NASA CR-54929
ADL 67180-00-04

NASA

ADVANCED STUDIES ON MULTI-LAYER INSULATION SYSTEMS

prepared for

NATIONAL AERONAUTICS AND SPACE ADMINISTRATION

NAS 3-6283

ARTHUR D. LITTLE, INC.

Requests for copies of this report should be referred to

National Aeronautics and Space Administration
Office of Scientific and Technical Information
Attention: AFSS-A
Washington, D.C. 20546

NASA CR-54929
ADL 67180-00-04

FINAL REPORT

ADVANCED STUDIES ON MULTI-LAYER INSULATION SYSTEMS

prepared for

NATIONAL AERONAUTICS AND SPACE ADMINISTRATION

June 1, 1966

CONTRACT NAS3-6283

Technical Management
NASA Lewis Research Center
Cleveland, Ohio
Liquid Rocket Technology Branch
James R. Barber

ARTHUR D. LITTLE, INC.
Acorn Park
Cambridge, Massachusetts 02140

TABLE OF CONTENTS

ACKNOWLEDGMENTS

The following personnel of Arthur D. Little, Inc., were associated with this program:

Igor A. Black	Richard B. Hinckley
Alfred G. Emslie	Frank E. Ruccia
Peter E. Glaser	Robert C. Reid ( )

We should like to acknowledge the assistance and co-operation of Mr. James R. Barber of the NASA Lewis Research Center, Liquid Rocket Technology Branch in the conduct of this work.

PART I

INTRODUCTION

I. INTRODUCTION

On March 2, 1965 Arthur D. Little, Inc. initiated work on "Advanced Studies on Multi-Layer Insulation Systems" under Contract No. NAS3-6283 with the NASA Lewis Research Center. This effort is, in part, a continuation of previous work accomplished under Contract Nos. NAS5-664, NASw-615 and NAS3-4181.

The heat leak into stored cryogenic propellants carried in space vehicles has an important effect on the quantities lost through vaporization, on the tank pressure limits, and on the utilization of the propellants. The heat leak rate to the propellants varies as the vehicle changes its environment, starting in the earth's atmosphere and ending in the vacuum of space. In all the environments, the heat leak to oxygen and, particularly, to hydrogen propellants must be limited and regulated in order to make the mission feasible and practical.

The means of limiting the heat flow in all the environments through the use of multi-layer insulations separately and in combination with other insulating media has received considerable attention.

Our studies both analytical and experimental, as reported herein, have dealt primarily with the performance of the insulating media in various environments.

Specifically, the present contract includes three major tasks:

(1) use of the previously developed emissometer to evaluate new radiation shield materials having lower emissivity than materials tested under previous contracts;

(2) operation of the flat plate thermal conductivity apparatus to evaluate new spacer materials to improve insulation efficiency, to obtain multi-layer insulation penetration heat leak data and to study the effect of perforations on the transient heat flow characteristics of multi-layer insulation systems; and

(3) to perform a series of insulated calorimeter tank experiments.

Although each task appears as a separate item in the contract, each has provided theoretical or experimental support for the others. As a matter of expedience and ease of reference, the detailed tasks are described in separate parts of this report; many of the interpretations and ideas were, however, derived through discussions between staff members engaged in the different areas.

A. <u>Experiments with the Thermal Conductivity Apparatus</u>

The purpose of this work was to obtain basic design information for evacuated multi-layer insulation systems and to evaluate their thermal performance experimentally. This information is intended to assist in the design of practical, lightweight insulation systems.

In particular, the objectives of this task are:

(1) To design and evaluate spacers that are light, have a low thermal conductivity, are insensitive to performance degradation caused by handling and application of compressive loads, and that readily return to the nearly uncompressed state after load release.

(2) To obtain and evaluate radiation shields with a lower emissivity than those currently available.

(3) To obtain data applicable to the design of a minimum heat leak configuration of a multi-layer insulation system penetrated by a pin or tube.

(4) To carry out measurements on multi-layer insulation systems in support of the calorimeter tank program.

Using an ADL Model-12 Calorimeter (flat plate thermal conductivity apparatus) equipped with a low compressive load attachment, we measured the thermal properties of several new spacer materials and material combinations with potentially better insulating performance than materials presently used for multi-layer insulations. We assembled the most promising materials into insulation systems and measured the heat flux passing through this system at compressive loads in the range between 0 to 15 psi.

In addition we obtained data on the performance degradation of multi-layer insulations caused by small diameter penetrations. For our study, we selected two typical multi-layer insulation systems, three sizes of penetrations, and two materials for penetrations. We studied the effect of thermal decoupling of a penetration from the multi-layer insulation on the heat flux through the entire system.

1. Conclusions

The following experimental results were obtained:

a. At zero compressive load, the heat flux through a multi-layer insulation with foam and glass mat sapcers (sample #3039) was higher than that through a multi-layer insulation with foam spacers only (sample #3040). Under load both insulations performed identically.

b. At zero compressive load the heat flux through a multi-layer insulation consisting of ten 0.00025 inch polyester film radiation shields aluminized on both sides and eleven 0.020 inch polyurethane foam spacers (2 lbs/ft^3 density) increased after each successive load application and release. The heat flux remained the same at 15 psi compressive load during three load applications.

c. The heat flux through a multi-layer insulation consisting of ten 0.00025 inch polyester film radiation shields, aluminized on both sides, and three layers of 0.003 inch silk netting for each spacer was lower than the heat flux through an insulation consisting of the same ten radiation shields but with spacers consisting each of two layers of 0.001 inch thick glass fabric. The weight of the first sample was one-half the weight of the second one, while the thickness of the first sample was approximately twice that of the second. In addition the silk netting was easier to handle than the glass fabric.

d. For the same compressive load the heat flux through a typical sample is lower before than after a 15 psi compressive load is applied.

e. System 11, when tested twice (samples #3041 and #3047), shows identical plots for heat flux vs. external compression even though several months past between the tests. These plots are not straight lines as theoretically predicted.

f. At zero external compression the heat flux through a sample with radiation shields perforated with 0.040-inch diameter holes, 2% open area, is twice as high as the heat flux through the similar sample with unperforated shields. At 15 psi compression, both samples conduct approximately the same amount of heat. Correlation between the data obtained from the thermal conductivity apparatus, emissometer and the theoretical estimates is very good.

g. The lightest practical spacer material is a 0.003-inch thick silk netting. This netting is dimensionally stable and easy to apply.

h. On the basis of thermal performance the uncut, 0.020-inch thick rigid polyurethane foam was the most efficient spacer material tested. Fragility of this material makes application difficult.

i. The total heat flux through insulation systems consisting of identical number of radiation shields of the same quality generally is lower for thicker spacers.

j. Heat flux passing through an insulation system with freshly prepared silver coated polyester radiation shields is lower than the heat flux through the same system, but with aluminum coated or gold coated radiation shields.

k. At no external compression the weight of the sample itself determines the lower limit of the heat flux through the sample.

l. Removal of a part of the spacer material decreases the weight of the spacer, the contact area between the shields and spacers, and, consequently, the total heat passing through the insulation layer.

m. Multi-layer insulations with spacers of two or more materials can be made more effective than single material spacers because each component can be selected to perform a single function. For example, the 0.003-inch thick silk netting together with foam or glass-paper discs or strips attached to the netting is a lightweight, dimensionally stable, easily applicable spacer system of a high thermal performance.

n. Extreme care must be exercised in assembly and installation of a multi-layer insulation penetrated by a pin to achieve a minimum heat loss through the assembly.

o. A "buffer zone" around a low conductivity penetration does not minimize the heat loss through the system if metal coated polyester film of 0.00025-inch thickness is used for radiation shields. On the contrary, the heat flux through the buffer zone adds to the total heat loss through the system. In the first approximation, the heat flux through a multi-layer insulation system penetrated by a low conductivity pin can be estimated by simply adding the heat flux calculated for an undisturbed sample of insulation and the heat flux calculated for the pin alone.

p. Theoretical work published in the literature describing the influence of the gas pressure on the thermal performance of the multi-layer insulation shows the relation only qualitatively. An attempt to use that data to estimate performance of a given insulation may lead to a considerable error.

B. The Emissometer Program

The objective of this program is to establish the emittance performance of vacuum metallized coatings placed on polyester film in terms of the coating thicknesses and exposure to various atmospheric environments. A second program objective was to evaluate the emittance properties of shield materials used in the insulation systems studied in the tank program and to aid in the selection of the shields.

The scope of this effort consisted of the specification, procurement and measurement of materials to be studied. Specifically, initial studies were conducted to select and specify coatings to be considered. The coatings finally selected were aluminum, gold, silver and copper. Whenever possible, coating samples were procured from commercial sources. Many samples were produced at Arthur D. Little, Inc. in the laboratory. Coating thickness was determined by electrical resistance methods generally, but other methods were also used. The emittances of various metal coatings in various thicknesses were measured in an emissometer developed in the previous contract. An environmental chamber was fabricated and samples were exposed in the chamber to humid air, carbon dioxide and salt air for 50 and 100 hour periods. Emittance measurements were taken after these exposure periods. During the progress of the work information obtained was used in selecting and specifying shield materials for the tank insulation and in establishing the quality of the purchased materials.

1. Conclusions

a. Each of the metals studied have different emittance values. Grouped in order of increasing emittance are silver, copper, gold and aluminum. Silver has an emittance of .011 at thicknesses greater than 1000 Angstroms (°A). Copper has an emittance value of .013 at thicknesses greater than 500°A. Gold has an emittance value of .017 at thicknesses greater than 1500°A. Aluminum has an emittance of .023 at thicknesses greater than 600°A. This data is summarized in Figure III-18.

b. Polyester film with the minimum coating thicknesses indicated above requires special ordering from commercial suppliers. Commercially available materials generally have thicknesses of 250°A or less.

c. The emittances of each metal studied have different degrees of stability when exposed to high humidity air, carbon dioxide and salt environments. Grouped in order of decreasing stability are aluminum, gold, silver and copper.

d. The emittance stability of silver and copper in the various environments studied are improved when thin protective coatings of silicon monoxide are applied over the primary coating. However, this protective coat generally results in a slight initial degradation in the emittance of the primary coating. The emittance of silver is increased to about .016 and the emittance of copper is increased to about .017. Gold and aluminum applied as a thin protective coat over silver resulted in serious emittance degradation of the surface.

e. The emittance of commercially produced samples was generally comparable to the emittance of laboratory produced samples. This applies to aluminum, gold and silver coatings. No commercially applied copper coatings were tested.

f. The determination of coating thickness using the wrought electrical resistivity of the metal and the measured resistance of the coating appears adequate. This method does not require specialized equipment, and can be done quickly and easily at any desired location on the coated film after it has been produced.

C. Insulated Tank Calorimeter

The purpose of this study was.

(1) to select insulation materials which were expected to yield improved performances of multi-layer insulation systems;

(2) to design and fabricate multi-layer insulation systems, apply them to calorimeter tanks, and measure and evaluate their thermal performance in a simulated space environment using liquid nitrogen; and

(3) to develop practical methods of applying insulation to vehicle-type tanks and achieve the optimum thermal performance for the least weight of insulation.

We have designed, fabricated and tested a total of seven multi-layer insulation systems. Four of these systems consisted of a foam substrate in addition to the multi-layers. One system contained a 6 inch diameter by 17 inch long penetration. Each system tested is described in Table IV-2. The thermal performance of each insulation system was measured in a test chamber which simulated the vacuum and a portion of the radiation spectrum found in the space environment. A group of seven experimental test series was conducted using the two test calorimeters and test chamber facilities fabricated under the previous contracts.

The heat flux and $\kappa\rho$ performance for each insulation system tested under space environment conditions are presented in Table IV-2 (Insulation Systems 8 thru 14). In addition the results obtained with systems in the two previous contracts are presented for comparison.

1. Conclusions

a. Commercial sources of good quality, low emittance shields have been identified. These consist of polyester film, vacuum metallized on both sides with aluminum, silver and gold and can be obtained on special order from the suppliers. The best emittance values obtained with these coatings have been .025, .011 (the silver was unprotected and new; emmitance degrades with time) and .017 respectively. One set of shields was obtained containing 1.9 per cent perforations for use in systems with expected gas leaks.

b. Commercial sources of lightweight spacer materials have been identified. These consist of glass fabric, silk nettings and combinations of silk and foams. Single layers of these materials have unit weights of .0042, .0012 and .0037 pounds per square foot respectively as compared to .0018 pounds per square foot representative of the unit weight of 1/4 mil Mylar. Multiple layers in spacers of the glass fabric and silk netting have good low load thermal performance. Each of the spacers could be easily fabricated into multi-layer insulation systems.

c. In the current program, the measured heat fluxes for the five shield systems tested ranged from .31 to 1.06 Btu/hr ft^2. System No. 14 consisting of gold coated shields and silk netting spacers, produced a $\kappa\rho$ product of .000273 Btu-in-lb/hr ft^5 °F, which is the lowest value obtained with any system in the entire tank program. The heat flux associated with this system was .33 Btu/hr ft^2 and is surpassed only by System No. 12 which produced a heat flux of .31 Btu/hr with a $\kappa\rho$ value of 0.0003 Btu-in-lb/hr ft^5 °F. Further improvement in the $\kappa\rho$ product of the systems tested can be expected if the insulations are not required to sustain pressure loadings.

d. The agreement in the insulation heat fluxes measured with tank calorimeter apparatus and with a flat plate thermal conductivity apparatus have been generally good. Also the predicted fluxes based on emittance measurements made on the shield surfaces with the emissometer instrument have been in good agreement with the measured system values. Thus, a great deal of confidence can be placed in the heat flux results obtained in the program.

e. Engineering relations have been developed to predict the effect of static gas pressure and gas flow in the insulation after certain empirical constants are evaluated. From tests conducted with helium gas in a five shield multi-layer insulation, a value for the gas accommodation coefficient of .65 was established for inner and outer boundary temperature of -320 and 80°F.

Penetration heat flow and temperature gradients were successfully measured in eight tests for a variety of conditions. The experimental techniques used in this investigation were demonstrated to be valid for isolating the penetration heat flows for a wide variety of boundary conditions. The measured heat flow and temperature gradients for one set of conditions are predicted by the analytical model with good accuracy. Generally, however, the conditions selected for the experimental model were not covered by the analysis performed in a previous contract. The analytical model gives good promise of predicting the heat transfer phenomena occurring within the penetration.

The technique of using angles of aluminum foil to seal the joints formed by the shields of the tank and penetration insulation against radiation leaks appears to be both effective and practical. While the data can only be used to demonstrate this factor indirectly, there are no significant heat flows that could be identified with this part of the insulation system.

PART II

TASK I A, EXPERIMENTAL PROGRAM - THERMAL CONDUCTIVITY APPARATUS

TABLE OF CONTENTS

II

LIST OF FIGURES

II

LIST OF FIGURES

II

(Continued)

LIST OF TABLES

II

LIST OF TABLES

II

(Continued)

LIST OF TABLES

II

(Continued)

II. TASK I A, THERMAL CONDUCTIVITY APPARATUS

A. SUMMARY

1. Purpose

The purpose of this work was to obtain basic design information for evacuated multi-layer insulation systems and to evaluate their thermal performance experimentally. This information is intended to assist in the design of practical, lightweight insulation systems.

In particular, the objectives of this task are:

a. To design and evaluate spacers that are light, have a low thermal conductivity, are insensitive to performance degradation caused by handling and application of compressive loads, and that readily return to the nearly uncompressed state after load release.

b. To evaluate radiation shields and to see if shields with a lower emissivity than those currently available can be obtained.

c. To obtain data applicable to the design of a minimum heat leak configuration of a multi-layer insulation system penetrated by a pin or tube.

d. To carry out measurements on multi-layer insulation systems in support of the calorimeter-tank program.

The purpose of this report is to describe the work performed and to state conclusions and recommendations resulting from this investigation.

2. Scope

Using an ADL Model-12 Calorimeter (flat plate thermal conductivity apparatus) equipped with a low compressive load attachment, we measured the thermal properties of several new spacer materials and material combinations with potentially better insulating performance than materials presently used for multi-layer insulations. We assembled the most promising materials into insulation systems and measured the heat flux passing through this system at compressive loads in the range between 0 and 15 psi.

We evaluated the performance of selected radiation shield materials with the Model-12 Calorimeter to substantiate data measured with the emissometer (see Section III).

In addition, we obtained data on the performance degradation of multi-layer insulations caused by small diameter penetrations. For our study we selected two typical multi-layer insulation systems, three sizes of penetrations, and two materials for penetrations. We studied the effect of thermal decoupling of a penetration from the multi-layer insulation on the heat flux through the entire system.

Finally, we supplied the required support to the calorimeter-tank program (see Section IV).

3. Program Findings

a. Experimental Results

The following experimental results were obtained:

(1) At zero compressive load, the heat flux through a multi-layer insulation with foam and glass mat spacers (sample #3039) was higher than that through a multi-layer insulation with foam spacers only (sample #3040). Under load both insulations performed identically.

(2) At zero compressive load the heat flux through a multi-layer insulation consisting of ten 0.00025-inch polyester film radiation shields aluminized on both sides and eleven 0.020-inch polyurethane foam spacers (2 lbs/ft^3 density) increased after each successive load application and release. The heat flux remained the same at 15 psi compressive load during three load applications.

(3) The heat flux through a multi-layer insulation consisting of ten 0.00025-inch polyester film radiation shields, aluminized on both sides, and three layers of 0.003-inch silk netting for each spacer was lower than the heat flux through an insulation consisting of the same ten radiation shields but with spacers consisting each of two layers of 0.001-inch thick glass fabric. The weight of the first sample was one-half the weight of the second one, while the thickness of the first sample was approximately twice that of the second. In addition, the silk netting was easier to handle than the glass fabric.

(4) For the same compressive load the heat flux through a typical sample is lower before than after a 15 psi compressive load is applied.

(5) System 11 when tested twice (samples #3041 and 3047) shows identical plots for heat flux vs. external compression even though several months past between the tests. These plots are not straight lines as theoretically predicted.

(6) At zero external compression the heat flux through a sample with radiation shields perforated with 0.040-inch diameter holes, 2% open area, is twice as high as the heat flux through the similar sample with unperforated shields. At 15 psi compression, both samples conduct approximately the same amount of heat. Correlation between the data obtained from the thermal conductivity apparatus, emissometer and the theoretical estimates is very good.

(7) The lightest practical spacer material is a 0.003-inch thick silk netting. This netting is dimensionally stable and easy to apply.

(8) On the basis of thermal performance the uncut, 0.020-inch thick rigid polyurethane foam was the most efficient spacer material tested. Fragility of this material makes application difficult.

(9) The total heat flux through insulation systems consisting of identical number of radiation shields of the same quality generally is lower for thicker spacers.

(10) Heat flux passing through an insulation system with freshly prepared silver coated polyester radiation shields is lower than the heat flux through the same system, but with aluminum coated or gold coated radiation shields.

(11) At no external compression the weight of the sample itself determines the lower limit of the heat flux through the sample.

(12) Removal of a part of the spacer material decreases the weight of the spacer, the contact area between the shields and spacers, and, consequently, the total heat passing through the insulation layer.

(13) Multi-layer insulations with spacers of two or more materials can be made more effective than single material spacers because each component can be selected to perform a single function. For example, the 0.003-inch thick silk netting together with foam or glass-paper discs

or strips attached to the netting is a lightweight, dimensionally stable, easily applicable spacer system of a high thermal performance.

(14) Extreme care must be exercised in assembly and installation of a multi-layer insulation penetrated by a pin to achieve a minimum heat loss through the assembly.

(15) A "buffer zone" around a low conductivity penetration does not minimize the heat loss through the system if metal coated polyester film of 0.00025-inch thickness is used for radiation shields. On the contrary, the heat flux through the buffer zone adds to the total heat loss through the system. In the first approximation, the heat flux through a multi-layer insulation system penetrated by a low conductivity pin can be estimated by simply adding the heat flux calculated for an undisturbed sample of insulation and the heat flux calculated for the pin alone.

(16) Theoretical work published in the literature describing the influence of the gas pressure on the thermal performance of the multi-layer insulation shows the relation only qualitatively. An attempt to use that data to estimate performance of a given insulation may lead to a considerable error.

b. Equipment

The following improvements and modifications of the equipment were accomplished:

(1) Pulsation of the boil-off gas flow at rates below 200 cc/hr was substantially reduced by using porous ceramic nozzles in the pressure controller and in the low boil-off meter.

(2) The operation of the low compressive load attachemnt has been improved by:

(a) Using an edge guard radiation shield. With this shield a 1/4-inch of the upper part of the edge of the sample can be observed through the window during the test.

(b) Incorporating precise pressure regulators to increase the sensitivity of the device. These regulators also permit to maintain and measure low bellows pressures corresponding to compressive loads of less than 0.01 psi.

(c) Providing better anchoring of the cold plate to the base plate of the apparatus. This modification permits continuous operation of the low load attachment from 0.01 psi to 15 psi.

(3) An adjustment which makes it possible to tilt the warm plate of thermal conductivity apparatus.

4. Recommendations

We recommend continuing investigations in the following areas;

a. Development of new methods of spacing the radiation shields. The investigation of composite material spacers already indicated their potential usefulness.

b. Effects of extremely low compressive loads (below 0.1 psi) on the heat flux through the insulation. Loads below 0.1 psi can be expected during application of the insulation, the effects of these loads will influence the final performance of the applied layer.

c. The recovery of the multi-layer insulation from multiple application of compressive loads including the influence of the maximum load applied and the length of application.

d. Application of the compressive load by a flexible cushion.

e. Penetrations of multi-layer insulations.

(1) Effect oc temperature distribution in the penetration on the total heat flux through the system.

(2) Effect of a pnentration on a multi-layer insulation with metallic radiation shields.

(3) Effect of a penetration on a multi-layer insulation with open spacer material.

B. INTRODUCTION

In Task I A the Government-owned thermal conductivity apparatus equipped with low compressive load attachment was used to evaluate new spacer materials combined into insulation systems in an effort to reduce insulation weight and to improve thermal performance. Of particular interest were materials insensitive to performance degradation caused by handling and application of compressive loads. and materials which return readily to the near uncompressed state after load release. These materials, as well as promising materials investigated during earlier programs, were examined in the compressive load range of 0 to 15 psi. Materials for this evaluation included low density foams, lightweight veils and composite spacers.

We investigated the effects of penetrations on the heat transfer through two multi-layer insulations. Because of the general interest, we briefly surveyed the literature on the effects of gas pressure on the thermal performance of the multi-layer insulation. We compared the experimental data which we obtained during Contract No. NASw-615 with the performance estimates based on this survey.

In addition, we tested three samples furnished by LeRC in order to determine the effects of an inflated pillow installed between the multi-layer insulation and the warm plate. All tests were accomplished at liquid nitorgen cold plate temperatures. Several tests were performed in support of the calorimeter-tank program.

We found several promising materials which merit further study, for example, compared to single material spacers, composite spacer materials were found to have a potentially superior performance.

C. APPARATUS

1. Description

To measure the heat flux passing through a multi-layer layer insulation we have designed and built under contract NAS5-664 a flat plate thermal conductivity apparatus shown in Figure II-1. The apparatus is described in detail in the Final Report under contract NASw-615 and in the Operating Manual which is supplied under this contract.

2. Maintenance

Thermal Conductivity Apparatus No. 3 had been stored for approximately six months prior to the beginning of this program. Before we started testing we inspected, cleaned, and regreased all O-rings and rubber vacuum seals. We inspected rubber hoses, serviced vacuum pumps, checked the vacuum system for leaks, tested vacuum gauges and repainted the warm and cold plates with 0.9 emissivity paint.

This preventive maintenance assured a satisfactory operation of the apparatus throughout the contract. The only difficulty which we experienced during the running of the apparatus was a failure of a plastic tube on the pressure controller. It occurred twice during the year causing incorrect readings of the boil-off rate. We suspect that the crack in the plastic tube was caused by vibration produced by pulsation of the boil-off flow from the guard vessel through the mercury in the pressure controller. Since the second failure occurred only at the very end of the project no attempt was made to improve the design.

3. Elimination of Gas Pulsation at Extremely Low Boil-Off Rates

At boil-off rates below 200 cc/hr gas flow from the measuring vessel pulsated at extremely slow rates causing the gas to discharge in bursts of bubbles at uneven intervals, each burst was accompanied by a small (not over 5 mm of oil) pressure drop. Apparently, the pressure required to form and push gas bubbles through the mercury in the pressure controller, and the oil in the low boil-off meter created the pulsation. We previously made several attempts to eliminate the gas pulsation. Wire screens and gauze cloth worked satisfactorily when new

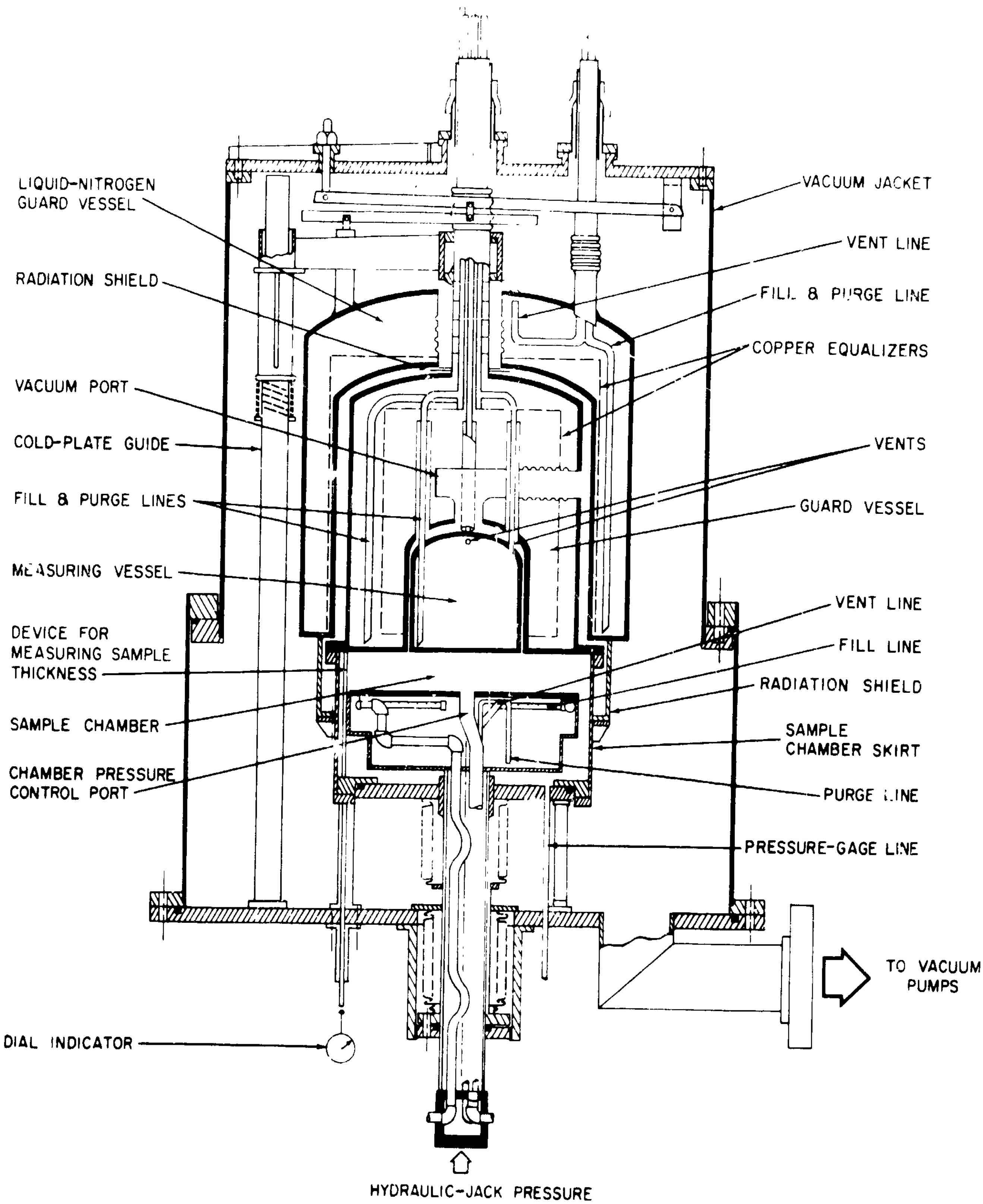

FIGURE II-1 CROSS-SECTION OF DOUBLE-GUARDED COLD-PLATE THERMAL-CONDUCTIVITY APPARATUS but failed after a short period. Nozzles of a few tenths of a millimeter diameter performed well at a particular constant flow rate but had to be exchanged for different flow rates.

From observations of the gas flow through the nozzle, we concluded that for each rate there exists a maximum size of bubble beyond which the gas flow becomes uneven. A small diameter nozzle, while discharging small diameter bubbles, caused a high pressure drop across the orifice and created an undesirably high pressure over the boiling liquid. A high pressure could cause a large gas leak in the boil-off system which, if not corrected, could result in erroneous measurements.

Because boil-off rate readings were being taken over a long period of time compared to the pulsation cycle, the effect of errors in the measurements tended to be averaged out. However, an improvement of the apparatus was desired.

We tested various nozzle designs and found that commercially available porous ceramic filters passed a large number of extremely small bubbles. By discharging various amounts of bubbles of constant size a ceramic filter provided a steady flow of gas for rates from 30 to 1000 cc/hr.

We installed ceramic filters for nozzles on the measuring vessel boil-off line in the pressure controller, and in the low boil-off meter. At gas flows over 1000 cc/hr, the bubbles created a foam above the surface of the oil; therefore, a high flow nozzle and a switch-over valve were added to the gas inlet line of the low boil-off meter. Figure II-2 shows both nozzles.

To even out the effects of the bubble discharge in the mercury pressure controller on the cryogen boiling in the measuring vessel, we added a surge chamber and a variable orifice (needle valve) to the discharge line between the vessel and the controller.

4. Measurement of the Total Boil-Off Gas Flow

To further increase the accuracy of the boil-off rate measurement, we installed a solenoid valve to interrupt the gas flow from the measuring vessel while the low boil-off meter is being actuated (when

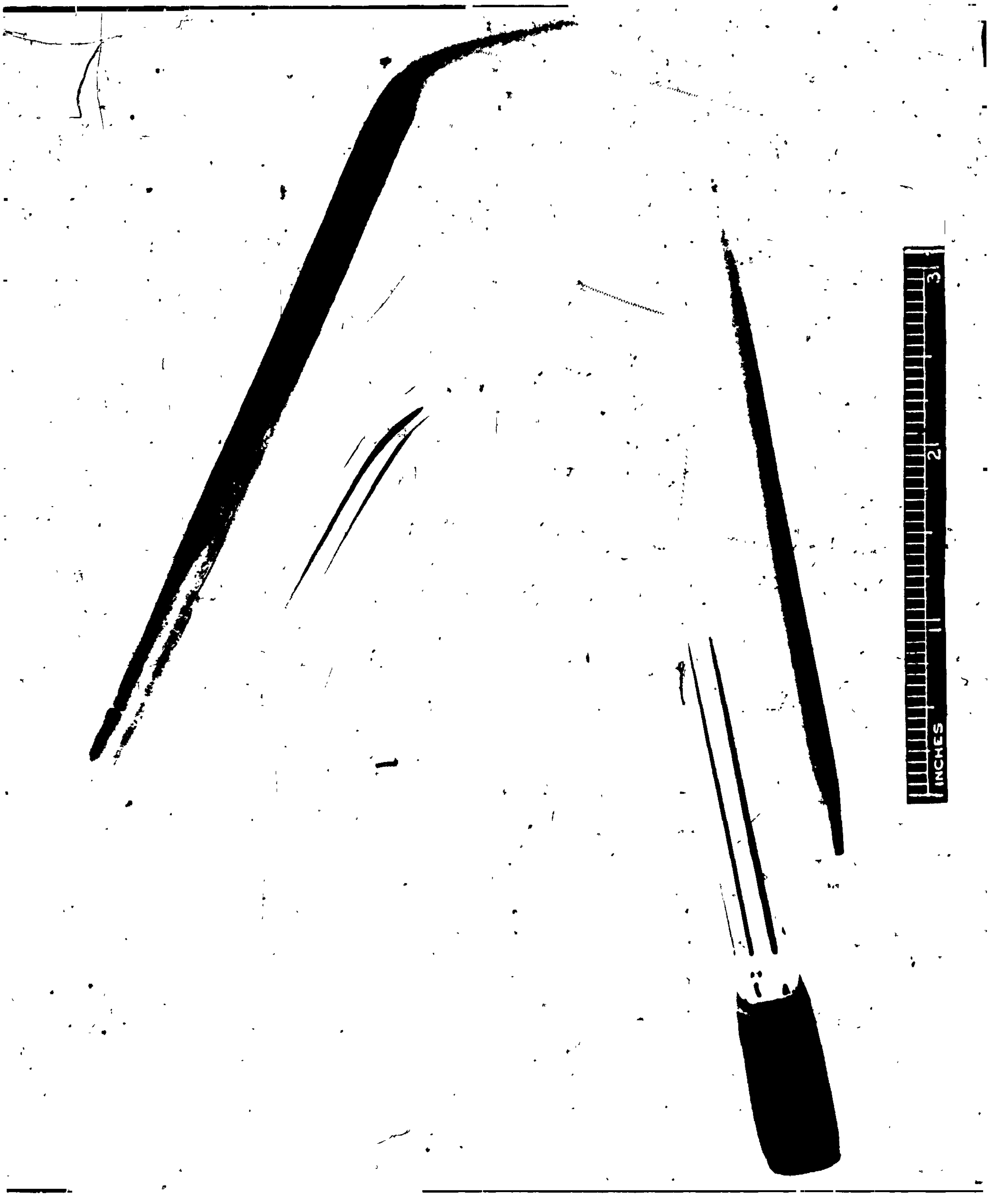

FIGURE II-2 NEW NOZZLES FOR LOW BOIL-OFF METER the oil is elevated to the upper level in the graduate and when the volume of the already measured gas is discharged from the meter).

Even though the time of the actuation process is short (only a few seconds in each 30-minute cycle), the total gas flow from the measuring vessel can be more accurately determined as a result of this modification.

5. Other Improvements in Operation of the Low Boil-Off Meter

We improved the ease of operation of the low boil-off meter by installing on the front panel of the device:

a. a manual valve which permits the operator to select one of the two discharge nozzles shown in Figure II-2 located under the oil level in the measuring tube.

b. a selector switch and two sets of photo-electric cells which are located at different heights of the measuring tube. By turning the switch the operator can select the volume of gas to be measured during one cycle of the meter.

Figure II-3 shows the improved low boil-off meter.

6. Improvements of the Low Compressive Load Attachment

a. Electrical Heater

In the test of the low load attachment (run No. 3037) during the previous contract (NAS3-4181), we found that the temperature of the floating plate (which now is the new warm plate of the calorimeter) was 20-30°F below the temperature of the water circulating through the ram (the original warm plate). To bring the temperature of the new warm plate closer to room temperature, we had two alternatives: to heat the water circulating through the ram or to add an electrical heater to the floating plate. We selected the latter method because it provides greater flexibility. We attached a 300-watt, 12-inch diameter by 1/32-inch thick flat electrical heater on the underside of the floating plate.

b. Guard Radiation Shield

When the low compressive load attachment was installed in the thermal conductivity apparatus, the sample chamber skirt had to be

FIGURE II-3 IMPROVED LOW BOIL-OFF METER

lowered so that it no longer protected the edges of the test sample from radiation of the 300°K vacuum jacket wall of the apparatus.

We therefore designed, manufactured, and installed a three-piece guard radiation shield to protect the sample edges. The shield was made from 1/16-inch thick copper, painted with 0.9 emissivity paint on all surfaces exposed to the 77°K temperature and to the sample, and polished on the surfaces viewing the 300°K temperature. The lower part of the shield was split in two pieces so that only one must be removed when the test sample is changed. Both pieces were bolted to the guard vessel 1/4-inch below the guard vessel flange. The 1/4-inch wide gap left between the shield and the guard vessel flange was shielded by the upper part of the radiation shield attached to the liquid nitrogen vessel. (See Figure II-4.) To observe the upper 1/4-inch of the test sample through the viewing windows in the vacuum jacket, we can lift the liquid nitrogen vessel and the part of the radiation shield attached to it at any time during a test using the mechanism already provided for this purpose.

c. Anchor Bolts

The cold plate was originally supported by four bolts which were anchored to the upper flange of the sample chamber skirt. In turn, the skirt was anchored to the base plate of the calorimeter. This arrangement was satisfactory when compressive loads of less than 2 psi (200-lb tension force on four bolts) were used. Compressive loads above 2 psi would have caused permanent distortion of the upper flange of the sample chamber skirt.

To permit application of compressive loads up to 15 psi without removing the low compressive load attachment, we installed eight bolts which support the cold plate directly from the base plate of the calorimeter and completely by-pass the flange of the sample chamber skirt. The bolts are of a split construction which permits the test sample to be easily removed.

Three additional bolts located 120 degrees apart permit the cold plate to be leveled before the other eight bolts are engaged and fastened.

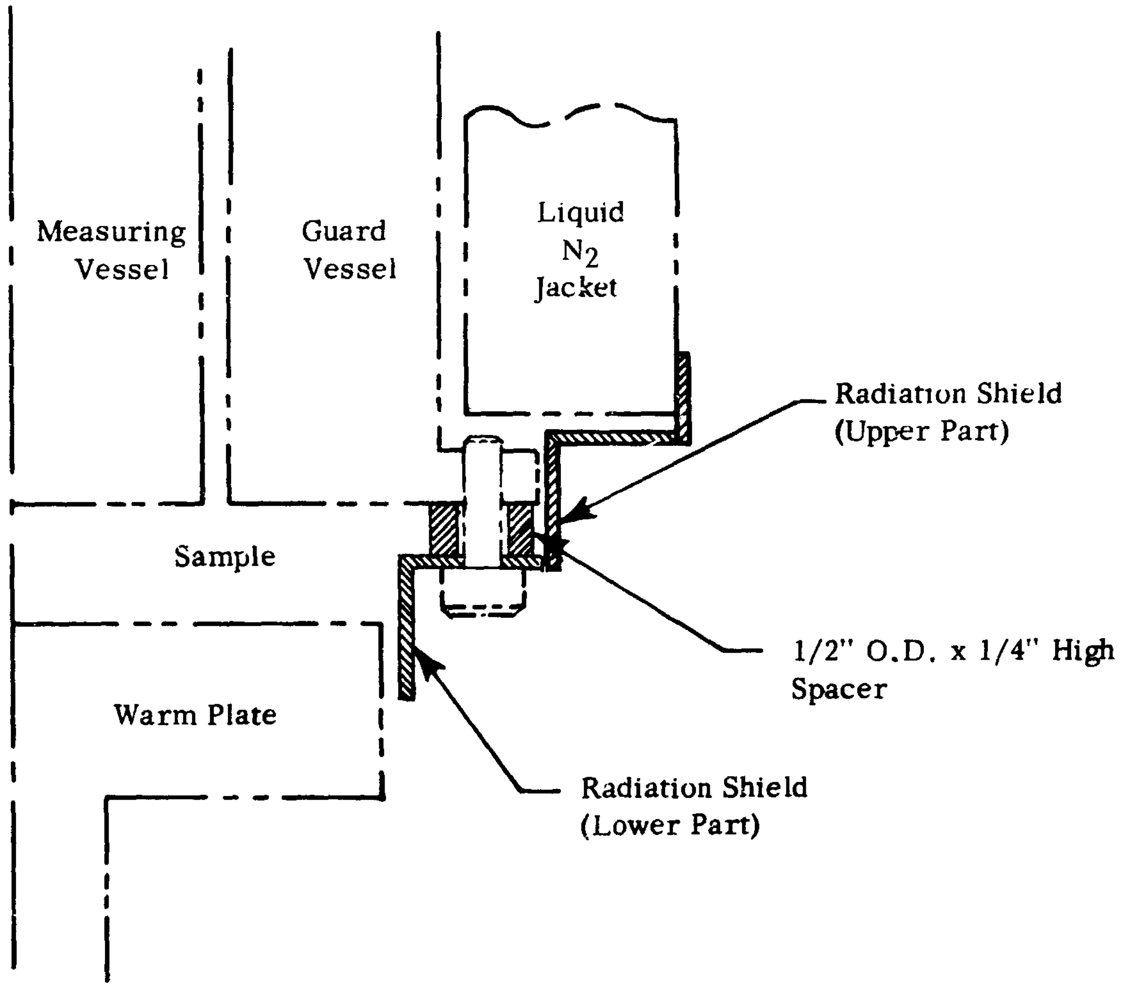

FIGURE II-4 ARRANGEMENT OF A GUARD RADIATION SHIELD FOR THE LOW COMPRESSIVE LOAD ATTACHMENT

d. Precise Pressure Regulator

The sensitivity of the standard gas pressure regulators was inadequate to pressurize the bellows. The regulators were difficult to adjust and the 0.5-psi gas pressure necessary to apply 0.01 psi compressive loads to the test sample was difficult to maintain constant.

We experimented with the device shown in Figure II-5 to apply loads below 0.01 psi. Due to minute leaks, this arrangement was unsatisfactory. Therefore, we searched for a commercial precision pressure regulator to control application of compressive loads to the sample as low as 0.001 psi.

We tested a Nullmatic Pressure Regulator, Series 40, made by Moore Product Company (Philadelphia) and found that regulators of this type with ranges of 0-50 inches H_2O and 0-200 inches H_2O can maintain constant pressure in the bellows down to 0.05 psig (corresponding to a 0.001 psi compressive load on the test sample). The new pressure regulator permits the gas pressure to be adjusted between 0.05 and 5 psig within $\pm$ 0.01 psig. The higher precision of pressure regulation has enabled us to improve the operation of the low compressive load attachment at and below 0.01 psi compression on the sample.

e. Increase of Device Sensitivity

In addition to the above described modifications, we further improved the sensitivity of the low load attachment by removing the spring which returns the stem of the dial indicator into its extended position. This spring exerted between 70 and 130 grams force (depending on the position of the dial indicator stem) per indicator. A force of 210 grams applied by 3 indicators to the floating plate corresponds to approximately 0.005 psi compression on the sample. After the spring was removed only 8 to 16 grams force was necessary to move one dial indicator.

In this modification the stem of the dial indicator depends on its own weight for the return stroke into the extended position. Therefore, the indicators were turned to a position with the stem down below the body. The bodies of the indicators were attached to the floating warm plate.

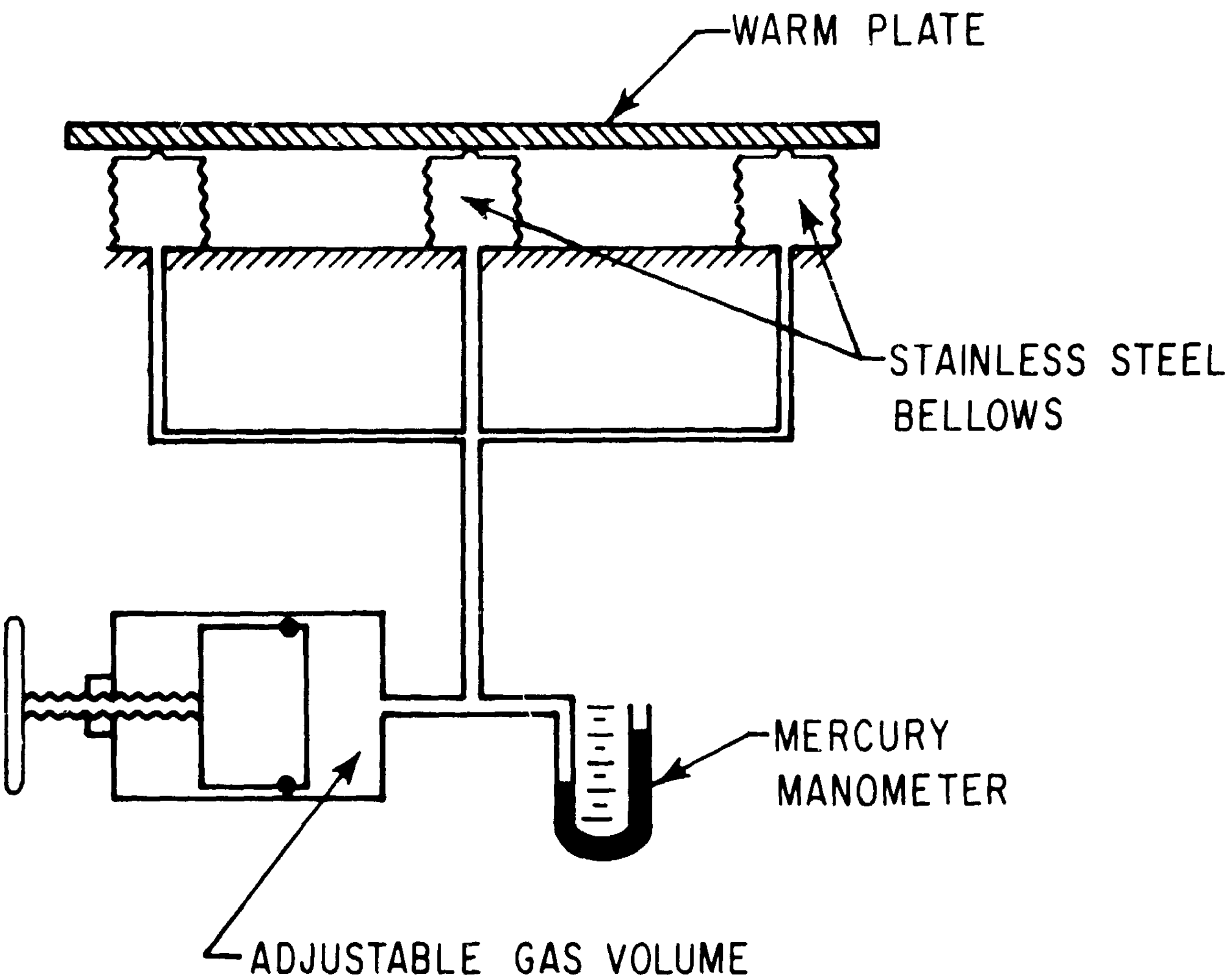

FIGURE II-5 EXPERIMENTAL GAS PRESSURE CONTROL SYSTEM FOR EXTREMELY LOW COMPRESSIVE LOADS

f. Various Methods of Load Application to the Test Sample

A compressive load can be transmitted to the sample by:

(1) applying a common gas pressure to all three bellows permitting the rigid floating warm plate to seek its own position (not necessarily a parallel one to the cold plate);

(2) applying a gas pressure individually to each of the three bellows maintaining the rigid warm plate parallel to the cold plate;

(3) placing a soft (for example, a flexible foam) cushion on top of the rigid warm plate and applying gas pressure in the same way as described in (2);

(4) a plastic inflatable cushion placed over the warm plate.

We tried these four methods. However, for most of the tests we used the method described under (1), because we found that:

-- if the sample is carefully assembled and placed concentrically on top of the warm plate, the latter floats parallel to the cold plate

-- a soft cushion placed over the warm plate may produce different results because of the elasticity of the cushion.

-- a plastic inflatable cushion does not produce a flat upper surface when inflated. As shown in Figure II-6 the top surface of the cushion is curled and uneven which may introduce local compressive loads.

To achieve an acceptable sensitivity the low load attachment already required three gas regulators and three pressure gauges (one for each pressure range). The method of load application described in (2) requires nine gas regulators and nine pressure gauges.

We installed two more gas regulators and two more pressure gauges for the compression range between 0.01 and 0.1 psi to investigate if the results depend on the method of compression applied to the sample. Figure II-7 shows the resulting panel board.

FIGURE II-6   INFLATABLE CUSHION

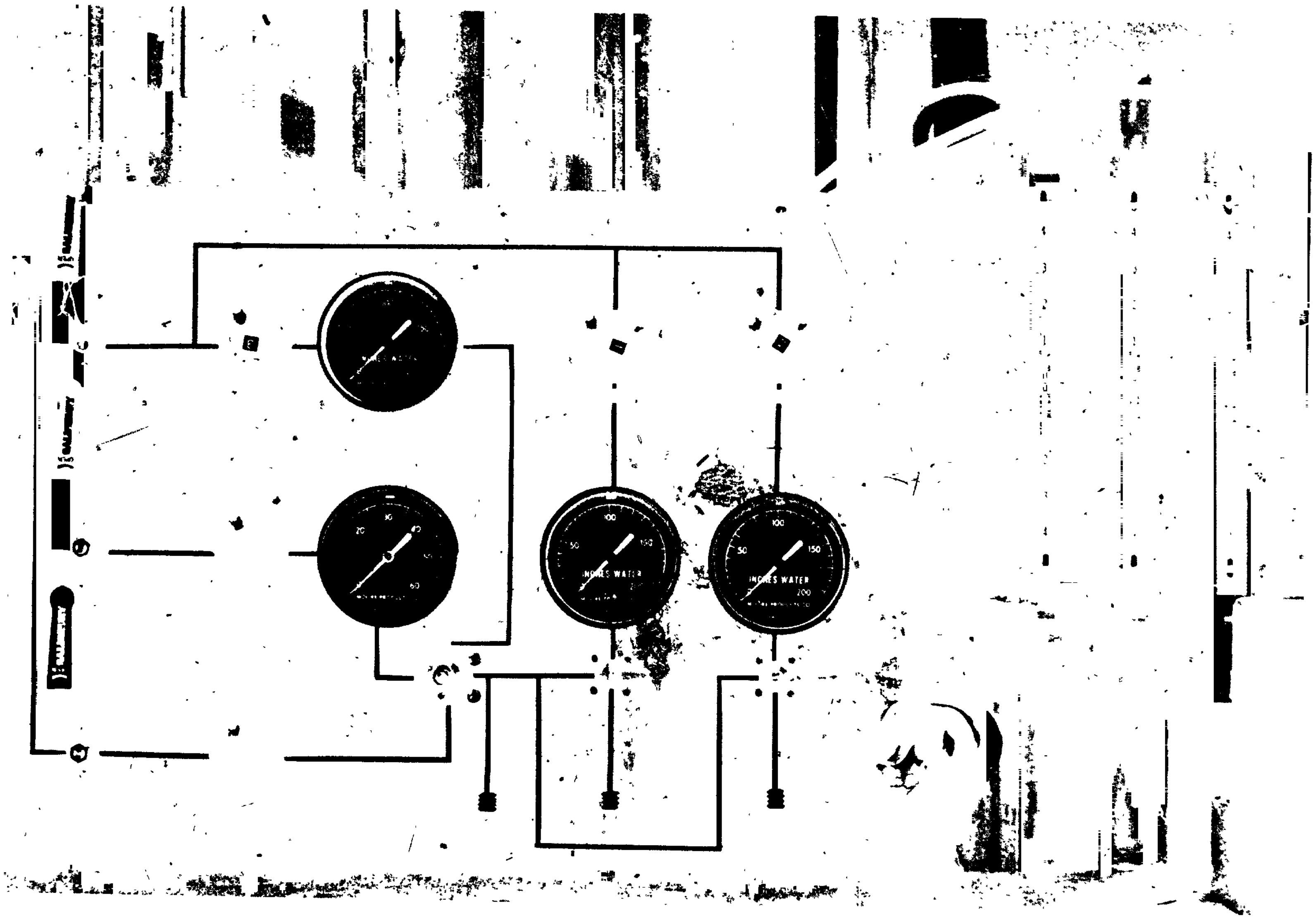

FIGURE II-7 CONTROL BOARD FOR THE LOW LOAD ATTACHMENT

g. Miscellaneous Improvements

Miscellaneous minor improvements were made on the low compressive load attachment, for example:

(1) We increased the inner diameter of the flating plate by 1/16 of an inch. This prevented the floating plate from rubbing against the original warm plate thereby eliminating frictional forces and increasing the accuracy of the measurement.

(2) We shortened the rivets which interfered with the movement of the needle in the dial indicators. This eliminated the occasional failure of the dial indicators to respond to the bellows' movements.

(3) The bellows were placed upside down to permit the line which carries the bellows' pressurizing gas to be on the stationary part of the bellows and to allow the bellows to move more freely.

Figure II-8 shows the low compressive load attachment after all improvements discussed above were completed.

h. Reproducibility of the Low Compressive Load Device

We tested the reproducibility of the low compressive load device with dead weights. Table II-1 shows the results. A 2.5-lb weight (corresponding to 0.02 psi compression of the sample) decreases the height of the bellows by approximately 0.020 inch. When a load is consecutively applied and released several times, the bellows returned to within ± 0.0015 inch of the position established during the first application of load.

We applied gas pressure to the bellows in 0.1-psi increments between 0 and 1 psig, using the new gas regulator. the results of the tests are shown in Figure II-9. All three bellows indicated undesirably high hysteresis effects, when extended beyond 0.150 inch. From these tests we concluded that in order to minimize hysteresis effect the bellows' travel as well as pressure increments during pressure increase (or decrease) must be limited to 1/2 the value used during the test, i.e. 0.080-inch and 1/2 PSID respectively.

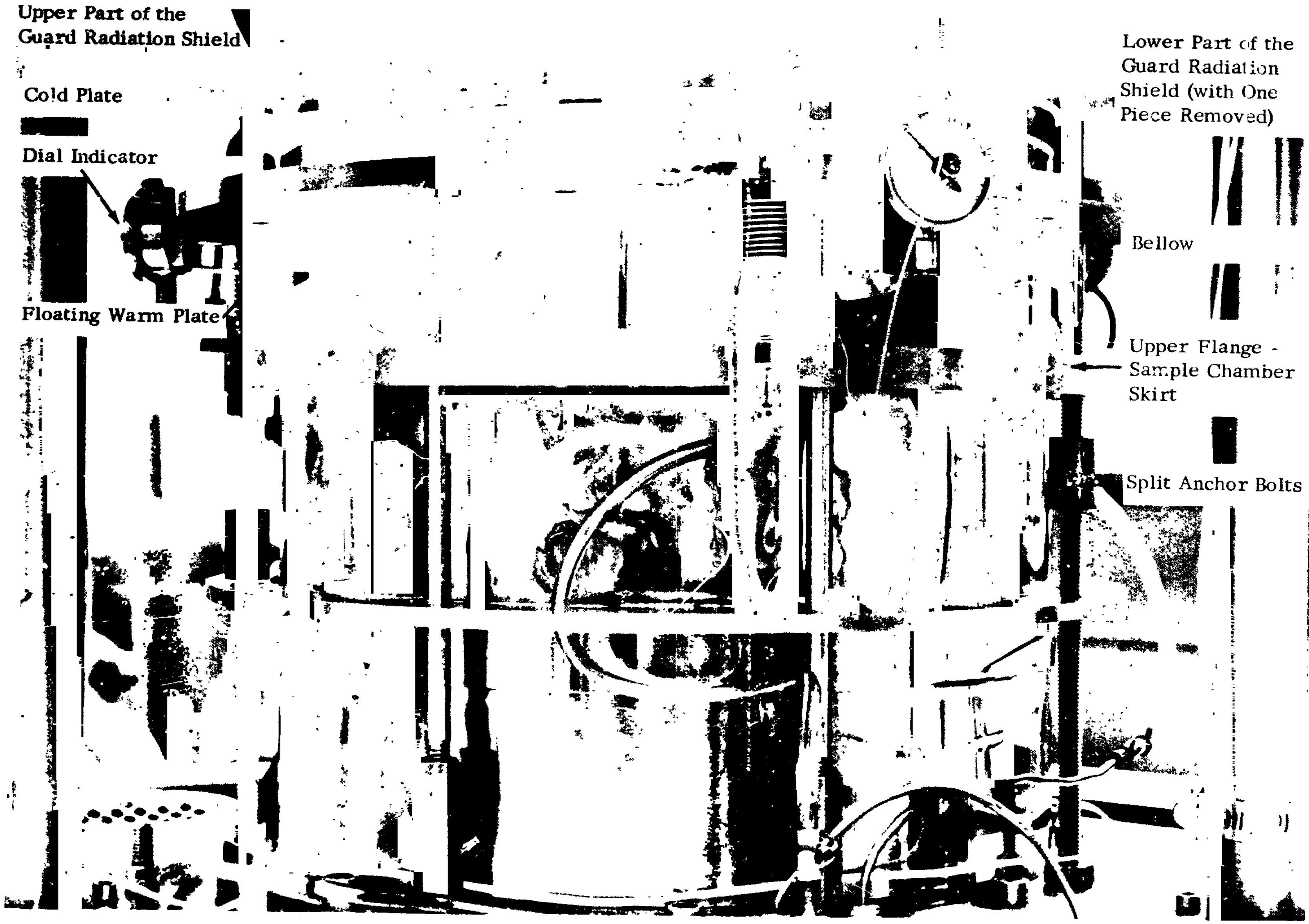

FIGURE II-8 LOW COMPRESSIVE LOAD ATTACHMENT

TABLE II-1

SENSITIVITY OF THE LOW COMPRESSIVE LOAD ATTACHMENT

Dead Weight: 2.52 lb (0.0223 psi on sample)

Gas Pressure: 28.7 psia (14 psig)

Initial Indicator Setting: Zero for all three bellows

Pressure Outside the Bellows: 14.7 psia

Bellow	Deflection At No Weight	Deflection Weight Added	D	Deflection Weight Removed	Deflection Weight Added	D	Weight Removed	Gas Pressure Removed	Repeatability
1	-.042	-.020	.022	-.043	-.022	.021	-.043	0	± .001
2	+.046	-.037	.017	+.044	-.038	.018	+.044	.003	± .0015
3	+.047	-.035	.018	+.045	-.038	.017	+.046	.003	± .0015

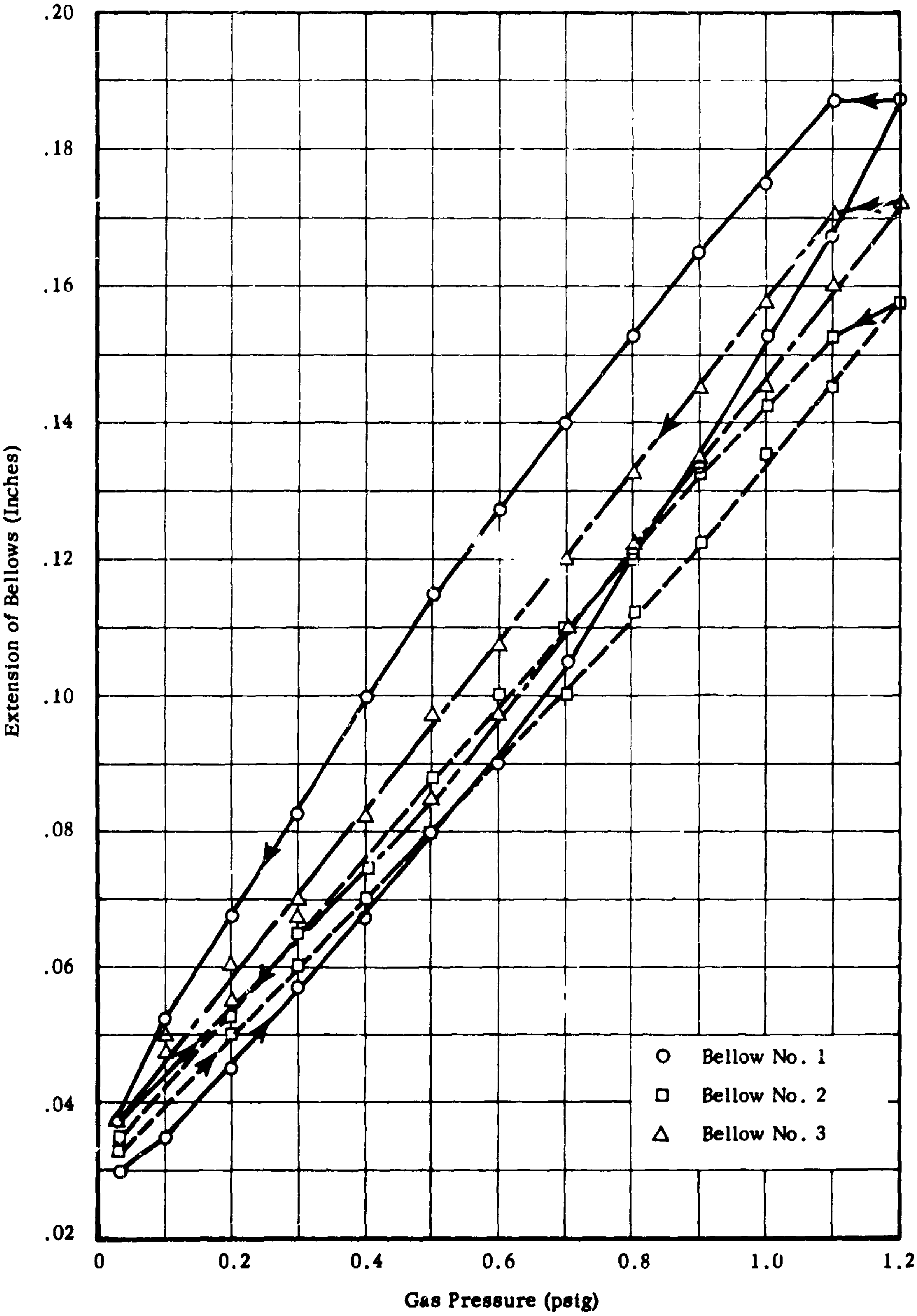

FIGURE II-9 APPLICATION OF GAS PRESSURE TO BELLOWS

D. DISCUSSION OF EXPERIMENTAL RESULTS

1. Description of Insulation Systems Tested

We investigated sixteen different insulation systems listed in Table II-2. Except systems No. 3 and 11 none of the systems were tested by us before (see appendix for a table listing all multi-layer insulation systems tested under Contracts Nos. NAS2-615, NAS5-664, and NAS3-4181).

Under this contract we were specifically searching for multi-layer insulation systems which show the lowest product of thermal conductivity and density; therefore, we tested insulations containing metal-coated plastic radiation shields only. To indicate possible improvements caused by spacer materials, we used standard radiation shields of 0.00025-inch thick polyester film coated with 400 Å thick layer of aluminum on both sides of the film.

To investigate the emissivity of various metal coatings on a plastic film we used our emissometer (see Section III). To correlate the emissometer data with our results we tested two systems, in one (#13) radiation shields were 0.00025-inch thick polyester film coated on both sides with 1700 to 3400 Å thick layer of gold, in another (#14) the shields were 0.0005-inch thick polyester film coated on both sides with 1000-2200 Å thick layer of silver.

To compare the performance of insulations, all tests were made on 10 radiation shield systems. Exceptions were systems Nos. 12, 15, and 16 where we tested systems with specific combinations to be used on a NASA tank.

2. Development of a New Spacer

a. Material Requirements

A suitable spacer material should be lightweight, a good thermal insulator and insensitive to compressive loads. The range of compressive loads to which multi-layer radiation shields may be exposed is 0-15 psi. In this range of compressive loads the heat flow through the insulation changes by almost two orders of magnitude, as shown by our experimental results.(1) Even compressive loads between 0.01 to 0.1 psi reduce drastically the insulating effectiveness of the multi-layer insulations. (See test No. 3037, Reference (1))

TABLF II-2 DESCRIPTION OF THE INSULATION SYSTEMS

System No.	Radiation Shield	Spacer material	Variable Investigated	Test No.	Component Supplier
1	1	Three--0.003" thick silk netting	Mech. compress.	3042	Jordan Marsh Co.
2	1	Two--0.003" thick silk netting	Mech. compress.	3071	Jordan Marsh Co.
3	1	One--0.020" thick 2 lb/ft^3 rigid polyurethane foam	Repeated mech. compression and penetrations	3040, 3043, 3054-68, 3070, 3078	Goodyear Co.
4	1	One--0.003" thick silk netting with Two--0.008" thick fiberglass paper	Mech. compress. and penetrations	3051, 3052 3079-3081	Jordan Marsh Co. Dexter & Sons, Inc.
5	1	One--0.003" thick silk netting with 0.004" thick x 1/2" wide glass paper strips on both sides of netting	Mech. compress.	3044	Jordan Marsh Co. Dexter & Sons, Inc.
6	1	One--0.003" thick silk netting with 0.008" thick x 1/2" wide glass paper strips and solid edge on both sides of net	Mech. compress.	3045	Jordan Marsh Co. Dexter & Sons, Inc.
7	1	One--0.003" thick silk netting with 0.008" thick x 1/4" wide glass paper strips on both sides of netting	Mech. compress.	3046	Jordan Marsh Co. Dexter & Sons, Inc.
8	4	One--0.003" thick silk netting with 0.008" thick x 1/4" dia. glass paper discs on both sides of netting, discs are all aligned	Mech. compress.	3049, 3050	Jordan Marsh Co. Dexter & Sons, Inc.
9	1	One--0.003" thick silk netting with 0.100" thick x 1/4" wide x 2" long flex. foam strips	Mech. compress.	3069	Jordan Marsh Co. Scott Paper Co.

TABLE II-2 cont'd

System No.	Radiation Shield	Spacer Material	Variable Investigated	Test No.	Component Supplier
10	1	One--0.003" thick silk netting with 0.100" thick x 1/4" wide x 2" long rigid foam strips	Mech. compress.	3073, 3074	
11	1	Two--0.001" thick glass fabric cloth	Mech. compress.	3041, 3047, 3048	
12	1	One-0.020" thick 2 lb/ft^3 polyurethane foam One-0.060" thick polyurethane foam cut to form grid 1/4" wide on 1-1/2" centers	Mech. compress.	3053, 3072	NASA
13	2	Two--0.003" thick silk netting	Mech. compress.	3077	Jordan Marsh Co. Hastings & Co., Inc.
14	3	One--0.003" thick silk netting with 0.100" thick x 1/4" wide x 2" long flex. foam strips	Mech. compress.	3075, 3076	Jordan Marsh Co. Gomar Manuf. Co.
15	1	15subassemblies each consisting of: 0.008" thick fiber glass mat, 0.030" thick polyurethane foam	Mech. compress.	3038, 3039	NASA
16	1	16subassemblies each consisting of: 0.025" thick 2 lb/ft^3 polyurethane foam	Repeated mech. compression	3082	NASA

Radiation Shields:

1. 0.00025" thick polyester film coated on both sides with 400 Å thick aluminum
2. 0.00025" thick polyester film, gold coated (1700-3400 Å) on both sides
3. 0.0005" thick polyester film, silver coated (1000-2200 Å) on both sides
4. 0.00025" thick polyester film coated on both sides with 400 Å thick aluminum and perforated with 0.047 dia. holes (1.88%)

These considerations dictated that we test all new insulation systems under compressive loadings from 0 to 15 psi, with special empahsis on the low compressive loads.

In order to minimize the effects of compressive loads an analytical model for the spacer was developed. Then a material for the spacer was selected based on analytical requir ments of the model.

b. Analytical Considerations

Heat transfer across an interface between two particles takes place by three different modes--thermal radiation, interstitial gas conduction, and particle-to-particle conduction. In the following discussion particle-to-particle conduction is considered to be controlling when (1) radiation has been reduced by the use of radiation shields to a small value which is constant for one insulation system and when (2) interstitial gas conduction is reduced to a small value by evacuation.

(1) Conduction Across Contact Areas

In analyses of particle-to-particle conduction the assumption has been made that two particles in contact can be represented by two shperes or two cylinders in contact with each other or a sphere or a cylinder in contact with a plane. It has been assumed that (1) the areas of contact are uniformly distributed over the entire apparent contact area, (2) the actual contact areas are all circular and of identical radius, (3) the asperities at the contact areas are deformed under a compressive load so that the average pressure exerted between the two surfaces is given by the hardness of the material, and (4) the surface film resistance between the particles can be neglected.

More recently, the view has been expressed that the uniform distribution of [illegible] al contact areas would exist only if the surfaces were perfectly flat and if they remain unchanged by compressive loading and the imposed thermal environment.[2] However, such ideal contacts do not exist in practice and large scale or macroscopic constrictions to heat flow are present. In fact, such constrictions may often dominate the thermal contact resistance

Experiments on friction and wear have indicated that multiple contacts are formed by elastic rather than plastic deformation.[3] In addition, the differential lateral thermal expansion between the surfaces which may result from temperature changes may be larger than the height of the asperities at the contact areas. An asperity may be plastically deformed at the first encounter with a mating surface; however, a subsequent lateral motion will increase the contact area so that the load may eventually be borne by elastic deformation.

In considering the heat transfer across an apparent contact area between two particles, two regions can be distinguished: the contact region and the non-contact region. In the non-contact region there are few or no microscopic contact areas. In the contact region there is a high density of micro-contacts. Therefore, the thermal contact resistance at an interface in the absence of an interstitial gas will consist of the macroscopic constriction resistance, the microscopic constriction resistance, and the surface film resistance. The flow of heat between two particles can be visualized to first be constricted by the large scale contact areas, then further constricted by the microscopic contacts within this area, and finally the heat will be forced to flow through any existing surface films. Therefore, the total contact resistance is given by the sum of these three individual resistances.

The macroscopic constriction resistance can be estimated by considering the classical problem of the determination of the contact area between t o elastic spheres pressed against each other under a mechanical load.[4] Thus, for a force F, the area of contact A_c is circular and proportional to the 2/3 power of the ratio of the force and Young's modulus of elasticity E.

$$A_c \sim \left(\frac{F}{E}\right)^{2/3} \qquad (1)$$

The same result is obtained when a sphere is pressed against a plane.

When two cylinders are pressed against each other, the contact area is elliptical and depends on F and E according to Equation 1. However, this result is not valid for all values of the angle formed by the axes of the two cylinders. When the cylinders are parallel, Equation 1 must be replaced by:

$$A_c \sim \left(\frac{F}{E}\right)^{1/2} \qquad (2)$$

Since Equation 1 cannot be converted to Equation 2 abruptly when the angle of the axes of the cylinders approaches zero, both 1 and 2 must be valid in different ranges of this angle. It is not clear what exactly these ranges are, but 1 is valid for angles close to 90 degrees while 2 is valid for angles close to zero degrees. Timoshenko[4] gives a table from which the proportionality constant in 1 can be computed for angles between 30 and 90 degrees only. This may mean that for angles smaller than 30 degrees Equation 1 is not valid and an expression such as Equation 2 should be used. Both of these formulae are applicable to multi-layer insulations with fibrous spacers because many fibers will be parallel rather than perpendicular to each other while in contact.

The microscopic constriction resistance will depend on the extent of the microscopic contact areas. The ratio of the macroscopic to microscopic constriction resistance can be calculated for a given material, geometry, and load when (1) the microhardness, elastic conformity modulus, and the radius of the macroscopic constriction region are known, and (2) it is assumed that the average size of the microscopic contact areas is of the same order of magnitude as the surface roughness. For several metals under relatively high loads, it has been shown that the macroscopic constriction resistance was approximately two orders of magnitude larger than the microscopic constriction resistance.[2] Hence, analyses which treat only one of these effects may be in error.

The disturbing effects of surface films on electrical contacts have been explored; however, their effect on thermal contact resistance is not clear.[5] In one instance, there was a considerable increase in thermal contact resistance with as much as 80% of the heat flow taking place across the interface surface film at pressures of 1μ

Hg.[6] However, the effect of relatively thin films on thermal contact resistance at low loads has not been established. The film resistance was generally neglected in many past investigations because most studies were limited to metallic surfaces with high contact pressures.

If there are surface films around microscopic contact areas, a quantum mechanical tunneling effect could provide a significant contribution to heat flow across small gaps, thereby causing an effective enlargement of the microscopic contact area.[5] The possible presence of cryopumped surface films of comparable thicknesses on liquid hydrogen tank thermal insulations could mean that the heat flow through such films could be of importance even in a vacuum environment.

The limited understanding of the behavior of the surface films and their properties under applied loads makes a theoretical estimate of their importance to thermal contact resistance between particles difficult. Because of this insufficient knowledge, the various derivations for the solid conduction contribution may be inadequate in predicting the effects of small compressive loads on the heat flow through multi-layer insulations. Therefore, it may be easier at this time to assess the overall effects experimentally while at the same time using the knowledge that does exist to guide the selection of promising spacer materials.

(2) Correlation of Experimental Results

The test results on effects of compressive loads are presented in the following sections and in Figures II-10 and II-14.

After we plotted the experimental results on logarithmic graph paper, it was apparent that all of the data could be fitted by straight lines. Moreover, the slopes of these lines lie between 0.44 and 2/3. This means that for the samples tested, the heat flow is proportional to a power between 0.44 and 2/3 of the compressive load.

If the heat flow is assumed to be proportional to the contact area between the individual components of the spacers and the dependence of the contact area on compressive load can be described by the Hertzian relation, then the heat flow should indeed be proportional to a power of about 2/3 or 1/2 of the compressive load. This result indicates that the macroscopic constriction resistance dominates the solid particle conduction resistance. The predominance of contact resistance indicates that its effects cannot be ignored in theoretical treatments of conduction through multi-layer insulations.

c. Single Material Spacers

We investigated three single materials for spacers: 0.020-inch thick, 2 lb/ft^3 density polyurethane foam (System 3, Test No. 3040), 0.001-inch thick fiber glass cloth (we used two sheets for each spacer, (System 11, Test No. 3041), and 0.003-inch thick, 14 x 14 mesh silk netting (we used three sheets for each spacer in System 1, Test No. 3C42 and two sheets for each spacer in System 2, Test No. 3071). We subjected the samples to external compression between 0 and 15 psi with the low load attachment of the thermal conductivity apparatus. The results of the test are presented in Tables II-3 through II-6. Figure II-10 shows the dependence of the heat flux on compressive loads for all four samples. For reference we show the theoretical curves representing the 1/2 and 2/3 powers of the external compression and results of the Test No. 3037 which was completed under Contract NAS3-4181 last year.

From Figure II-10 we observe that the slopes of the four curves fall between the slopes of the curve representing the 0.63 and 0.45 powers of the external compression on the sample.

Compared with the other samples, No. 3040 showed the lowest heat fluxes for every external compression setting tested. Sample No. 3041 is the thinnest sample tested, and it has the smallest resistance to heat flow. The four newly tested samples have ten radiation shields made from aluminized polyester films; therefore, we can assume that the radiation heat transfer is approximately the same for those samples. We conclude that the 0.020-inch thick foam spacer is the most efficient separator for radiation shields.

At the left lower corner of the figure we marked with a segment of a horizontal line the level of the heat flux when no external

TABLE II-3 EFFECT OF COMPRESSIVE LOAD ON THE HEAT LOSS THROUGH A FOAM SPACED MULTILAYER INSULATION

Sample No. 3040 (former 1070), System 3.

Sample Description: Ten radiation shields of 0.00025" thick x 10-1/2" diameter polyester film, aluminum coated on both sides and eleven spacers of 2.0 lb/ft^3 freon blown polyurethane foam 0.02" thick x 12" diameter.

Sample Weight: 0.0474 lb

Sample Chamber Pressure: Less than 5×10^{-5} torr

Warm Plate Emittance: 0.9

Cold Plate Emittance: 0.9

Warm Plate Temperature: $43 \pm 2^{\circ}F$

Cold Plate Temperature: $-320^{\circ}F$

Mechanical Compression on Sample psi	Sample Density lb/ft^3	Heat Flux $Btu/hr\ ft^2$	Thermal Conductivity $Btu\text{-}in/hr\ ft^2\ {}^{\circ}F$	Sample Thickness in	Test Date	Test No.
0	1.39	0.20	0.33×10^{-3}	0.595	4/15/65	a
0	1.44	0.06	0.096×10^{-3}	0.576	4/15/65	b
0.011	1.69	0.36	0.49×10^{-3}	0.488	4/16/65	c
0.22	2.14	1.00	1.07×10^{-3}	0.385	4/16/65	d
1.0	2.63	3.77	3.30×10^{-3}	0.314	4/16/65	e
10.3	3.03	9.00	6.80×10^{-3}	0.273	4/16/65	f

TABLE II-4 EFFECT OF COMPRESSIVE LOAD ON THE HEAT FLUX THROUGH A GLASS FABRIC SPACED MULTILAYER INSULATION

Sample No. 3041, System 11.

Sample Description: Ten 0.00025" thick x 11" diameter polyester film radiation shields, aluminum coated on both sides
Twenty-one 0.001" thick x 12" diameter glass fabric spacers

Sample Weight: 0.076 lb

Sample Chamber Pressure: Less than 5×10^{-5} torr

Warm Plate Emittance: 0.9

Cold Plate Emittance: 0.9

Warm Plate Temperature: $40 \pm 2^{\circ}F$

Cold Plate Temperature: $-320^{\circ}F$

Mechanical Compression psi	Sample Density lb/ft^3	Heat Flux $Btu/hr\ ft^2$	Thermal Conductivity $Btu\text{-}in/hr\ ft^2\ {}^{\circ}F$	Sample Thickness in	Test Date	Test No.
0.011*	11.4	0.44	0.13×10^{-3}	0.11	5/ 5/65	a
0.10	25.2	6.6	0.9×10^{-3}	0.050	5/ 6/65	b
1.0	33.1	32	3.3×10^{-3}	0.038	5/ 6/65	c
14.2	48.3	126	9.3×10^{-3}	0.026	5/ 6/65	d
0	10.5	0.57	--	0.12	5/ 7/65	e
0	9.65	0.35	0.13×10^{-3}	0.13	5/ 7/65	f
0	9.65	0.35	0.13×10^{-3}	0.13	5/11/65	g

*This run was made before the sensitivity of the low compressive load device was improved; we believe that the external compression on the sample was lower than the reading indicated.

TABLE II-5 EFFECT OF COMPRESSIVE LOAD ON THE HEAT LOSS THROUGH A MULTILAYER INSULATION WITH THREE SILK NETTINGS FOR EACH SPACER

Sample No. 3042, System 1.

Sample Description: Ten 0.00025" thick x 11" diameter polyester film radiation shields, aluminum coated on both sides
Thirty-three 0.003" thick x 12" diameter silk netting

Sample Weight: 0.041 lb

Sample Chamber Pressure: Below 5×10^{-5} torr

Warm Plate Emittance: 0.9

Cold Plate Emittance: 0.9

Warm Plate Temperature: $70 \pm 5^{\circ}F$

Cold Plate Temperature: $-320^{\circ}F$

Mechanical Compression psi	Sample Density lb/ft^3	Heat Flux $Btu/hr\ ft^2$	Thermal Conductivity $Btu\text{-}in/hr\ ft^2\ {}^{\circ}F$	Sample Thickness in	Test Date	Test No.
0	1.62	0.285	0.36×10^{-3}	0.42	5/15/65	a
0	1.39	0.20	0.25×10^{-3}	0.49	5/18/65	b
0.01	3.25	0.57	0.30×10^{-3}	0.21	5/18/65	c
0.11	4.26	1.25	0.51×10^{-3}	0.16	5/18/65	d
1.0	4.87	3.35	1.2×10^{-3}	0.14	5/18/65	e
15.6	15.8	16.25	1.8×10^{-3}	0.043	5/19/65	f
1.0	3.59	4.6	2.2×10^{-3}	0.19	5/19/65	g
0.11	2.96	1.7	1.0×10^{-3}	0.23	5/19/65	h
0.01	2.62	0.71	0.47×10^{-3}	0.26	5/19/65	i

TABLE II-6 EFFECT OF REPEATED COMPRESSIVE LOADS ON THE HEAT LOSS THROUGH A MULTILAYER INSULATION WITH TWO SILK NETTINGS FOR EACH SPACER

Sample No. 3071, System 2.

Sample Description: Ten radiation shields of 0.00025" thick x 11" diameter polyester film, aluminum coated on both sides and twenty-two 12" diameter, 0.003" thick silk netting

Sample Weight: 0.031 lb

Sample Chamber Pressure: Below 5×10^{-5} torr

Warm and Cold Plate Emittance: 0.9

Warm Plate Temperature: $71 \pm 3^{\circ}$F

Cold Plate Temperature: -320°F

Mechanical Compression psi	Sample Density lb/ft^3	Heat Flux $Btu/hr\ ft^2$	Thermal Conductivity $Btu\text{-}in/Hr\ ft^2\ {}^{\circ}F$	Sample Thickness in	Test Date	Test No.
0	0.75	0.32	0.55×10^{-3}	0.682	12/22/65	a
0.01	2.5	0.56	0.29×10^{-3}	0.205	12/28/65	b
0.1	4.0	1.4	0.48×10^{-3}	0.130	12/29/65	c
1.0	9.0	6.9	0.89×10^{-3}	0.057	12/29/65	d
15	11.7	37	4.2×10^{-3}	0.044	12/30/65	f
1.0	10	8.8	2.4×10^{-3}	0.051	12/30/65	g
0.1	5.4	1.8	0.44×10^{-3}	0.095	12/30/65	h
0.01	3.3	0.61	0.24×10^{-3}	0.154	12/31/65	i
0	1.4	0.31	0.30×10^{-3}	0.369	1/ 1/66	j

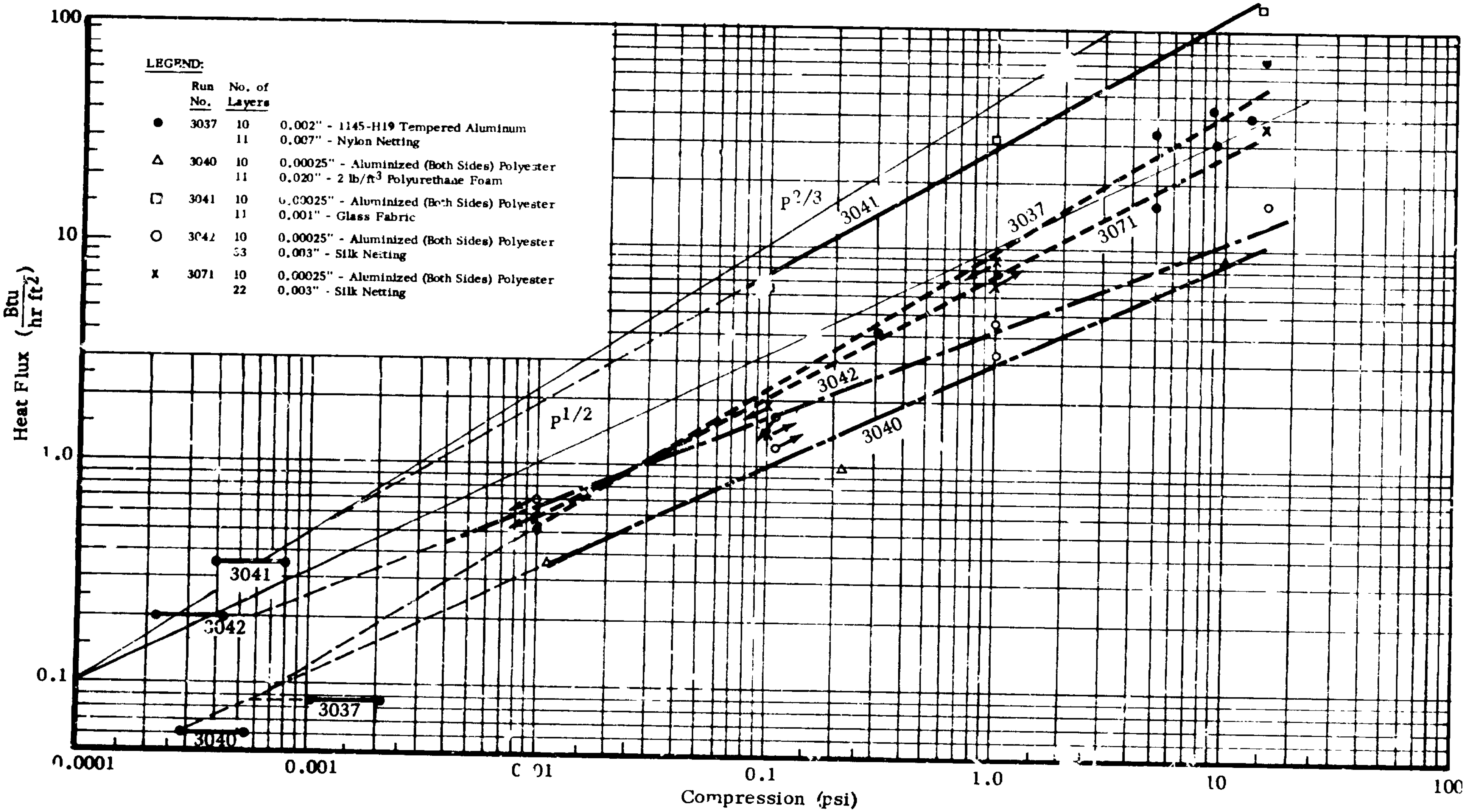

FIGURE II-10 EFFECT OF A COMPRESSIVE LOAD ON THE HEAT FLUX THROUGH MULTI-LAYER INSULATIONS WITH SINGLE MATERIAL SPACERS compression was applied to the samples. The segment ends are located relative to the vertical axis so that the right end point marks the ratio (in psi) of total sample weight to the sample area, i.e., the compression applied to the lowest surface of the sample by the weight of the sample. Similarly, the left end point of the segment marks one-half of the same ratio, i.e., the mean compression applied to the sample by its own weight.

Extending the curves in Figure II-10 to the heat flux levels corresponding to no external compression, we find that the intersections of these two lines fall in four cases (except sample 3071) near the marked segments.

We conclude:

(1) The mean compression applied by weight of the sample is between 0.0002 and 0.001 psi.

(2) At no exte nal compression the weight of the sample puts the lower limit on the heat flux through the sample.

The weight of the insulation plays an important part in the final selection of the insulation. To compare the insulations on the basis of the thermal performance and weight the product of heat flux and weight (per unit area) as a function of external compression is shown in Figure II-11. This figure shows that, if both the weight and thermal performance of the insulation are considered, sample Nos. 3040, 3042 and 3071 are approximately equal. Sample No. 3040 performs better at low compression and worse at higher compression than do samples No. 3042. The same can be siad about sample Nos. 3037 and 3041. However, the performance of sample Nos. 3040, 3042 and 3071 is significantly better than that of sample Nos. 3037 and 3041.

Note that test No. 3040 was performed on the sample supplied to us by NASA. It was previously tested at NASA Lewis Research Center during the test No. 1070.

A similar sample was tested by us in 1965 (No. 1064, see Reference (1)). Comparing the two samples, we observe that at zero external compressive load the heat flux passing through sample No. 1064 was about twice that for

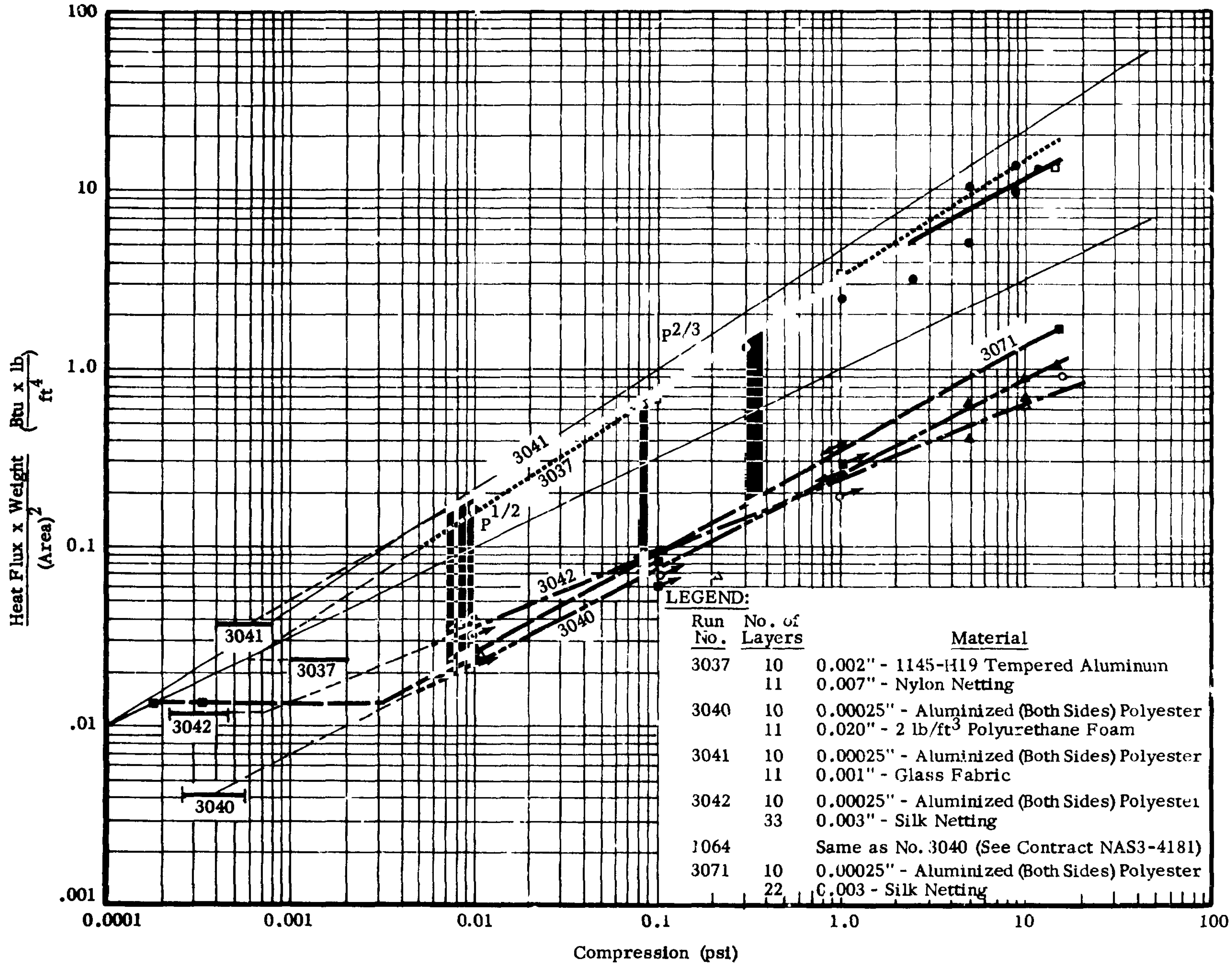

FIGURE II-11 EFFECT OF EXTERNAL COMPRESSION ON THE PRODUCT OF HEAT FLUX AND SAMPLE WEIGHT PER UNIT AREA sample No. 3040. Also, sample No. 1064 was 0.685 inch thick compared with 0.576 inch for the optimum setting in test No. 3040. We believe that variation in handling of the samples before the test may have produced such differences. The control sample (No. 3040) was kept flat for several weeks in the shipping container before it was installed in the apparatus.

In tests Nos. 3042 and 3071 (System 1 and 2) both samples have an identical spacer material: 0.003-inch thick silk netting; however, in sample No. 3042 three layers of netting were used to each spacer while only two layers of the same netting were used for each spacer in sample No. 3071. In Figure II-10 we observe that at 0.01 psi compression the heat flux is nearly the same for both samples; however, the slope of the curve for sample No. 3071 is higher than for sample No. 3042. The heat flux through sample No. 3071 is double that through sample No. 3042 at 15 psi compression.

Since the heat flux is nearly the same at compression below 0.1 psi for both insulations the product of heat flux and weight is smaller for sample No. 3071 at these compressions. This would indicate that an insulation similar to System 2 is preferable when compressive loads due only to application and insulation weight are expected.

d. Multi-Material Spacer

(1) General

After considering various single spacer materials, we came to the conclusion that it is difficult to find a material which has the following properties desired in a spacer:

(a) Acceptable low thermal conductivity;

(b) Light weight;

(c) Dimensional stability coupled with an acceptable tensile strength for ease of application;

(d) Acceptable compressive load carrying characteristics.

Table II-7 compares better performing single spacer materials which we have tested. We found that silk netting is by far the lightest spacer. Dimensional stability and the tensile strength of

TABLE II-7 COMPARISON OF VARIOUS SPACER MATERIALS

Spacer Material	Thickness in	Weight lb/ft^2	Dimensional Stability	Tensile Strength
Foam	0.020	3.3×10^{-3}	Good	Poor
Glass Paper	0.03	10.9×10^{-3}	Fair	Poor
Glass Paper	0.04	6.1×10^{-3}	Fair	Poor
Crinkled Polyester Film	0.00025	1.5×10^{-3}	Poor	Excellent
Glass Fabric	0.0020	3.8×10^{-3}	Poor	Poor
Silk Netting	0.0035	1.2×10^{-3}	Good	Good

the netting are good; however, the performance of a 10 shield sample was poor even when 3 nettings per one spacer were used (System 1, Sample No. 3042) compared to a multi-layer insulation with foam spacers (see Figure II-10).

A foam spacer has low tensile strength and is relatively heavy, but the thermal conductivity of the foam is low. The foam spacer can sustain a moderate compressive load.

Because no single spacer material has the desired characteristics we decided to combine two or more materials into one spacer system. Each material in the system was selected to perform a specific function. For example, a light strong material such as silk netting can be used to give the system dimensional stability and tensile strength required for handling during application of the insulation; foam which has desirable thermal properties can be attached to the netting to give the system superior thermal properties. To reduce the weight of the system, foam in the form of strips or disks with a selected ratio of the total to open area can be assembled with the netting.

(2) Silk Netting and Glass Paper System

Since the foam was not immediately available, we used glass paper instead of foam for the first series of tests. We tested samples of ten 0.00025-inch thick aluminized (on both sides) polyester film shields with the following systems as spacers:

(a) 0.004-inch thick, 1/2-inch wide strips of glass paper sewed on 1 1/2-inch centers to both sides of a 12-inch diameter silk netting (Sample No. 3044).

(b) 12-inch diameter silk netting placed between two layers of 0.008-inch thick glass paper cut to a configuration shown in Figure II-12 (Sample No. 3045).

(c) 0.008-inch thick, 1/4-inch wide strips of glass paper sewed on 1 1/2-inch centers to both sides of a 12-inch diameter silk netting (Sample No. 3046).

In assembling the above-described samples, we placed even numbered spacers with strips at right angle to the strips on all odd numbered spacers.

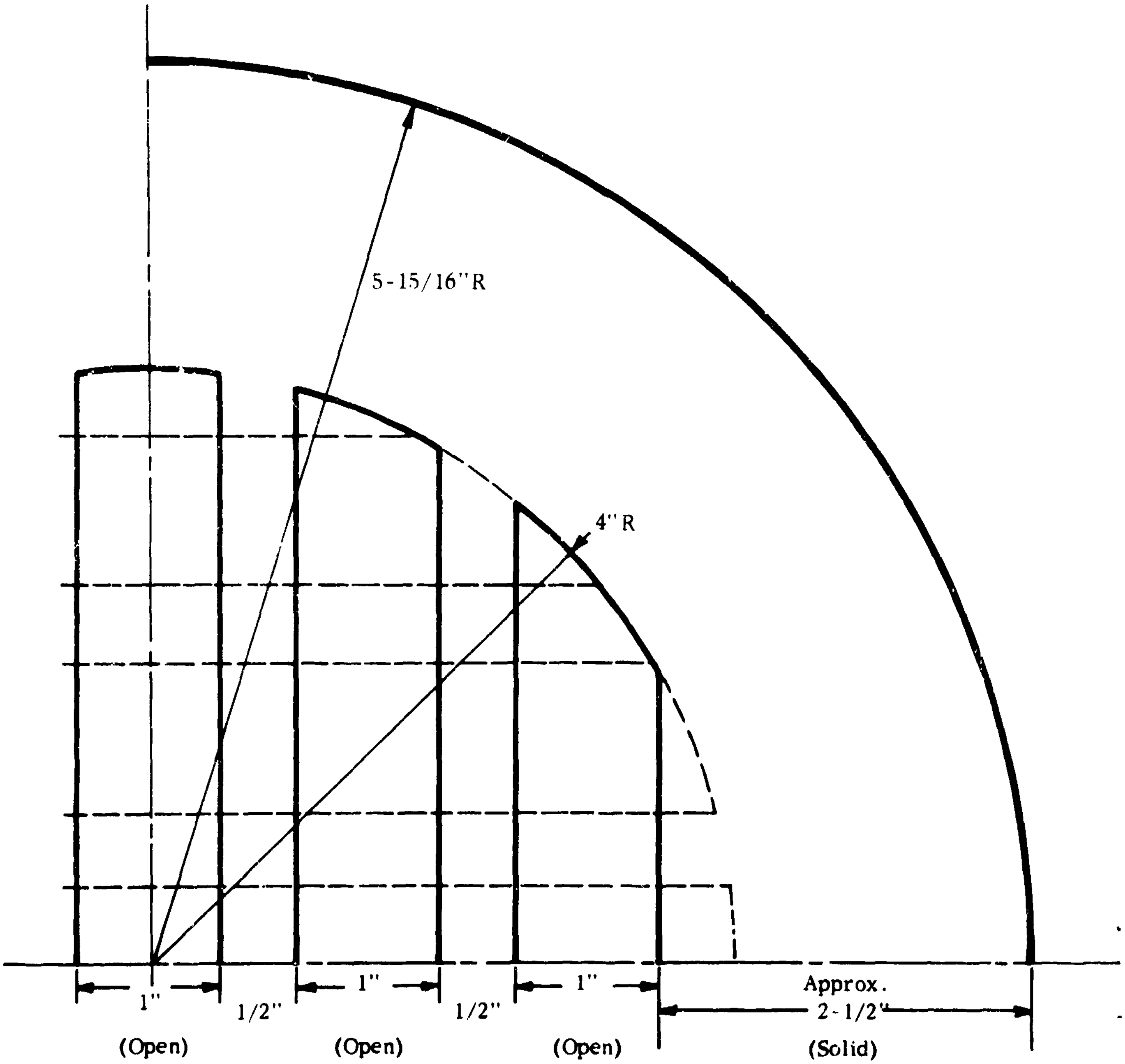

FIGURE II-12 CONFIGURATION OF GLASS MAT SPACER IN SAMPLE NO. 3045

(d) 0.008-inch thick by 9/32-inch diameter disks of glass paper placed on 1 1/2-inch centers on both sides of the silk netting. 0.006-inch diameter thread held the stacked disks together (Sample No. 3049, Figure II-13). Sample No. 3050 is identical to Sample No. 3049 with the thread removed.

(e) Two 0.008-inch thick, 12-inch diameter disks of glass paper placed on both sides of the 12-inch diameter silk netting (Sample No. 3051).

Tables II-8 through II-13 and Figures II-14 and II-16 show the results of tests. The relatively high heat fluxes through Sample No. 3044 (Table II-8) were at first attributed to the use of a thin spacer (0.011-inch theoretical thickness), and to the absence of a well defined buffer zone around the sample edge. Therefore, we prepared Sample No. 3045 using a glass paper of a double thickness (0.008-inch) cut to a configuration shown in Figure II-12. We used spacers of the same shape before (Samples No. 3027 and 3028, Reference (7)) achieving acceptable results. This configuration provided a 2-inch wide buffer zone with 1/2-inch side strips of glass paper spaced on 1 1/2-inch centers inside an 8-inch diameter central part of the sample. Table II-9 shows the results of tests. At zero external compressive load both samples (Nos. 3044 and 3045) show approximately the same heat flux; however, at 15 psi external compression heat flow through Sample No. 3045 is less than the heat flow through Sample No. 3044.

Note that the load distribution in Sample No. 3045 is different than that in Sample No. 3044. A large portion of the load is carried by the 2-inch wide buffer zone; therefore, effective compression on the inner part located under measuring vessel is reduced. Calculations show that when the sample is exposed to a 1425 lb load which corresponds to 15 psi mean compression on the sample, the effective compression on the portion of the sample under measuring vessel is only 3.15 psi.

Since at zero external compression no improvement was achieved with Sample No. 3045 which incorporated a wide buffer zone, we decided that the buffer zone rendered by a simple continuation of the spacer was sufficient.

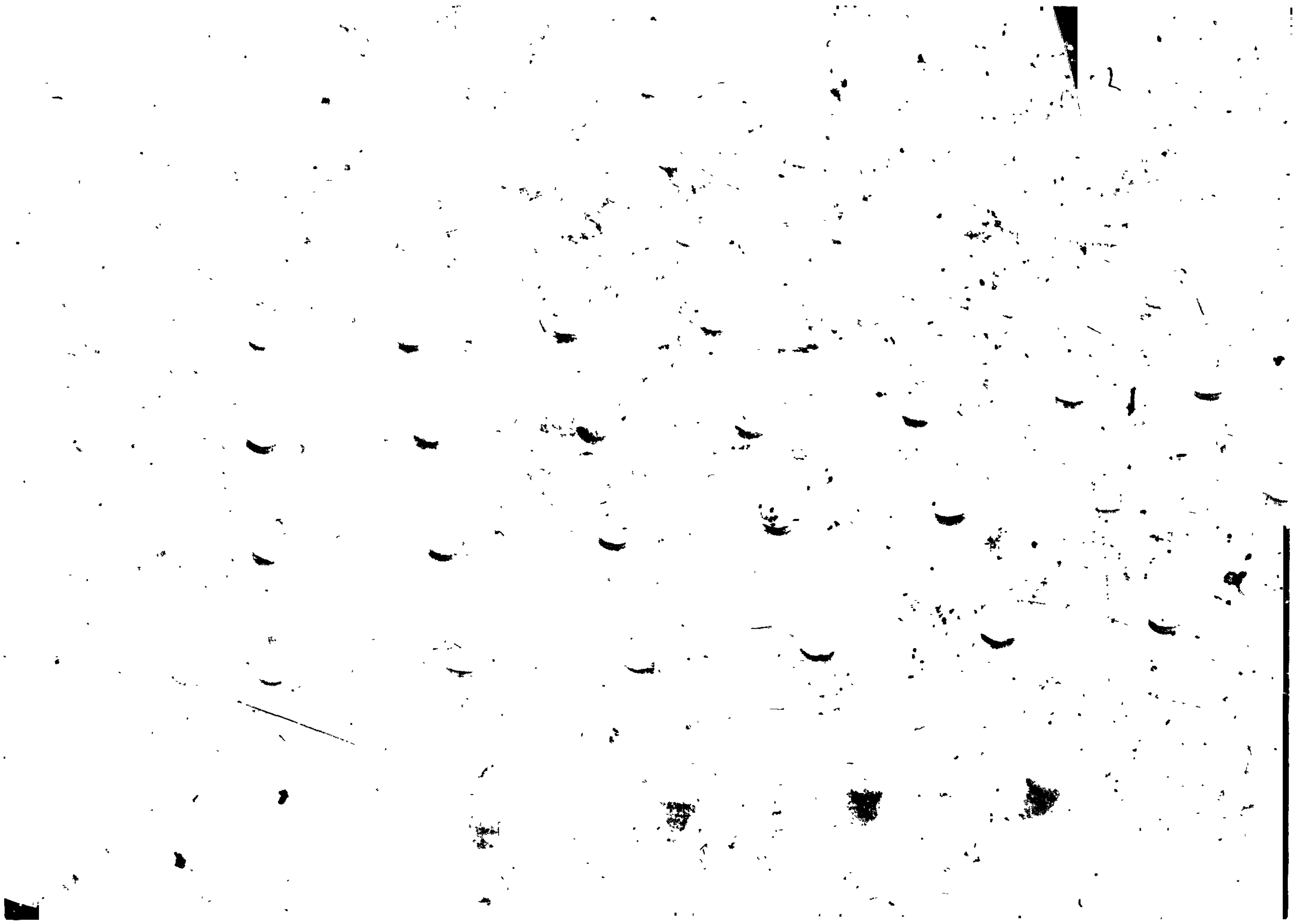

FIGURE II-13 SAMPLE NO. 3049 WITH COMPOSITE MATERIAL SPACER

TABLE II-8 EFFECT OF COMPRESSIVE LOADS ON THE HEAT LOSS THROUGH A MULTILAYER INSULATION WITH TWO-MATERIAL SPACER

Sample No. 3044, System 5.

Sample Description: Ten radiation shields of 0.00025" thick x 11" diameter polyester film, aluminum coated on both sides and eleven 12" diameter, 0.003" thick silk nettings with 0.004" thick x 1/2" wide glass paper strips sewed on both sides of silk netting 1" apart

Sample Weight: 0.058 lb

Sample Chamber Pressure: Less than 2×10^{-5} torr

Warm and Cold Plate Emittance: 0.9

Warm Plate Temperature: $70^{\circ} \pm 3^{\circ}F$

Cold Plate Temperature: $-320^{\circ}F$

Mechanical Compression psi	Sample Density lb/ft^3	Heat Flux $Btu/hr\ ft^2$	Thermal Conductivity $Btu\text{-}in/hr\ ft^2\ {}^{\circ}F$	Sample Thickness in	Test Date	Test No.
0	1.73	0.304	0.42×10^{-3}	0.536	6/15/65	a
0.005	3.22	0.600	0.44×10^{-3}	0.288	6/16/65	b
0.01	3.41	1.20	0.83×10^{-3}	0.271	6/17/65	c
0.1	4.86	2.10	1.0×10^{-3}	0.190	6/17/65	d
1.0	7.33	7.17	2.3×10^{-3}	0.126	6/17/65	e
7.0	9.50	13.15	3.3×10^{-3}	0.097	6/17/65	f
15.0	13.00	22.7	4.1×10^{-3}	0.071	6/17/65	g
7.0	10.20	16.2	3.7×10^{-3}	0.090	6/17/65	h
2.5	-	10.5	-	-	6/17/65	j
1.0	8.50	7.76	2.2×10^{-3}	0.109	6/18/65	k
0.1	5.55	2.22	0.95×10^{-3}	0.167	6/18/65	l
0.01	4.00	0.770	0.46×10^{-3}	0.231	6/18/65	m
0.005	3.60	0.655	0.43×10^{-3}	0.256	6/18/65	n
0.001	3.21	0.486	0.36×10^{-3}	0.288	6/18/65	o
0	1.44	0.300	0.49×10^{-3}	0.645	6/18/65	p

TABLE II-9 EFFECT OF COMPRESSIVE LOADS ON THE HEAT LOSS THROUGH A MULTILAYER INSULATION WITH TWO-MATERIAL SPACER

Sample No. 3045, System 6.

Sample Description: Ten radiation shields of 0.00025" thick x 11" diameter polyester film, aluminum coated on both sides and eleven 12" diameter 0.003" thick silk nettings with 0.010" thick glass paper sewed on both sides of silk netting

Sample Weight: 0.153 lb

Sample Chamber Pressure: Less than 2×10^{-5} torr

Warm and Cold Plate Emittance: 0.9

Warm Plate Temperature: $7.2 \pm 4^{\circ}F$

Cold Plate Temperature: $-320^{\circ}F$

Mechanical Compression psi	Sample Density lb/ft^3	Heat Flux $Btu/hr\ ft^2$	Thermal Conductivity $Btu\text{-}in/hr\ ft^2\ ^{\circ}F$	Sample Thickness in	Test Date	Test No.
0	1.55	0.458	-	0.677	6/28/65	b
0	1.49	0.280	0.50×10^{-3}	0.705	6/29/65	c
0.01	1.96	0.972	1.3×10^{-3}	0.536	6/30/65	d
0.1	2.32	1.71	2.0×10^{-3}	0.453	6/30/65	e
1.0	3.00	2.80	2.4×10^{-3}	0.338	6/30/65	f
15.0	4.55	6.34	3.7×10^{-3}	0.231	6/30/65	g
1.0	3.17	2.64	2.2×10^{-3}	0.331	6/30/65	h
0.1	2.64	1.60	1.6×10^{-3}	0.398	6/30/65	i
0.01	2.11	0.764	0.97×10^{-3}	0.498	7/ 1/65	j
0	1.62	0.321	0.53×10^{-3}	0.650	7/ 1/65	k

We tested sample No. 3046 which had a construction identical to that of sample No. 3044, except that the strips were made from a glass paper of double thickness and 1/2 the width of the strips used in sample No. 3044. The weight of both samples was approximately the same, but the theoretical thickness of sample No. 3046 was almost double that of sample No. 3044. Under test the true thickness of sample No. 3046 was only 20 to 40% greater than that of sample No. 3044 at the corresponding - ompressions.

Table II-10 presents the test results for sample No. 3046. The results are plotted in Figure II-14. An increase in the sample thickness and a decrease in the macroscopic contact area (due to a decrease in the strip width) resulted in lower heat fluxes through sample No. 3046 compared to those through sample No. 3044 for the corresponding values of compressive loads.

Strips of a load carrying material were a convenient way to reduce the contact area and the weight of the glass mat decreasing the total weight of the sample. Further reduction in the weight of the sample can be achieved by removing the parts of the strips which do not carry load. At low compression the load is supported only in the areas where two strips of the neighboring spacers are crossing each other. Removal of the portion of the strips not loaded heaves a configuration where separate squares (or circles) are attached to both sides of the silk netting.

At the initial stages of the assembly, we attempted to use unperforated radiation shields for sample No. 3049; however, we found it difficult to maintain the shields crinkle free when the latter were placed over assembly pins. By using perforated shields the assembly difficulty was eliminated, but the heat flux was high partially due to perforations in the shields as we will discuss in section II-D-7b. The sample was assembled on a series of needles fastened in a styrofoam block as shown in Fgiure II-15. Table II-11 presents the test results for sample No. 3049. The results are plotted in Figure II-14. The heat flux through the sample exposed to zero external compression is 0.65 Btu/hr ft^2 or approximately 3 times higher

TABLE II-10 EFFECT OF REPEATED APPLICATION OF COMPRESSIVE LOADS ON THE HEAT LOSS THROUGH A MULTILAYER INSULATION WITH TWO-MATERIAL SPACER

Sample No. 3046 , System 7.

Sample Description: Ten radiation shields of 0.00025" thick x 11" diameter polyester film, aluminum coated on both sides and eleven 12" diameter, 0.003" thick silk nettings with 0.008" thick x 1/4" wide glass paper strips sewed on both sides of silk netting 1-1/4" apart

Sample Weight: 0.061 lb

Sample Chamber Pressure: Less than 1×10^{-5} torr

Warm and Cold Plate Emittance: 0.9

Warm Plate Temperature: $70^{o} \pm 2^{o}F$

Cold Plate Temperature: $-320^{o}F$

Mechanical Compression psi	Sample Density lb/ft^3	Heat Flux $Btu/hr\ ft^2$	Thermal Conductivity $Btu\text{-}in/hr\ ft^2\ {}^oF$	Sample Thickness in	Test Date	Test No.
0	1.4	0.219	0.38×10^{-3}	0.675	7/ 7/65	b
0.01	2.3	0.322	0.36×10^{-3}	0.411	7/ 9/65	d
0.1	3.3	1.065	0.79×10^{-3}	0.288	7/ 9/65	e
1.0	3.8	5.070	3.3×10^{-3}	0.254	7/ 9/65	f
15	11.3	18.68	4.1×10^{-3}	0.085	7/ 9/65	g
1.0	6.7	6.35	2.4×10^{-3}	0.146	7/ 9/65	h
0.1	5.5	2.97	1.3×10^{-3}	0.174	7/ 9/65	i
0.01	4.8	1.88	0.94×10^{-3}	0.199	7/ 9/65	j
0	1.9	0.183	0.20×10^{-3}	0.510	7/10/65	k
0	1.9	0.189	0.25×10^{-3}	0.513	7/12/65	l
0.01	3.0	0.436	0.36×10^{-3}	0.317	7/12/65	m
0.1	4.2	1.40	0.82×10^{-3}	0.228	7/13/65	n

TABLE II-10 (contd)

Mechanical Compression psi	Sample Density lb/ft^3	Heat Flux $Btu/hr\ ft^2$	Thermal Conductivity $Btu\text{-}in/hr\ ft^2\ {}^oF$	Sample Thickness in	Test Date	Test No.
1.0	7.2	6.44	2.2×10^{-3}	0.134	7/13/65	o
15	12.3	19.35	3.9×10^{-3}	0.078	7/13/65	p
1.0	8.0	7.42	2.3×10^{-3}	0.121	7/13/65	r
0.1	5.5	2.80	1.3×10^{-3}	0.176	7/13/65	s
0.01	3.2	0.564	0.44×10^{-3}	0.300	7/13/65	t
0	2.5	0.148	0.14×10^{-3}	0.379	7/14/65	u
0.01	3.0	0.372	0.25×10^{-3}	0.315	7/14/65	v
1.0	4.7	5.60	2.9×10^{-3}	0.204	7/14/65	w
15	12.3	20.75	4.2×10^{-3}	0.078	7/14/65	x
0.01	3.1	0.493	0.39×10^{-3}	0.306	7/15/65	y

Compression was released to 0 before 0.1 psi was applied.

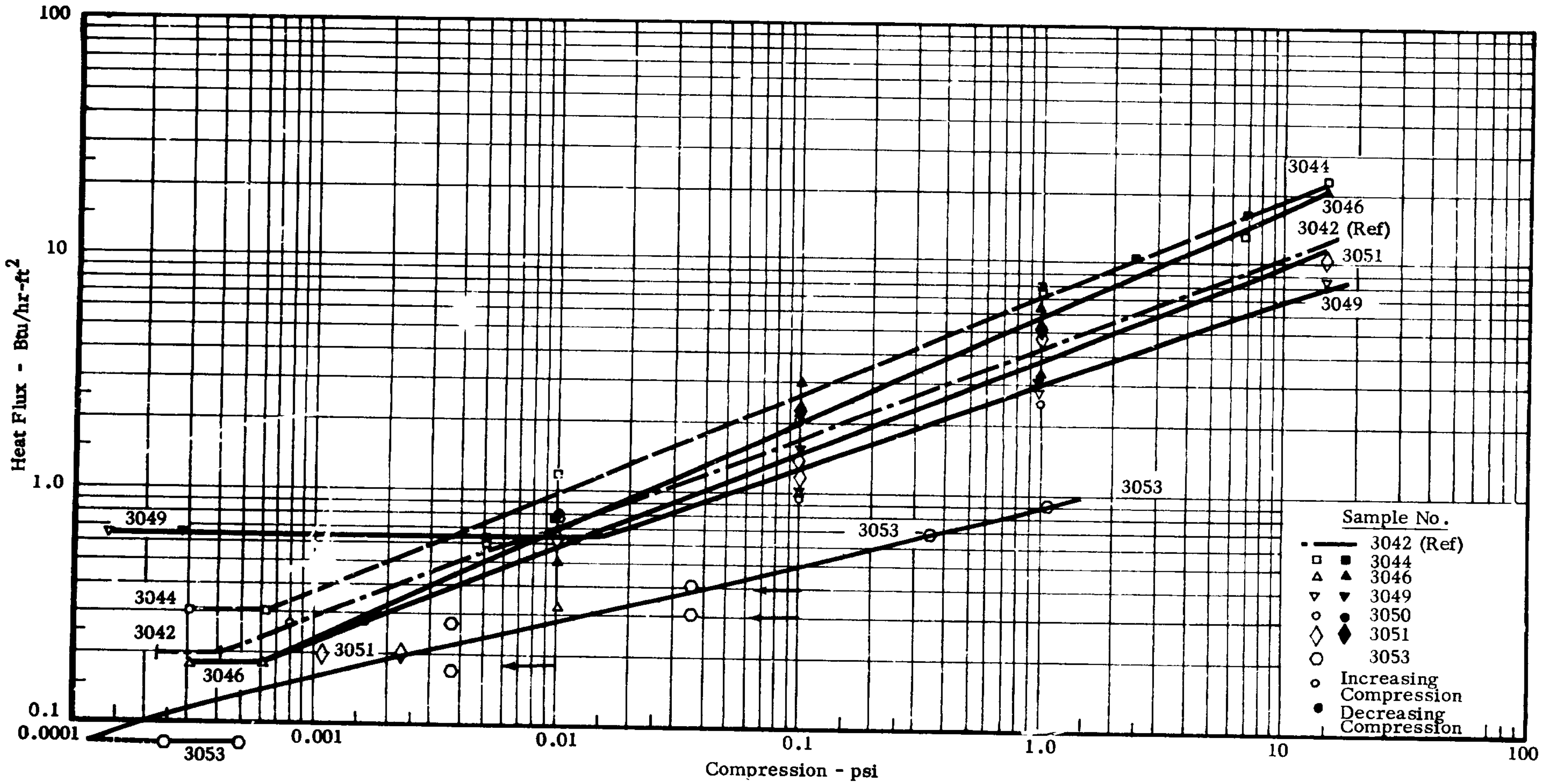

FIGURE II-14 THERMAL PERFORMANCE OF VARIOUS MULTI-LAYER INSULATIONS UNDER COMPRESSIVE LOADS

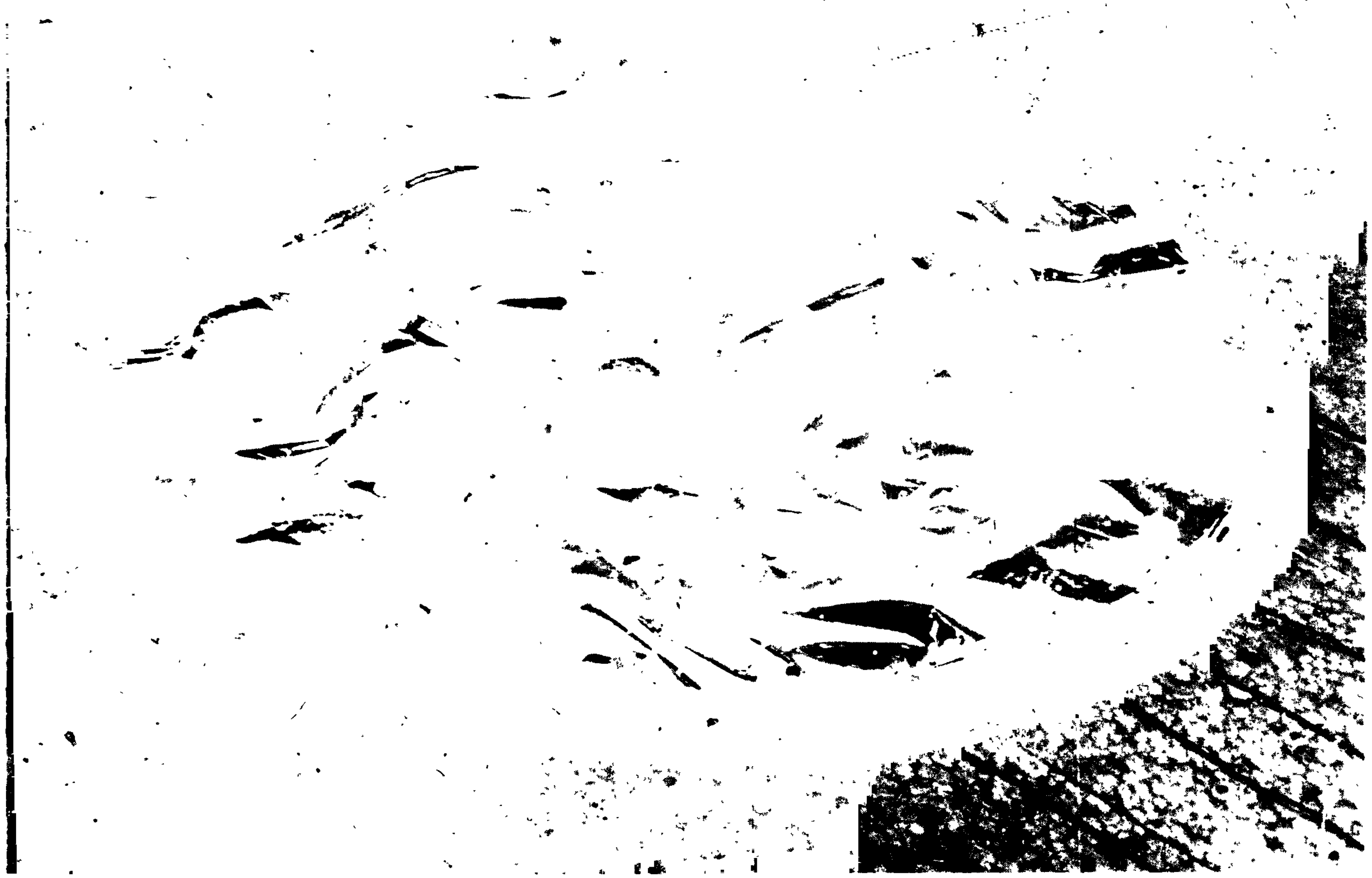

FIGURE II-15 ASSEMBLY OF SAMPLE NO. 3049

TABLE II-11 EFFECT OF COMPRESSIVE LOAD ON THE HEAT LOSS THROUGH A MULTILAYER INSULATION WITH TWO-MATERIAL SPACER

Sample No. 3049, System 8.

Sample Description: Ten radiation shields of 0.00025" thick x 11" diameter perforated polyester film, aluminum coated on both sides and eleven 12" diameter, 0.003" thick silk nettings with 1/4" diameter x 0.008" thick glass paper disks sewed on both sides of silk netting on 1-1/2" centers with 0.006" diameter thread

Sample Weight: 0.027 lb

Sample Chamber Pressure: Less than 1×10^{-5} torr

Warm and Cold Plate Emittance: 0.9

Warm Plate Temperature: $70 \pm 4^{o}F$

Cold Plate Temperature: $-320^{o}F$

Mechanical Compression psi	Sample Density lb/ft^3	Heat Flux $Btu/hr\ ft^2$	Thermal Conductivity $Btu\text{-}in/hr\ ft^2\ ^{o}F$	Sample Thickness in	Test Date	Test No.
0	0.81	0.658	0.96×10^{-3}	0.551	8/5/65	a
0.01	1.0	0.790	0.89×10^{-3}	0.440	8/6/65	b
0.10	1.6	1.05	0.83×10^{-3}	0.309	8/6/65	c
1.0	2.6	2.68	1.21×10^{-3}	0.176	8/6/65	d
15.0	6.1	7.85	1.48×10^{-3}	0.074	8/6/65	e
1.0	3.6	3.04	0.98×10^{-3}	0.126	8/6/65	f
0.1	2.3	1.48	0.75×10^{-3}	0.196	8/6/65	g
0	1.1	0.742	0.77×10^{-3}	0.406	8/6/65	h

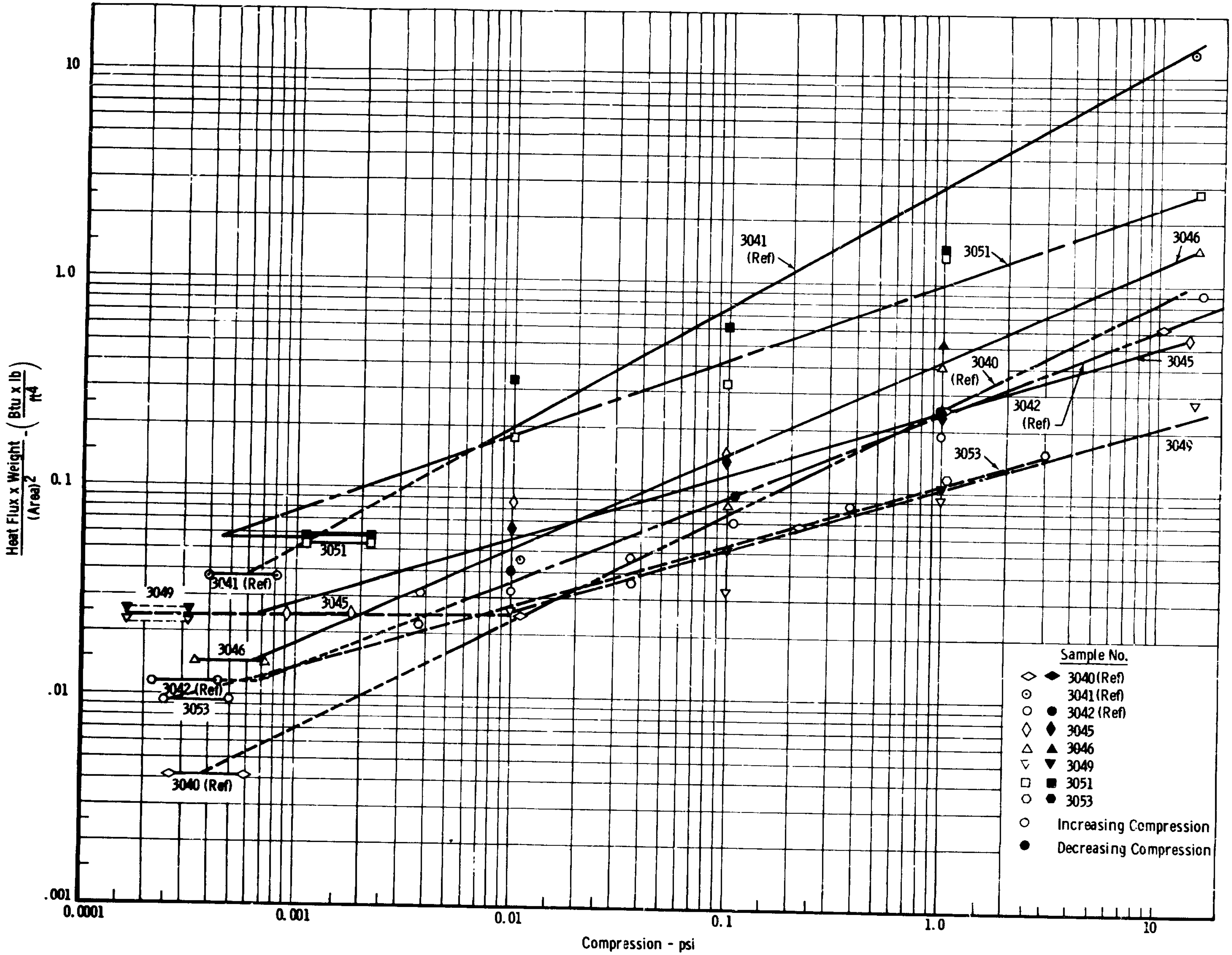

FIGURE II-16 EFFECT OF EXTERNAL COMPRESSION ON THE PRODUCT OF HEAT FLUX AND SAMPLE WEIGHT PER UNIT AREA than that for sample No. 3046 at zero compression. However, a large part of the heat flux is due to perforations in the shields. At 15 psi external compression where radiation accounts only for a small percentage of the total heat flux the latter is 2.5 times smaller in sample No. 3049 than in sample No. 3046 at the corresponding compression. We concluded that the heat conduction through the solid is smaller in sample No. 3049 than it is in sample No. 3046.

To estimate the portion of the heat flux which is contributed by 0.006 inch diameter thread holding the glass paper discs, we removed the thread and retested the sample. Table II-12 shows the test results. The test showed that the thread contributed approximately 7% of the total heat flux. These results later were supported by calculations assuming the thermal conductivity of the thread to be 1.4 Btu-in/hr ft^2 °F—typical for a plastic material.

For comparison (and as the beginning of a series of tests investigating penetrations), we assembled sample No. 3051 which was composed of 10 radiation shields and eleven spacers each consisting of two 12 inch diameter glass paper discs with 12 inch diameter silk netting disc in between. The test results are shown in Table II-13 and are plotted in Figure II-14.

We can compare results of all six tests we had run both on the basis of heat transferred through the sample of 10 radiation shields and on the basis of the product of the heat flux and weight of the sample which is even more significant for space application than heat flux alone. From Figures II-14 and II-16 we can draw the following conclusions:

(a) Decreased contact area between shields and spacer helps to decrease the total heat transferred through the insulation layers, especially at elevated external compression. The gain is even more noticeable when the products of heat flux and weight are compared for various insulation schemes.

(b) Comparing results for samples Nos. 3046 and 3051 we observe that under a compressive load the heat flux through the sample with uncut spacers is lower than for the sample with cut spacers.

TABLE II-12 EFFECT OF COMPRESSIVE LOAD ON THE HEAT LOSS THROUGH A MULTILAYER INSULATION (SYSTEM 8) WITH NYLON THEAD REMOVED

Sample No. 3050 , System 8.

Sample Description: Same as Sample 3049, except threads were removed

Sample Weight: 0.027 lb

Sample Chamber Pressure: 4×10^{-5} torr

Warm and Cold Plate Emittance: 0.9

Warm Plate Temperature: $73^{o} \pm 5^{o}F$

Cold Plate Temperature: $-320^{o}F$

Mechanical Compression psi	Sample Density lb/ft^3	Heat Flux $Btu/hr\ ft^2$	Thermal Conductivity $Btu\text{-}in/hr\ ft^2\ {}^{o}F$	Sample Thickness in	Test Date	Test No.
0	0.87	0.615	0.81×10^{-3}	0.515	8/10/65	a
0.01	1.1	0.780	0.77×10^{-3}	0.391	8/11/65	b
0.1	1.6	0.962	0.68×10^{-3}	0.275	8/11/65	c
1.0	2.2	2.46	1.27×10^{-3}	0.201	8/11/65	d
15	5.0	10.3	2.35×10^{-3}	0.089	8/11/65	e
1.0	3.7	3.17	0.97×10^{-3}	0.119	8/11/65	f
0.1	2.2	1.12	0.59×10^{-3}	0.204	8/11/65	g
0.01	1.7	0.882	0.60×10^{-3}	0.266	8/11/65	h
0	1.2	0.698	0.66×10^{-3}	0.371	8/12/65	i

TABLE II-13 EFFECT OF COMPRESSIVE LOAD ON THE HEAT LOSS THROUGH A MULTILAYER INSULATION WITH GALSS FIBER-SILK NETTING-GLASS FIBER SPACER

Sample No. 3051, System 4.

Sample Description: Ten radiation shields of 0.00025" thick x 11" diameter polyester film, aluminum coated on both sides and eleven 12" diameter, 0.003" thick silk nettings with twenty-two 12" diameter, 0.008" thick glass paper disks placed on both sides of silk netting

Sample Weight: 0.213 lb

Sample Chamber Pressure: 7×10^{-6} torr

Warm and Cold Plate Emittance: 0.9

Warm Plate Temperature: $73 \pm 5^{o}F$

Cold Plate Temperature: $-320^{o}F$

Mechanical Compression psi	Sample Density lb/ft^3	Heat Flux $Btu/hr\ ft^2$	Thermal Conductivity $Btu\text{-}in/hr\ ft^2\ {}^oF$	Sample Thickness in	Test Date	Test No.
0	5.9	0.198	0.28×10^{-3}	0.565	8/16/65	a
0.01	6.9	0.642	0.79×10^{-3}	0.481	8/16/65	b
0.1	8.0	1.20	1.3×10^{-3}	0.413	8/16/65	c common gas pressure
0.075	8.0	1.37	1.5×10^{-3}	0.415	8/16/65	c-1 parallel
0.1	8.0	1.42	1.5×10^{-3}	0.412	8/16/65	c-2 plates
1.0	10.6	4.88	4.0×10^{-3}	0.315	8/17/65	d
15	14.6	9.99	5.8×10^{-3}	0.225	8/17/65	e
1.0	11.3	5.30	4.0×10^{-3}	0.294	8/17/65	f
0.1	8.7	2.22	2.1×10^{-3}	0.381	8/17/65	g
0.01	7.6	1.20	1.3×10^{-3}	0.436	8/18/65	h
0	5.9	0.214	0.31×10^{-3}	0.567	8/19/65	i

Apparently the gains achieved by reducing the contact area are cancelled by the compression of the sample.

(3) Foam Spaced Multi-Layer Insulation

Table II-14 presents the description and the test for sample No. 3053. This sample was submitted to us by NASA. Each spacer of the sample consisted of two layers of foam (see Figure II-17). Although this was a thick sample it had only 9 shields. The heat loss through this thick sample was far lower than through the thinner samples tested previously (see Figure II-14). Compared on the basis of the product of heat flux and weight samples Nos. 3049 and 3053 had a similar performance between 0.01 and 3 psi compressions. To avoid crushing of the foam we did not apply compression over 3 psi. The load distribution between the measured and guard portion in the sample is different in sample No. 3053 from that in samples with evenly distributed load due to the ring-shaped buffer zone. The portion of the sample under the measuring vessel of the test apparatus experienced a load smaller than 3 psi mean compression of the sample.

(4) Combined Silk Netting and Foam Spacers

We assembled two ten-radiation shield samples with spacers constructed as shown in Figure II-18: 0.100-inch thick by 1/4-inch wide by 2 1/4-inch long strips of polyurethane foam were placed on 1 1/2-inch centers and heat sealed to one side of 0.003-inch thick silk netting. Silk netting provided dimensional stability for the spacer while the foam strips were intended to provide high thermal resistance.

In sample No. 3069 we used flexible foam strips while in sample No. 3073 strips were made from rigid foam. Tables II-15 and II-16 show results of the tests. The tests are compared to test 3053 in Figures II-19 and II-20.

When we examine the above tables and figures we conclude:

(a) The insulation samples spaced with a rigid foam spacer had the lowest heat flux at all compressive loads.

(b) Samples 3069 and 3073 exposed to compression over 0.1 psi were compressed beyond their elastic limit, causing a high

TABLE II-14 EFFECT OF COMPRESSIVE LOAD ON THE HEAT LOSS THROUGH A MULTILAYER INSULATION WITH COMPOSITE FOAM SPACER

Sample No. 3053, System I2.

Sample Description	Nine layers of each: (1) aluminized polyester film (1) 0.025" thick polyurethane foam (1) 0.060" thick polyurethane foam cut to form a grid with 7/32" wide strips on 1-7/6 centers
Sample Weight:	0.12 lb
Sample Chamber Pressure:	Less than 1×10^{-5} torr
Warm and Cold Plate Emittance:	0.9
Warm Plate Temperature:	70°F
Cold Plate Temperature:	-320°F

Mech. Comp. on Sample psi	Sample Density lb/ft^3	Heat Flux $Btu/hr\ ft^2$	Thermal Conductivity $Btu\text{-}in/hr\ ft^2\ °F$	Sample Thickness in	Test Date	Test No.
0	1.3	0.076	0.25×10^{-3}	1.266	8/26/65	a
0.0035	1.4	0.173	0.51×10^{-3}	1.150	8/26/65	b
0.035	1.5	0.289	0.75×10^{-3}	1.048	8/26/65	c
0.35	1.9	0.697	1.5×10^{-3}	0.859	8/26/65	d
1.06	1.9	0.905	1.9×10^{-3}	0.847	8/26/65	e
0.035	1.7	0.369	0.93×10^{-3}	0.947	8/27/65	f
0.0035	1.6	0.258	0.68×10^{-3}	1.019	8/27/65	g
0	1.4	0.076	0.23×10^{-3}	1.145	8/27/65	h

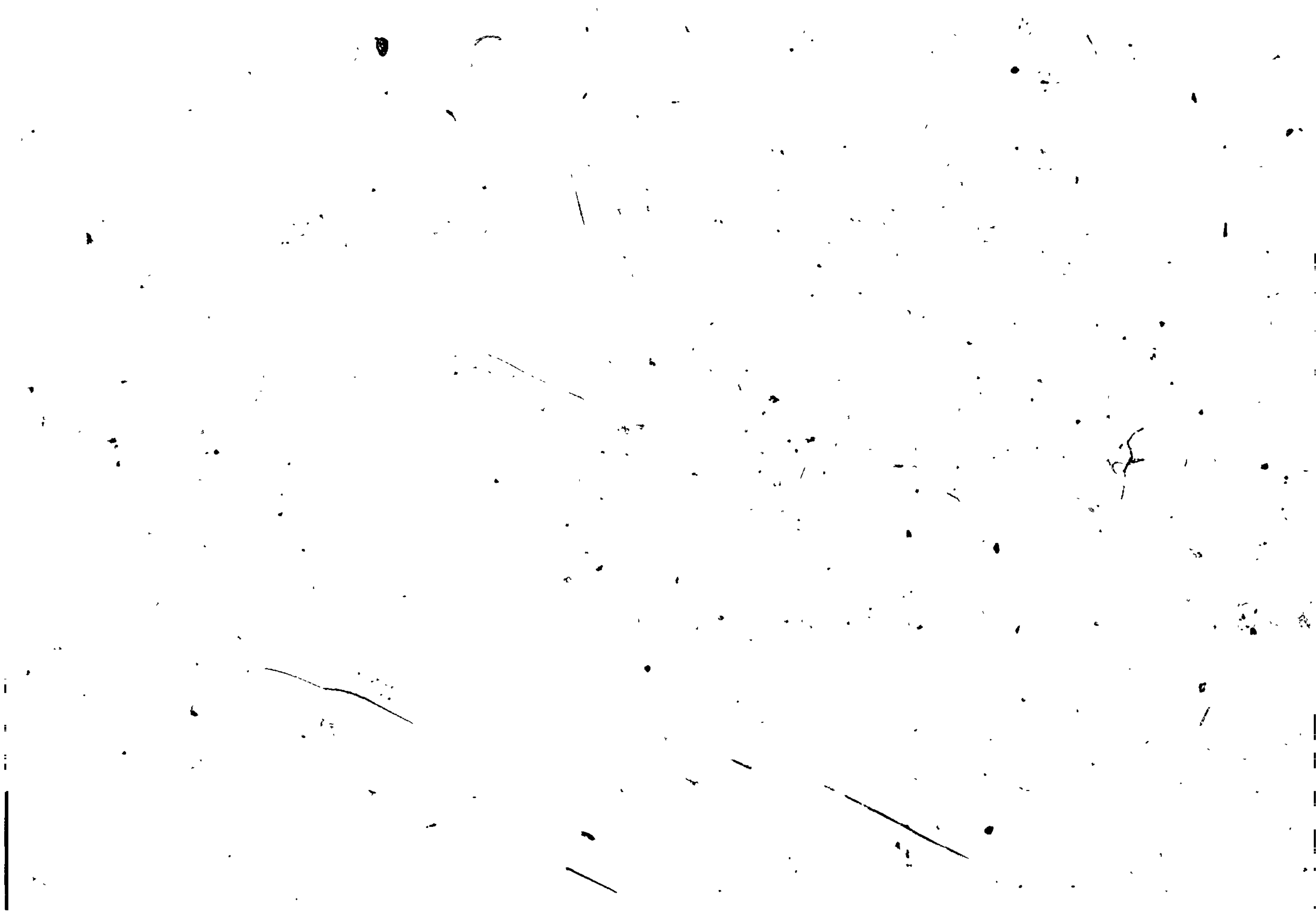

FIGURE II-17 MULTILAYER INSULATION WITH COMPOSITE FOAM SPACER (SAMPLE 3053)

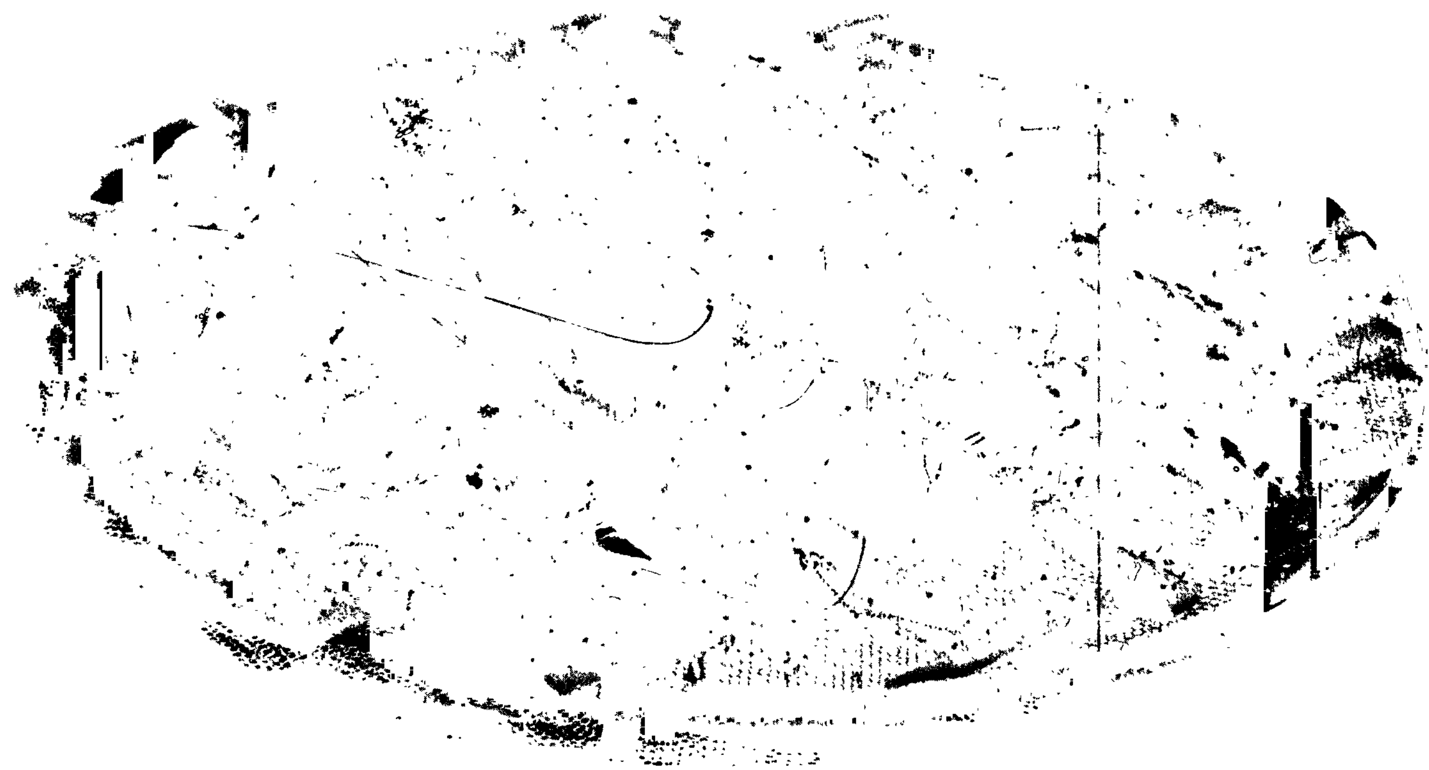

FIGURE II-18 MULTILAYER INSULATION WITH POLYURETHANE FOAM STRIPS - SILK NETTING SPACER (SAMPLES 3069 AND 3073)

TABLE II-15 EFFECT OF COMPRESSIVE LOAD ON THE HEAT LOSS THROUGH A MULTILAYER INSULATION WITH FLEXIBLE POLYURETHANE FOAM STRIPS-SILK NETTING SPACERS

Sample No. 3069, System 9.

Sample Description: Ten radiation shields of 0.00025" thick x 11" diameter polyester film, aluminum coated on both sides and eleven spacers of 0.003" thick x 12" diameter silk netting with 0.100" thick x 1/4" wide x 2-1/4" long flexible polyurethane foam (Scott Paper Co.) strips heat sealed to netting by a polyester film strip

Sample Weight: 0.059 lb

Sample Chamber Pressure: Below 5×10^{-5} torr

Warm and Cold Plate Emittance: 0.9

Warm Plate Temperature: $70 \pm 5^{\circ}F$

Cold Plate Temperature: $-320^{\circ}F$

Mechanical Compression psi	Sample Density lb/ft^3	Heat Flux $Btu/hr\ ft^2$	Thermal Conductivity $Btu\text{-}in/hr\ ft^2\ ^{\circ}F$	Sample Thickness in	Test Date	Test No.
0	0.74	0.17	0.55×10^{-3}	1.259	11/28/65	a
0.01	0.98	0.33	0.80×10^{-3}	0.948	12/ 2/65	b
0.1	1.2	0.65	1.3×10^{-3}	0.775	12/ 5/65	c
1.0	3.6	6.7	4.4×10^{-3}	0.259	12/ 6/65	d
15.0	8.6	66	1.8×10^{-3}	0.108	12/ 6/65	e
1.0	7.4	16	5.2×10^{-3}	0.126	12/ 6/65	f
0.1	4.3	2.4	1.3×10^{-3}	0.217	12/ 7/65	g
0.01	2.9	0.94	0.77×10^{-3}	0.322	12/ 7/65	h
0	2.2	0.67	0.73×10^{-3}	0.428	12/ 8/65	i
0	1.4	0.30	0.53×10^{-3}	0.685	12/ 8/65	j
0	0.97	0.32	-	0.960	12/ 9/65	k

TABLE II-16 EFFECT OF COMPRESSIVE LOAD ON THE HEAT LOSS THROUGH A MULTILAYER INSULATION WITH RIGID POLYURETHANE FOAM STRIPS--SILK NETTING SPACERS

Sample No. 3073, System 10

Sample Description: Ten radiation shields of 0.00025" thick x 11" diameter polyester film, aluminum coated on both sides and eleven spacers of 0.005" thick x 12" diameter silk netting with 0.100" thick x 1/4" wide x 2-1/4" long rigid polyurethane foam strips heat sealed to netting by a polyester film strip

Sample Weight: 0.055 lb

Sample Chamber Pressure: Below 5×10^{-5} torr

Warm and Cold Plate Emittance: 0.9

Warm Plate Temperature: 70 ± 5°F

Cold Plate Temperature: -320°F

Comments: A soft cushion consisting of 3 layers of 0.070" thick flexible polyurethane foam was placed between the test sample and warm plate. Three thermocouples were mounted on the upper (toward the sample) face of the cushion. The temperature of these thermocouples was monitored at 70°F

Mechanical Compression psi	Sample Density lb/ft^3	Heat Flux $Btu/hr\ ft^2$	Thermal Conductivity $Btu\text{-}in/hr\ ft^2\ °F$	Distance Between Plates in	Test Date	Test No.
0	0.62	0.10	0.36×10^{-3}	1.417	2/2/66	c
0.01	0.9	0.19	0.48×10^{-3}	0.975	2/3/66	d
0.1	1.1	0.47	0.98×10^{-3}	0.814	2/3/66	e
3.0	2.4	9.00	8.5×10^{-3}	0.366	2/4/66	f
15.0	4.4	24.9	13×10^{-3}	0.200	2/4/66	g
3.0	3.5	11.8	7.6×10^{-3}	0.250	2/4/66	h
0.1	1.7	1.24	1.6×10^{-3}	0.518	2/4/66	i
0.01	1.4	0.47	$.76 \times 10^{-3}$	0.640	2/7/66	j
0	0.84	0.12	$.32 \times 10^{-3}$	1.044	2/12/66	m

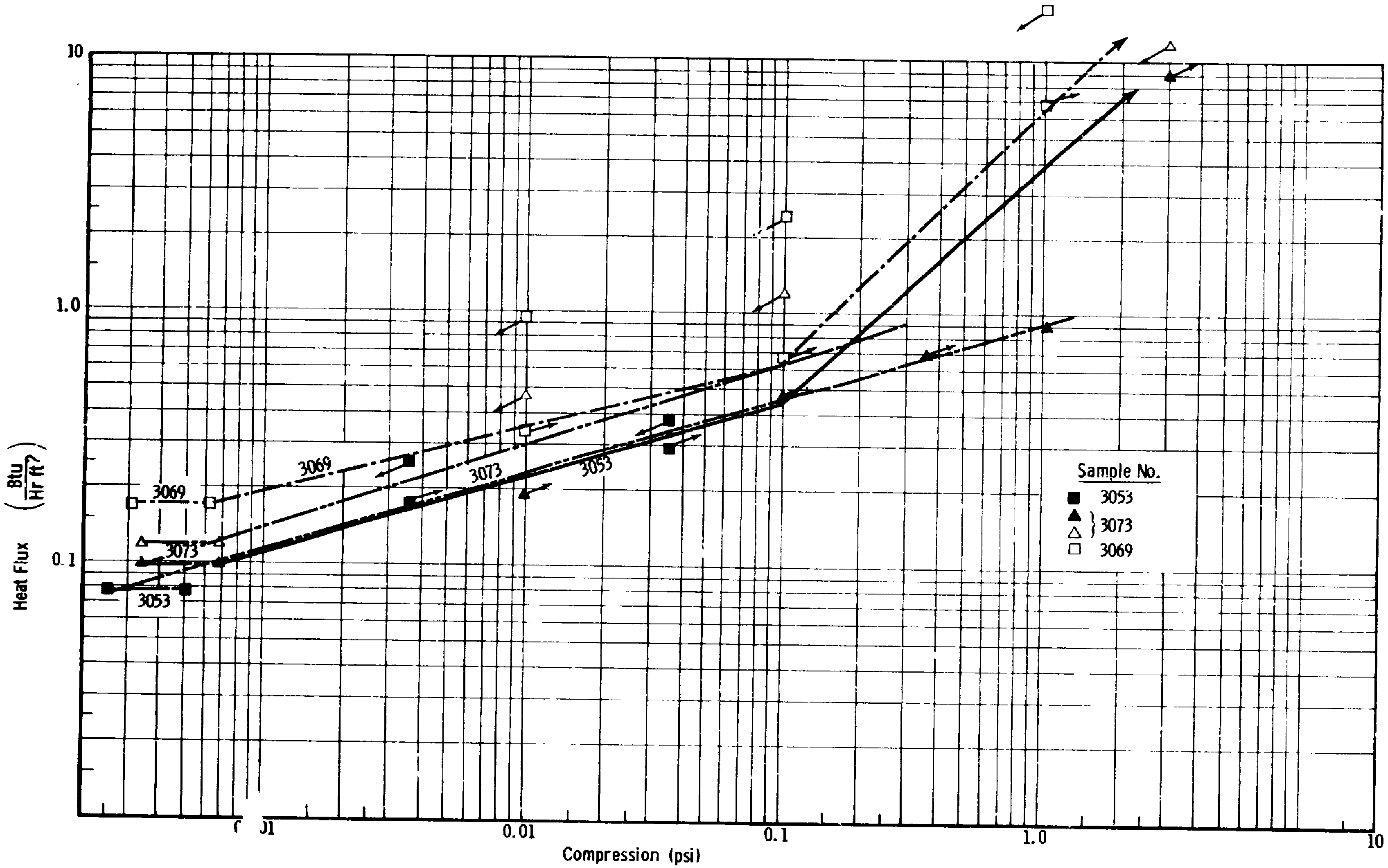

FIGURE II-19 THERMAL PERFORMANCE OF MULTI-LAYER INSULATION WITH FOAM STRIPS - SILK NETTING SPACERS

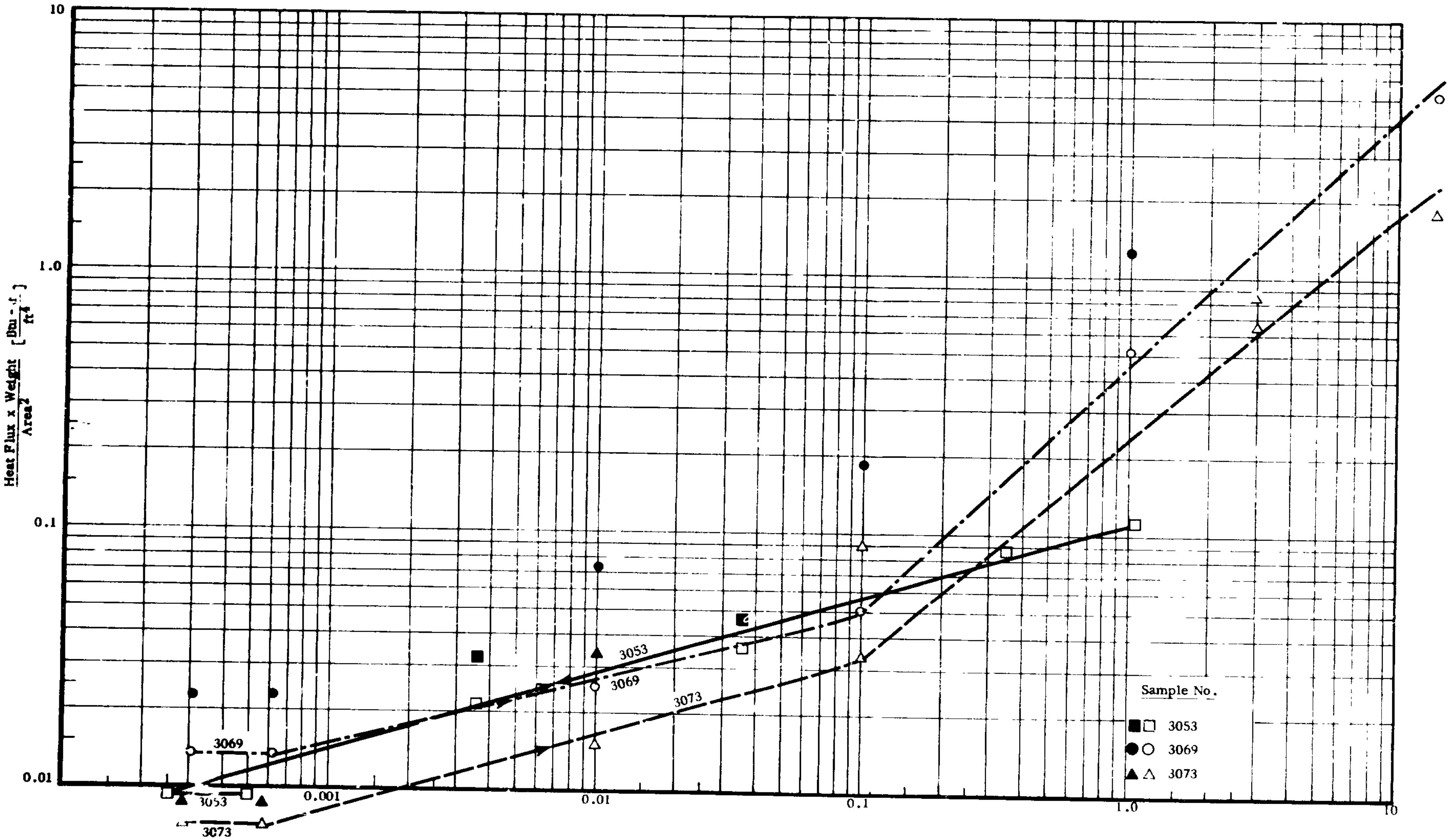

FIGURE II-20 PRODUCT OF HEAT FLUX AND WEIGHT FOR MULTI-LAYER INSULATIONS WITH SILK NETTING - FOAM SPACERS increase in the heat flux, and fail to return after load release along the same curve.

(c) Comparing samples on the basis of the products of heat flux and weight, sample No. 3073 at compression below 0.1 psi had the best performance of any sample tested during this program.

3. Tests of Three-Blanket Systems

We tested two systems (No. 15 and 16, Table II-2) which represent a mock-up of a blanket-type insulation. Each blanket in system 15 (sample No. 3039) consisted of three 0.00025-inch thick aluminum coated (on both sides) polyester radiation shields spaced with 0.020-inch thick polyurethane foam. The last foam spacer toward the cold side was replaced by an 0.008-inch thick fiberglass mat spacer. This assembly was placed between two polyester-aluminum-polyester laminates 0.002-inch thick each. Sample 3039 consisted of three such blankets. Construction of this sample is shown in Figure II-21. An extra 0.020-inch thick foam spacer was placed against the cold plate to prevent a thermal short between measuring and guard vessels through the laminated boundary.

Similarly, sample 3082 (Figure II-22) consisted of three subassemblies. Each subassembly had, however, six 0.00025-inch thick aluminum coated polyester radiation shields. The shields were spaced with two pieces of 0.025-inch thick polyurethane foam. Only one piece of foam was used to space the assembly from each of the two 0.003-inch thick polyester-aluminum-polyester laminated boundaries. The test results for both samples are presented in Tables II-17, II-18. In Figure II-23, we plotted the heat flux vs. compressive load for both tests and compared the resulting curves to the curve for the simple ten shield-foam spaced system (3040).

From Figure II-23 we conclude:

a, The slope of the lines corresponding to all three tests are identical--approximately 0.5.

b. Sample 3082 which has the larger number of radiation shields had a lower heat flux at all compressive loads.

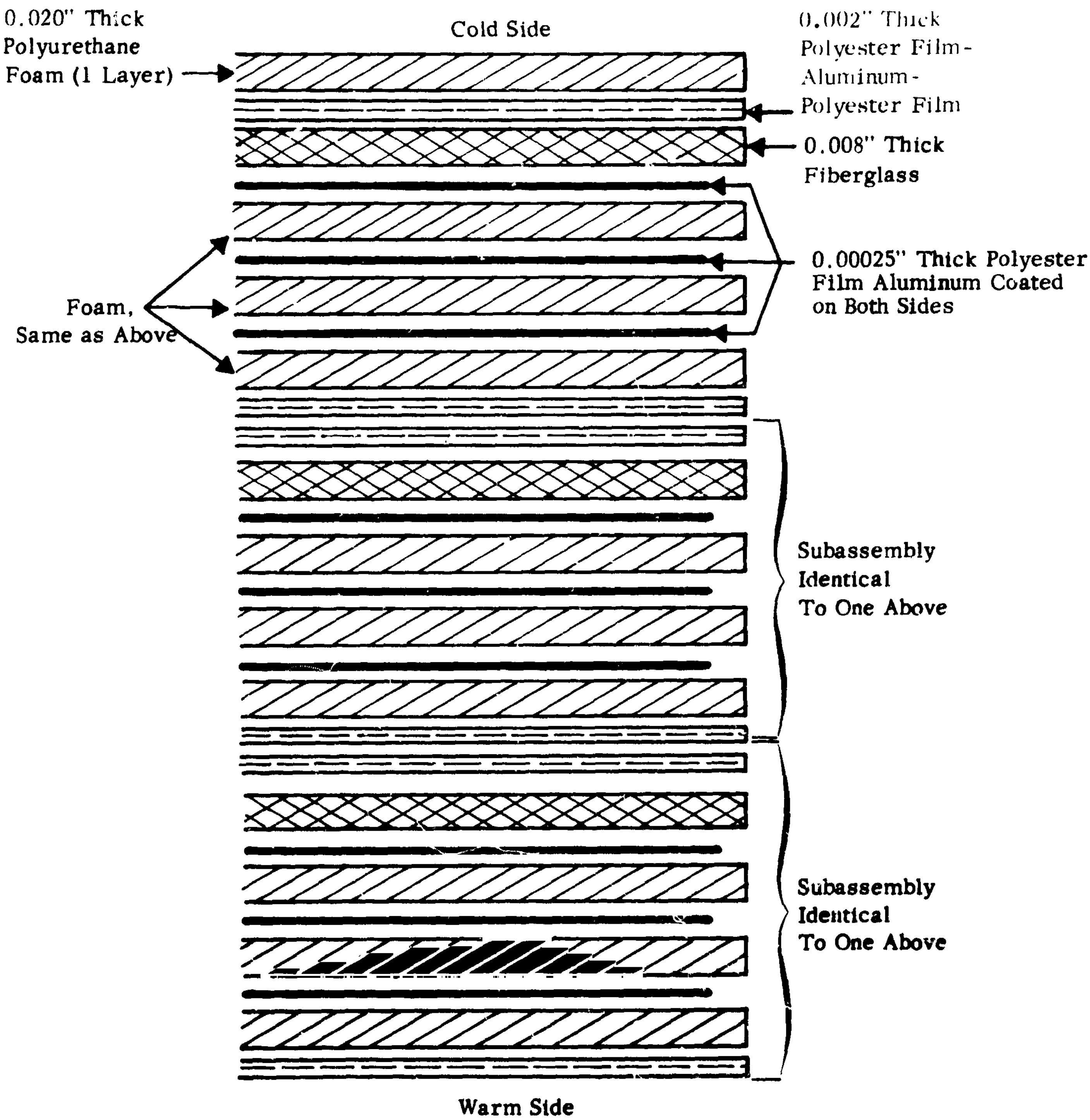

FIGURE II-21 STRUCTURE OF SAMPLE NO. 3039 (AND NO. 1069)

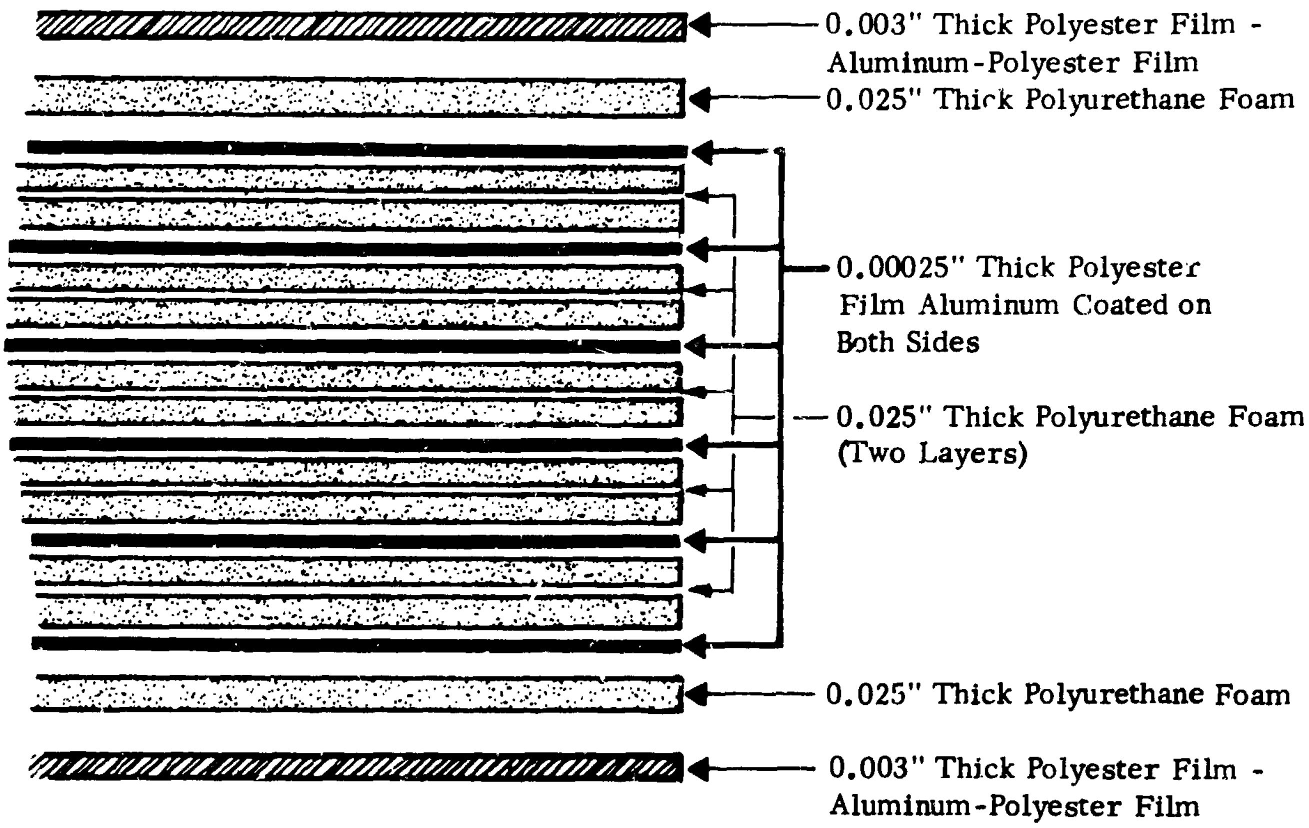

FIGURE II-22 CONSTRUCTION OF ONE SUBASSEMBLY FOR SAMPLE NO. 3082

TABLE II-17 EFFECT OF COMPRESSIVE LOAD ON HEAT LOSS THROUGH A THREE-BLANKET MULTILAYER SYSTEM

Sample No. 3039, System 15.

Sample Description: (i) 0.020" thick x 12" diameter polyurethane foam spacer (directly under the cold plate) +

(3) Subassemblies, each consisting of:

- (2) 0.002" thick x 10-1/2" diameter polyester-aluminum-polyester laminated boundaries
- (1) 0.008" thick x 12" diameter Fiberglas layer (first toward cold boundary)
- (3) 0.00025" thick x 10-1/2" diameter polyester film shields aluminized on both sides
- (3) 0.020" thick x 12" diameter polyurethane foam spacers

Sample Weight: 0.134 lbs

Sample Chamber Pressure: Less than 1 x 10^{-5} torr

Warm and Cold Plates Emittance: 0.9

Warm Plate Temperature: 43 ± 2°F

Cold Plate Temperature: -320°F

External Compression psi	Sample Density lb/ft^3	Heat Flux Btu/hr ft^2	Thermal Conductivity Btu-in/hr ft^2 $^{\circ}$F	Sample Thickness in	Test Date	Test No.
0	2.16	0.646	1.76 x 10^{-3}	0.996	3/31/65	a
0	2.54	0.430	1.00 x 10^{-3}	0.844	4/1/65	b
0	2.95	0.420	0.84 x 10^{-3}	0.729	4/2/65	c
0	3.05	0.420	0.82 x 10^{-3}	0.705	4/2/65	d
0	3.14	0.447	0.85 x 10^{-3}	0.686	4/3/65	e
0.01	3.16	0.447	0.84 x 10^{-3}	0.680	4/5/65	f
0.06	4.20	0.954	1.34 x 10^{-3}	0.511	4/6/65	g
0.58	5.35	2.211	2.43 x 10^{-3}	0.401	4/6/65	h
9	6.90	8.090	6.80 x 10^{-3}	0.312	4/6/65	j
4	6.31	5.150	4.70 x 10^{-3}	0.340	4/6/65	i

TABLE II-18 EFFECT OF REPEATED APPLICATION OF COMPRESSIVE LOAD ON THE HEAT LOSS THROUGH A THREE-BLANKET MULTILAYER SYSTEM

Sample No. 3082, System 16.

Sample Description: (3) Subassemblies, each consisting of:
(2) 0.003" thick x 11" diameter polyester-aluminum-polyester laminated boundaries
(6) 0.00025" thick x 11" diameter polyester shields aluminized on both sides
(12) 0.025" thick x 12" diameter polyurethane foam spacers
The top cold polyester-aluminum-polyester boundary was removed in order for the cold plate to be in contact with spacer material.

Sample Weight: 0.223 lbs

Sample Chamber Pressure: Less than 1×10^{-5} torr

Warm and Cold Plate Emittance: 0.9

Warm Plate Temperature: 70° ± 2°F

Cold Plate Temperature: -320°F

Mechanical Compression psi	Sample Density lb/ft^3	Heat Flux $Btu/hr\ ft^2$	Thermal Conductivity $Btu\text{-}in/hr\ ft^2\ °F$	Sample Thickness in	Test Date	Test No.
15	5.4	6.65	12×10^{-3}	0.713	3/18/66	a
2	4.8	3.18	6.6×10^{-3}	0.805	3/18/66	b
0.1	4.0	0.570	1.4×10^{-3}	0.761	3/21/66	c
0.01	3.7	0.141	0.38×10^{-3}	1.044	3/22/66	d
0	3.2	0.052	0.16×10^{-3}	1.210	3/23/66	e
15	5.4	6.65	12×10^{-3}	0.712	3/23/66	f
2	5.0	3.96	7.9×10^{-3}	0.774	3/23/66	g
0.1	4.4	0.945	2.1×10^{-3}	0.880	3/24/66	h
0.01	3.7	0.219	0.58×10^{-3}	1.041	3/24/66	i
0	3.2	0.058	0.18×10^{-3}	1.207	3/30/66	j
15	5.5	7.04	13×10^{-3}	0.707	3/30/66	k
2	5.0	4.35	8.5×10^{-3}	0.767	3/30/66	l
0.1	4.3	0.807	1.9×10^{-3}	0.906	3/31/66	m
0.01	4.0	0.324	0.80×10^{-3}	0.968	3/31/66	n
0	3.2	0.072	0.22×10^{-3}	1.222	4/1/66	o

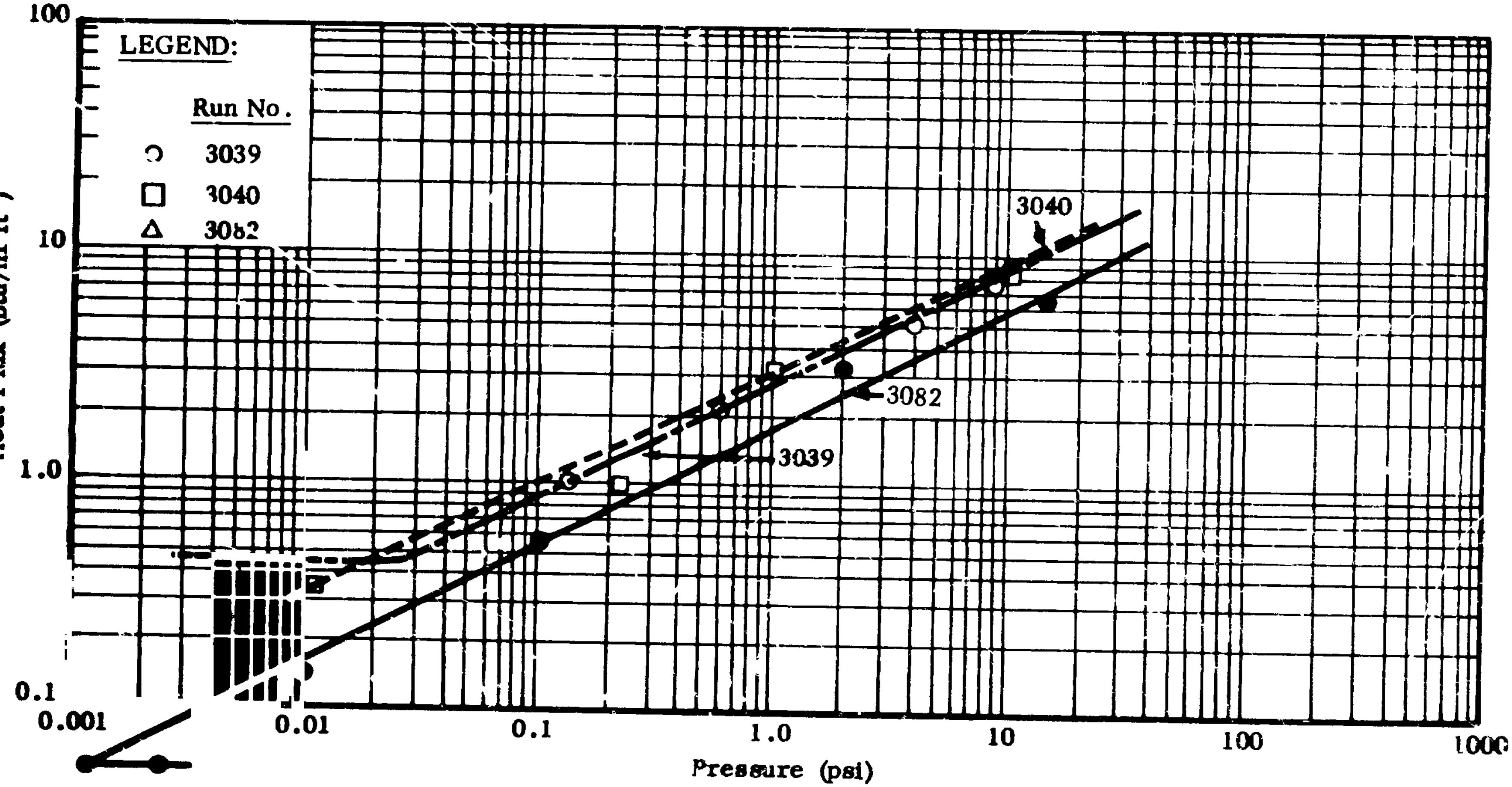

FIGURE II-23 EFFECT OF EXTERNAL COMPRESSION ON THE HEAT FLUX THROUGH MULTI-LAYER INSULATIONS - SAMPLE NOS. 3039, 3040, AND 3082

c. The heat flux through sample No. 3039, which has more radiation shields than sample No. 3040, is slightly lower than the heat flux through sample No. 3040 for external compression above 0.01 psi.

d. The unguarded edge of the sample No. 3039 may have caused a high heat flux at zero compressive load.

4. <u>Effects of Repeated Load Application on Samples of Multi-Layer Insulations</u>

It is important for an application engineer to know the behavior of a multi-layer insulation when it is exposed one or more times to a compressive load and left to recover after the load is removed.

In our previous investigations[(1)] we found that neither the heat loss through an insulation layer nor the layer's thickness are the same before and after the insulation was compressed. Our equipment, however, was then not sensitive enough to make a thorough study of this subject.

The new more sensitive low compressive load attachment (see Section IIC-6) to the thermal conductivity apparatus permitted us to conduct an investigation of the recovery pattern demonstrated by various insulations after a compressive load was applied and removed a single or repeated number of times.

Investigation of the load application and recovery pattern of various insulations requires a study of the method of load application: sudden or slow load application; duration under the load; maximum intensity of the load; and the method of recovery: sudden or slow; time allowed for recovery before the measurement is taken.

We measured heat fluxes through three samples repeating more than once the loading sequence.

For the first sample we selected a multi-layer insulation supplied by NASA consisting of ten aluminum coated (on both sides) polyester film radiation shields spaced with eleven 12-inch diameter, 0.020 inch thick, 2 lb/ft^3 density polyurethane foam discs (system 3).

Table II-19 presents a description and the test results for system 3. The sample was subjected to compressive loads for the first

TABLE II-19 EFFECT OF REPEATED APPLICATION OF COMPRESSIVE LOADS ON THE HEAT LOSS THROUGH A FOAM SPACED MULTILAYER INSULATION

Sample No. 3043 (Former 3040), System 3

Sample Description: Ten radiation shields of 0.00025" thick x 10-1/2" diameter polyester film, aluminum coated on both sides and eleven spacers of 2.0 lb/ft^3 Freon blown polyurethane foam 0.02" thick x 12" diameter

Sample Weight: 0.0474 lb

Sample Chamber Pressure: Less than 3×10^{-5} torr

Warm and Cold Plate Emittance: 0.9

***Warm Plate Temperature:** $71^{o} \pm 2^{o}F$ for runs a through j; $40^{o}F$ for runs k through n

Cold Plate Temperature: $-320^{o}F$

Mechanical Compression psi	Sample Density lb/ft^3	Heat Flux $Btu/hr\ ft^2$	Thermal Conductivity $Btu\text{-}in/hr\ ft^2\ {}^{o}F$	Sample Thickness in	Test Date	Test No.
0	1.39	0.154	-	0.594	5/26/65	a
0	1.38	0.193	-	0.600	5/27/65	b
0	1.44	0.127	0.19×10^{-3}	0.576	5/28/65	c
0.01	1.71	0.369	0.45×10^{-3}	0.483	5/28/65	d
0.1	2.18	1.54	1.5×10^{-3}	0.379	5/31/65	e
1.0	2.56	5.25	4.3×10^{-3}	0.323	6/1/65	f
15.0	3.36	14.95	9.4×10^{-3}	0.246	6/1/65	g
0.1	2.34	1.88	1.7×10^{-3}	0.353	6/1/65	i
0.01	2.14	0.73	0.72×10^{-3}	0.386	6/2/65	j
0.01	2.14	0.58	0.57×10^{-3}	0.389	6/2/65	k*
0.1	2.32	1.29	1.2×10^{-3}	0.356	6/2/65	l*
1.0	2.69	4.61	3.6×10^{-3}	0.307	6/2/65	m*
15.0	3.39	12.1	7.5×10^{-3}	0.244	6/2/65	n*

time by NASA (No. 1070). We applied compressive loads to the same sample for the second time (see Section II-D-2-c, Sample No. 3040); finally, after storing the sample for 1 1/2 months, we compressed the sample consecutively for the third and fourth time. Table II-20 shows the thickness of the sample for various compressive loads as recorded during the three consecutive compression cycles. A noticeable change in sample thickness occurred between the third and the fourth load application; however, comparing the values during load release after the third load application with those values during the fourth load application, we find that the thickness of the sample for the corresponding loads are identical. The third load application was performed at a 70°F warm plate temperature and the fourth one at 40°F warm plate temperature. Correcting for the difference in warm plate temperature, the heat fluxes for the corresponding loads remained the same for the third and fourth load applications. As Figure II-24 shows, this was not the case for the second and the fourth load applications which were performed at the same temperature of the warm plate (40°F).

After each application of the load, we discovered small loose particles on the radiation shields. These particles broke loose from the foam spacer.

A similar test was repeated on system 7. The sample had ten aluminum coated (on both sides) polyester film radiation shields spaced with eleven composite material spacers. Table II-10 and Figure II-25 present the description and the test results for the sample.

Sample 3082 which consisted of the same radiation shield and spacer materials as sample 3040 but was assembled into a system consisting of 3 subassemblies (Figure II-22) exhibited a behavior similar to that of sample 3040 under repeated application of the compressive loads.

The loads were applied to sample 3082 in a different sequence than to sample 3040. After the calorimeter was evacuated and filled with liquid nitrogen a 15 psi compressive load was applied to the sample, the total exposure time was 1 3/4 hours--just enough to bring the calorimeter to equilibrium and record data for 1 1/4 hours. Then the compression

TABLE II-20 REPEATED COMPRESSION OF A MULTI-LAYER INSULATION WITH FOAM SPACER

Compression psi	Sample Thickness (inch) Compressed 2nd Time (Sample No. 3040)	Compressed 3rd Time	Compressed 4th Time
0	0.576	0.576	0.576
0.010	0.488	0.483	0.389
0.1	-	0.379	0.356
0.22	0.385	-	-
1.0	0.314	0.323	0.307
10	0.273	-	-
15	-	0.246	0.244
0.1	-	0.353	-
0.01	-	0.386	-
Temperature of the Warm Plate	40°F	70°F	40°F

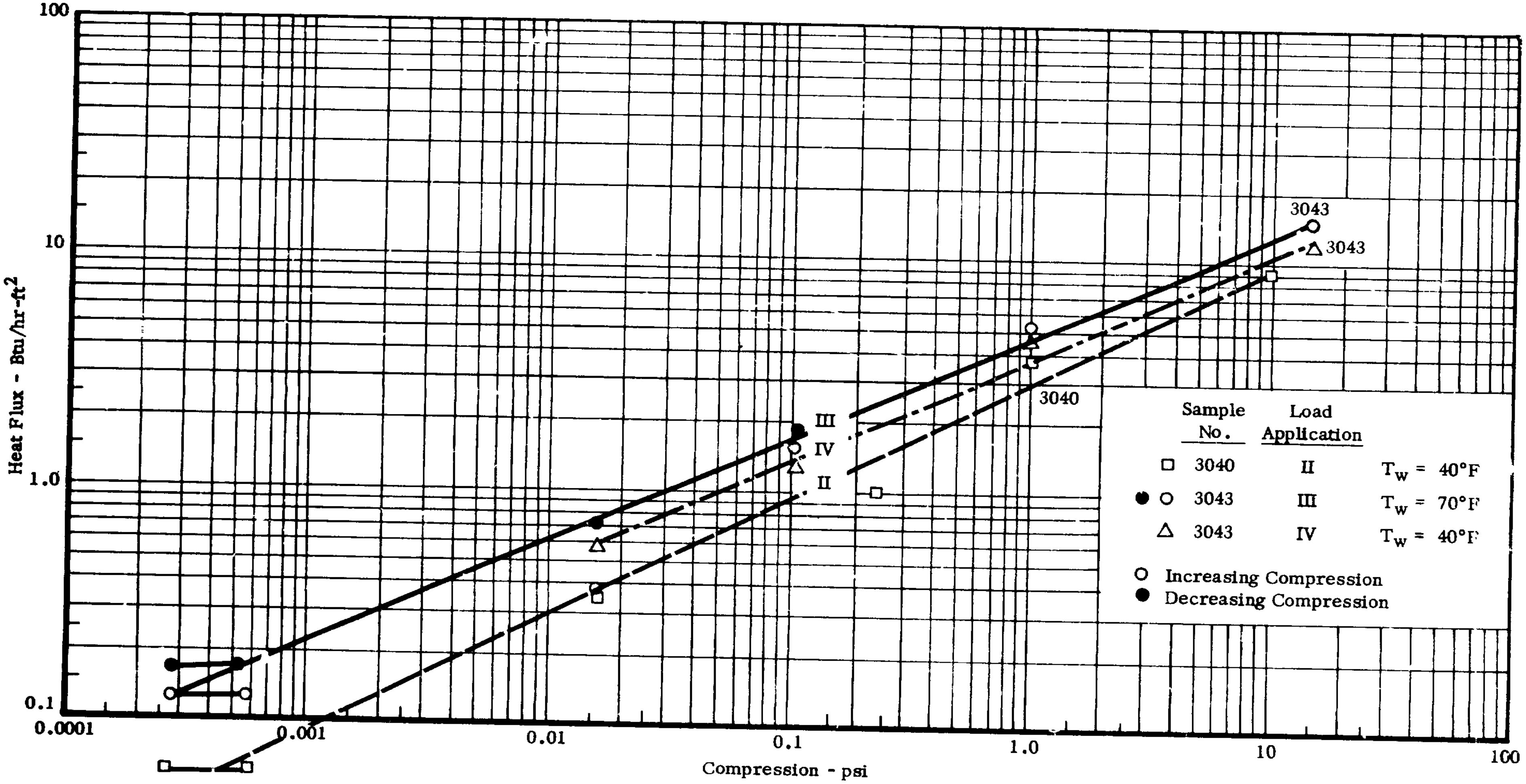

FIGURE II-24 REPEATED APPLICATION OF COMPRESSIVE LOADS TO A SAMPLE OF MULTI-LAYER INSULATION WITH 0.020" THICK FOAM SPACER

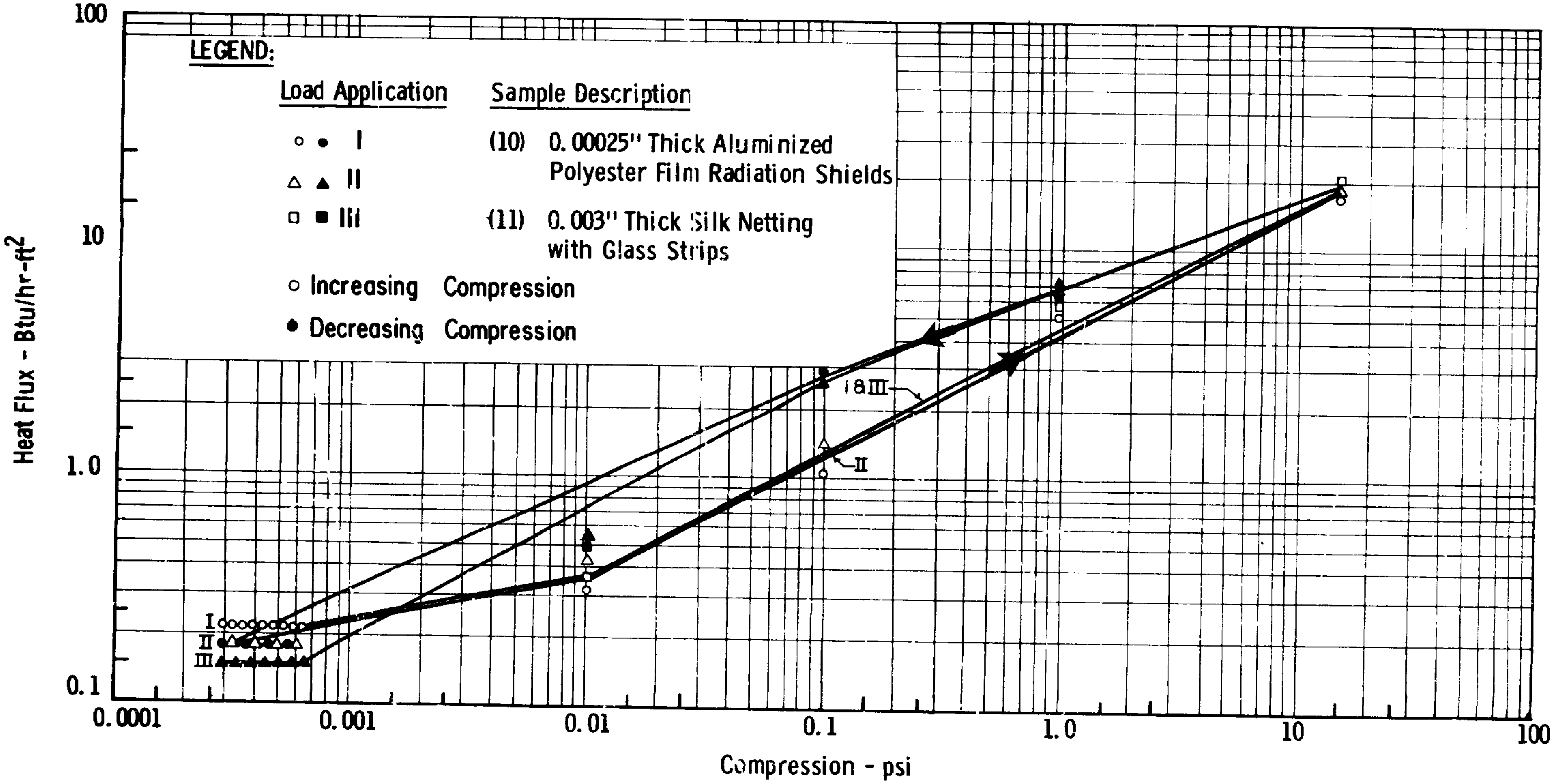

FIGURE II-25 REPEATED APPLICATION OF COMPRESSIVE LOADS TO A SAMPLE OF MULTI-LAYER INSULATION WITH COMPOSITE SPACER (SAMPLE No. 3046) load was reduced to 2 psi. Data were again recorded at equilibrium. The process was repeated at 0.1, 0.01, and 0 compression. This cycle was repeated two more times. During the second and third cycles the sample was exposed to a compressive load of 15 psi for 8 hours each time.

In spite of the variation in application of compressive loads the two samples behaved in a similar manner. As expected, sample 3082 which had 18 radiation shields and 36 spacers had a lower heat flux at all compressive loads than the heat flux through sample 3040 which had only 10 shields and 11 spacers.

Table II-18 and Figure II-26 show the results of the test.

Because the information which we have obtained was limited, definite trends in the behavior of the insulation were not established. Our observations indicate that:

a. The thickness of the sample (#3040, 3043, 3082, Systems 3 and 1) with foam spacers decreased slightly after each successive compression cycle presumably due to crushing of the foam cells under pressure, simultaneously the heat flux steadily increased.

b. The thickness of the sample (#3046, System 7) spaced with strips of glass paper attached to the silk carrier was drastically reduced during the first compression cycle, thereafter the sample became resilient; however, the resiliency of the sample is, apparently, time dependent.

c. The greatest variation of the heat flux from the theoretically predicted relationship (see Section II-D-2-f) occurred during the first cycle.

d. The variation of the heat flux from the theoretically predicted relationship was smaller during the decompression part of the cycle.

e. After the sample was subjected three times to full compression cycles, the increase in heat flux was negligible.

5. Effects of Load Application Methods

a. Effect of Plate Parallelness

As we already described in Section II-C-6-f, the compressive load to the sample can be applied in various ways.

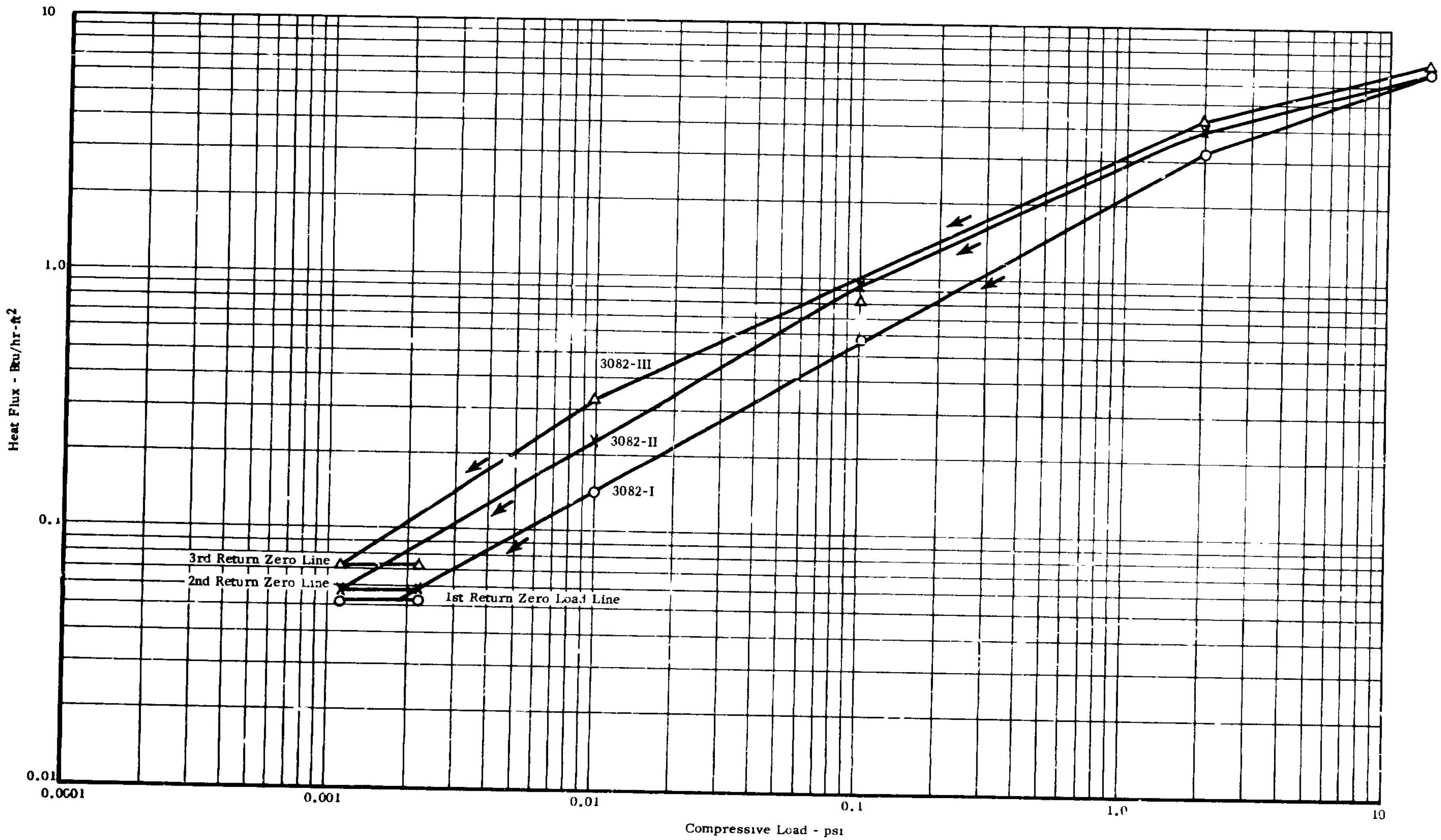

FIGURE II-26 REPEATED APPLICATION OF COMPRESSIVE LOADS TO A SAMPLE OF MULTI-LAYER INSULATION WITH TWO LAYERS OF FOAM FOR EACH SPACER

During test No. 3051 (see Table II-13) we applied 0.1 psi compression to the sample in two different ways:

(1) By applying a common gas pressure to all three bellows.

(2) By applying a gas pressure individually to each of the three bellows.

When method (1) was applied, the warm plate was floating 0.070-inch off from being parallel to the cold plate. This was unusual; in most tests the plates were parallel within 0.020-inch or closer. We found that when the gas pressure was applied to each individual bellows to keep warm and cold plates parallel the measured heat flux was 18% higher than in the case when a common gas pressure was applied to all three bellows. In the case of non-parallel plates, the compressive load is distributed unevenly: the highest compression is always near the edge of the sample and the heat flows preferentially to the guard vessel so that the heat flow to the measuring vessel is smaller than when the plates are parallel. In all tests following test No. 3051 we attempted to maintain the plate parallel within 0.010 inch.

b. Loads Applied with Flexible Cushion

As we already described in Section II-C-6-f, the compressive load to the sample may be applied by a soft cushion rather than a rigid plate. We made two tests to see if significant variation in heat flux will be caused by a load application with a soft cushion.

During the first test we used three 0.070-inch thick discs of flexible polyurethane foam as a soft cushion. We tested system 12 compressing it between soft warm plate and rigid cold plate (test No. 3072). Table II-21 presents results of test 3072. These results are compared in Figure II-27 to the previously obtained results when the same sample was tested between two rigid plates (test No. 3053, Table II-14). Figure II-27 shows that application of a compressive load by a flexible cushion causes the heat flux to be higher for the corresponding loads. Due to the structure of the sample (see Figure II-17) a flexible cushion applies loads not only on the high points but also between the strips causing a certain amount of bridging and thereby increasing total

TABLE II-21 EFFECT OF COMPRESSIVE LOAD ON THE HEAT LOSS THROUGH A MULTILAYER INSULATION WITH A FOAM-GRID SPACER

Sample No. 3072 (same as 3053), System 12.

Sample Description: Nine layers of each:
(1) 0.0025" thick aluminized polyester film
(1) 0.020" thick polyurethane foam
(1) 0.060" thick polyurethane foam cut to form a grid with 7/32" wide strips on 1-7/16 centers

Sample Weight: 0.12 lb

Sample Chamber Pressure: less than 1×10^{-5} torr

Warm and Cold Plate Emittance: 0.9

Warm Plate Temperature: 70°F

Cold Plate Temperature: -320°F

Comments: A soft cushion consisting of 3 layers of 0.070" thick flexible polyurethane foam was placed between the test sample and warm plate. Three thermocouples were mounted on the upper (toward the sample) face of the cushion. The temperature of these thermocouples was monitored at 70°F.

Mech. Comp. on Sample psi	Heat Flux Btu/hr ft^2	Distance Between Plates Inch	Test Date	Test No.
0	0.16	1.439	1/14/66	
0	0.13	1.464	1/19/66	b
0.0035	0.23	1.259	1/20/66	c
0.035	0.32	1.173	1/20/66	d
0.70	1.7	0.855	1/23/66	e
5.25	4.5	0.695	1/23/66	f
0.70	2.8	0.745	1/24/66	g
0.0035	0.51	0.969	1/24/66	h
0	0.17	1.207	1/26/66	j

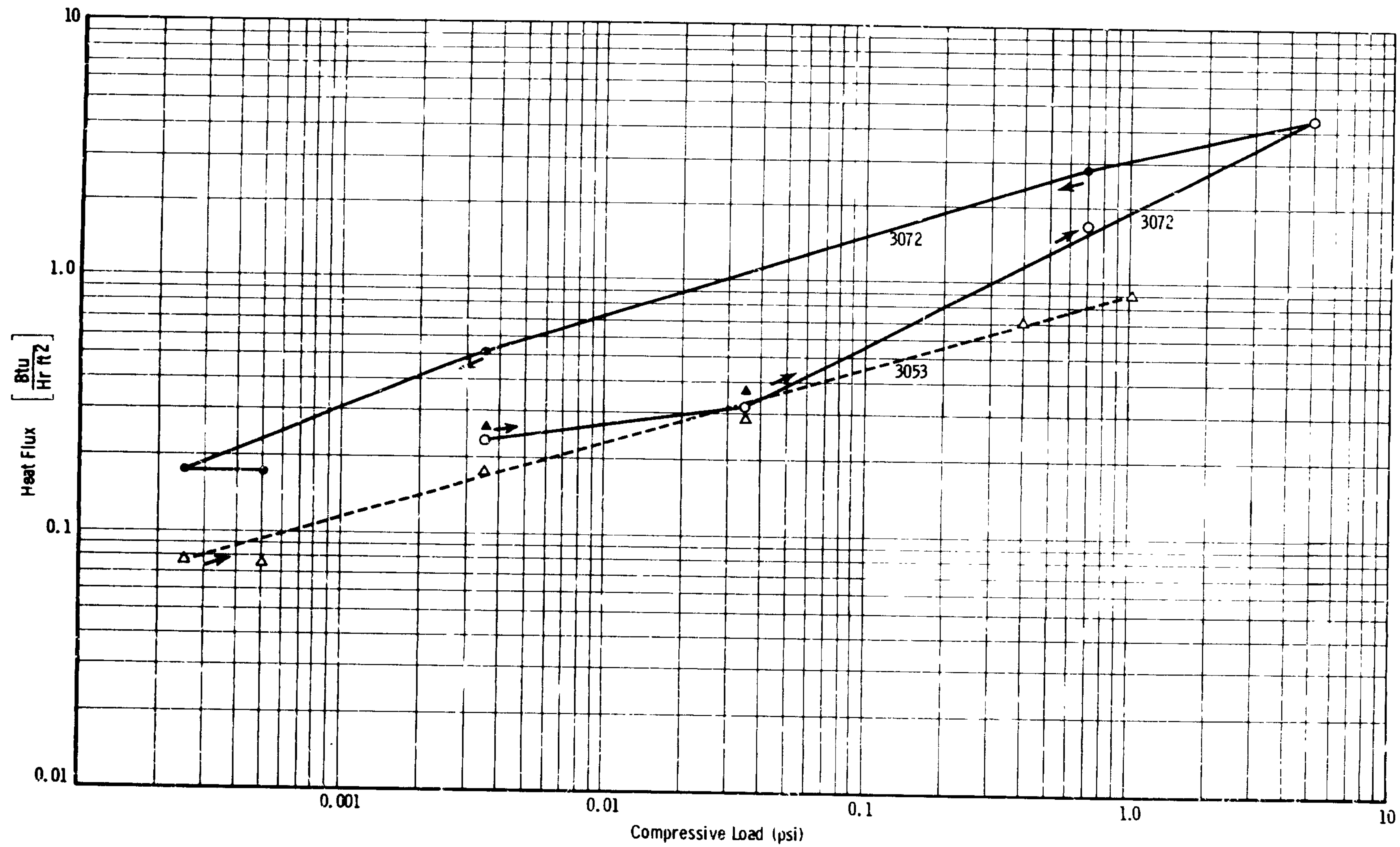

FIGURE II-27 EFFECT OF COMPRESSION ON THE HEAT FLUX THROUGH A MULTI-LAYER INSULATION WITH COMPOSITE FOAM SPACER area of contact between adjacent radiation shield and the spacer. We estimate that the bridging begins to influence the heat flux for compressive load above 0.04 psi, causing the slope of the line to increase. The section of the line corresponding to the heat flux at a compressive load of zero may actually have been recorded at a compressive load higher than zero but below the sensitivity of the apparatus. The heat flux was measured at the maximum separation of the cold and warm plates. By decreasing the plate separation only 0.025-inch, the heat flux increased to 0.16 Btu/hr ft^2. If the plate separation would have been increased slightly a lower heat flux may have resulted. Original minimum heat flux (in test 3053) was achieved at a plate separation of 1.266 inches. Adding 0.210-inch for the soft cushion we expect to reach the same condition at 1.476-inch between plates. The maximum available plate separation was 1.464 or 0.012 below the required value.

To see if the heat flux remains the same when a compressive load was applied with an inflatable cushion (see Figure II-6) to the sample rather than with a soft pad, tests No. 3073 and 3074 were run on system 10 (Figure II-18).

Test No. 3073 (Table II-16) was run with three layers of a 0.070-inch thick polyurethane flexible foam placed on top of the warm plate. The same system was compressed with an inflatable cushion in test No. 3074. The test results are shown in Table II-22 and are compared with results of test 3073 in Figure II-28.

The lower heat flux for corresponding loads applied by an inflatable cushion may be caused by the fact that the top of the inflatable cushion may be more rigid than the soft flexible foam, causing less bridging between the contact points.

6. Variation of Heat Flux Due to Change in Number of Shields

We conducted tests of two samples (#3075 and 3076) in support of our insulated tank program. One sample (system 14) consisted of five 0.0005 inch thick silver-coated polyester radiation shields with six spacers of 0.003 inch thick silk netting with 0.100 inch thick x 1/4 inch wide x 2 inch long flexible polyurethane foam (Scott Paper Company)

TABLE II-22 APPLICATION OF COMPRESSIVE LOAD WITH AN INFLATABLE CUSHION

Sample No. 3074 (same as 30/3), System 10.

Sample Description:	Ten radiation shields of 0.00025" thick x 11" diameter polyester film, aluminum coated on both sides and eleven spacers of 0.003" thick x 12" diameter silk netting with 0.100" thick x 1/4" wide x 2" long rigid polyurethane foam strips heat sealed to netting by a polyester film strip
Sample Weight:	0.055 lb
Sample Chamber Pressure:	Below 5×10^{-5} torr
Warm and Cold Plate Emittance:	0.9
Warm Plate Temperature:	70 ± 5°F
Cold Plate Temperature:	-320°F
Comments:	An inflatable flexible cushion (made by Goodyear Co.) was placed between the test sample and warm plate. Three thermocouples were mounted on the upper (toward the sample) face of the cushion. The temperature of these thermocouples was monitored at 70°F. The compression on the sample was applied by inflation of the cushion.

Mech. Comp. On Sample psi	Heat Flux Btu/hr ft^2	Distance Between Plates in	Test Date	Test No.
0.08	0.59	1.417	2/16/66	a
0.01	0.31	1.417	2/17/66	b
0	0.13	1.471	2/17/66	c

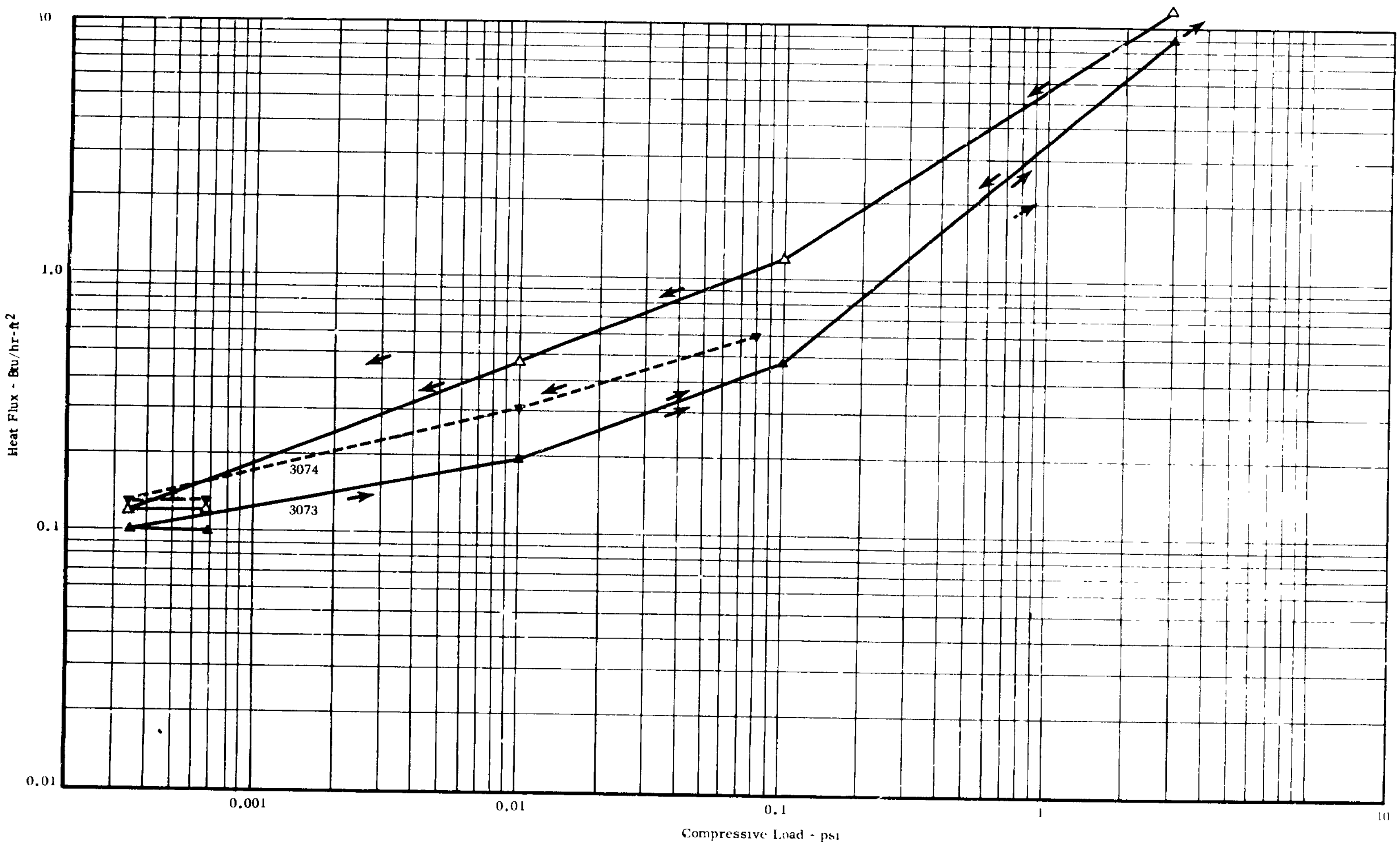

FIGURE II-28 EFFECT ON THE HEAT FLUX OF A COMPRESSIVE LOAD APPLIED BY ELASTIC OR INFLATABLE CUSHION strips heat sealed to the netting by a polyester film strip. A ten shield sample from the same materials was tested to assure that the performance of a five shield sample can be predicted from the test results of a ten shield sample. Table II-23 presents the results of these tests. The lowest heat flux obtained for a five shield sample was 0.26 Btu/ft^2 hr. Because a ten shield sample is more compressed by its own weight than a similar five shield sample, we expected the heat flux through a ten shield sample to be higher than one-half the heat flux through the five shield sample. Applying a correction for the extra compression we estimated the heat flux through the ten shield sample to be approximately 0.18 Btu/ft^2 hr. The experimental results supported the estimated value.

Theoretical lines shown in Figure II-7 of Reference (1) could be corrected in the same manner, which would provide a far better correlation between these lines and the emperimental points plotted in the same figure.

7. Development of New Radiation Shields

a. Effect of Radiation Shield Quality

We tested sample No. 3047 which was identical to sample No. 3041 (see Section II-D-2-c) except that the radiation shields were made from the newly received batch of aluminized polyester film manufactured to our specifications. The radiation shields for the tank insulation system (see Section IV) were made from the same batch of material.

Test results are presented in Table II-24.

The sample was subjected to compressive loads from 0 to 15 psi. The results of the tests are plotted in Figure II-29. Test results for sample No. 3041 are plotted in the same figure for reference. The heat fluxes for sample No. 3047 are consistently lower (except for 1.0 psi compression) than the heat fluxes for corresponding compression applied to sample No. 3041. However, comparing the thermal performance of the two samples based on the density (see Table II-25) we observe that the correspondence between the heat flux and density is much closer than between heat flux and compression. This can be explained by a poorer

TABLE II-23 EFFECT OF RADIATION SHIELD NUMBER

Sample Description: Radiation shields: 0.0005 inch thick x 11 inch diameter polyester film silver coated both sides; spacers: 0.003 inch thick x 1¼ inch diameter silk netting with 0.100 inch thick x 1/4 inch wide x 2 inch long flexible polyurethane foam (Scott Paper Company) strips heat sealed to netting by a polyester film strip.

Sample Chamber Pressure: Below 1×10^{-5}

Warm and Cold Plate Emittance: 0.9

Warm Plate Temperature: $70^{\circ} \pm 5^{\circ}F$

Cold Plate Temperature: $-320^{\circ}F$

No. of Spacers	No. of Radiation Shields	Weight of Sample lb.	Mech. Compr. on Sample	Heat Flux $\frac{Btu}{Hr\ ft^2}$	Sample Thk'n (inch)	Test Date	Test No.
6	5	0.041	0	0.26	0.861	2/19/66	3075a
			0	0.26	0.808	2/21/66	3075c
			0	0.31	0.784	2/22/66	3075d
			0.01	0.37	0.584	2/22/66	3075f
			0.10	1.06	0.416	2/23/66	3075g
11	10	0.076	0	0.16	1.365	2/25/66	3076b
			0	0.18	1.340	2/27/66	3076c
			0	0.17	1.397	1/3/66	3076d

TABLE II-24 TEST RESULTS

Sample No. 3047 (Same as 3041 with shields prepared by other manufacturer), System 11.

Sample Description:	Ten radiation shields of 0.00025" thick x 11" diameter polyester film, aluminum coated on both sides and twenty-two 0.001" thick x 12" diameter glass fabric spacers
Sample Weight:	0.0788 lb
Sample Chamber Pressure:	Less than 5×10^{-6} torr
Warm and Cold Plate Emittance:	0.9
Warm Plate Temperature:	70° ± 5°F
Cold Plate Temperature:	-320°F

Mech. Comp. on Sample psi	Sample Density lb/ft^3	Heat Flux $Btu/hr\ ft^2$	Thermal Conductivity $Btu\text{-}in/hr\ ft^2\ °F$	Sample Thickness in	Test Date	Test No.
0	5.2	0.216	0.13×10^{-3}	0.236	7/19/65	a
0.005	7.6	0.311	0.13×10^{-3}	0.164	7/20/65	b
0.01	8.0	0.329	0.13×10^{-3}	0.155	7/21/65	c
0.1	23	5.75	1.2×10^{-3}	0.054	7/22/65	d
1.0	27	42.4	5.0×10^{-3}	0.046	7/22/65	e
15	48	105.7	7.0×10^{-3}	0.026	7/22/65	f
1.0	28	75.0	8.6×10^{-3}	0.045	7/22/65	g
0.1	25	12.4	1.6×10^{-3}	0.049	7/22/65	h
0.01	21	2.68	0.40×10^{-3}	0.058	7/22/65	i
0	10	0.344	0.10×10^{-3}	0.120	7/23/65	j

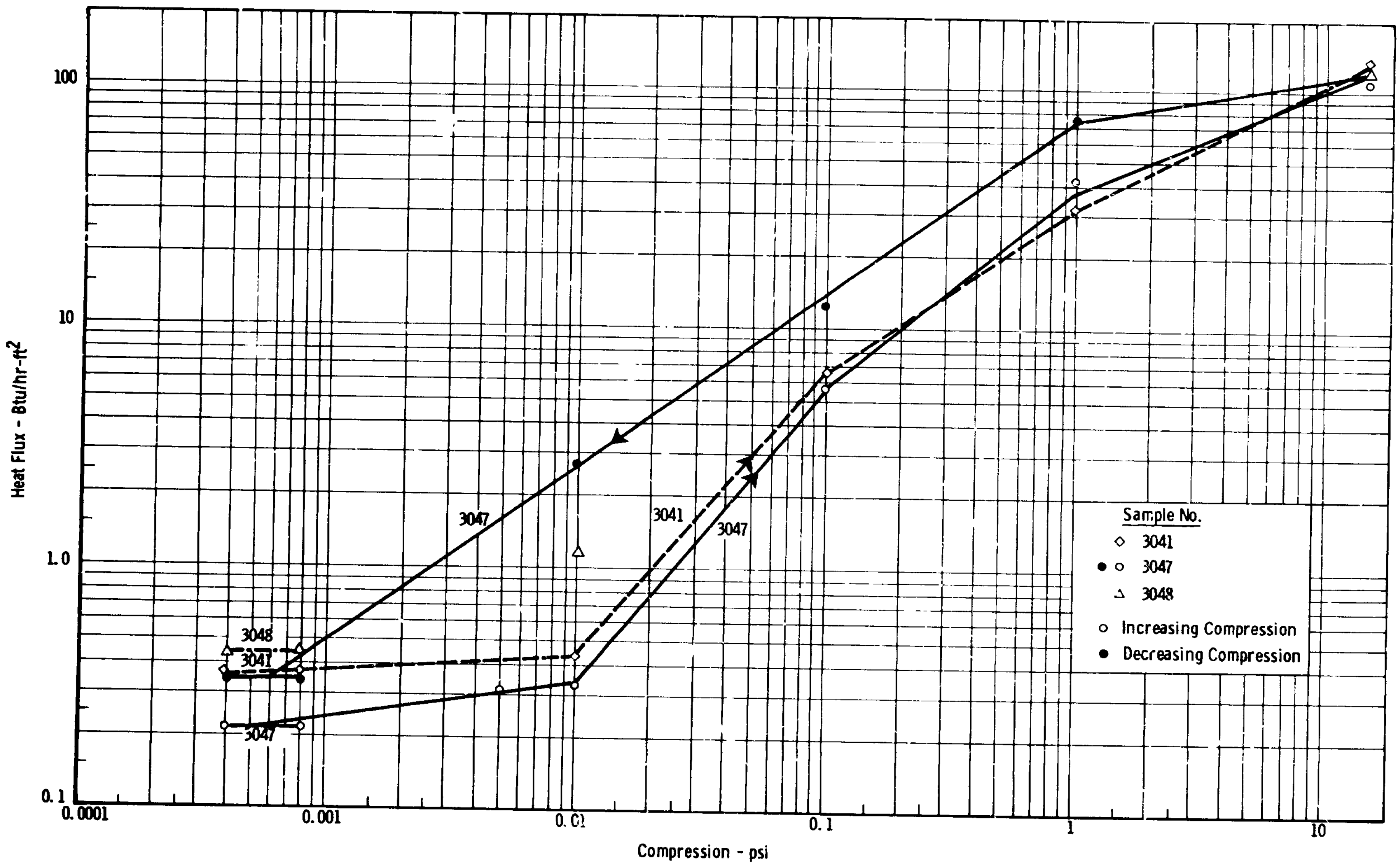

FIGURE II-29 EFFECT OF RADIATION SHIELD QUALITY

TABLE II-25 COMPARISON OF THERMAL PERFORMANCE BASED ON DENSITY

	Sample No. 3047		Sample No. 3041	
Compression psi	Density lb/ft^3	Heat Flux $Btu/hr\ ft^2$	Density lb/ft^3	Heat Flux $Btu/hr\ ft^2$
0.01	8	0.329	11.4	0.44
0.1	23	5.75	25.2	6.6
1.0	27	42.4	33.1	32
15	48	106	48.3	126
0	10	0.344	9.65	0.35

precision of the low load device during the test of sample No. 3041. As described in Section II-C-6 of this report, several revisions were made to improve the performance of the low load device.

Studying Figure II-29 the following observation can be made in regard to the test results:

Both samples, even though tested several months apart, show identical shape of the plot. The plot of heat flux versus external compression recorded for increasing compression is not a straight line. An explanation may be in the fact that two pieces of woven mat were placed together to form one spacer, under compression the mats may have slipped sideways from their original position. This may also explain the heat flux being much higher for all corresponding compression when the load on the sample was decreasing.

b. Effect of Perforations

Table II-26 presents the description and test results for Sample No. 3048. This sample is identical to Sample No. 3047 except that the radiation shields were perforated (2% open area) with 0.047 diameter holes.

The heat fluxes through Sample No. 3048 are higher for low compressive loads than the corresponding heat fluxes for Sample No. 3047 with unperforated shields; while for compression above 1 psi, when the conduction component of the heat flux is considerably higher than the radiation component, the heat flux for both samples are nearly identical. According to the results of the tests run on the ADL Emissometer, the emissivity of the unperforated shield is approximately 1/2 of that for the perforated shield.

Comparing the ratio of the emissometer results to the ratio of heat flux through the ten shield samples measured by the calorimeter at 0 compression, we find that the ratios are in both cases nearly the same. Examining the theoretical predictions made in Reference (7) Figure II-VI-10, we expect for the shields perforated with small diameter holes and 2% open area the heat flux to increase by a factor of two compared to the heat flux through unperforated shields.

TABLE II-26 EFFECT OF PERFORATION ON THE HEAT LOSS THROUGH A MULTILAYER INSULATION WITH GLASS FABRIC SPACER

Sample No. 3048, System 11

Sample Description: Same as Sample 3047, except perforated radiation shields were used

Sample Weight: 0.0781 lb

Sample Chamber Pressure: Less than 1×10^{-5} torr

Warm and Cold Plate Emittance: 0.9

Warm Plate Temperature: 70°F

Cold Plate Temperature: -320°F

Mech. Comp. on Sample psi	Sample Density lb/ft^3	Heat Flux $Btu/hr\ ft^2$	Thermal Conductivity $Btu\text{-}in/hr\ ft^2\ °F$	Sample Thickness in	Test Date	Test No.
0	6.0	0.437	0.23×10^{-3}	0.207	7/27/65	a
0.01	14	1.15	0.22×10^{-3}	0.086	7/28/65	b
1.0	31	41.2	4.2×10^{-3}	0.040	7/28/65	c
15	35	120	11×10^{-3}	0.035	7/28/65	d
0	5.8	0.522	0.28×10^{-3}	0.210	7/29/65	e

We conclude that the correlation between the data received in the thermal conductivity apparatus, emissometer and the theoretical estimates is very good.

8. Edge Effects

a. NASA Composite Sample

After the calorimeter was checked out, we began the first series of tests on system 15 sent to us by NASA Lewis Research Center. The materials used in this sample and the order of assembly were shown in Figure II-21. The data which we received in our first test (No. 3038) are presented in Table II-27. The observed heat flux was three times higher than that measured by NASA during the test of the same sample in calorimeter No. 1 in Cleveland.

The increase in heat flux was due to the thermal radiation from the 300°K wall of the vacuum jacket to the edge of the sample. The sample had no edge guarding buffer zone, and the low compressive load device had no radiation guard shield at the sample edges. With NASA approval, we cut the radiation shields of the sample to a 10-1/2-inch diameter, which provided a 3/4-inch wide buffer zone. The ratio of the buffer zone width to the thickness of the sample was 1 to 1, which was only one-half that indicated by theoretical considerations. Therefore, in addition, we installed a three-piece radiation guard shield described in Section II-C-6-b on the low compressive load device.

The test No. 3039 (see Table II-17) made after these changes showed the heat flux through the sample to be 0.43 Btu/ft^2 hr. This value is approximately the same as that obtained at NASA earlier when the sample was tested in calorimeter No. 1 in Cleveland (Sample 1069).

9. Effect of Penetration on the Heat Flux through the Evacuated Multi-Layer Insulation

We performed tests on two typical evacuated multi-layer insulations (systems 3 and 4) each system had 10 radiation shields made from 0.00025-inch thick polyester film aluminized on both sides and eleven spacers. System 3 had 0.020-inch thick foam spacers (foam supplied by

TABLE II-27 TEST RESULTS

Sample No. 3038 (former 1069), System 15

Sample Description: (1) 0.020" thick polyurethane foam spacer (directly under the cold plate) +
(3) Subassemblies, each consisting of:
(2) 0.002" thick mylar-aluminum-mylar laminated boundaries
(1) 0.008" thick Fiberglas layer (first toward cold boundary)
(3) 0.00025" thick mylar shields, aluminized both sides
(3) 0.020" thick polyurethane foam spacers

External Compression of the Sample: Below 0.01 psi, not measurable

Sample Chamber Pressure: Less than 1×10^{-5} torr

Warm Plate Emissivity: 0.9

Cold Plate Emissivity: 0.9

Warm Plate Temperature: 41 ± 1°F

Cold Plate Temperature: -320°F

Sample Thickness in	Heat Flux Btu/hr ft^2	Test Date	Test Number
0.919	1.65	3/23/65	a
0.902	1.40	3/24/65	b
0.750	1.24	3/25/65	c

Union Carbide Corporation). Each spacer for system 4 consisted of 0.003-inch thick silk netting sandwiched between two 0.008-inch thick glass paper sheets.

The structure of the second sample permitted us to keep the total thickness of each spacer approximately 0.019-inch, or nearly the same as that of one foam spacer.

Eleven penetration experiments were carried out; three were made on system 4 and eight on system 3. The conditions for each test are described in Tables II-28 and II-29 and repeated in Tables II-30 and II-32 for easy reference. In the various tests, nylon and stainless steel pins and stainless steel tubes were used. Various methods of attaching these penetrations to the warm and cold plates were tried; also, the hole size cut in the radiation shields and sample thicknesses were varied.

The data may be analyzed in a simple manner and the predicted increase in heat flux correlated well with the actual measured values. The theory is discussed below in section d and a comparison between values determined from theory and experiment is made last.

a. Effect of the Buffer Zone on an Unpenetrated Sample

To study the effect of a buffer zone on the heat flux through the multi-layer insulation, we began with testing samples of the two insulations described above in the virgin (uncut) condition. Later we cut a hole in the center of each radiation shield, reassembled and tested the samples again. No hole was cut in the spacers.

The radius of the hole was selected in accordance with theoretical considerations which show that an effective buffer zone for a pure aluminum radiation shield must be twice the thickness of the sample.

Tables II-30 and II-31 show the test results for the two systems. Examining the tables we find:

Removal of the radiation shields from the buffer zone causes a large increase in the heat loss through the samples. For the sample with the foam spacer, the heat loss is increased by 0.266 Btu/hr which is equivalent to the heat loss through approximately 3.3 sq ft of the

TABLE II-28 HEAT LOSS THROUGH A GLASS FIBER SPACED MULTILAYER INSULATION PENETRATED BY A PIN

Sample Description:	Ten radiation shields of 0.00025" thick x 11" diameter polyester film, aluminum coated on both sides and eleven 12" diameter, 0.003" thick silk nettings with twenty-two 12" diameter, 0.008" thick glass paper disks placed on both sides of silk netting
Sample Weight:	0.213 lb (uncut)
Sample Chamber Pressure:	Below 1×10^{-5} torr
Warm and Cold Plate Emittance:	0.9
Warm Plate Temperature:	$70 \pm 5^{o}F$
Cold Plate Temperature:	$-320^{o}F$

Buffer Zone Diameter (inch)	Penetration	Heat Flux (Btu/hr)	Sample Thickness (inch)	Date	Sample No.
0	none	0.046	0.567	8/19/65	3051
2.51	none	0.155	0.571	8/24/65	3052
2.51	0.020" dia s.s. pin	1.15	0.599	9/22/65	3056
2.51	0.032" dia nylon pin	1.00	0.576	9/28/65	3058
2.51	0.020" dia s.s. pin	1.10	0.599	10/17/65	3060

TABLE II-29 HEAT LOSS THROUGH FOAM SPACED MULTILAYER INSULATION PENETRATED BY A PIN

Sample Description: Ten radiation shields of 0.00025" thick x 11" diameter polyester film, aluminum coated on both sides and eleven 12" diameter, 0.020" thick polyester foam (Union Carbide Corp.) spacers

Sample Weight: 0.047 lb (uncut)

Sample Chamber Pressure: Below 1×10^{-5} torr

Warm and Cold Plate Emittance: 0.9

Warm Plate Temperature: $70 \pm 5^{o}C$

Cold Plate Temperature: $-320^{o}F$

Buffer Zone Diameter (inch)	Penetration	Heat Flux (Btu/hr)	Sample Thickness (inch)	Date	Sample No.
0	none	0.0172	0.407	9/16/65	3054
1.88	none	0.283	0.408	9/19/65	3055
1.88	0.020" dia s.s. pin x 0.716 lg	0.468	0.436	10/15/65	3062
0.25	0.020" dia s.s. pin x 0.716 lg	0.122	0.416	10/28/65	3065
0.040	0.020" dia s.s. pin x 0.716 lg	0.106	0.414	11/6/65	3066a 1# force
0.040	0.020" dia s.s. pin x 0.716 lg	0.118	0.414	11/7/65	3066b 2# force
1.88	0.020" dia s.s. pin x 0.602 lg	0.416	0.414	11/16/65	3067 Hot plate mount
1.88	0.020" dia s.s. pin x 0.420 lg	0.473	0.384	11/22/65	3068b

TABLE II-30 HEAT LOSS THROUGH A MULTILAYER INSUALTION WITH A GLASS FIBER BUFFER ZONE

Sample Description:	Ten radiation shields of 0.00025" thick x 11" diameter polyester film, aluminum coated on both sides and eleven 12" diameter, 0.003" thick silk nettings with twenty two 12" diameter, 0.008" thick glass paper disks placed on both sides of silk netting
Sample Weight:	0.213 lb (uncut)
Sample Chamber Pressure:	Below 1×10^{-5} torr
Warm and Cold Plate Emittance:	0.9
Warm Plate Temperature:	$70 \pm 5^{o}F$
Cold Plate Temperature:	$-320^{o}F$

Buffer Zone Diameter (inch)	Heat Flux (Btu/hr)	Sample Thickness (inch)	Date	Sample No.
0	0.046	0.567	8/19/65	3051
2.51	0.155	0.571	8/24/65	3052

TABLE II-31 HEAT LOSS THROUGH A MULTILAYER INSULATION WITH FOAM BUFFER ZONE

Sample Description:	Ten radiation shields of 0.00025" thick x 11" diameter polyester film, aluminum coated on both sides and eleven 12" diameter, 0.020" thick polyester foam (Union Carbide Corp.) spacers
Sample Weight:	0.047 lb (uncut)
Sample Chamber Pressure:	Below 1×10^{-5} torr
Warm and Cold Plate Emittance:	0.9
Warm Plate Temperature:	$70 \pm 5^{\circ}C$
Cold Plate Temperature:	$-320^{\circ}F$

Buffer Zone Diameter (inch)	Heat Flux (Btu/hr)	Sample Thickness (inch)	Date	Sample No.
0	0.0172	0.407	9/16/65	3054
1.88	0.283	0.408	9/19/65	3055

uncut insulation. For the other sample, the heat loss is increased by 0.109 Btu/hr which is equivalent to the heat loss through approximately 1/2 sq ft of the uncut insulation. (Note that the efficiency of the multi-layer insulation layer with glass paper is poorer than that of the insulation spaced with foam.)

Calculations show that the heat which would pass by radiation through an empty hole of the diameter equivalent to the diameter of the buffer zone (1.88-inch diameter for foamed spaced sample and 2.51-inch diameter for glass paper spacer) between the boundaries of the same emissivity (0.9) as that of the warm and cold plates of the thermal conductivity apparatus is 2.1 Btu/hr and 3.7 Btu/hr, respectively.

The tests indicate that both spacers intercept a large percentage of radiation. Denser glass paper provides a better radiation barrier than the less dense foam.

A fair correlation of these test results can be achieved by assuming that heat flux through the buffer zone is independent of the heat flux through the multi-layer insulation, and that the total heat flux through the system is simply a summation of the two. See further discussion of this subject in Section IID-9d.

b. Influence of Sample Assembly Method on the Heat Flux through the Sample with a Pin

We installed penetrations into samples Nos. 3052 and 3055 which were already provided with buffer zones described in the previous section.

The upper end of a 0.020-inch diameter stainless steel pin penetration was screwed into the cold plate of the test apparatus. The pin was made 0.020-inch longer than the thickness of the sample measured under zero external compressive load during the testing of the samples described above. The pin was forced through the center of each sample. The lower end of the pin was brought into contact with the surface of the warm plate.

Addition of a 0.020-inch diameter stainless steel penetration to samples Nos. 3052 and 3055 increased the total heat flow passing through the samples by 1.0 Btu/hr and 1.5 Btu/hr, respectively, for glass paper and foam spaced systems. Calculations show that the heat expected to be conducted through 0.020-inch diameter, 0.42-inch long stainless steel pin alone is only 0.18 Btu/hr.

A gross discrepancy between the estimated and experimental results was obvious. To check if this discrepancy can be attributed to the relatively high conductance of the stainless pin, a 0.032-inch diameter nylon pin instead of the stainless pin was installed in both insulation systems.

Substitution of the stainless steel pin by a nylon pin decreased the heat loss through the sample spaced with glass paper by 0.15 Btu/hr or approximately by the difference between conduction of stainless steel and nylon pins. However, in the case of the foam spaced system, the heat flux was decreased by 0.75 Btu/hr for the same substitution of the pins.

The test results seem to indicate that the method of assembly, a local compression of the sample caused by the pin, or a thermal coupling between the pin and the sample, may have adversely influenced the system performance.

To eliminate the possibility that the unexpectedly high heat flux was due to a local compression caused by forcing the pin through the sample, we changed the procedure for assembly of the test sample. Previously, we forced the pin (installed in the cold plate of the calorimeter) through the center of the sample after the latter was completely assembled. The new procedure called for the following six steps:

(1) Punch an 0.045-inch diameter hole through the center of each spacer.

(2) Assemble the sample over a hori ontal 12-inch diameter disc with an 0.042-inch o.d. x 0.025-inch i.d. tubing placed vertically in the center of the disc.

(3) Move the sample with the disc into the calorimeter and insert the 0.020-inch diameter S.S. pin into the 0.025-inch i.d. tubing.

(4) Pull the tubing out, leaving the sample on the pin.

(5) Bring up the warm plate within 1/16 inch below the lower end of the sample.

(6) Remove supporting disc.

This procedure diminishes the chance that the sample is constrained by the pin from moving freely in the vertical direction, and causing local compression of the sample. Sample No. 3060 was assembled using the new procedure. The results of the test are shown in Table II-30 along with results of other tests on similar samples. Since the heat flux through sample No. 3060 was approximately the same as that through sample No. 3056, we concluded that this method of assembly was still not satisfactory.

Examining sample No. 3060 after the test, we noticed the ease with which the lower spacers can slip from the pin which has a length equal to the thickness of the sample. To prevent the slippage of the lower layers of the sample from the pin, we extended the length of the pin 0.300 inch past the lower layer of the sample and drilled an 0.300-inch deep hole in the center of the warm plate. This arrangement permitted us to bury the end of the pin in the warm plate before the disc supporting the sample against the cold plate during the assembly is removed (Step 6 above).

The hole in the warm plate was tapped (the same as the hole in the center of the cold plate) which will allow us to anchor the same pin into the cold or warm plate at will.

The results of the test on sample No. 3062, which was identical to sample No. 3057, except for the length of the pin, is shown in Table II-32. Results of previous tests of the same insulation system with the pin are also shown in the same table for comparison.

The heat loss through the system with a longer pin was four times smaller than the heat flux through the same system with a shorter pin. We cannot explain the decrease in heat flux by an increase in the pin length. Therefore, we concluded that an improved method of assembly possible with a longer pin was responsible for the decrease in the heat flow.

As discussed later in section d, the total heat flux through sample No. 3062 can be easily estimated by a single summation of heat fluxes which are expected to pass through each separate component of the

TABLE II-32 EFFECT OF THE PIN LENGTH ON THE HEAT FLUX THROUGH A FOAM SPACED MULTILAYER INSULATION PENETRATED BY A PIN

Sample Description:	Ten radiation shields of 0.00025" thick x 11" diameter polyester film, aluminum coated on both sides and eleven 12" diameter, 0.020" thick polyester foam (Union Carbide Corp.) spacers
Sample Weight:	0.047 lb (uncut)
Sample Chamber Pressure:	Below 1×10^{-5} torr
Warm and Cold Plate Emittance:	0.9
Warm Plate Temperature:	$70 \pm 5^{o}C$
Cold Plate Temperature:	$-320^{o}F$

Buffer Zone Diameter (inch)	Penetration	Heat Flux (Btu/hr)	Sample Thickness (inch)	Date	Sample No.
1.88	0.020" dia s.s. pin x 0.426" lg	1.816	0.426	9/24/65	3057
1.88	0.020" dia s.s. pin x 0.716" lg	0.468	0.436	10/15/65	3062

assembly; i.e., through the pin, through the buffer zone, and through the rest of the multi-layer insulation.

c. Effect of the Buffer Zone on the Heat Flux through a Sample with a Penetration

To observe the effect caused by a decrease in the diameter of the buffer zone on the heat flux through a multi-layer insulation penetrated by a pin, we assembled and tested sample No. 3065. This sample used 0.020-inch thick foam for the spacers and was similar to sample No. 3062, except that the diameter of the hole cut in the center of each radiation shield was decreased from 1.88 inches to 1/4 inch. Result of the test is shown in Table II-29 The total heat flux through the sample is reduced by a factor of four when compared to the heat flux through sample No. 3062. The experimentally obtained heat flux corresponds closely to the one estimated for the theoretical model developed in section d.

To check if this trend continues when the buffer zone width is further decreased, we tested sample No. 3066. We punched an 0.040-inch diameter hole in the center of each radiation shield of this sample. All the spacers already used in earlier tests had 0.040-inch diameter holes in the center. The test results were presented in Table II-29. For reference, we show in the same table, test results for samples No. 3062 and 3065. We concluded from these tests that for a system consisting of a multi-layer insulation using metal coated polyester film radiation shields and a small diameter low conductivity pin placed between the same temperature boundaries as the insulation layer, no buffer zone is required. An addition of a buffer zone to a system described above merely increases the total heat flux in proportion to the diameter of the buffer zone.

Note that basically the same conclusion can be drawn from examining tests of sample No. 3049 which was penetrated by a series of nylon threads and sample No. 3050 with nylon threads removed (see Section IID-2, page II-54).

To examine whether contact pressure between the end of the pin and the warm plate will significantly change the total heat flux through the pin-insulation system, we pressed the warm plate against the pin with one and then two lbs force (tests Nos. 3066a and 3066b). Assuming the end of the pin is flat, these forces produce 3,300 psi and 6,600 psi pressure on the pin. We observed no significant change in the total heat flux through the system.

To investigate further the influence of contact resistance between the plate and the pin on the total heat flux through the pin-insulation system, we screwed the pin into the warm plate and pressed the other end of the pin against the cold plate. Test No. 3067 in Table II-29 shows the results of the run. Comparing this result to the result of test No. 3062, which was performed with the pin mounted in the cold plate, we find only a 10% decrease in the heat flux. These two tests (Nos. 3066b and 3067) indicate that the contact between the end of the pin and the calorimeter plates is acceptable. Test No. 3067 also supports our belief that unexplainably high heat fluxes received during tests Nos. 3057 and 3059 were caused by an improper assembly of the samples.

To satisfy ourselves again that the high heat flux received in test No. 3057 can be explained only by assuming that the sample was improperly assembled, we tested sample No. 3068 which was assembled in exactly the same way as sample No. 3062, but the length of the pin was shortened to 0.420-inch long (same as in sample No. 3057). Unfortunately, when attempting to free one of the dial indicators on the low load device, we must have bent the pin since only when we reached the thickness of 0.384 were we able to feel compression exerted on the top of the pin. When the apparatus was opened, we found the pin to be bent. However, in spite of the fact that the sample was compressed 0.020 inch beyond the point which we believed to be zero compression, the total heat flux through the system was approximately the same as during test No. 3062 (sample with a 0.300-inch longer pin) and only 1/4 of the heat flux experienced during test No. 3057.

d. Correlation of the Results

The experimental heat flux values for various sizes and types of pin penetrations have been presented in the previous Section in Tables

II-28 and II-29. Before attempting to interpret these results, it is well to emphasize that (a) the temperature of the penetration's ends was fixed and known in all tests, and (b) the penetrations were made from low conductivity material. In many actual applications of multi-layer insulations, the temperature of the penetration's warm end is not known and is certainly less than the outer shield temperature, and, in addition, the penetrations could be made of high conductivity materials. The model we suggest below may well have to be modified for such conditions, but only an experimental program can determine the degree of modification.

Assumptions for establishing a model which will allow an estimation of heat leak through the multi-layer insulation penetrated by a pin are as follows:

(1) The penetration cross section, length, and physical properties are known. A good thermal contact is maintained between the pin and the cold surface. The temperature of the hot end of the penetration is known (or estimated by some external heat transfer analyses).

(2) The spacer material is not removed from the buffer zone even though the shields may be cut to make the shield perforation area-to-penetration area ratio quite large. There is no limitation as to the size of the hole in the shield compared to the penetration hole (except, of course, it cannot be smaller) and, in fact, the shields may touch the penetration in one or more places.

(3) The penetration holes are "lined-up".

We will discuss later in this section some of the effects of modifying these ground rules.

(1) Suggested Model

While we realize that the computation of penetration heat leaks in multi-layer insulations is, in theory, very difficult when possible interactions between the shields, spacers, and penetrations are considered, we were motivated to suggest first a simple model to determine the degree of sophistication necessary. Fortunately, we found that in essentially all cases studied experimentally, a simple model yielded quite satisfactory results. The model is outlined below:

The heat leak through a multi-layer insulation containing low-conductivity penetrations may be calculated by summing, separately, the heat leaks for:

(a) the insulated area containing no penetrations;

(b) the penetration;

(c) the buffer zone--the area not containing the penetration but where the radiation shields are perforated. We assume that the buffer zone contains spacer material but no radiation shield material.

In this model, we have purposely omitted any interaction effects. The actual computation of the three heat flux components outlined above in (a) through (c) is discussed and the sum compared to measured values.

These components are designated in Equation 3 below:

$$Q_T = Q_p + Q_h + Q_o\ (A_T - A_h)/A_T \qquad (3)$$

where Q_T = total heat leak through the system;

Q_p = heat leak through the penetration(s) only;

Q_h = heat leak due only to conduction in the spacer material of the buffer zone;

Q_o = heat leak through the same multi-layer insulation containing no penetrations;

A_T = total cross sectional area of the sample;

A_h = total cross sectional area of the buffer zone.

The heat flux for the unpenetrated insulation, Q_o, is determined experimentally or from standard estimation methods. The heat leak through a constant area penetration, Q_p, is determined from Fourier's Law:

$$Q_p = \frac{A_p}{L_p} \int_{T_{cold}}^{T_{hot}} k_p \, dT \qquad (4)$$

where A_p = the cross sectional area of the penetration;

L_p = the penetration length;

k_p = the penetration conductivity.

Heat leak through the buffer zone, Q_h, is assumed to be:

$$Q_h = \frac{(A_h - A_p)}{L} k_h(T_{hot} - T_{cold}) \tag{5}$$

where L = actual cumulative thickness of all the spacers;

k_h = average conductivity of a system consisting of the spacer material without radiation shields.

(2) Comparison of Model with Experimental Results

(a) Parameters Constant in All Tests

(i) A_T is the total sample area, i.e., the area of a circle about 6-1/4 inches in diameter, = $\pi(6\text{-}1/4)^2/4$ = 30 sq in.

(ii) T_{hot} = 70°F

(iii) T_{cold} = -320°F

(iv) $\int_{-320}^{70} k_p dT \simeq$ 238 Btu/hr-in for stainless steel

$\simeq$ 6.6Btu/hr-in for nylon (this value may be low)

(b) Heat Flux through Insulation without Holes and Penetrations

From Tables II-28 and II-29, the value of Q_h for the two insulation systems studied in this work were found to be

Q_h = 0.046 Btu/hr and

Q_h = 0.017 Btu/hr, respectively.

(c) Heat Flux through Insulation with Holes but No Penetrations

If a hole is cut in the radiation shield, but the spacer left intact, and if the hole size is not large compared to the total insulation area, then an increase in heat flux is observed. The actual heat flux through a sample with the hole can be calculated from equation 3, with $Q_p = 0$. Equation 3 can be written in another form:

$$Q_T = q_T A_T = q_h A_h + q_o (A_T - A_h) \qquad (6)$$

or

$$q_h = q_T (A_T/A_h) - q_o (A_T - A_h)/A_h \qquad (7)$$

where $q_o = \frac{Q_o}{A_T}$ = heat flux in the insulation with no holes;

$q_T = \frac{Q_T}{A_T}$ = heat flux in the insulation with holes;

$q_h = \frac{Q_h}{A_h}$ = heat flux through the hole area;

A_h = hole area

A_T = total insulation area.

In our work, q_T was measured for insulation system 4 in test 3052 and for system 3 in tests 3055 and 3063. Values of q_h should be in the range of heat fluxes encountered with isotrophic (e.g., powder) insulations.

We compared, not our measured q_h, but rather the effective thermal conductivity, $k_h = (q_h/A_h)\ (\Delta X/\Delta T)$*, against typical values reported by the NBS between the same warm and cold temperatures. Typically, such NBS values of k_h ranged from 10 to 20 microwatts/cm-°K. In our tests 3052, 3055, and 3063, we measured values of k_h as 3, 11, and 30 microwatts/cm-°K. The variation is somewhat larher than desired. The low value was determined on the system using silk netting and glass paper spacers while the values of 11 and 30 were made on the system using polyurethane foam. The latter two values should have been identical. The only difference in the tests was the hole size; the larger value of k_h being associated with the smaller hole size. Apparently, there is some perturbation of the shield temperature distribution in the neighborhood of holes, and this effect is more pronounced for small holes,

* The value of ΔX to use in the equation was taken as the actual (uncompressed) thickness of the eleven spacers, i.e., for 0.020 inch thick polyurethane: $\Delta X = (11)(0.020) = 0.22$ in.

especially with the real experimental difficulties of lining up small diameter holes in an actual test.

Based upon the hole tests, we have chosen the values of k_h = 3 microwatts/cm-°K for system 3051 and 10 microwatts/cm-°K for large hole (>1 in) and 30 microwatts/cm-°K for holes <1 inch in insulation system 3054. These are reasonable values and minor variations would not significantly change the calculated total heat flux with penetrations present.

(d) Heat Flux Due to Penetrations

We have experimented with both stainless steel and nylon penetrations. Some of the stainless steel penetrations were pins while others were thin wall tubes packed with foam. The heat flux through the foam should be based on the $\bar{k}$ values determined for holes in the foam-spacer insulation system (3054) and since, for foam, we previously chose a value of k_p= 30 microwatts/cm-°K for those holes with a diameter less than 1 inch, that some value is chosen here for determining the heat flux through the tubes.

The incremental heat leak due to penetrations alone was assumed to be:

$$Q_p = A_p \; k_p(T) \; dT/dX_p \qquad (8)$$

or

$$Q_p = \frac{A_p}{L_p} \int_{T_c}^{T_h} k_p(T) \; dT \qquad (9)$$

Values of A_p and L_p may be determined from the data in Tables II-28 and II-29. T_h = 70°F = 530°R, and T_c = -320°F = 140°R are known from the same table. Thermal conductivity integrals were obtained from Reference (8). For stainless steel this integral is 238 Btu/in-hr and for nylon, 6.6 Btu/in-hr for a temperature range of 70 to -320°F. Table II-33 summarizes the calculated penetration heat leak for all tests as determined by Equation 9.

TABLE II-33

CALCULATED HEAT LEAK DUE ONLY TO PENETRATIONS

Test	A_p in^2	L_p in	$\int_{-320}^{70} k_p\,dt$ Btu/in-hr	Q_p Btu/hr
3062	3.14×10^{-4}	0.739	238	0.10
3065	3.14	0.739	238	0.10
3066	3.14	0.716	238	0.11
3067	3.14	0.602	238	0.12
3068	3.14	0.420	238	0.18
3070	8.0	0.423	6.6	0.012
3078	7.9	0.760	238	0.25
3079	8.0	0.810	6.6	0.006
3080	8.0	0.810	6.6	0.006
3081	7.9	0.760	238	0.25

(e) Combined Calculated Heat Fluxes

The total heat flux for insulations with both holes and penetrations is estimated from Equation 3. In both insulation systems tested the value of A_T is about 95 in^2.

The various contributions to Q_{tot} are shown in Table II-34.

(f) Comparison Between Calculated and Experimental Values

The last two columns in Table II-34 show the experimentally measured value of heat flux and the difference between the experimental and calculated values. The agreement is quite good. In some cases, the calculated heat leak depends predominantly on the penetration contribution; in other tests, the hole contribution predominates; and in the nylon pin tests, the bulk of the heat leak is through the non-perforated portion. Still, in all these cases, the simple calculational technique appears reliable.

Of course, this suggested procedure is not exact. No interaction between the holes, shields, pins, etc., has been taken into account. We simply suggest this method as a first, and reasonably reliable, technique to determine the effect of a penetration. We conclude that when the temperature at each end of the penetration is the same as that of the insulation boundary a large buffer zone is quite undesirable, especially if the spacer material alone (without radiation shields) is a poor insulator.

10. Support of the Tank-Calorimeter Program

Tests 3041, 3042, and 3071 (systems 11, 1 and 2) which are discussed in Section II-D-2-c; tests 3047 and 3048 (system 11) which are discussed in Section II-D-7-a and b; test 3069 (system 9) which is discussed in Section II-D-2-d; and, finally, tests 3075 and 3077 (systems 13 and 14) which are presented in Tables II-23 and II-35 were performed in support of the tank insulation program. Correlation of these tests with the results received from the tank experiments are discussed further in Section IV of this report.

TABLE II-34 COMPARISON OF CALCULATED AND EXPERIMENTAL VALUES FOR THE MULTILAYER INSULATION PENETRATED BY THE PIN

Test No.	Penetration Material	Penetration Description	Q_p Btu/hr	Hole Diameter in	A_h in^2	Q_h Btu/hr	$\frac{A_t - A_h}{A_t}$	$Q_o x (\frac{A_t - A_h}{A_t}) \frac{Btu}{hr}$	Q_t Btu/hr	Q_{meas} Btu/hr	$Q_t - Q_{meas}$ Btu/hr
3062	S.Steel	pin,0.020"	0.10	1.88	2.79	0.24	0.97	0.016	0.36	0.47	0.12
3065	"	" "	0.10	0.25	.049	0.013	>0.99	0.017	0.13	0.12	-0.01
3066	"	" "	0.11	0.040	.0013	<0.001	>0.99	0.017	0.13	0.12	-0.01
3067	"	" "	0.12	1.88	2.79	0.24	0.97	0.016	0.38	0.42	0.04
3068	"	" "	0.18	1.88	2.79	0.24	0.97	0.016	0.44	0.47	0.03
3070	Nylon	" ,0.032"	0.012	0.040	.0013	<0.001	>0.99	0.017	0.029	0.05	0.02
3078	S.Steel	tube,0.25"O.D. 0.001"thick	0.25	0.281	.062	0.016	>0.99	0.017	0.29	0.36	0.07
3079	Nylon	pin,0.032"	0.006	0.040	.0013	< .001	>0.99	0.046	0.052	0.063	0.01
3080	"	" "	0.006	0.281	.062	0.003	>0.99	0.046	0.055	0.042	-0.01
3081	S.Steel	tube,0.25"O.D. 0.001"thick	0.25	0.281	.062	0.016	>0.99	0.046	0.31	0.32	-0.01

TABLE II-35

TESTS OF A MULTILAYER INSULATION WITH GOLD COATED RADIATION SHIELDS

Sample No. 3077, System 13.

Sample Description: Five radiation shields of 0.00025" thick x 11" diameter polyester film, gold coated on both sides and 18 12" diameter, 0.003" thick silk netting

Sample Weight: 0.03#

Sample Chamber Pressure: below 5×10^{-5} torr

Warm and Cold Plate Emittance: 0.9

Warm Plate Temperature: 80°F 5°F (except during run "a" where temperature was 70°F)

Cold Plate Temperature: -320°F

MECHANICAL COMPRESSION PSI	SAMPLE DENSITY lb/ft^3	HEAT FLUX $Btu/hr\ ft^2$	THERMAL CONDUCTIVITY $\frac{Btu\text{-}in}{hr\ ft^2\ °F}$	SAMPLE THICKNESS inch	TEST DATE	TEST NO.
0	1.05	0.28	0.33×10^{-3}	0.453	3.6.66	a
0	1.05	0.32	0.36×10^{-3}	0.453	3.8.66	b
0.01	1.5	0.55	0.43×10^{-3}	0.315	3.8.66	c
0.10	5.3	2.11	0.46×10^{-3}	0.090	3.8.66	d

11. Effects of Gas Pressure on the Performance of Multi-Layer Insulation

In certain pressure ranges, the thermal conductivity of a multilayer insulation is strongly affected by the residual gas pressure. At high pressures, the effect is not important since in this range the gas conductivity is essentially independent of pressure; at very low pressures, there is a negligible amount of gas present and the conduction of heat through the gas is small compared to solid conduction and radiation effects. In between these two extremes, gas conduction plays an important role and the conductivity of gases in this range increases with an increase in pressure. The net result of these considerations is that a plot of k (effective) vs. pressure yields an "S" shape curve. We discuss below some of the pertinent results of existing theory and experiment and indicate the hazards of attempting to calculate *a priori* quantitative effects of pressure on the thermal effectiveness of any given insulation.

a. Theory

Many investigators have studied the problem of the effect of pressure on gas thermal conductivity; evacuated fibers and powders, and the simpler case of conduction between flat plates or coaxial cylinders have also been considered.

It is not the purpose of this brief section to review the papers in the field, although some representative papers are noted in the bibliography (9-16). Most of these papers and books allude the "S" curve referred to above. It is important to note, however, that even though different derivations are employed, all of the theoretical treatments reduce to the following form:

$$k_g = \frac{C_1}{1 + C_2 \frac{T^n}{Pd} \left(\frac{2-\alpha}{\alpha}\right)} \tag{10}$$

where k_g refers to the effective gas conductivity in the evacuated insulation;

C_1 is obviously the value of k_g as P becomes large;

C_2 is a constant which may incorporate knowledge about some particular insulation such as fiber size and density (for fiber insulations); C_2 also contains some dimensional constants. Values of C_2 for particulate or multi-layer shields are often assumed to be of the form(s)

$$C_2 = P_o L_o/T_o^n \tag{11}$$

where P_o, L_o, and T_o refer to a base set of conditions, i.e., the conditions P_o, T_o, where the gas mean free path L_o is measured;

T is the average temperature in the insulation;

P is the average pressure in the insulation;

d is the spacing between solid surfaces or between particles (in a particulate insulation such as powder);

n is a constant, often taken to be unity, but occasionally expressed as (n' + 0.5) where n' is obtained for various gases from the table on page 149 of reference 9;

α is the accommodation coefficient.

If one is interested in a particular insulation with fixed T, α, d, but with variable P, then Equation 10 becomes

$$k_g = \frac{C_1}{1 + C_2'/P} \tag{12}$$

where $C_2' = (C_2T^n/d)\ (2-\alpha)/\alpha$

Equation 12 when combined with other parallel conductances (i.e., of radiation k_r, and solid conduction k_s) will yield the typical "S" curve referred to above,

$$k = k_r + k_s + k_g \tag{13}$$

since k_r and k_s are not functions of gas pressure.

As usually plotted, so as to cover wide ranges, log k and log P are the usual variables. From Equation 12, it is easily seen that

$$(d \log k_g/d \log P) = \frac{1}{\frac{P}{C_2} + 1},$$

thus the slope of the curve log k_s vs log P is always less than unity. (Wang[6] has simplified Equation 12 to a form $k_g = C_3P$ so that he predicts a slope $(d \log k_g/d \log P)$ of unity.

The use of an equation of the type of 10 to express k_g is now generally accepted. The actual fitting of experimental data, a priori, with this equation (and with Equations 11 and 12) is, however, difficult. The reasons for this are discussed below.

b. Comparison of Equation 10 with Experimental Data

(1) Variables

(a) Pressure

The pressure referred to in Equation 10 is the pressure within the insulation. Ordinarily, however, it is measured exterior to the insulation and any gradient neglected. In a truly equilibrium situation, this assumption is warranted, but if much outgassing is taking place, then the interior pressure may be considerably greater than the exterior value.

(b) Temperature

No truly satisfactory way exists for defining the temperature to use in Equation 10. It is certainly less than the warm source and more than the cold sink, but the theoretical value to use depends upon the values of the accommodation coefficients. If $\alpha = 1$, then theory indicates that

$$1/T^{1/2} = 1/2 \left[\frac{1}{T_H^{1/2}} + \frac{1}{T_c^{1/2}}\right] \qquad (14)$$

where T_H and T_c refer to the source and sink temperature. Since α is not ordinarily known (see below), T is usually estimated as $(T_H + T_c)/2$ but this introduces an error into any results obtained.

(c) Spacing

The spacing d between the sink and source may be approximated for ideal situations where these are parallel planes held a given distance apart. One may set up a kinetic theory probability function to describe the distance traveled by a molecule desorbing from one plate and traveling in a straight line to the other plate. Some angular distribution law (such as the cosine law) must be assumed. For particulate insulations or those with nettings, fibers, or foams, the distance d is very difficult even to estimate approximately. Ordinarily it is chosen for simplicity to be a typical spacing dimension or a cell-dimension and not specified any more accurately.

(d) Accommodation Coefficients

The value of α cannot be determined except very approximately. For example, Scott[16] lists some "typical" values in Table 6.2 and Kennard[12] shows more on page 323. Other tabulations are available, but these illustrate the wide ranges of α which can be expected. For example, for He gas, the following values are quoted:

Scott	300°K	$\alpha = 0.3$
	76°K	$\alpha = 0.4$
	20°K	$\alpha = 0.6$
Kennard	403°K	$\alpha = 0.32$ (glass)
	? °K	$\alpha = 0.44$ (on bright platinum)
	? °K	$\alpha = 0.91$ (on black platinum)
	? °K	$\alpha = 0.07$ (on clean tungsten)
	? °K	$\alpha = 0.18$-0.19 (on clean heated tungsten)
	79°K	$\alpha = 0.025$ (on clean tungsten)

It appears that α increases as T decreases and is smaller for clean bright surfaces. Any *a priori* accurate estimate of α is, however, impossible. (In fact, Equation 10 is really a simplification, in that α for both surfaces has been assumed equal, a fact not necessarily true.)

(2) Discussion

The brief discussion of the variables in Equation 10 should make it obvious that it is essentially impossible to use this equation to predict k_g for any particular insulation at some given T_H, T_c, spacing, and pressure. The real utility of the equation is that it shows the general effect of these variables on the value of k_g. Such considerations also point out the hazard in comparing two insulations at the same pressure. For example, a small-cell foam insulation may show a smaller value of k_g at a given P,T than one with an open netting since the characteristic dimension "d" would be lower than the netting d and then the value of C_2' in Equation 12 would be smaller. (However, the use of high-density, small pore, foams may also increase k_g so that k (from Equation 13) would remain essentially the same.

To illustrate the use of Equation 10 with Equation 11 to determine C_2, and with the following conditions, Figure II-30 was plotted.

d = 0.030 in;
P_o = 1 atm;
T_o = 288°K = 15°C;
T = 188°K (arithmetic average between 25°C and 77°K);
L_o = 18.6 x 10^{-6} cm (at T_o, P_o);
n = 1.15;
C_1 = k (T_o, P_o) = 0.53 Btu-in/hr-ft^2-°F
gas = helium

Values of α = 1, 0.4, and 0.2 were chosen and a value of (k_r + k_s) 1.5 x 10^{-4} was chosen to agree with some of the insulation tests made at Arthur D. LIttle, Inc. As an example of such a test, sample No. 3005, which contains 10 shields of 0.002 in tempered aluminum, with 11 spacers of 1/8 x 1/8 silk netting (about 0.022 in thick) was used with liquid nitrogen as the cold sink and with a hot plate near 25°C. Helium was the residual gas. d for this case is about 0.022 in (although it may be somewhat less, considering the lesser distance for molecule-netting collisions). The actual experimental data for this test are

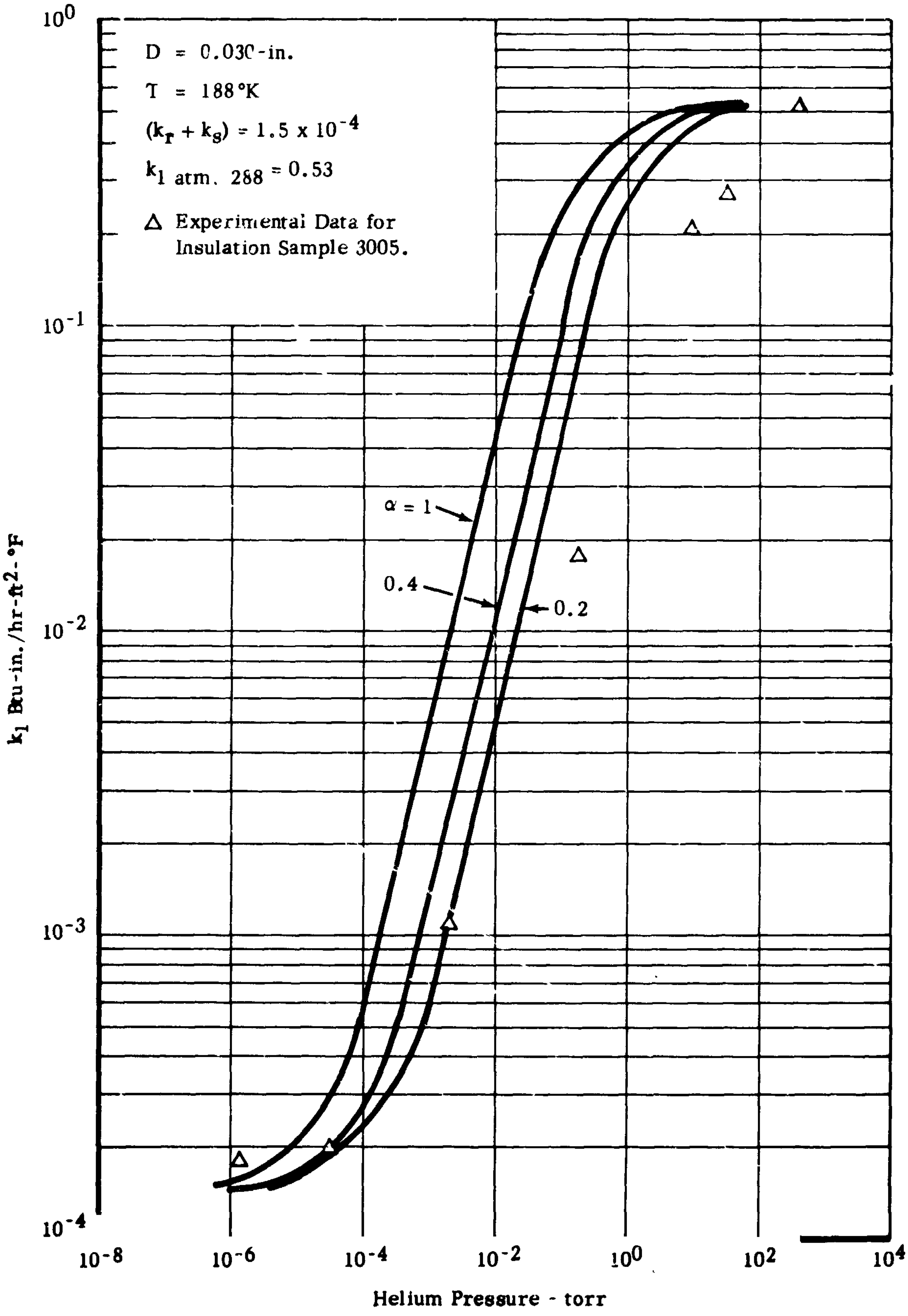

FIGURE II-30 EFFECT OF HELIUM GAS PRESSURE ON AN INSULATION shown in Figure II-30 as triangles. The check between experiment and theory is neither good nor bad. In view of the current state of the theory, the agreement is about as good as can be expected. Other comparisons could be made but they show nothing new.

In summary, therefore, the theory now existing to correlate a gas conductivity in an evacuated insulation has been sufficiently developed to indicate the dependence of this conductivity on the principal experimental variables, but it has not been developed to the degree where one can make an <u>a priori</u> estimation of k_g with any degree of assurance. Until we can delineate more clearly the values of α and d to use, developments are likely to be slow.

REFERENCES

1. Basic Investigations of Multilayer Insulation Systems, Final Report, Contract NAS-3-4181, Oct. 1964, NASA CR-54191.

2. Clausing, A. M. and Chao, B. T., Thermal Contact Resistance in a Vacuum Environment, ASME paper 64-HT-16, Heat Transfer Conference, Cleveland, Ohio, April 1964.

3. Archard, J. F., Elastic Deformation and Laws of Friction, Proc. Roy. Soc. (London) A, 243, 1957, p 190.

4. Timoshenko, S. and Goodier, J. N., "Theory of Elasticity", McGraw-Hill Book Co., New York, 1951, p 372.

5. Holm, R., Electrical Contacts Handbook, Springer Verlag, Berlin, 1958.

6. Sanderson, P. D., Heat Transfer from the Uranium Fuel to the Magnov Can in a Gas-Cooled Reactor, ASME Int. Heat Transfer Conference, Part 1, 1961, p 53.

7. Liquid Propellant Losses during Space Flight, Final Report, Contract NASw-615, Arthur D. Little, Inc., Report No. 65008-00-04, Oct. 1963.

8. A Compendium of the Properties of Materials at Low Temperature, Part IV, WADD-TR-60-56, December 1961.

9. ASD-TDR-63-574, "Investigation of the Thermal Properties of High Temperature Insulation Materials", Air Force Materials Laboratory, July 1963.

10. "Thermal Conductivity of Non-Metallic Materials", Contract NAS8-1567, 27 March-27 April 1962, NASA George C. Marshall Space Flight Center, Huntsville, Alabama.

11. Wang, D. I-J., "Multiple Layer Insulations", Chapter in Aerodynamically Heated Structures, Ed. P. E. Glaser, Prentice-Hall, 1962, p 95.

12. Kennard, E. H., Kinetic Theory of Gases, McGraw-Hill Book Co., 1938, Ch. VIII.

13. ASD-TDR-62-88, "Investigation of Materials for Vacuum Insulation Up to 4000°F", January 1962.

14. Hnilicka, M. P., Advances in Cryogenic Engineering, Vol. 5, 199 (1959).

15. Riede, P. M. and Wang, D. I-J., Advances in Cryogenic Engineering, Vol. 5, 209 (1959).

16. Scott, R. B., Cryogenic Engineering, D. Van Nostrand, New York (1959).

PART III

TASK I B, EMISSOMETER

TABLE OF CONTENTS

III

LIST OF TABLES

III

LIST OF FIGURES

III

LIST OF FIGURES

III
(Continued)

III. TASK I B, EMISSOMETER

A. Summary

The emissometer program is a continuation and expansion of the effort initiated during the previous Contract NAS3-4181. The objective of this program is to establish the emittance performance of vacuum metallized coatings placed on polyester film in terms of the coating thicknesses and exposure to various atmospheric environments. A second program objective was to evaluate the emittance properties of shield materials used in the insulation systems studied in the tank program and to aid in the selection of the shields.

The scope of this effort consisted of the specification, procurement and measurement of materials to be studied. Specifically, initial studies were conducted to select and specify and coatings to be considered. The coatings finally selected were aluminum, gold, silver and copper. Whenever possible, coating samples were procured from commercial sources. Many samples were produced at Arthur D. Little, Inc. in the laboratory. Coating thickness was determined by electrical resistance methods generally but other methods were also used. The emittances of various metal coatings in various thicknesses were measured in an emissometer developed in the previous contract. An environmental chamber was fabricated and samples were exposed in the chamber to humid air, carbon dioxide and salt air for 50 and 100 hour periods. Emittance measurements were taken after these exposure periods. During the progress of the work the information obtained was used in selecting and specifying shield materials for the tank insulation and in establishing the quality of the purchased materials.

Conclusions

1. Each of the metals studied have different emittance values. Grouped in order of increasing emittance are silver, copper, gold and aluminum. Silver has an emittance of .011 at thicknesses greater than 1000 Angstroms(°A). Copper has an emittance value of .013 at thicknesses greater than 500 °A. Gold has an emittance value of .017 at thicknesses greater than 1500 °A. Aluminum has an emittance of .023 at thicknesses greater than 600°A. This data is summarized in Figure III-1.

2. Polyester film with the minimum coating thicknesses indicated above requires special ordering from commercial suppliers. Commercially available materials generally have thicknesses of 250°A or less.

3. The emittances of each metal studied have different degrees of stability when exposed to high humidity air, carbon dioxide and salt environments. Grouped in order of decreasing stability are aluminum, gold, silver and copper.

4. The emittance stability of silver and copper in the various environments studied are improved when thin protective coatings of silicon monoxide are applied over the primary coating. However, this protective coat generally results in a slight initial degradation in the emittance of the primary coating. The emittance of silver is increased to about .016 and the emittance of copper is increased to about .017. Gold and aluminum applied as a thin protective coat over silver resulted in serious emittance degradation of the surface.

5. The emittance of commercially produced samples was generally comparable to the emittance of laboratory produced samples. This applies to aluminum, gold and silver coatings. No commercially applied copper coatings were tested.

6. The determination of coating thickness using the wrought electrical resistivity of the metal and the measured resistance of the coating appears adequate. This method does not require specialized equipment, and can be done quickly and easily at any desired location on the coated film after it has been produced.

Recommendations

1. Coatings for shield materials require further screening to establish the effects of mechanical environments, principally accoustical and lower frequency vibrations, superimposed upon the atmospheric environments.

2. Suppliers for producing metallized polyester film should be qualified by NASA. This involves the establishment of specifications which set production and performance requirements as well as preliminary measurement and testing standards.

3. The emittances of silicon monoxide protected silver and copper coatings are competitive with the emittance of gold. However, there is very little commercial practice established in the application of silicon monoxide coatings. Improved technology in this area may result in shield materials less expensive than gold but of comparable surface emittance performance with gold.

B. Introduction

In previous contracts we obtained design information on the thermal properties of various insulation systems applicable for cryogenic liquid storage tanks on spacecraft. In particular, the thermal performance of a number of multi-layer insulation systems was studied as a function of different variables such as compressive loads, gas pressures, boundary temperatures, number of layers or radiation shields and spacers, configurations of the sample, and materials for the radiation shield and spacers.

From this work it was apparent that additional basic design information would be needed. The infrared surface emittance of shield materials, being one of the most important factors in MLI performance, was selected for further study. A program was established in the current contract to produce, identify and test practical lightweight shield materials which exhibit low surface emittances.

The thermal performance of any multi-layer insulation system is directly dependent upon the emissivity of the shields. The control of surface emissivity is difficult, and wide variations in this value occur even in shields almost identically constructed. The surface emissivity depends primarily upon the metal used and its purity. Factors which degrade the basic emittance of the metals include the smoothness of the surface and the presence of contaminants, oxides or the like on the surface. Where shields are formed by metal coatings on substrate films, the thickness of the coating and method of deposition are also significant parameters.

It is important, therefore, that the properties of high thermal performance shields be identified so that uniform thermal performance can be expected from the shields when they are incorporated into a multi-layer insulation. This involves the measurement and interpretation of the emissivity values obtained with different shield materials both under ide conditions and after exposure to various envirorments expected during the intended use of the insulation systems.

The emissivity of a pure, non-oxidized, strain-free material is directly related to its electrical resistivity. Metals with low electrical resistivity include gold, aluminum, copper and silver. Of these four, gold reacts least with the natural environment, and, therefore, maintains an emissivity more constant with time. The others are more chemically active and form surface oxides or sulfides, as the case may be, on exposure to the air. Aluminum oxide is thin and transparent to infrared radiation; whereas, in the case of copper, the oxide form and in the case of silver the sulfide form increase greatly the emittance of the surface. Therefore, some protective transparent coating must be applied over copper or silver coatings to prevent this degradation.

Except in the case of aluminum, factors such as cost, weight, and fragility dictates that these metals be utilized as a coating on a substrate, such as polyester film. Because aluminum has low density, is inexpensive and can be obtained as extremely thin foil in many sizes, shields can be constructed entirely of metal. However, additional weight reduction, by a factor of 2 can be achieved even with aluminum by applying it to polyester film.

Generally, coatings produced by vacuum metallizing techniques are less than 250 Angstroms thick. These coatings are produced commercially for decorative purposes, for use in electrical capacitors and for other purposes which do not warrant heavier coatings. Under ordinary viewing conditions, These commercial coatings appear opaque. However, wher all the light sources are removed from the viewing side, it is evident that the coatings instead are quite transparent. The solar disc can be seen through an aluminum coating less than about 500 °A thick and through a gold coating less than about 2000 °A thick. Thus, the transparency of commercial film in the visible radiation spectrum raises questions about the transparency of the same film to infrared radiation.

According to Holland[1] some of the important parameters for production of high quality reflective surfaces are chamber pressure during vaporization, evaporation or deposition rate, incident angle of the vapor on the coating surface and the cleanliness of the surface. The latter establishes the degree of adhesion between the coating and substrate and, therefore, determines the performance of the coating. The former factors effect the surface emittance of the coating directly. For example, large incident angles and/or low evaporation rates produce a granular surface structure which degrades the emittance of the surface. When the chamber pressures are high (greater than .1 micron) and evaporation rates are low, sufficient vapor reacts with gas in the chanber to reduce the purity of the metallic coating and, thereby, increases the coating's emittance.

To eliminate or reduce the importance of these factors in our studies procedures were adopted in which the vapor incidence angle was less than 20 degrees and the chamber pressures were less than 10^{-4} mm Hg. the deposition rates were varied from a few Angstroms per second to a few hundred per second. Every attempt was made to deposit at rates greater than 25 Angstroms per second. The suppliers who also provided metallized film for both the emissometer and tank programs were asked to follow similar procedures.

C. Experimental Equipment

1. Emissometer

a. Principal of Operation

The emissometer measures the total hemispherical emittance of samples of candidate radiation shield materials. It has been designed to permit fairly rapid measurements, i.e., about two hours per sample, and can be used for comparative measurements without estensive calibration.

The emissometer uses the receiver disc principle. A circular, thin-metal blackened disc, about 2.25 inches in diameter, is placed closely adjacent, and parallel, to a circular sample piece in an evacuated space. The back side of the receiver disc, (also blackened), is surrounded by a black cavity held at a temperature low with respect to the sample temperature. The receiver disc exchanges heat with the sample on one side and with the black cavity on the other side principally by radiative heat transfer. The geometry is such that the heat transfer between the sample, the receiver disc and the black cavity is essentially like that between three infinite parallel planes as shown in Figure III-2. Hence, a heat balance on the disc once steady-state temperatures have been attained, yields the equation:

$$e_s \sigma (T_s^4 - T_D^4) = \sigma (T_D^4 - T_c^4) \qquad (1)$$

or

$$e_s = \frac{T_D^4 - T_c^4}{T_s^4 - T_D^4}$$

where,

e_s = the total hemispherical emittance of the sample

T_D = the receiver disc temperature

T_c = the cavity temperature

T_s = the sample temperature

Thus, if the sample temperature, the cavity temperature, and the disc temperature are measured, the emissivity of the sample can be determined. In our apparatus the sample temperature is maintained constant at a value of 93°F. The cavity temperature is maintained at the temperature of liquid nitrogen (77°K) and the receiver disc temperature is measured with a thermocouple.

b. Description

An assembly drawing of the apparatus is shown in Figure III-3. Only the vacuum vessel with internal parts is shown. The vacuum pumping system is shown schematically in Figure III-4. A liquid nitrogen supply system, and instrumentation for controlling sample temperature and reading the thermocouple outputs are also required.

Referring to Figure III-3 the sample is mounted on the lower surface of the sample holder block, part 9. Its temperature is maintained at a fixed level by means of a heater, part 28. A controller with thermistor sensing element monitors the temperature and controls the heat input to maintain a preset level within ± 0.25°F. The temperature of the sample holder is accurately measured by an imbedded copper-constantan thermocouple

The receiver disc is immediately adjacent to the sample surface. The disc is blackened on both sides with platinum black.

It is extremely important to insure that the major heat input to the disc is the radiative transfer from the sample and the major heat flow from the disc is due to its radiative interchange with the surrounding cold, black cavity. The construction places strong emphasis on minimizing extraneous heat inputs to or outputs from the disc. The disc is suspended by six 0.003 inch diameter stainless steel wires which pass radially outward to a mounting ring, part 6. A copper-constantan thermocouple made of 0.001 inch diameter wire is mounted on the ear surface of the receiver disc; the two leads pass downward and connect to heavier thermocouple leads, which then pass out through the vacuum shell.

For low emissivity samples, the radiative flux received by the disc is very low and the disc temperature approaches that of the cavity. The mounting ring, to which both the support wires and the thermocouple leads are connected (thermally, but not electrically, in the case of the thermocouple leads) is cooled to the same temperature as the cavity, i.e., 77°K. Conductive heat leaks from the disc, through the supports and thermocouple leads, are thereby minimized for low emissivity samples. Thus, even for low emissivity samples, the conductive heat leaks are small compared to the radiative transfer on which the measurement depends, and good accuracy is maintained.

The black cavity around the receiver disc is formed by a copper tube with a flat end piece, cooled by a flow of liquid nitrogen passing through tubes soldered to its exterior. The interior of the cavity is blackened with the 3M Brand Velvet Coating #9564 black paint. The geometrical arrangement of the cavity and mounting ring (with baffles) is such as to prevent radiation from the warm walls of the chamber from passing into the cavity and reaching the disc.

The sample holder can be moved axially in its mounting tube and is adjusted so the surface of the sample is in a plane established by four points on the end of the tube. The sample is placed on the sample holder and set in position with the sample holder sub-assembly, parts 1, 2 and 9, removed from the vacuum vessel. The sub-assembly is then inserted into the vessel; the construction insures that the sample face will be positioned, parallel to the receiver disc and at a fixed distance from it. In this way, samples of various thicknesses can be emplaced on the holder and the same axial space between the sample surface and the receiver disc surface is maintained from test to test. Variations in the measurement due to change in geometry of the set-up are thereby eliminated.

The receiver disc and its mounting ring are incorporated in a second sub-assembly, consisting primarily of parts 13, 3, 4, 6, 7, 8 and 26, that can be removed from the vacuum vessel to facilitate inspection of the receiver disc, calibration of its thermocouples and alignment of the receiver disc with the sample surface.

The vacuum vessel and black cavity, principally parts 12, 14, 15, 30 and 31 comprise the third major sub-assembly. Part 32 is a port for connecting the roughing vacuum pump. The liquid nitrogen coolant tubes, part 17, pass into the chamber through pantleg arrangements, parts 16 and 18 Four penetrations are made, two inputs and two outputs. The two liquid nitrogen circuits will be connected in series external to the vacuum vessel so that only one liquid nitrogen input is required.

The vacuum pumping train, shown schematically in Figure III-4, consists of a high vacuum valve connected to the flange on the vessel, a chevron baffle at room temperature, a 2 inch oil diffusion pump and a forepump, which also serves as a roughing pump. When the chamber is not under vacuum, the high vacuum valve will be kept closed and the diffusion pump running.

c. Operation

In a typical test the sample will be mounted on the sample holder by means of a double sided adhesive tape and inserted into the emissometer. The system is then evacuated. First, with the foreline valve closed and the roughing valve open, the chamber is pumped down to about 200 microns. Then with the roughing valve closed and the foreline and high vacuum valves open, evacuation continues down to a level of about 10^{-6} torr. Just before the high vacuum valve is opened, the cylindrical cavity and receiver disc mounting ring will be cooled by passing liquid nitrogen through the cooling tubes. These cold surfaces protect the sample, the receiver disc and the interior of the cavity from oil backstreaming from the diffusion pump. The cavity cooldown and pumpdown to the 10^{-6} torr range takes about one hour. After the cavity is cooled, an additional hour is required for the receiver disc to reach its equilibrium temperature. During this time, the sample holder temperature, hence, the sample temperature is maintained constant by the heater-controller. Measurement of the steady-state temperature of the receiver disc and of the sample holder temperature is all that is required for the completion of the test, since the temperature of the cavity is known.

d. Error Analysis

(1) Approach

The device has been designed so that the steady-state radiant heat transfer between the fixed temperature sample, the floating receiver disc and the fixed temperature cold cavity closely approximate that which would occur between three infinite parallel planes as shown in Figure III-2. In the idealized situation of Figure III-2, all surfaces except the sample surface are perfectly black, the sample emittance can be related to the system temperatures by Equation (1).

The approach used in the determination of sample emittance is to measure the three temperatures, assume Equation (1) applies, and use it to calculate sample emittance.

The measurement of the three temperatures involves errors of a random nature, such as might be associated with any temperature measurement using thermocouples or other thermometric device. These errors combine to cause random errors in emittance determination. In addition certain fixed errors can be identified that are associated with the fact that Equation (1) does not apply exactly to conditions in the Emissometer. These errors are, in essence, designed into the instrument and are not strictly an error in measurement. Development of a relationship between instrument parameters and the sample emittance to replace Equation (1) would be extremely complex and would still involve considerable uncertainty. Hence, the approach of using Equation (1) and considering departures from the idealized conditions of Figure III-2 as giving rise to fixed errors has merit.

The fixed errors are due to the following factors:

1) Geometry of the instrument is different than geometry of Figure III-2.
2) The emittance of the receiver disc is less than 1.
3) The emittance of the cavity is less than 1.
4. Conductive heat leaks from the receiver disc via supports and thermocouples are present. These upset the purely radiative heat transfer.

Random and fixed errors are discussed in detail in the next two sections.

(2) Random Errors Due to Temperature Measurement

The uncertainties in measuring (or otherwise evaluating) temperatures combine to result in a total uncertainty in emittance determination according to the relation:

$$(\Delta e_s)^2 = \left(\frac{\partial e_s}{\partial T_s} \cdot \Delta T_s\right)^2 + \left(\frac{\partial e_s}{\partial T_D} \cdot \Delta T_D\right)^2 + \left(\frac{\partial e_s}{\partial T_c} \cdot \Delta T_c\right)^2 \quad (2) \tag{2}$$

where Δe_s, ΔT_s, ΔT_D and ΔT_c are uncertainty intervals. The percentage error in e_s is then given by

$$\frac{\Delta e_s}{e_s} \times 100 = 100 \times \sqrt{\left(\frac{\partial e_s}{\partial T_s} \cdot \frac{\Delta T_s}{e_s}\right)^2 + \left(\frac{\partial e_s}{\partial T_D} \cdot \frac{\Delta T_D}{e_s}\right)^2 + \left(\frac{\partial e_s}{\partial T_c} \cdot \frac{\Delta T_c}{e_s}\right)^2} \tag{3}$$

It should be noted that if the uncertainties in temperatures are expressed as $\pm$ values, the error in e_s will be a $\pm$ value. The coefficient $\frac{\partial e_s}{\partial T_s}$ can be determined from Equation (1) and is given by the relation

$$\frac{\partial e_s}{\partial T_s} = - \frac{4 e_s (1+e_s)}{T_s} \tag{4}$$

In this and following expressions, it is assumed that $\left(\frac{T_c}{T_s}\right)^4 << 1$. so that

$$\frac{\partial e_s}{\partial T_s} \cdot \frac{\Delta T_s}{e_s} = -4(1+e_s) \frac{\Delta T_s}{T_s} \tag{5}$$

This term may be interpreted as the error in emittance determination due to the uncertainty in sample temperature measurement. This temperature is measured with a calibrated copper-constantan thermocouple that uses an automatic ice point reference junction. A conservative estimate of the uncertainty in measurement is $\pm$ 0.5°R. Values of the per cent error in sample emittance due to sample temperature uncertainty, i.e.,

$\pm \frac{\partial e_s}{\partial T_s} \cdot \frac{\Delta T_s}{e_s} \times 100$ for a range of sample emittances are shown in Table III-1.

The coefficient $\frac{\partial e_s}{\partial T_D}$ as determined from Equation (1) is

$$\frac{\partial e_s}{\partial T_D} = \frac{4(1+e_s)^{5/4}}{T_s} \left[e_s + \left(\frac{T_c}{T_s}\right)^4 \right]^{3/4} \tag{6}$$

so that

$$\frac{\partial e_s}{\partial T_D} \cdot \frac{\Delta T_D}{e_s} = \frac{4(1+e_s)^{5/4}}{e_s T_s} \left[e_s + \left(\frac{T_c}{T_s}\right)^4 \right]^{3/4} \cdot \Delta T_D \qquad (7)$$

The disc temperature is also measured with a calibrated copper-constantan thermocouple using an automatic ice point reference junction. Care is taken to insure that the disc reaches an equilibrium temperature, i.e., that steady-state heat transfer conditions prevail. Hence, a conservative estimate of the error in disc temperature measurement is also ± 0.5°R. The corresponding errors in emittance determination due to uncertainties in disc temperature are shown in Table III-1.

The coefficient $\frac{\partial e_s}{\partial T_c}$ as determined from Equation (1) is

$$\frac{\partial e_s}{\partial T_c} = - \frac{4T_c^{\,3}(1+e_s)}{T_s^{\,4}} \qquad (8)$$

so that

$$\frac{\partial e_s}{\partial T_c} \cdot \frac{\Delta T_c}{e_s} = - \frac{4T_c^{\,3}}{T_s^{\,4}} \cdot \frac{(1+e_s)}{e_s} \cdot \Delta T_c \qquad (9)$$

The cavity temperature is not measured; instead, reliance is placed on the constancy of the atmospheric boiling point of liquid nitrogen. The liquid admitted to the cooling tubes bonded to the cavity discharges to atmospheric pressure. The discharge is a two-phase flow indicating that boiling occurs in the tube. Since the pressure drop through the tube is small, it is reasonable to assume that the temperature of the liquid is very close to the boiling point at ambient pressure. The design of the instrument insures intimate thermal contact between the boiling liquid and the cavity walls and an essentially isothermal wall. Variations in atmospheric pressure do cause a variation in the liquid boiling point. In calculations of emittance from Equation (1), a constant cavity temperature of 77.4°K is assumed. This corresponds to an atmospheric pressure of 30 inches Hg. Local variations in atmospheric pressure seldom exceed ± 0.5 inches Hg about this mean.

The corresponding variation in boiling point is $\pm 0.28°R$. For the purposes of this analysis, therefore, a conservative estimate of the uncertainty in cavity temperature is $\pm$ 0.5°R. The corresponding errors in the determination of sample emittance due to uncertainty in cavity temperature are shown in Table III-1.

The total random errors in sample emittance calculated from Equation (3) are also shown in Table III-1. The table shows that even for very low sample emittances random errors due to temperature measurement are not likely to exceed $\pm$ 1.8%.

(3) Fixed Errors

(a) Geometry

An error due to the geometry of the instrument may be defined to account for the fact that the sample, receiver disc and cavity do not precisely duplicate heat transfer conditions existing between infinite parallel planes, on which Equation (1) is based. To simplify the evaluation of this and other fixed errors, we assume that only the error being evaluated exists. Thus, in considering the geometry error, we assume the disc and cavity emittances to be unity and no conductive heat leaks from the receiver disc to the surroundings. It is also fair to assume that the receiver disc has negligible thickness (actual thickness, .010 inches). For the real geometry shown schematically in Figure III-5, a heat balance on the disc yields the following relation between the sample emittance and other system parameters:

$$e_s = \frac{(2-\phi)(u_D - u_c)}{(u_s - u_c)F_{Ds} - \phi\ (u_D - u_c)} \qquad (10)$$

where

$$\phi \equiv \frac{1}{A_D} \int_o^{r_s} 2\pi r dr F_{rD}^{\ 2}$$

A_D = area of the receiver disc (one side)

r = radius of elemental ring dr on sample surface

F_{rD} = radiative view factor from elemental ring on sample to receiver disc

r_s = outside radius of sample (1.250 inches)

u = σT^4

F_{Ds} = view factor from receiver disc to sample

If we define an apparent sample emittance by

$$e_{sa} = \frac{u_D - u_c}{u_s - u_c} \qquad (11)$$

i.e., one calculated using Equation (1), and note that for the geometry of Figure III-4,

$$F_{Ds} \simeq 1 \text{ (actual value 0.994)}$$

It follows that the fractional error in sample emittance determination is given by

$$\frac{e_s - e_{sa}}{e_s} = \frac{(1-\phi)(1-e_s)}{1 + (1-\phi)(1-e_s)} \qquad (12)$$

The parameter ϕ has been evaluated by graphical integration for the geometry of Figure III-5 and is found to have a value of 0.944. Equation (12) has been used to calculate the percentage errors attributable to geometry shown in Table III-2, i.e., $\left(\frac{e_s - e_{sa}}{e_s}\right) \times 100$.

It should be noted that this error is always positive, which, by its definition, means that if the geometry error were the only one present, the true sample emittance would be greater than the apparent one.

(b) Receiver Disc Emittance

The emittance of the receiver disc is somewhat less than unity. Over the disc temperature range of 189°R to 463°R, corresponding to sample emittances from .01 to 1.0, its emittance is thought to be greater than 0.9.[3]

In evaluating the error associated with a disc emittance less than unity, we assume that the cavity has an emittance of 1.0, that heat transfer between sample disc and cavity is like that between infinite parallel planes and that conductive heat leaks from the disc to surroundings are negligible. Then a heat balance on the disc yields the following relation between sample emittance and other parameters

$$e_s = \frac{e_D(u_D-u_c)}{(u_s-u_D) - (1-e_D)\ (u_D-u_c)} \tag{13}$$

Equation (13) and the definition of apparent emittance, Equation (11), lead to the following expression for the error in sample emittance:

$$\frac{e_s-e_{sa}}{e_s} = - \frac{(1-e_s)(1-e_D)}{e_D+e_s(1-e_D)} \tag{14}$$

Equation (14) has been used to calculate the errors attributable to receiver disc emittance shown in Table II-2. In the calculation a receiver disc emittance of 0.9 was assumed.

(c) Cavity Emittance

The effective emittance of the cavity is also less than unity. The inner surfaces of the cavity are painted with 3M Velvet coating, which, at liquid nitrogen temperature, is thought to have an emittance of about 0.75.(1) However, this substantial decrement from unity is greatly offset by the geometry of the cavity which, because of its large area in relation to the disc, simulates a highly absorbing surface. In evaluating this error, we assume the emittance of the disc is 1.0, that the heat transfer between sample and disc is like that between infinite parallel plates, and that conductive heat leaks from the disc to surroundings are negligible. Then a heat balance on the receiver disc, in which the cavity geometry of Figure III-6 and a cavity surface emittance of 0.75 are used in the calculation of heat transfer from the disc to the cavity, yields the following relation between sample emittance and other parameters.

$$e_s = \frac{u_D - u_c}{u_s - u_D} \quad [1- \frac{A_D}{A_c} (1-e_{ce})] \tag{15}$$

where A_c = cross section area of cavity = 19.6 in^2

e_{ce} = effective emittance at the inlet of the cavity

The cavity is cylindrical with $\frac{L}{D}$ = 1 and a surface emittance of 0.75 so that e_{ce} = 0.92.[4] Using the apparent emittance defined in Equation (11) one can obtain the following relationship for error in sample emittance.

$$\frac{e_s - e_{sa}}{e_s} = - \frac{\frac{A_D}{A_c}(1-e_{ce})}{1-\frac{A_D}{A_c}(1-e_{ce})} \tag{16}$$

This error, unlike the other errors, is independent of sample emittance. Its value, as calculated from Equation (16), is shown in Table III-2.

(d) Conductive Heat Leaks From Disc

Heat flow from the disc through the disc supporting wires and thermocouples are thermally connected to a structure which is at liquid nitrogen temperature (i.e., T_c). Conductive heat flow through them represents a departure from the conditions presumed by Equation (1) which we consider gives rise to an error. In evaluating this error, we assume the emittance of the disc equals 1.0, the heat transfer between the sample and disc and disc and cavity is like that between infinite parallel plates, and the emittance of the cavity equals 1.0. Then a heat balance on the disc yields the following relation for emittance of the sample in terms of other parameters:

$$e_s = \frac{u_D - u_c}{u_s - u_D} + \frac{q_L}{(u_s - u_D)A_D} \tag{17}$$

where q_L = heat leak from disc to structure through support wires and thermocouples

Again, using the apparent emittance defined by Equation (11) one can develop the following relationship for the error in emittance determination.

$$\frac{e_s - e_{sa}}{e_s} = \frac{(1+e_s)}{e_s} \cdot \frac{q_L}{q_L + A_D(u_s - u_c)} \tag{18}$$

The heat leak, q_L, is essentially pure conduction through the supports and thermocouples and is, therefore, proportional to (T_D-T_c). Thus q_L is a function of the disc temperature which, in turn, is a function of the sample emittance. We have evaluated the heat leak for various sample emittances and the corresponding disc temperatures obtained from Equation (1) and used these values to calculate the errors in sample emittance shown in Table III-2.

The construction of the instrument, whereby the disc supports and thermocouples are heat stationed to nitrogen cooled surfaces is important. It results in maintaining the error due to conductive heat leak at a reasonably low value, even for very low sample emittances where the total heat flow to the disc by radiation is small. If the disc supports were terminated on a room temperature surface, the conductive heat leak would increase with decreasing disc temperature so as to introduce large errors in measurements of low emittances.

(e) Total Fixed Errors

The fixed errors described in the previous sections can be added together to establish the total fixed error of the instrument, taking care to observe the polarity of each error. The total errors are tabluated in Table III-2. The negative errors dominate for all emittance values so that, in general, the instrument indicates a higher emittance than the true value. Based on the estimates used to generate the table, the maximum fixed error that might be expected over the emittance range shown is less than 6 per cent.

f. Calibration Tests

To our knowledge no absolute low emittance standards are available. Hence, calibration of the emissometer in an absolute sense is not possible. However, we have performed some tests to determine the response of the instrument to changes in emittance in the low emittance range to verify its performance to the degree possible. The approach used was to increase the emittance of an aluminum foil sample which had an initial measured emittance of $.020^5$ by painting black rings of known area on the sample. (Paint was 3M Velvet coating with a room temperature emittance of 0.93.) With this approach, the effective sample emittance after the addition of each ring could be estimated. Estimated values up to 0.28 were produced and the measured value compared to the estimated value. The basis for the estimated value may be derived with reference to Figure III-7. We assume the disc emittance is 1.0. Then, the heat transfer from the sample shown in the figure to the receiver disc is given by:

$$q_{sD} = (u_s - u_D)\ (A_1 e_s F_{1D} + A_2 e_p F_{2D} + A_3 e_s F_{3D}) \tag{19}$$

where
q_{sD} = heat transfer from sample to disc
A_1 = sample area inside black ring
A_2 = area of black ring
A_3 = sample area outside black ring
e_s = emittance of unpainted sample
e_p = emittance of black paint
F_{1D} = view factor from A_1 to disc
F_{2D} = view factor from A_2 to disc
F_{3D} = view factor from A_3 to disc

Since

$$A_1 F_{1D} + A_2 F_{2D} + A_3 F_{3D} = A_D F_{Ds} \tag{20}$$

one can write

$$q_{sD} = (u_s - u_D)[A_2 F_{2D}(e_p - e_s) + A_D F_{Ds} e_s] \tag{21}$$

Equation (21)can be applied to more than one painted ring by using the sum of the AF's for each ring in place of A_2F_{2D}.

For the painted sample we now define an effective emittance, e_{se}, that will cause the same heat transfer to the receiver disc, so that

$$e_{se}(u_s - u_D)\ A_s F_{sD} \equiv q_{sD} \tag{22}$$

Combining Equations (21) and (22) and noting that

$$A_s F_{sD} = A_D F_{Ds} \tag{23}$$

we get

$$e_{se} = \frac{A_2\ F_{2D}}{A_D\ F_{Ds}} (e_p - e_s) + e_s \tag{24}$$

Calculations have shown that F_{2D} and F_{Ds} are essentially 1.0 for the painted rings used in our tests. Therefore, Equation (24) may be simplified to

$$e_{se} = \frac{A_2}{A_D} (e_p - e_s) + e_s \tag{25}$$

where for multiple rings, A_2 is simply the total painted area. If the emittance of the unpainted e_s sample, the emittance of the paint, e_p, and the total area of the painted rings, A_2, are known, the effective emittance can be calculated from Equation (25). the equation shows that the slope of a plot of e_{se} vs. the area ratio $\frac{A_2}{A_D}$ should have the value $(e_p - e_s)$.

A photograph of the painted sample used in the test is shown in Figure III-8. The rings were added one at a time to obtain increments in effective emittance. The value of the effective emittance, as measured with the emissometer, are shown plotted against the area ratic in Figure III-9. The dashed line is faired through the data in the figure. The solid line shows the effective emittance calculated from Equation (25), assuming that the initial sample emittance is identical to the measured initial sample emittance. The latter assumption may not be precisely true, but small errors in the initial emittance will not have much effect on the plot. The figure shows that the measured effective emittance is greater than the calculated effective emittance. The percentage difference between measured emittance and estimated emittance is less than 7 per cent for the data shown in the figure. These results are in qualitative agreement with the results of the analysis of fixed errors.

2. Bell Jar Sample Production

The samples used in the Emissometer Program were produced mainly at the Arthur D. Little, Inc. facilities in an 18 inch diameter bell jar. A number of samples were obtained from materials purchased in the tank program from commercial suppliers.

The bell jar system is shown in Figure III-10. It is manufactured by the High Vacuum Equipment Corporation. The vacuum system consists of a 4 inch diffusion pump, 30 cfm forepump, liquid nitrogen trap and associated valving. Power and instrumentation leads were passed through a number of the twenty port feed throughs located on the bell jar collar. A 12/24 volt, 150-300 amp power supply was used for resistance heating of the melt boats. A second system having a 7.5 kv, .02 amp rating was used for glow discharge cleaning of the sample surface.

Polyester film of 1/4 mil thickness was used as the substrate for the coatings. This film was mounted on to an 8 inch diameter, 1/4 inch thick aluminum disc which was horizontally supported at the high point in the bell jar point along the center line. The crystal sensor of the film thickness monitor was mounted at the center of the disc on the substrate surface facing the boat (crucible in which the coating material is vaporized). The electrically heated boat was located 20 inches and directly below the coating surface. A corona discharge ring of about 7 inch diameter was located about 4 inches below the sample mounting disc.

In order to metallize a sample substrate, a predetermined amount of pure metal was placed into the boat. The glass bell jar was placed in position and the working space evacuated to 25-50 microns. The corona ring was then activated for a period of about one minute to ion clean the sample surface. The working space was next evacuated to below 5×10^{-5} mm Hg pressure level and the boat heated to vaporization temperature of the metallizing material. Based upon experience a power setting was developed to achieve specific rates of vaporization. On occasion the metal was completely vaporized. On others the duration of the vaporization period was determined from the thickness monitor.

3. Thin Film Thickness Measurement

Three different techniques were used to establish thickness values of aluminum, gold, silver and copper coatings that were deposited on 1/4 mil polyester film by vacuum metallizing techniques. In the first method, the thickness was computed from the electrical resistance of the metal coating measured between known fixed boundaries. In the second method, the measurements were made while the films are being produced by measuring the frequency change in a vibrating crystal due to the accumulation of coating material. Third, during the production of samples, the mass of vaporized metal was used to establish the coating thickness.

a. Resistance Method Parallel Bar Electrode

The resistance method is the one most widely used by commercial vacuum metallizers for the measurement of film thickness in production. The accepted unit of measurement is the ohm per square. The resistance between the ends of a right prism is proportional to its length and inversely proportional to its cross sectional area in accordance with the following relation:

$$R_B = \rho \frac{\ell}{A} \tag{1}$$

where R_B = the electrical resistance

ρ = the resistivity of the material (Figure III-13)

ℓ = the distance between the electrodes

A = the cross sectional area, product of w and t where w is the sample width and t the coating thickness

Replacing A in Equation 1 with its equivalent and setting length equal to width, then the resistance or ohms per square is proportional to 1/t. In the tank program, all resistance measurements have been taken with a parallel bar device having a two-inch space. Therefore, the measuring square is 2 inches on a side. The resistance of the film between the two electrodes is measured with a resistance bridge of high accuracy. The measuring equipment and sample are shown in Figure III-11.

The measurements are made by cutting a sample from the film using the two by three inch micarta block which also serves to protect the knife edges of the electrodes when the head is not in use. The sample is then set on a cushioned surface and the measuring head set on the sample across the narrow side of the sample and at right angles to long side. The resistance is measured while hand pressure is being applied to the measuring head to assure uniform contact with the sample. The many measurements made with this system show that measurements made on the same sample over a period of months are repeatable within about 5 per cent.

b. Resistance Method Two-Point Electrode

As indicated above, a sample must be cut out of the sheet in order to measure the coating resistance with the parallel bar measuring head. This is not usually desirable because measurements cannot be made directly on the material to be used in the insulation system but must be made on the discard material. Further, the number of data taken are limited because cutting out, measuring, cataloging and storing the samples is tedious and time consuming. Thus, the design of a two-point electrode measuring head was carried out on the basis that the new head would give an ohm per square reading that was identical to the parallel electrode head. This work resulted in the design shown in Figure III-12. When connected to the measuring bridge in the same manner as the head utilizing parallel knife edges, coating thickness of a shield could be determined at any location (except close to the edges.)

c. Thickness Determination - Melt Methods

The vapor leaving the surface of a molten metal has flux distribution which is according to Lambert's cosine law[5]. A consequence of this is that if the surface of the melt is made to coincide with the surface of a sphere and facing inward, then the vapor will deposit on this interior surface producing a coating whose thickness is uniform throughout. This is made use of in the bell jar production of vacuum metallized coatings on polyester film. The coating, in most instances, was produced from weighed amounts of metal placed into a boat. The boat was heated at the metal boiling point until all the metal disappeared from the boat.

The diameter of the ficticious coating sphere was set equal to the distance from the boat to the sample. Using the wrought properties of the metal, the required mass of metal was computed from the sphere diameter, the coating thickness desired and the metal density. For example, the usual space between the boat and sample was 20 inches. This resulted in a sphere whose area is 1260 square inches. The coating volume corresponding to a coating thickness of 250 Angstroms (approximately 1.0 micro inch) is 1260 $in^2 \times 10^{-6}$ in = 1.26×10^{-3} cu. in. For an aluminum coating (density approximately 0.1 lb/in^2) a melt weight of .0573 grams is required.

In the actual coating productions, the molten metal must be contained in a cavity. If the walls of the cavity extend significantly above the melt surface, some of the low angle vapor molecules will impinge on the surface and become redirected and alter the distribution. However, in all but a few circumstances, the boats were made shallow so that the distribution of the molecular flux in the region of surface to be coated was essentially a cosine distributor.

These procedures worked well with silver, gold and copper coating materials. However, boats could not be used successfully with aluminum because of its high capillarity. The molten aluminum would rise to the edges of the boat and overflow. The boat required large power supplies and the aluminum would vaporize both towards and away from the sample. Thus, to make the aluminum vaporization, we used an electrically heated sinusoidially shaped element. The molten aluminum clings to the trough of the element and forms a series of point source vaporization pools. Therefore, we could not use the melt method for computing applied metal thickness.

d. <u>Vibrating Crystal Method</u>

During the preparation of a number of samples, the thickness and growth rate of the coatings was established from a Speedivac, vibrating crystal, Film Thickness Monitor manufactured by Edwards High Vacuum Ltd. of England.

The accumulation coating material on the sensitive element, which is a crystal, causes the element natural frequency to shift. The associated instrumentation measures the frequency change which can, for a particular coating, be directly related to thickness (assuming wrought metal properties).

e. Comparison of Thickness Measurements

The metal coating thickness of each sample produced in the bell jar was measured by at least two methods and, when possible, by three methods. The thickness data for each sample are presented in Table III-3. Since resistance was used as the primary thickness measurements for the tank insulation shield, the results obtained with this method are compared with the melt method results in Figure III-14a and with the crystal method in Figure III-14b.

As indicated in Figure 13a, the measurements obtained with the melt method agree with the resistance method to within ± 20 per cent. Several measurements at thickness below 500 Angstroms show very poor agreement. These measurements were usually the first taken with a particular coating metal when coating procedures were being established and the use of high heating rates may have caused loss of melt from the boat by splatter. This would reduce the amount of metal coated on film and the resistance measurements would reflect the smaller coating thickness present.

There is less data taken with the crystal film thickness monitor then with the other two methods. However, the crystal measurements also agree within $\pm$ 20 per cent of the resistance determined thicknesses.

The melt and crystal thickness determinations represent absolute measures of metal mass applied to a unit surface. Their agreement with the resistance determination shows the latter to be a valid method for establishing coating thickness.

4. Atmospheric Environment Chamber

A chamber was constructed to produce four atmospheric environments in which specific shield materials could be placed for extended periods and a study made of the environment effect on the surface emittance. The chamber was constructed of marine plywood and was approximately 36 inches wide, 36 inches deep and 44 inches high. All the outside surfaces were insulated with a 1/2 inch thickness of Fiberglas wool. A see-through port was provided in the front for observing the samples and monitoring instruments located within the chamber.

The following environments were produced with the environmental chamber:

a) Air, 45 per cent relative humidity, 95°F (Code "A45")
b) Air, 95 per cent relative humidity, 95°F (Code "A95")
c) Salt air, 95°F (Code "S")
d) Carbon Dioxide, 95°F (Code "C")

The environmental chamber and associated systems are shown schematically in Figure III-15. The interior of the chamber was maintained at a temperature of 95°F through use of an electrical heater. A thermostatic device was used to actuate the heater and maintain appropriate temperature control. Temperature gradients within the chamber were minimized with an internally mounted fan which provided forced circulation. A dry and wet bulb thermometer was mounted within the chamber and was observed through the glass view port. A water reservoir 10 inches wide, 25 1/2 inches long and 10 inches deep was mounted into the bottom of the chamber with its top open to the chamber interior. Bottled gas was used to supply gas to the chamber. The flow to the chamber was controlled by a pressure regulator and measured with a flow meter.

a. Humid Atmosphere

The humid atmosphere conditions were obtained by bubbling high purity bottled air through the water reservoir. The gas flow was set at about 1 ft^3 per hour. By controlling the temperature of the water, the humidity could be maintained at any desired level up to 95 per cent for extended periods. Thus, with the chamber temperature controlled at 95°F, the humidity could set at the required values, 45 and 95 per cent, by control of the reservior temperature.

b. Salt Atmosphere

The salt atmosphere was obtained by bubbling compressed air through a salt solution. The water in the reservior was brought to a weight concentration 2.35 per cent by the addition of chemically pure sodium chloride. Air at the rate 1 ft^3 per minute was passed to a submerged gas distributor having three 0.1 inch diameter orifices. Simultaneously the chamber was maintained at 95°F through use of the thermostated electric heater and fan circulator.

c. Carbon Dioxide Atmosphere

The carbon dioxide environment was achieved with bottled gas fed directly to the chamber at a flow rate of about 1 cubic foot per hour. As in other tests, the temperature within the chamber was thermostatically controlled at 95°F. No water was present in the reservior when the CO_2 atmospheric tests were performed.

D. Experimental Results and Discussion

The following coatings, vacuum metallized on polyester film, were studied: gold, gold over aluminum, aluminum, silver and copper. Thin coatings of gold, aluminum and silicon monoxide over silver and silicon monoxide coatings over copper were also studied. The majority of the test samples were produced at Arthur D. Little, Inc. in the equipment described previously. The remaining samples were obtained from material purchased for the radiation shields used in the tank program insulation. Aside from the laboratory production of samples, the experimental work consisted in measuring the coating thicknesses and in measuring the surface emittances of the coatings both in the "fresh" state and after undergoing the various environments discussed previously.

In Table III-4 are presented in chronological order all the emittance measurements made in the program with the emissometer. This is provided as a matter of record and is also a continuation of the similar record presented in the Final Report CR 54191 of Contract NAS3-4181. The receiver disc used in the emissometer is listed along with the test number and date for each sample. A description of the sample is provided in terms of the type of coating or material, its thickness and where obtained or by whom produced. Similar information is provided for any succeeding substrate or substrates. A sample identifying number is also provided which permits ready access to the stored sample data and other pertinent information. The test number and/or sample number are cross referenced in other tables where particular groupings of the emittance data are used. In a number of tests information is provided in column five which identifies the environment which immediately preceded the emittance measurement. Where no information is provided in this column, it is assumed that the sample was in an ambient air environment. The last column contains the measured emittance of the sample.

1. Aluminum

a. Emittance and Thickness

The emittance and thickness measurements made on aluminized polyester film are presented in Table III-5. The data in this table prior to the performance of environmental tests are also presented in Figure III-16. Among the coatings measured were those produced commercially and those produced by Arthur D. Little, Inc. in the eighteen inch bell jar. In addition, the samples include those coated on one side as well as those coated on both sides of the polyester film. The coating thicknesses range from 150 to 1400 Angstroms.

There is a grouping of the data which indicates a variation of emittance with coating thickness below 600 Angstroms. At above 600 Angstroms, the emittance is generally independent of thickness and has an average value of about .0225 and band limits between .02 and .025. Below 600 Angstroms the average value increases with decreasing thickness and the band limits also increase.

The effect on emittance due to the presence of a coating on the opposite film surface was also investigated. All the solid data points in Figure III-16 represent two sided coatings while open data points are for one sided coatings. The emittance values obtained indicate that for a particular coating thickness the absolute values and band limits for each group are comparable. Therefore, the emittances of the coatings investigated appear independent of the presences of similar coatings on the opposite surface.

Shield materials for the perforated and unperforated insulations, System No. 8 and 9 respectively, were purchased from two sources because of questionable delivery. The specifications called for the coating thickness of each side of the Mylar film to be 600 Angstroms ± 100 Angstroms. The coating thicknesses on the material received from National Research Corporation of Cambridge, Massachusetts (NRC) was generally less than specified and the coating thickness on the material that was received from Hy-Sil Manufacturing Corporation of Revere, Massachusetts was generally greater than specified. The former had a high lustre while the latter was dull looking.

Screening measurements of the emittance were performed on both shield materials. Though the NRC coatings were about half the thickness of the Hy-Sil coatings, their emittance was lower as shown below.

Test	Source	Emitttance	Thickness Angstroms
284	NRC	.0236	430
285	NRC	.0273	450
288	NRC	.0227	445
286	Hy-Sil	.0327	777
287	Hy-Sil	.0335	732
289	Hy-Sil	.0324	772

These data are also shown in Figure III-16 The emittances of the NRC material group with the majority of the data. The Hy-Sil material has higher emittances by about 30 per cent.

The question arises as to the reason for the inferior emittance values obtained with the thicker coating. From the literature[(5)] it is evident that the rate of coating application and number of passes required to achieve a given thickness are variables equal in importance to the coating thickness. Based on the available information, it appears that the NRC coating was applied "rapidly" in a single pass in the recommended manner. On the other hand, the Hy-Sil coating was applied at a "slow" rate and several passes through the coater were required to achieve the specified thickness.

The data obtained in emissometer test 304 are also outside the area where the largest number of data are located. The sample used in the emittance test was prepared from the NRC material which was used as a base. The coating thickness was increased to 885 Angstroms by vacuum metallizing by three successive slow (estimate 2 to 5 Angstroms per second deposition rate) evaporations. Thus, as can be seen from the resulting emittance value of .0415 obtained, that thickness alone, as discussed above for the Hy-Sil material, is no guarantee of emittance performance of the surface.

After the NRC shield material was perforated with .047 diameter holes in the amount of 1.88 per cent of the film area, tests No. 310 and 311 were performed with the emissometer. The increase in emittance from a nominal value of .027 to an effective value of .040 (test 310) is confirmed by calculations presented in Part IV, i.e., the computed effective emittance of the perforated shields is .045.

b. Environmental Effects

One aluminum coated sample produced in the bell jar was placed in each of the four environments for 50 and 100 hour periods. A second sample, produced by the National Research Corporation of Cambridge for the tank insulation shields, was placed in the two humidity environments only. The results obtained are presented in Tables III-12 through III-15) and are summarized in Figure III-17.

The bell jar produced sample experienced no changes in emittance in any of the environments investigated. Also the coating adhesion remained acceptable, i.e., no coating lift-off in scotch tape test after 100 hours in each environment.

The commercial sample experienced about 15 per cent increase in emittance at the end of the 100 hour test in the A45 environment. At the start of the A95 environment, a sample of the same material had an initial emittance value of .0225. There was no emittance degradation in the first 50 hours of test. In the following 50 hours the emittance degraded by an order of magnitude. Adhesion remained good at the end of the test. Eighty per cent of the sample area had a milky appearance which, when inspected with a microscope, was made up of many tiny close spaced diffuse areas. The remaining twenty per cent of the sample area of the disc remained specular in appearance.

c. Conclusions

Aluminized films with average emittance values of .022 are obtainable commercially. These films should have a minimum coating thickness of 600 Angstroms and should be applied rapidly in a single pass. Adhesion of the coatings produced commercially and in the laboratory is acceptable, based on the scotch tape test, for all environments tested. The bell jar produced material experienced no degradation in emittance in the environmental tests. The commercial product (purchased material produced on roll to roll equipment) experienced estensive degradation in the 95 per cent R.H., 95°F environment. Thus, the commercial aluminum coatings have the potential for acceptable performance. Further study and comparisons between laboratory and commercial samples are required.

2. Gold Coatings

a. Emittance and Thickness

The emittance and thickness measurements made on gold metallized polyester film are presented in Table III-6 and are shown in Figure III-18. These data are taken from seven samples produced at Arthur D. Little, Inc. in the eighteen inch bell jar. Two samples are taken from material received from National Metallizing Division of Standard Packaging Corporation and eighteen samples were taken from three different batches of material received from Hastings & Company, Inc. (emittance values for coating thicknesses greater than 2300 Angstroms are not shown on the Figure.)

The average emittance of about .025 was obtained with 250°A thick gold coatings. This value decreases to about .017 at a coating thickness of 1500°A. Beyond 1500°A the emittance value of the gold remains constant. This trend is evident in the data though some of the values spread between .015 and .025 at a thickness of 1000°A. Actually the higher values in this region are attributed to the use of impure gold (23K) in the coating preparation. All other values were obtained with samples prepared from gold of 99.9 per cent or greater purity.

Based upon the emittance data discussed above, aluminum and gold coatings are opaque to infrared radiation at thicknesses greater than 600°A and 1500°A respectively. It was thought that the emittance of gold at thickness less than 1500 could be improved by applying the gold coatings over aluminun coatings. A number of samples consisting of aluminum substrate overcoated with gold were prepared. The pertinent data are presented in Table III-7. The emittance values of the composite coatings are compared to those obtained for plain gold coatings below.

Test No.	Coating Metals	Thickness of Gold Coating(°A)	Emittance
277	Gold	488	.019
278	Gold	1415	.015
292	Gold	1000	.021
293	Gold	1410	.028
296	Gold	1900	.019
297	Gold	322	.025
276	Gold/Aluminum	498/320	.022
280	Gold/Aluminum	1300/455	.014
319	Gold/Aluminum	166/430	.018
321	Gold/Aluminum	413/307	.018
356	Gold/Aluminum	83/344	.026

From the comparison above it is evident that above 500°A there is no improvement in the emittance when the gold is coated over aluminum. Based on the data represented by tests 319 and 356, the indications are that, as the gold coating thickness decreases below 500 Angstroms, the surface emittance approaches the value corresponding to that of the aluminum undercoat.

b. Environmental Effects

Three gold coated samples were placed in each of the four environments for 50 and 100 hour periods. The results obtained are presented in Tables III-12 thru III-15 and are summarized in Figure III-19.

A45 Environment

All samples showed no change in the emittance value (within experimental limits) and adhesion remained acceptable (zero per cent lift-off) for 100 hours.

A95 Environment

The coating of one sample produced a 30 per cent lift-off after 100 hours. A second sample showed an emittance increase of 30 per cent after 50 hours and remained unchanged after 100 hours. All other samples remained unchanged.

CO_2 Environment

Of the three samples two showed emittance increases of 15 and 20 per cent. The coating adhesion, for each sample, remained acceptable throughout the test period.

Salt Environment

Only two samples were affected by the salt environment. The scotch tape test produced 40 per cent lift-off on one sample. The emittance of a second sample (330-B) produced a net increase in emittance of 12 per cent after 100 hours.

c. Conclusions

Emittance values of about .017 can be expected from commerical vacuum deposited gold coatings at thicknesses greater than 1500 Angstroms. The coating emittances and adhesion appear to be generally stable for all environments tested. Through better quality control and possibly improved manufacturing processes the commercial product can be made acceptable on the basis of the criteria established in this program. Gold coatings are suited for use in multi-layer insulations and their use for this purpose should be extended.

3. Silver and Silver Combination Coatings

a. Emittance and Thickness

(1) Silver

The emittance and thickness measurements made on silver metallized polyester film are presented in Table III-8 and in Figure III-20. These data are taken from thirteen samples produced at Arthur D. Little, Inc. in the eighteen inch bell jar. Two samples are taken from material purchased from G. T. Schjeldahl and two samples are taken from material purchased from the Gomar Manufacturing Company.

An average emittance of 0.011 was obtained with silver coatings at thicknesses greater than 1000 Angstroms. At 100 Angstroms thickness the emittance is approximately .02 and decreases asymptotically to .011 with increasing coating thickness. These data are taken from fresh coatings and from coatings that were stored in nitrogen and ambient air environments for periods up to 1000 hours. The type and duration of these environments do not have an apparent effect on the emittance values. It is to be noted that silver coatings only a few hundred Angstroms thick produce surface emittances below that of the best aluminum coatings.

Four measurements on samples prepared from the Gomar manufactured material, approximately one moth after its receipt, produced values that were significantly greater than those measured previously with other silver coatings including the as-received Gomar material. See Table IV-16 for comparison of emittance data and Figure III-20. This material had been stored in a metal container which contained an atmosphere of nitrogen gas. As indicated above, other silver coatings tested after a month in both nitrogen and ambient air environments show comparable emittance values. The higher emittance values of these particular samples are believed to be the result of the tight packing of the inner layers of the received roll which resulted in a wrinkled film after unrolling.

(2) Silicon Monoxide/Silver Coatings

As will be shown later, the 95°F humid environments do increase the emittance of silver coatings. Thus, methods for protecting the silver without seriously degrading the emittance were investigated. These methods included the addition of extremely thin coatings of silicon monoxide, gold and aluminum to the silver.

Silicon monoxide in nominal thicknesses of 70 and 150 Angstroms was applied over silver coatings generally greater than 745 Angstroms thick. Of the ten samples tested, seven were produced at Arthur D. Little, Inc. in the eighteen inch bell jar and three were obtained from material purchased from the G. T. Schjeldahl Company. The silicon monoxide coatings on all samples were measured during production with thin film thickness monitors of the crystal type discussed previously.

A comparison of the results presented in Tables III-8 and 9 indicates that the emittance value is increased as much as .005 by the silicon monoxide coatings. There is no clear evidence that the 150°A coatings increase the surface emittance by a larger factor than the 70°A coatings.

(3) Gold and Aluminum/Silver Coatings

In our discussions with vacuum metallizers, it was evident that they considered silicon monoxide coatings difficult to produce. It was also the coating with which they all had acquired the least practice. We, therefore, investigated the use of gold and aluminum coatings in thickness of 100°Angstroms or less for providing protection to the silver coatings since they are more chamically stable than silver.

Two samples, Nos. 64 and 68 were prepared. The former consisted of a 103°A gold coating vacuum metallized over a silver coating of 810°A. The latter consisted of a 83°A aluminum coating over a silver coating of 820°A. The emtttance results, obtained in Tests 329, 381, and 384, show the emittance to be significantly increased over that obtained for pure silver coatings. The table below summarizes these results.

Sample No.	Description	Test No.	Emittance
20-1	Silver, 953°A, ADL	364	.012
20-2	Silver, 1230°A, ADL	365	.013
25-1	Silver 1210°A, ADL	337	.011
64	Gold, 103°A, ADL/Silver 810°A, ADL	379	.024
68	Al, 83°A, ADL/Silver 820°A, ADL	381	.033
68	Al, 83°A, ADL/Silver 820°A, ADL	384	.039

b. Environmental Effects

(1) Silver Coatings

One silver coated sample was placed in each of the two humidity environments for 50 and 100 hour periods. The results obtained are presented in Tables III-12 and 13 and Figure III-21. Both environments affect emittance and adhesion of the coatings. In the A45 environment the emittance is increased about 20 per cent in 100 hours. After 50 hours, the scotch tape test resulted in about 10 per cent coating lift-off. In the A95 environment there is about 30 per cent increase in coating emittance in 100 hours; most of the increase takes place in the first 50 hours. The scotch tape test indicates progressive deterioration of coating adhesion which amounts to about 40 per cent after 100 hours of test.

The CO_2 environment has resulted in an emittance degradation of about 40 per cent in 100 hours. Adhesion in this period remained acceptable. No apparent changes in the appearance of the coating had taken place after 100 hours in the environment.

The salt environment produced an anomalous situation in that the emittance improved and the adhesion degraded as the time of the immersion in the environment increased. The emittance decreased from an initial value of .020 to .0165 at the end of 100 hours. This decrease amounts to about 15 per cent and was progressive. On the other hand, the adherence decreased to 50 per cent at the end of 100 hours and further to 100 per cent at the end of 100 hours. Again, no apparent changes in the appearance of the coatings had taken place after 100 hours.

(2) Silicon Monoxide/Silver Coatings

One silicon monoxide/silver coated sample was placed in each of the four environments for 50 and 100 hour periods. The results obtained are presented in Tables III-9 and 12 thru 15 and Figure III-21.

The A45 environment produced no emittance or adhesion degradation in the sample. The A95 environment degraded both factors. For example, the starting emittance value of Sample No. 43 was .0141. This is about average for samples with its SiO and silver thickness. There is a slight but continual degrading of the emittance in the 50 and 100 hour tests, resulting in an over-all increase of about 20 per cent. The adhesion of metal to film is affected by the first 50 hour test but appears not to become progressive in the 100 hour test. About 60 per cent of the surface had a milky appearance. The other 40 per cent appeared unaffected. Under a microscope, a milky area had a very fine granular appearance. It was not determined whether the SiO or the silver coatings or both had been affected by the A95 environment.

c. Conclusions

Emittance values of .011 were obtained with silver coatings greater than 1000°A in thickness. Dry atmospheric air or nitrogen atmospheres appear to produce no noticeable degradation in the value in 1000 hours. Thin overcoats of gold, aluminum and silicon monoxide degrade the surface emittance; the gold and aluminum cause serious degradation while the silicon monoxide increases the emittance from .011 to about .016. Humidity environments of 45 and 95 per cent relative humidity, 95°F degrade both the emittance and adhesion of the silver coatings. The silicon monoxide/silver coatings are not affected by the A45 environment. In all other environments the emittance or the adhesion is degraded. These coatings not as stable as the gold coatings.

4. Copper Coatings

a. Emittance and Thickness

(1) Copper Coatings

The emittance and thickness measurements made on five samples of copper metallized polyester film are presented in Table III-10. These samples were produced by Arthur D. Little, Inc. in the eighteen inch bell jar. Coating thickness ranged from 540 to 1500 Angstroms An average value .013 was obtained for the coating emittances.

(2) Silicon Monoxide/Copper

As will be shown later, the copper coatings deteriorated when placed in the high humidity environments. Thus, 75°A of silicon monoxide protective coatings were applied over the 760°A of copper in five samples. These coatings added about .004 to the bare copper emittance values of .013. The resulting value of .017 is better than that obtained with the best aluminum coatings.

b. Environmental Effects

(1) Copper Coatings

One copper coated sample was placed in each of the two humidity environments. Sample No. 58 in the A45 environment showed about 30 per cent increase in emittance with the largest portion of the increase occurring in the first 50 hours. Adhesion of the coating remained acceptable during the test period.

The coating of Sample No. 59 degraded seriously in the A95 environment. In 100 hours the emittance increased almost 100 per cent. Adhesion of the coating remained acceptable during the test period. No further tests were run. See Figure III-22.

(2) Silicon Monoxide/Copper Coatings

One SiO/copper sample was placed in each of the four environments. The data are summarized in Tables III-11 thru 15. The protective coating resulted in no apparent emittance changes in all environments except the A95. The emittance was progressively deteriorated from a value of .017 to .025 at the completion of the 100 hour test. The coating adhesion was likewise degraded only by the A95 environment. The scotch tape test showed a 10 per cent lift-off after 50 hours. This value remained unchanged at 100 hours. See Figure III-22.

c. Conclusions

Emittance values of .013 were obtained with bare copper coatings over a thickness range of 500 to 1500°A. As is generally known, humid atmospheres have a serious effect on the emittance of the coatings. A silicon monoxide protective coating markedly reduces the effects of environment and produces a material acceptable for use in multi-layer insulations. The emittance values obtained are comparable to those obtained with gold and SiO/coated silver.

5. Sources of Metallized Film

The manufacturers of metallized coatings used in the current program are identified in the Table III-16. Metallized polyester films were purchased from these suppliers using the specification presented in Table III-17 as basis for establishing the requirements of the purchase orders. Since there are no industry standards for identifying the thickness and emittance of metallized coatings, the purchase of materials in some cases was based upon the performance of sample materials. The thickness and emittance of the samples was determined using procedures described previously. The manufacturer was then requested to provide materials manufactured in the same manner as the samples.

TABLE III-1

RANDOM ERRORS; + VARIES IN %

Source of Error	Equation for Calculation	True Sample Emittance 1.0	0.5	0.1	0.05	0.01
Sample Temperature	(5)	.726	.544	.399	.381	.365
Disc Temperature	(7)	.866	.721	.773	.865	1.525
Cavity Temperature	(9)	.012	.018	.064	.122	.885
Total Error		1.13	.90	.87	.95	1.80

TABLE III-2

FIXED ERRORS; VALUES IN %

Source of Error	Equation for Calculation	True Sample Emittance 1.0	0.5	0.1	0.05	0.01
Geometry	(12)	0	2.70	4.80	5.00	5.20
Receiver Disc Emittance	(14)	0	-5.26	-9.89	-10.50	-11.00
Cavity Emittance	(16)	-1.65	-1.65	-1.65	-1.65	-1.65
Conductive heat leaks from disc		0.49	0.63	1.39	1.94	3.75
Total Error		-1.16	-3.58	-5.35	-5.21	-3.70

TABLE III-3

COATING THICKNESSES
COMPARISON OF MELT, RESISTANCE AND CRYSTAL MEASUREMENTS

Sample No.	Metal	Thickness (°A)		
		Melt	Resistance	Crystal
1	Gold	340	166	
2-1	Gold	500	498	
2-2	Gold	500	488	
3-1	Gold	500	413	
3-2	Gold	500	322	
5-1	Aluminum	500	230	
5-2	Aluminum	500	253	
6-1	Aluminum	500	186	
7-1	Aluminum	1500	505	
8-1	Aluminum	1500	448	
8-2	Aluminum	1500	440	
9-1	Aluminum	3000	1030	
9-2	Aluminum	3000	1395	
12-1	Gold	1400	1415	
12-2	Gold	1400	1300	
14-1	Gold	1500	1335	
14-2	Gold	1500	1080	
16-1	Silver	500	104	
16-2	Silver	500	83	
17-1	Silver	500	436	
17-2	Silver	500	427	
20-1	Silver	1000	953	
20-2	Silver	1000	1230	
21-1	Silver	1500	1430	
21-2	Silver	1500	1150	
22-1	Silver	500	415	
23-1	Silver	500	432	
24-1	Silver	1500	-	1500
25-1	Silver	1500	1210	1410
26-1	Silver	2500	-	4000
27-1	Silver	2500	2325	3200
29-1	Copper	670	540	
30-1	Copper	1500	1475	
30-2	Copper	1500	1500	
35-1	Gold	750	940	
35-2	Gold	750	783	
36	Silver	600	762	750
42	Silver	600	745	666
48	Aluminum	-	862	790
58	Copper	-	675	761
64	Silver	-	820	810
68	Silver	-	-	820

TABLE III-4

EMISSOMETER DATA SUMMARY

Test Date	Disc No.	Test No.	Sample No.	Sample Description	Envir. Code/Hrs	Emittance
10/19/64	3	227		1145-H25 al. foil, 1 mil, polished side clean		.0398
10/19/64	3	228		114 H25 al. foil, 1 mil, polished with finger prints		.0361
10/20/64	3	229		1145-H25 al. foil, 1 mil, pol. side, fing. pr. removed		.0334
10/20/64	3	230		1145-H25 al. foil, 1 mil, polished with finger prints		.0311
10/20/64	3	231		1145-H25 al. foil, 1 mil, unpolished side		.0196
10/20/64	3	232		Black cavity calib., boil water temp.		.961
10/21/64	3	233		1100-H14 al. foil, 1.2 mil, washed in non-etch detergent		.0255
10/21/64	3	234		1100-H14 al. foil, 1.2 mil, chemic. polished altrex cleaning after		.0299
10/21/64	3	235		Al. tape, 3M		.0318
10/22/64	3	236		Al. tape, 3M, attached masking tape		.0293
10/22/64	3	237		Black dacron cloth with black silicone rubber pigment		.912
10/22/64	3	238		1100-H14 Alcoa Aluminum, 1.2 mil, chem. polished		.0218
10/23/64	3	239		1100-H14 Alcoa Aluminum, spray coated with #9900 booth coaters		.0274
10/23/64	3	240		1145-H25 al. foil, 1 mil, polished side		.0198
10/23/64	3	241		1145-H25 al. foil, 1 mil, unpolished side		.0201
10/23/64	3	242		1145-H25 al. foil, 1 mil, unpolished cleaned with alchol		.0201
12/8/64	3	243		P-1807A rubberized nylon		.928
12/8/64	3	244		P-1807A rubberized nylon(same samples as 243)		.906

TABLE III-4

EMISSOMETER DATA SUMMARY

Test Date	Disc No.	Test No.	Sample No.	Sample Description	Envir. Code/Hrs	Emittance
12/8/64	3	245		Dacron, polyurethane coated		.943
12/8/64	3	246		Nomex HT-1		.857
12/9/64	3	247		Nomex HT-1, P-5995		.804
12/9/64	3	248		Black polyethlene, 4 mil		.868
12/9/64	3	249		Dacron Fabric, 44-003 DuPont Fairprene		.862
12/10/64	3	250		Glass fabric 116, 5812 DuPont Fairprene		.878
12/10/64	3	251		Porous al. foil #10		.0324
12/10/64	3	252		Black cavity calib., boiling water temp.		.968
12/11/64	3	253		Porous al. foil #7		.0450
12/11/64	3	254		Plain filament dacron cloth #3537		.888
12/11/64	3	255		Nylon twill, type 200, Style 301		.888
12/14/64	3	256		Dacron fabric, polyurethane coating, Cat-323		.906
12/29/64	3	257		Al. Mylar film, 3/4 mil Roll A		.0444
12/29/64	3	258		Al. Mylar film, 3/4 mil Mylar side Roll B		.0903
12/29/64	3	259		Al. Mylar film, 3/4 mil alum. side Roll B		.0665
12/30/64	3	260		Silver Mylar film, 3/4 mil, Mylar side		.535
12/30/64	3	261		Silver Mylar film, 3/4 mil, silver side		.0564
12/30/64	3	262		Alum. Mylar, 3/4 mil inside Roll A		.0520
12/30/64	3	263		Alum. Mylar, 3/4 mil inside Roll B		.0818
12/31/64	3	264		Alum. Mylar, 3/4 mil outside Roil A Mylar side		.540

TABLE III-4

EMISSOMETER DATA SUMMARY

Test Date	Disc No.	Test No.	Sample No.	Sample Description	Envir. Code/Hrs	Emittance
1/8/65	3	265		Nylon metallized fabric		.136
1/8/65	3	266		Aluminum Mylar, 3/4 mil, inside Roll B		.0802
1/8/65	3	267		Aluminum Mylar, 3/4 mil, inside Roll B		.553
1/26/65	3	268		Aluminum foil without DOP plasterizer		.0284
1/26/65	3	269		Aluminum foil with .1 cc DOP plasterizer		Abort.
1/27/65	3	270		Aluminum foil with 11 mg DOP plasterizer		.178
5/11/65	3	271		1145-H-25 al. foil, 1 mil, unpolished side		.0244
5/11/65	3	271A		1145-H25 al. foil, 1 mil, unpolished side		.0201
5/11/65	3	271B		1145-H25 al. foil, 1 mil, unpolished side		.0203
5/11/65	3	272		1145-H25 al. foil, 1 mil, unpolished side		.0205
6/15/65	4	273		1145-H25 al. foil, 1 mil, unpolished 3M blacked		.954
6/15/65	4	273A		Sample 273 with added 3M spray coat		.961
6/16/65	4	274		Gold Plate on 304SS, XHV-8, see Test 134		.0416
6/17/65	4	275		Alum. Mylar, 320°A, 1/4 mil		.0354
6/18/65	4	276		Gold over aluminum coated on Mylar, 498°A, 1/2 mil		.0218
6/21/65	4	277		Gold coated Mylar, 488°A, 1/4 mil		.0186
6/21/65	4	278		Gold coated Mylar, 1415°A, 1/4 mil		.0151
6/21/65	4	279		Alum. Mylar one side only, 1395°A, 1/4 mil		.0226
6/22/6	4	280		Gold, 1300°A, ADL/Al - 455°A, NRC/Mylar, 1/4 mil		.0144
6/22/65	4	281		Alum. 1 mil unpolished		.0227

TABLE III-4

EMISSOMETER DATA SUMMARY

Test Date	Disc No.	Test No.	Sample No.	Sample Description	Envir. Code/Hrs	Emittance
6/23/66	4	282		Alum. Mylar, 1030°A, 1/4 mil		.0220
6/23/65	4	283		Alum. Mylar, 525°A, 1/4 mil		.0260
6/24/65	4	284		Alum. Mylar, 430°A, NRC 62465		.0236
6/24/65	4	285		Alum. Mylar, 450°A, NRC 62465		.0273
6/24/65	4	286		Alum. Mylar, 777°A, 1/4 mil, Hy-Sil		.0327
6/25/65	4	287		Alum. Mylar, 732°A, 1/4 mil, Hy-Sil		.0335
6/26/65	4	288		Alum. Mylar, 445°A, NRC 62465		.0227
6/25/65	4	289		Alum. Mylar, 772°A, 1/4 mil, Hy-Sil		.0324
6/25/65	4	290		Gold on metal plate Sample No. 1		.0226
6/28/65	4	291		Gold on metal plate Sample No. 2		.0239
6/28/65	4	292		Gold coated polyester film, 1000°A, 1/4 mil, NRC 62664		.0215
7/8/65	5	293		Gold, 1410°A, ADL/Aluminum ( ) NRC/Mylar, 1/4 mil		.0275
7/9/65	5	294		Gold plate on metal, finger printed surface, Sample No. 2		.0128 (value doubtful)
7/12/65	5	295		Test No. 294 rerun		.0270
7/12/65	5	296		Gold, 1900 °A, ADL/Aluminum ( ) NRC/Mylar, 1/4 mil		.0191
7/13/65	5	297	3-2	Gold, 322°A, ADL/Mylar, 1/4 mil		.0246
7/13/65	5	298		Gold plate on metal, clean surface, Sample No. 2		.0216
7/14/65	5	299		Gold plate on metal, finger printed surface, Sample No. 2		.0273
7/15/65	5	300		Aluminum, 346°A, NRC/Mylar 1/4 mil		.0251
7/15/65	5	301		Aluminum, 455°A, NRC/Mylar, 1/4 mil		.0226

TABLE III-4

EMISSOMETER DATA SUMMARY

Test Date	Disc No.	Test No.	Sample No.	Sample Description	Envir. Code/Hrs	Emittance
7/15/65	5	302	11-2	Aluminum, 555°A, ADL and NRC/Mylar, 1/4 mil		.0226
7/16/65	5	303	10-1	Aluminum, 665°A, ADL/Mylar, 1/4 mil		.0255
7/19/65	5	304	10-2	Aluminum, 885°A, ADL and NRC/Mylar, 1/4 mil		.0415
7/20/65	5	305	7-2	Aluminum, 1090°A, ADL and NRC/Mylar, 1/4 mil		.0224
7/21/65	5	306	7-1	Aluminum, 505°A, ADL/Mylar, 1/4 mil		.0213
7/22/65	5	307		Aluminum, 380°A, NRC/Mylar, 1/4 mil		.0266
7/23/65	5	308	8-1	Aluminum, 448°A, ADL/Mylar, 1/4 mil		.0225
7/23/65	5	309	8-2	Aluminum, 440°A, ADL/Mylar, 1/4 mil		.0221
7/27/65	5	310		Aluminum, 455°A, NRC/Mylar, 1/4 mil, 2% perforations		.0479
7/28/65	5	311		Aluminum, 342°A, NRC/Mylar, 1/4 mil, 2% perforations		.0400
7/28/65	5	312		Aluminum, 310°A, NRC/Mylar, 1/4 mil		.0250
7/29/65	5	313	11-1	Aluminum, 146°A, ADL/Mylar, 1/4 mil		.0421
7/30/65	5	314		Aluminum 350°A, NRC/Mylar, 1/4 mil		.0311
7/30/65	5	315		Aluminum, 1145-H25, 1 mil (oily surface)		.0251
8/2/65	5	316	6-1	Aluminum, 186°A, ADL/Mylar, 1/4 mil		.0279
8/3/65	5	317		Aluminum, 253°A, ADL/Mylar, 1/4 mil		.0267
8/4/65	5	318	5-1	Aluminum, 230°A, ADL/Mylar, 1/4 mil		.0365
8/4/65	5	319	1	Gold, 166°A, ADL/Aluminum, 350°A, NRC/Mylar, 1/4 mil		.0179
8/5/65	5	320		Aluminum, 430°A, NRC/Mylar, 1/4 mil		.0240
8/5/65	5	321	3-1	Gold, 413°A, ADL/Aluminum, 307°A, NRC/Mylar, 1/4 mil		.0178

TABLE III-4

EMISSOMETER DATA SUMMARY

Test Date	Disc No.	Test No.	Sample No.	Sample Description	Envir. Code/Hrs	Emittance
8/6/65	5	322		Aluminum, 307°A, NRC/Mylar, 1/4 mil		.0264
8/6/65	5	323		Aluminum, 455°A, NRC/Mylar, 1/4 mil		.0255
8/10/65	5	324		Aluminum, 772°A, Hy-Sil/Mylar, 1/4 mil		.0247
8/18/65	5	325	15-2	Aluminum, 1230°A, ADL-NRC/Mylar, 1/4 mil		.0197
		326		Blank		
8/23/65	5	327	XHV-5	Gold, .0003" plate/304 SS, 1/8"		.0966
8/23/65	5	328	15-1	Aluminum, 807°A, ADL/Mylar, 1/4 mil		.0244
8/25/65	5	329		Silver, 436°A, ADL/Mylar, 1/4 mil		.0172
8/25/65	5	330		Silver, 427°A, ADL/Mylar, 1/4 mil		.0128
8/26/65	5	331	28-1	Silver, 900°A, ADL/Dexter Paper, .011"		.2590
8/27/65	5	332	28-2	Silver, 900°A, ADL/Glass fabric, Style 104, .0025"		.5280
9/7/65	5*	333		Black cavity, LN_2, TC No. 1 calibration		-
9/7/65	5	334		Black cavity, LN_2, TC No. 2 calibration		-
9/8/65	5	335		Silver, 2325°A, ADL/Mylar, 1/4 mil		.0109
9/8/65	5	336		Silver, 2325°A, ADL/Silicone oxide, 150°A, ADL/Mylar, 1/4 mil		.0163
9/9/65	5	337		Silver, 1210°A, ADL/Mylar, 1/4 mil		.0110
9/9/65	5	338		Silver, 1210°A, ADL/Silicone oxide, 340°A, ADL/Mylar, 1/4 mil		.0154
9/10/65	5	339	(23-2)	Silver, 432°A, ADL/Silicone oxide, 75°A, ADL/Mylar, 1/4 mil		.0124
9/13/65	5	340	(23-1)	Silver, 432°A, ADL/Mylar, 1/4 mil		.0099
9/13/65	5	341	(29-1)	Copper, 540°A, ADL/Mylar, 1/4 mil		.0133

*Broken thermocouples on receiver disc replaced 3 September 1965.

TABLE III-4

EMISSOMETER DATA SUMMARY

Test Date	Disc No.	Test No.	Sample No.	Sample Description	Envir. Code/Hrs	Emittance
9/13/65	5	342	(29-2)	Copper, 540°A, ADL/Silicone oxide, 150°A, ADL/Mylar 1/4 mil		.0170
9/13/65	5	343		Black paint, 3M/aluminum disc, 1/8", ADL		.890
9/14/65	5	344		Aluminum foil, .001		.0179
9/14/65	5	345		Aluminum foil, .001		.0169
9/14/65	5	346		Black cavity, LN_2, T.C. calibration		-
9/14/65	5	347		Black cavity, boiling H_2O		.979
9/15/65	5	348		Black cavity, LN_2, T.C. calibration		-
9/16/65	5	349		Black cavity, LN_2, T.C. calibration		-
9/21/65	5	350	(302)	Aluminum foil, .001/aluminum disc, 1/8"		.0177
9/22/65	5	351	(13-1)	Gold, 25°A, ADL/Mylar, 1/4 mil		.115
9/22/65	5	352		Black paint, 3M/aluminum disc, 1/8"		.887
9/23/65	5	353		Aluminum foil, .001		.0204
9/23/65	5	354	(302)	Aluminum foil, .001		.0188
9/23/65	5	355	(30-2)	Copper, 1500°A/Mylar, 1/4 mil		.0142
9/[illegible]/65	5	356	(13-2)	Gold, 83°A, **ADL/Aluminum** ( )°A		.026
9/28/65	5	357	(30-1)	Copper, 1475°A, ADL/Mylar, 1/4 mil, plate contact 25%		.0144
9/28/65	5	358	(30-1)	Copper, 1475°A, ADL/Mylar, 1/4 mil, plate contact 25%		.0125
9/28/65	5	359	(14-1)	Gold, 1335°A, ADL/Mylar, 1/4 mil		.0148
9/29/65	5	360	(16-2)	Silver, 83°A/Mylar, 1/4 mil		.0206

TABLE III-4

EMISSOMETER DATA SUMMARY

Test Date	Disc No.	Test No.	Sample No.	Sample Description	Envir. Code/Hrs	Emittance
9/29/65	5	361	(16-1)	Silver, 104°A/Mylar, 1/4 mil, stored GN_2		.0191
9/30/65	5	362	(18-1)	Silver, 294°A/Mylar, 1/4 mil		.0158
9/30/65	5	363	(18-2)	Silver, 353°A/Mylar, 1/4 mil		.0153
10/1/65	5	364	(20-1)	Silver, 953°A, ADL/Mylar, 1/4 mil		.0118
10/1/65	5	365	(20-2)	Silver 1230°A, ADL/Mylar, 1/4 mil		.0130
10/5/65	5	366	(303A)	Gold, 350°A, Hastings/Mylar, 1/4 mil		.0204
10/6/65	5	367	(303B)	Gold, 235°A, Hastings/Mylar, 1/4 mil		.0234
10/15/65	5	368		Black cavity LN_2, T.C. calibration		-
10/15/65	5	369		Black cavity, boiling H_2O		.998
10/15/65	5	370	34-2	Mylar, 1/4 mil		.349
10/15/65	5	371	35-2	Gold, 783°A, ADL/Mylar, 1/4 mil		.015
10/18/65	5	372	20-1	Silver 935°A, ADL/Mylar, 1/4 mil		.0145
10/18/65	5	373	20-2	Silver, 1230°A, ADL/Mylar, 1/4 mil		.0111
10/18/65	5	374	304A	Gold, 920°A, Hastings/Mylar, 1/4 mil		.0234
10/18/65	5	375	304B	Gold, 750°A, Hastings/Mylar, 1/4 mil		.0231
10/19/65	5	376	36	Silver, 762°A, ADL/Mylar, 1/4 mil		.016
10/20/65	5	377	42	SiO, 75°A, ADL/Silver, 745°A, ADL/Mylar, 1/4 mil		.016
10/20/65	5	378	53	Copper, 675°A, ADL/Mylar, 1/4 mil		.0126
10/20/65	5	379	64	Gold, 103°A, ADL/Silver, 810°A, ADL/Mylar, 1/4 mil		.024
10/20/65	5	380		Black cavity, LN_2, T.C. calibration		-

TABLE III-4

EMISSOMETER DATA SUMMARY

Test Date	Disc No.	Test No.	Sample No.	Sample Description	Envir. Code/Hrs	Emittance
10/25/65	5	381	68	Aluminum 83 Å ADL/Silver 820 Å ADL/Mylar, 1/4 mil		.033
10/25/65	5	382	-	Black cavity, LN_2, T.C. Calibration		-
10/25/65	5	383	-	Black cavity, Boiling H_2O		1.006
10/26/65	5	384	68	Aluminum 83 Å ADL/Silver 820 Å ADL/Mylar, 1/4 mil		.0386
10/26/65	5	385	18-2	Silver 353 Å ADL/Mylar, 1/4 mil		.0152
10/26/65	5	386	306A	Aluminum 482 Å NASA/Mylar, 1/4 mil		.0218
10/26/65	5	387	52	SiO 75 Å ADL/Copper 761 Å ADL/Mylar 1/4 mil		.0179
10/27/65	5	388	48	Aluminum 862 Å ADL/Mylar, 1/4 mil		.0210
10/27/65	5	389	36	Silver 762 Å ADL/Mylar, 1/4 mil		.0133
10/27/65	5	390	20-1	Silver 953 Å ADL/Mylar, 1/4 mil		.0151
10/28/65	5	391	305	Aluminum 376 Å NRC/Mylar, 1/4 mil		.0316
10/19/65	5	392	302	Aluminum .001" foil		.0214
10/28/65	5	393	306B	Aluminum 249 Å NASA/Mylar, 1/4 mil		.0310
10/28/65	5	394	308	Gold 240 Å NM/Mylar, 1/4 mil		.0214
10/28/65	5	395	309	Gold 244 Å NM/Mylar, 1/4 mil		.0222
10/28/65	5	396	307B	Aluminum 475 Å NASA/Mylar, 1/4 mil		.0221
10/29/65	5	397	307A	Aluminum 300 Å NASA/Mylar, 1/4 mil		.0273
10/29/65	5	398	20-2	Silver 12[illegible]0 Å Mylar, 1/4 mil		.022
11/1/65	5	399	306B	Aluminum 249 Å NASA/Myla , 1/4 mil		.0322
11/8/65	5	400	36	Silver 762 Å ADL/Mylar, 1/4 mil		.0161

TABLE III-4

EMISSOMETER DATA SUMMARY

Test Date	Disc No.	Test No.	Sample No.	Sample Description	Envir. Code/Hrs	Emittance
11/8/65	5	401	58	Copper 675Å ADL/Mylar, 1/4 mil		.0167
11/9/65	5	402	-	Black Cavity, LN_2, TC, Calibration		.021
11/9/65	5	403	48	Aluminum 862Å ADL/Mylar, 1/4 mil		.021
11/9/65	5	404	302	Aluminum .001 Foil		.021
11/10/65	5	405	310	Paint Alum. Epoxy on Anodized Magnesium/MIT No. 4		.312
11/10/65	5	406	308	Gold 240Å NM/Mylar, 1/4 mil		.0211
11/12/65	5	407	304A	Gold 920Å Hast./Mylar, 1/4 mil		.025
11/12/65	5	408	311	Paint, Epoxy, Resinweld, on Anodized Magnesium/MIT No. 6		.543
11/13/65	5	409	312	Paint, Gray, over primer on Anodized Magnesium/MIT No. 9		.762
11/15/65	5	410	52	SiO 75Å ADL/Copper 761Å ADL/Mylar, 1/4 mil		.0178
11/15/65	5	411	42	SiO 75Å ADL/Silver 745Å ADL/Mylar, 1/4 mil		.0152
11/15/65	5	412	35-2	Gold 783Å ADL/Mylar, 1/4 mil		.0159
11/15/65	5	413	313	Anodized (Chromic-Acid) on Aluminum/MIT No. 1		.577
11/15/65	5	414	305	Aluminum 376Å NRC/Mylar, 1/4 mil		.025
11/16/65	5	415	318	Paint, Epoxy, on Sheri-Williams, Silverbrite on Anodized Magnesium/MIT No. 8		.725
11/17/65	5	416	314	Paint, Chromate on Aluminum/MIT No. 2		.0475
11/17/65	5	417	315	Anodized, Dyed Black on Alum./MIT No. 3		.720
11/19/65	5	418	316	Paint, Aluminum Epoxy (Amicon) on Anodized Magnesium/MIT No. 5		.336
11/19/65	5	419	304A	Gold 1000Å Hast./Mylar, 1/4 mil		.025

TABLE III-4

EMISSOMETER DATA SUMMARY

Test Date	Disc No.	Test No.	Sample No.	Sample Description	Envir. Code/Hrs	Emittance
11/19/65	5	420	317	Anodized on Aluminum/MIT No. 7		.546
11/22/65	5	421	313	Anodized, Chromic-Acid, on Alum./MIT No. 1		.575
11/22/65	5	422	35-2	Cold 783Å ADL/Mylar, 1/4 mil		.0148
11/23/65	5	423	308	Gold 240Å Nat. Met./Mylar, 1/2 mil		.0235
11/23/65	5	424	305	Aluminum 376Å NRC/Mylar, 1/4 mil		.0291
11/24/65	5	425	42	SiO 75Å ADL/Silver 745Å ADL/Mylar, 1/4 mil		.0165
11/24/65	5	426	36	Silver 762Å ADL/Mylar, 1/4 mil		.016
11/26/65	5	427	48	Aluminum 862Å ADL/Mylar, 1/4 mil		.0195
11/26/65	5	428	52	SiO 75Å ADL/Copper 761Å ADL/Mylar, 1/4 mil		.0173
11/29/65	5	429	304A	Gold 920Å Hastings/Mylar, 1/4 mil		.0234
11/29/65	5	430	319	Paint, Aluminum Epoxy, on Anodized Magnesium/MIT No. 10		.267
11/30/65	5	431	320	Paint, Aluminum Epoxy, on Anodized Magnesium/MIT No. 11		.267
11/30/65	5	432	58	Copper 675Å ADL/Mylar, 1/4 mil		.0174
12/1/65	5	433	321	Aluminum, 435 Å, NRC/Mylar 1/4 mil	A95/0	.0225
12/1/65	5	434	322	Gold, 212 Å, Nat. Met/Mylar 1/2 mil	A95/0	.0211
12/2/65	5	435	43	SiO, 75 Å, ADL/Silver, 745 A, ADL/1/4 mil Mylar	A95/0	.0141
12/6/65	5	436	37	Silver, 762 Å, ADL/1/4 mil Mylar	A95/0	.0111
12/7/65	5	437	49	Aluminum, 862 Å, ADL/1/4 mil Mylar	A95/0	.0184
12/7/65	5	438	53	SiO 75 Å, ADL/Copper, 761 Å, ADL/1/4 mil Mylar	A95/0	.0174
12/8/65	5	439	35-1	Gold, 940 Å, ADL/1/4 mil Mylar	A95/0	.014

TABLE III-4

EMISSOMETER DATA SUMMARY

Test Date	Disc No.	Test No.	Sample No.	Sample Description	Envir. Code/Hrs	Emittance
12/8/65	5	440	304B	Gold, 920 Å, Hastings/1/4 mil Mylar	A95/0	.021
12/8/65	5	441	59	Copper, 761 Å, ADL/1/4 mil Mylar	A95/0	.012
12/13/65	5	442	49	Aluminum, 862 Å, ADL/1/4 mil Mylar	A95/50	.0225
12/14/65	5	443	43	SiO, 75 Å, ADL/Silver, 745 Å, ADL/1/4 mil Mylar	A95/50	.0199
12/14/65	5	444	35-1	Gold, 940 Å, ADL/1/4 mil Mylar	A95/0	.0145
12/14/65	5	445	304B	Gold, 920 Å, Hastings/1/4 mil M[illegible]ar	A95/50	.023
12/15/65	5	446	53	SiO, 75 Å, ADL/Copper 761 Å, A[illegible] [illegible]/4 mil Mylar	A95/50	.0212
12/15/65	5	447	59	Copper, 761 Å, ADL/1/4 mil Mylar	A95/50	.0437
12/15/65	5	448	325	Silver, 635 Å, Gomer/Mylar, 1/2 mil	-	.0136
12/15/65	5	449	-	ALKYD Resin, 10 mil, ADL/	-	.404
12/16/65	5	450	326	Silver, 537 Å, Gomar/Mylar, 1/2 mil	-	.0119
12/20/65	5	451	37	Silver, 762 Å, ADL/1/4 mil Mylar	A95/50	.0114
12/20/65	5	452	321	Aluminum, 435 Å, NRC/1/4 mil Mylar	A95/50	.0229
12/23/65	5	453	324	Aluminum filled epoxy, MIT, Sample No. 13	-	.339
12/23/65	5	454	323	Aluminum filled epoxy, MIT, Sample No. 12	-	.3342
12/27/65	5	455	322	Gold, 212 Å, Nat. Met/1/2 mil Mylar	A95/50	.0271
12/28/65	5	456	53	SiO, 75 A, ADL/Copper, 761 Å, ADL/1/4 mil Mylar	A95/100	.0254
12/28/65	5	457	327A	Silver, 1150 Å, Schjeldahl/1/4 mil Mylar	-	.0104

TABLE III-4

EMISSOMETER DATA SUMMARY

Test Date	Disc No.	Test No.	Sample No.	Sample Description	Envir. Code/Hrs	Emittance
12/29/65	5	458	327B	Silver, 1010 Å, Schjeldahl/1/4 mil Mylar	-	.0102
12/29/65	5	459	328A	SiO, 60 Å/Silver 1463 Å, Schjeldahl/1/4 mil Mylar	-	.0116
12/30/65	5	460	328B	SiO, 150 Å/Silver 1550 Å, Schjeldahl/1/4 mil Mylar	-	.0154
12/31/65	5	461	329	SiO, 80 Å/Silver 742 Å, Schjeldahl/1/4 mil	-	.0142
12/16/65	5	462	-	ALKYD Resin, 20 mil, ADL/	-	.534
1/11/66	5	463	330A	Gold, 1840 Å, Hastings/Mylar, 1/4 mil		.0146
1/11/66	5	464	331	AZ31B, Dow 17, 60? Cat-A-Lac/MIT No. 14		.365
1/12/66	5	465	330B	Gold, 2072 Å, Hastings/Mylar, 1/4 mil		.0127
1/13/66	5	466	304B	Gold, 920 Å, Hastings/Mylar, 1/4 mil	A95/100	.0225
1/14/66	5	467	337A	Silver, 1680 Å, Gomar/Mylar, 1/2 mil		.0109
1/14/66	5	468	337B	Silver, 1650 Å, Gomar/Mylar, 1/2 mil		.0103
1/17/66	5	469	321	Aluminum, 435 Å, NRC/Mylar, 1/4 mil	A95/100	.243
1/17/66	5	470	59	Copper, 675 Å, ADL/Mylar, 1/4 mil	A95/100	.0713
1/17/66	5	471	322	Gold, 212 Å, Nat. Metal./Mylar, 1/2 mil	A95/100	.0271
1/17/66	5	472	43	SiO, 75 Å, ADL/Silver, 745 Å, ADL/Mylar, 1/4 mil	A95/100	.0175
1/17/66	5	473	66531-2	Alkyd Resin, 10 mil, ADL		.705
1/18/66	5	474	37	Silver, 762 Å, ADL/Mylar, 1/4 mil	A95/100	.0147
1/18/66	5	475	35-1	Gold, 940 Å, ADL/Mylar, 1/4 mil	A95/100	.014
1/18/66	5	476	49	Aluminum, 862 Å, ADL/Mylar, 1/4 mil	A95/100	.0206

TABLE III-4

EMISSOMETER DATA SUMMARY

Test Date	Disc No.	Test No.	Sample No.	Sample Description	Envir. Code/Hrs	Emittance
1/18/66	5	477	66531-11	Alkyd Resin, 10 mil, ADL		.770
1/19/66	5	478	338B	Silver, 1400 Å, Gomar/Mylar, 1/2 mil		Abort
1/19/66	5	479	-	LN_2 Calibration		-
1/19/66	5	480	338B	Silver, 1400 Å, Gomar/Mylar, 1/2 mil		.0116
1/19/66	5	481	337B	Silver, 1650 Å, Gomar/Mylar, 1/2 mil		.0107
1/19/66	5	482	66531-9	Alkyd Resin, 10 mil, ADL		.806
1/19/66	5	483	66531-1	Alkyd Resin, 10 mil, ADL		.820
1/20/66	5	484	338A	Silver, 1400 Å, Gomar/Mylar, 1/2 mil		.022
1/21/66	5	485	34-1	Gold, 1020 Å, ADL/Mylar, 1/4 mil		.0152
1/24/66	5	486	333	Gold, 953 Å, Hastings/Mylar, 1/4 mil		.0259
1/24/66	5	487	50	Aluminum, 862 Å, ADL/Mylar, 1/4 mil		.0203
1/24/66	5	488	44	SiO, 75 Å, ADL/Silver, 745 Å, ADL/Mylar, 1/4 mil		.0150
1/24/66	5	489	54	Sio, 75 Å, ADL/Copper, 761 Å, ADL/Mylar, 1/4 mil		.0170
1/25/66	5	490	66531-1	Alkyd Resin, 10 mil, ADL		.812
1/25/66	5	491	51	Aluminum, 862 Å, ADL/Mylar, 1/4 mil		.0191
1/25/66	5	492	66531-1D	Alkyd Resin, 10 mil, ADL		[illegible]
1/27/66	5	493	339	Polyurethane, Rigid Foam, NASA(Linde)		.450
1/28/66	5	494	34-1	Gold, 1020 Å, ADL/Mylar, 1/4 mil	CO_2/50	.0148
1/31/66	5	495	333	Gold, 953 Å, Hastings/Mylar, 1/4 mil	CO_2/50	.0273

TABLE III-4

EMISSOMETER DATA SUMMARY

Test Date	Disc No.	Test No.	Sample No.	Sample Description	Envir. Code/Hrs	Emittance
1/31/66	5	496	330A	Gold, 1840 Å, Hastings/Mylar, 1/4 mil	CO_2/50	.0146
1/31/66	5	497	50	Aluminum, 862 Å, ADL/Mylar, 1/4 mil	CO_2/50	.0192
1/31/66	5	498	66531-1W	Alkyd Resin, 10 mil, ADL		.760
1/31/66	5	499	66531-1W	Alkyd Resin, 10 mil, ADL		.825
2/1/66	5	500	54	SiO, 75 Å, ADL/Copper, 761 Å, ADL/Mylar, 1/4 mil	CO_2/50	
2/1/66	5	501	44	SiO, 75 Å, ADL/Silver, 745 Å, ADL/Mylar, 1/4 mil	CO_2/50	.01500
2/2/66	5	502	45	Sio, 75 Å, ADL/Silver, 745 Å, ADL/Mylar, 1/4 mil		.0198
2/3/66	5	503	336	Gold, 1050 Å, Hastings/Mylar, 1/4 mil		.0228
2/4/66	5	504	-	Alkyd Resin, 10 mil ADL		.795
2/4/66	5	505	55	SiO, 75 Å, ADL/Copper, 761 Å, ADL/Mylar, 1/4 mil		.0223
2/4/66	5	506	33-2	Gold, 455 Å, ADL/Mylar, 1/4 mil	CO_2/100	.0154
2/7/66	5	507	50	Aluminum, 862 Å, ADL/Mylar, 1/4 mil	CO_2/100	.0184
2/8/66	5	508	34-1	Gold, 1020 Å, ADL/Mylar, 1/4 mil	CO_2/100	.0187
2/8/66	5	509	44	SiO, 75 Å, ADL/Silver, 745 Å, ADL/Mylar, 1/4 mil	CO_2/100	.0207
2/9/66	5	510	340	Silver, 985 Å, Gomar, Mylar 1/2 mil		.0175
2/9/66	5	511	340	Repeat Test No. 510		.0179
2/10/66	5	512	-	LN_2 Calibration		-
2/10/66	5	513	341	Silver, 1000 Å, Gomar/Mylar, 1/2 mil		.0101
2/10/66	5	514	342	Silver, 1000 Å, Gomar/Mylar, 1/2 mil		.0103
2/10/66	5	515	54	SiO, 75 Å, ADL/Copper, 761 Å, ADL/Mylar, 1/4 mil	CO_2/100	.0166

TABLE III-4

EMISSOMETER DATA SUMMARY

Test Date	Disc No.	Test No.	Sample No.	Sample Description	Envir. Code/Hrs	Emittance
2/11/66	5	516	333	Gold, 953 Å, Hastings/Mylar, 1/4 mil	CO_2/100	.0299
2/11/66	5	517	330A	Gold, 1840 Å, Hastings/Mylar, 1/4 mil	CO_2/100	.0153
2/11/66	5	518	33-2	Gold, 455 Å, ADL/Mylar, 1/4 mil	S95/50	.0153
2/14/66	5	519	51	Aluminum, 862 A, ADL/Mylar, 1/4 mil	S95/50	.0187
2/15/66	5	520	330B	Gold, 2072 Å, Hastings/Mylar, 1/4 mil	S95/50	.0160
2/15/66	5	521	344	Silver, plated on Invar		.0130
2/16/66	5	522	45	SiO, 75 Å, ADL/Silver, 745 Å, ADL/Mylar, 1/4 mil	S95/50	.0179
2/17/66	5	523	336	Gold, 1050 Å, Hastings, Mylar, 1/4 mil	S95/50	.0225
2/17/66	5	524	55	SiO, 75 Å, ADL/Copper, 761 Å, ADL/Mylar, 1/4 mil	S95/50	.0248
2/18/66	5	525	345	Silver, 1300 Å, Gomar		.0242
2/22/66	5	526	343A	Gold, 2220 Å, Gomar		.019
2/23/66	5	527	343B	Gold, 3100 A, Hastings		.0176
2/24/66	5	528	-	Black, 3M Paint, Calibration check		.866
2/24/66	5	529	346A	Silver, 1290 Å, Gomar		.0342
2/28/66	5	530	346B	Silver, 2210 Å, Gomar		.0158
2/28/66	5	531	345	Silver, 1300 Å, Gomar		.0187
2/28/66	5	532	33-2	Gold, 455 Å, ADL/Mylar, 1/4 mil	S95/100	.0152
2/28/66	5	533	347	Silver, plated on Invar and polished		.0132

TABLE III-5

DATA SUMMARY

EMITTANCE PROGRAM SAMPLES

GROUP 2 - ALUMINUM

Sample No.	Coating Thick. (Å)	Condition Code	Condition Hours	Emittance Test	Emittance ε	Condition Code	Condition Hours	Emittance Test	Emittance ε	Condition Code	Condition Hours	Emittance Test	Emittance ε	Condition Code	Condition Hours	Emittance Test	Emittance ε
5-1	230	AA	1775	318	.0365												
6-1	186	AA	1490	316	.0279												
6-2	525	AA	790	283	.026												
7-1	505	AA	1440	306	.0213												
7-2	1090	AA	1416	305	.0224												
8-1	448	AA	1416	308	.0225												
8-2	440	AA	1416	309	.0221												
9-1	1030	AA	695	282	.022												
9-2	1395	AA	650	279	.0226												
10-1	665	AA	1200	303	.0255												
11-1	148	AA	1490	313	.0421												
11-2	555	AA	1180	302	.0227												
15-1	807	AA	168	328	.024												
15-2	1230	AA	48	325	.020												
5-2	253	AA	1750	317	.026												
10-2	855	AA	1320	304	.0415												
48	862	N	196	388	.021	A45	50	403	.021	A45	100	427	.02				
49	862	N	935	437	.018	A95	50	442	.023	A95	100	476	.0206				

Codes	Conditioning Environment
AA	Air, Ambient
Axx	Air, xx per cent Relative Humidity
S	Salt Atmosphere
C	Carbon Dioxide
N	Nitrogen

Group No.	Coating
1	Gold
2	Aluminum
3	Gold/Aluminum
4	Silver
5	SiO/Silver
6	Copper
7	SiO/Copper
8	Rhodium

TABLE III-5

DATA SUMMARY

EMITTANCE PROGRAM SAMPLES

GROUP 2 - ALUMINUM

Sample No.	Coating Thick. (Å)	Condition Code	Condition Hours	Emittance Test	Emittance ε	Condition Code	Condition Hours	Emittance Test	Emittance ε	Condition Code	Condition Hours	Emittance Test	Emittance ε	Condition Code	Condition Hours	Emittance Test	Emittance ε
50	862	N_2	3mo.	487	.020	CO_2	50	497	.019	CO_2	100	507	.018				
51	862	N_2	3mo.	491	.019	S95	50	519	.019	S95	100	535	.020				
305	376	AA	5 mo	391	.0316	A45	50	414	.025	A45	100	424	.0291				
306A	482	AA		386	.022												
306B	249	AA		393	.031	AA		399	.032								
307A	300	AA		397	.027												
307B	475	AA		396	.022												
321	435	AAS	6 mo	433	.023	A95	50	452	.0229	A95	100	469	.243				

Codes	Conditioning Environment
AA	Air, Ambient
Axx	Air, xx per cent Relative Humidity
S	Salt Atmosphere
C	Carbon Dioxide
N	Nitrogen

Group No.	Coating	Group No.	Coating
1	Gold	6	Copper
2	Aluminum	7	SiO/Copper
3	Gold/Aluminum	8	Rhodium
4	Silver		
5	SiO/Silver		

TABLE III-6

DATA SUMMARY

EMITTANCE PROGRAM SAMPLES

GROUP 1 - GOLD

Sample No.	Coating Thick. (Å)	Condition		Emittance		Condition		Emittance		Condition		Emittance		Condition		Emittance	
		Code	Hours	Test	ε	Code	Hours	Test	ε	Code	Hours	Test	ε	Code	Hours	Test	ε
2-2	488	AA	840	277	.0185												
3-2	322	AA	1350	297	.0246												
12-1	1415	AA	576	278	.015												
13-1	25	AA	2780	351	.116												
14-1	1335	AA	2890	359	.015												
31-1	262																
31-2	278																
32-1	202																
32-2	190																
33-1	515																
33-2	455	N_2	4mo.	506	.015	S95	50	518	.015	S95	100	532	.015				
34-1	1020	N_2	4mo.	485	.0152	CO_2	50	494	.0148	CO2	100	508	.019				
34-2	860	Aborted															
35-1	940	N	1510	439	.014	A95	50	444	.015	A95	100	475	.014				
35-2	783	GN_2	240	371	.015	A45	50	412	.016	A45	100	422	.015				
303-A	350	AA		366	.020												
303-B	235	AA		367	.023												
304-A	920	AA		374	.023	AA		407	.025	A45	50	419	.025	A45	100	429	023

Codes	Conditioning Environment
AA	Air, Ambient
Axx	Air, xx per cent Relative Humidity
S	Salt Atmosphere
C	Carbon Dioxide
N	Nitrogen

Group No.	Coating
1	Gold
2	Aluminum
3	Gold/Aluminum
4	Silver
5	SiO/Silver
6	Copper
7	SiO/Copper
8	Rhodium

TABLE III-6

DATA SUMMARY

EMITTANCE PROGRAM SAMPLES

GROUP 1 - GOLD

Sample No.	Coating Thick. (Å)	Condition Code	Condition Hours	Emittance Test	Emittance ε	Condition Code	Condition Hours	Emittance Test	Emittance ε	Condition Code	Condition Hours	Emittance Test	Emittance ε	Condition Code	Condition Hours	Emittance Test	Emittance ε
304-B	750	AA	-	375	.023	AA	1152	440	.021	A95	50	445	.023	A95	100	466	.023
308	240	AA	-	394	.021	A45	50	406	.020	A45	100	423	.024				
322	212	AAS	-	434	.021	A95	50	455	.027	A95	100	471	.027				
330A	1840	AA		463	..015	CO_2	50	496	.015	CO_2	100	517	.015				
330B	2070	AA		465	.013	S95	50	520	.016	S95	100	534	.0144				
333	953	AA	-	486	.026	CO_2	50	495	.027	CO_2	100	516	.030				
336	1050	AA	-	503	.023	S95	50	[illegible]	.0225	S95	100	537	.020				
343A	2220	-	-	526	.019												
343B	3100	-	-	527	.018												
351A	2080	-	-	545	.0145												
351B	3310	-	-	542	.0201												
352A	2600	-	-	550	.0176												
352B	3340	-	-	551	.0166												
353A	2200	-	-	546	.0195												
353B	3360	-	-	549	.0173												
354A	1740	-	-	547	.0166												
354B	2140	-	-	548	.0146												

Codes	Conditioning Environment
AA	Air, Ambient
Axx	Air, xx per cent Relative Humidity
S	Salt Atmosphere
C	Carbon Dioxide
N	Nitrogen

Group No.	Coating	Group No.	Coating
1	Gold	6	Copper
2	Aluminum	7	SiO/Copper
3	Gold/Aluminum	8	Rhodium
4	Silver		
5	SiO/Silver		

TABLE III- 7

DATA SUMMARY

EMITTANCE PROGRAM SAMPLES

GROUP 3 - GOLD/ALUMINUM

Sample No.	Coating Thick. (Å)	Condition		Emittance		Condition		Emittance		Condition		Emittance		Condition		Emittance	
		Code	Hours	Test	ε	Code	Hours	Test	ε	Code	Hours	Test	ε	Code	Hours	Test	ε
1	166/430	AA	2130	319	.0179												
2-1	498/320	AA	840	276	.022												
3-1	413/307	AA	1170	321	.0178												
12-2	1300/455	AA	600	280	.0144												
13-2	83/334	AA	2830	356	.026												
14-2	1080/370	AA	Abor	ted Test													

Codes	Conditioning Environment
AA	Air, Ambient
Axx	Air, xx per cent Relative Humidity
S	Salt Atmosphere
C	Carbon Dioxide
N	Nitrogen

Group No.	Coating
1	Gold
2	Aluminum
3	Gold/Aluminum
4	Silver
5	SiO/Silver
6	Copper
7	SiO/Copper
8	Rhodium

TABLE III-8

DATA SUMMARY

EMITTANCE PROGRAM SAMPLES

GROUP 4 - SILVER

Sample No.	Coating Thick. (Å)	Condition Code	Condition Hours	Emittance Test	Emittance ε	Condition Code	Condition Hours	Emittance Test	Emittance ε	Condition Code	Condition Hours	Emittance Test	Emittance ε	Condition Code	Condition Hours	Emittance Test	Emittance ε
-1	104	N	960	361	.019												
16-2	83	AA	960	360	.021												
17-1	436	N	137	329	.017												
17-2	427	AA	141	330	.013												
18-1	294	N	960	362	.016												
18-2	353	AA	960	363	.015	AA	364	385	.015								
19-1	390	Aborted Test															
19-2	445	Aborted Test															
20-1	953	N	865	364	.012	AA	408	372	.015	AAS	192	390	.015				
20-2	1230	AA	865	365	.013	AA	408	373	.011	AAS	240	398	.022				
21-1	1430	N															
21-2	1150	AA															
22-1	415	N															
23-1	432	AA	264	340	.010												
25-1	1210	AA	192	337	.011												
27-1	2325	AA	144	335	.011												
36	762	N	220	376	.016	N	192	389	.013	A45	50	400	.018	A45	100	426	.016
37	762	N	1270	436	.0111	A95	50	451	.0114	A95	100	474	.0147				

Codes	Conditioning Environment
AA	Air, Ambient
Axx	Air, xx per cent Relative Humidity
S	Salt Atmosphere
C	Carbon Dioxide
N	Nitrogen
AAS	Air, Ambient, Sho

Group No.	Coating
1	Gold
2	Aluminum
3	Gold/Aluminum
4	Silver
5	SiO/Silver
6	Copper
7	SiO/Copper
8	Rhodium
9	Miscellaneous

Note: 300 Series Sample numbers are commercial products.

TABLE III-8

DATA SUMMARY

EMITTANCE PROGRAM SAMPLES

GROUP 4 - SILVER

Sample No.	Coating Thick. (Å)	Condition		Emittance		Condition		Emittance		Condition		Emittance		Condition		Emittance	
		Code	Hours	Test	ε	Code	Hours	Test	ε	Code	Hours	Test	ε	Code	Hours	Test	ε
38	762																
39	762																
40	762																
41	762																
325	635	AAS		448	.0136												
326	537	AAS		450	.0119												
327A	1150	AA		457	.0104												
327B	1010	AA		458	.0102												
337A	1680	N_2		467	.0109												
3378	1650	N_2		468	.0103												
338A	1400	N_2		484	.0218	Test aborted-value obtained inconclusive											
338B	2000	N_2		478	.0116	AA	6	480	.0114								
340	985	N_2	-	510	.0175	-	-	511	.0179								
341	1000	N_2	-	513	.0101												
342	1000	N_2	-	514	.0103												
345	1300	-	-	525	.0242	-	-	531	.0187								
346A	1290	-	-	529	.0342												
346B	2210	-	-	530	.0158												

Codes	Conditioning Environment
AA	Air, Ambient
Axx	Air, xx per cent Relative Humidity
S	Salt Atmosphere
C	Carbon Dioxide
N	Nitrogen

Group No.	Coating
1	Gold
2	Aluminum
3	Gold/Aluminum
4	Silver
5	SiO/Silver
6	Copper
7	SiO/Copper
8	Rhodium

Note: 300 Series numbers samples are commercial products.

TABLE III-9

DATA SUMMARY

EMITTANCE PROGRAM SAMPLES

GROUP 5 - SiO/SILVER

Sample No.	Coating Thick. (Å)	Condition		Emittance		Condition		Emittance		Condition		Emittance		Condition		Emittance	
		Code	Hours	Test	ε	Code	Hours	Test	ε	Code	Hours	Test	ε	Code	Hours	Test	ε
22-2	/415																
23-2	75/432	AA	264	339	.012												
24-1	150/1200	AA															
24-2	150/1200	AA															
25-2	150/1210	AA	192	338	.015												
26-1	150/2250	AA															
26-2	150/2250	AA															
27-2	150/2325	AA	144	336	.016												
42	75/745	N	120	377	.016	A45	50	411	.015	A45	100	425	.0165				
43	75/745	N	1125	435	.014	A95	50	443	.016	A95	100	472	.0175				
44	75/745	N	3mo.	488	.015	CO_2	50	501	.015	CO_2	100	509	.0207				
45	75/745	N	$3\frac{1}{2}$mo.	502	.02	S95	50	522	.018	S95	100	536	.0165				
46	75/745																
47	75/745																
328A	60/1463	AA		459	.0116												
328B	150/1550	AA		460	.0154												
329	80/742	AA		461	.0142												

Codes	Conditioning Environment
AA	Air, Ambient
Axx	Air, xx per cent Relative Humidity
S	Salt Atmosphere
C	Carbon Dioxide
N	Nitrogen

Group No.	Coating
1	Gold
2	Aluminum
3	Gold/Aluminum
4	Silver
5	SiO/Silver
6	Copper
7	SiO/Copper
8	Rhodium

Note: 300 Series numbered samples are commercial products.

TABLE III- 10

DATA SUMMARY

EMITTANCE PROGRAM SAMPLES

GROUP 6 - COPPER

Sample No.	Coating Thick. (Å)	Condition		Emittance		Condition		Emittance		Condition		Emittance		Condition		Emittance	
		Code	Hours	Test	ε	Code	Hours	Test	ε	Code	Hours	Test	ε	Code	Hours	Test	ε
29-1	540	AA	72	341	.011												
30-1	1475	AA	336	357	.014												
30-2	1500	AA	311	355	.014												
58	675	N	24	378	.013	A45	50	401	.016	A45	100	432	.017				
59	675	N	1357	441	.012	A95	50	447	.0437	A95	100	470	.071				
60	675																
61	675																
62	675																
63	675																

Codes	Conditioning Environment
AA	Air, Ambient
Axx	Air, xx per cent Relative Humidity
S	Salt Atmosphere
C	Carbon Dioxide
N	Nitrogen

Group No.	Coating
1	Gold
2	Aluminum
3	Gold/Aluminum
4	Silver
5	SiO/Silver
6	Copper
7	SiO/Copper
8	Rhodium

TABLE III-11

DATA SUMMARY

EMITTANCE PROGRAM SAMPLES

GROUP 7 - SiO/COPPER

Sample No.	Coating Thick. (Å)	Condition Code	Condition Hours	Emittance Test	Emittance ε	Condition Code	Condition Hours	Emittance Test	Emittance ε	Condition Code	Condition Hours	Emittance Test	Emittance ε	Condition Code	Condition Hours	Emittance Test	Emittance ε
29-2	150/540	AA	72	342	.017												
52	75/761	N	120	387	.018	A45	50	410	.018	A45	100	428	.017				
53	75/761	N	1152	438	.0174	A95	50	446	.021	A95	100	456	.025				
54	75/761	N_2	3mo.	489	.017	CO_2	50	500	.018	CO_2	100	515	.017				
55	75/761	N_2	3½mo.	505	.023	S95	50	524	.025	S95	100	539	.026				
56	75/761																
57	75/761																

Codes	Conditioning Environment
AA	Air, Ambient
Axx	Air, xx per cent Relative Humidity
S	Salt Atmosphere
C	Carbon Dioxide
N	Nitrogen

Group No.	Coating
1	Gold
2	Aluminum
3	Gold/Aluminum
4	Silver
5	SiO/Silver
6	Copper
7	SiO/Copper
8	Rhodium

TABLE III-12

SUMMARY OF COATING CONDITIONING TESTS

Test Series A-45

Air Atmosphere of 45 Percent Relative Humidity and Temperature of 95°F

Sample No.	Metal Coating	Th'K Å	Source	ε Start	Tape Test	ε 50 hr	Tape Test	ε 100 hr	Tape Test
48	Aluminum	790	ADL	.021	0%	.021	0%	.0195	0%
35-2	Gold	783	ADL	.015	0%	.0159	0%	.0148	0%
36	Silver	762	ADL	.0133	0%	.0181	10%	.016	10%
42	SiO/Silver	75/745	ADL	.0160	0%	.0152	1%	.0165	0%
58	Copper	675	ADL	.013	0%	.0167	0%	.0174	0%
52	SiO/Copper	75/761	ADL	.0179	0%	.0178	0%	.0173	0%
305	Aluminum(1)	376	NRC	.0136(2)	0%	.025	0%	.0291	0%
304-A	Gold(1)	1000	Hast.	.025	0%	.025	0%	.0234	0%
308	Gold(1)	240	Nat. Met.	.0214	0%	.0211	0%	.0235	0%

(1)Purchased samples are coated on both sides

(2)Questionable value; previous measurements indicate this value has a range of .023 to .027

TABLE III-13

SUMMARY OF COATING CONDITIONING TESTS

TEST SERIES A-95

AIR ATMOSPHERE OF 95 PER CENT RELATIVE HUMIDITY AND TEMPERATURE OF 95°F

Film	Source	Sample No.	Th'k °A	ε Start	Tape Test	ε 50 hr.	Tape Test	ε 100 hr.	Tape Test
Al	ADL	49	862	.0184	0%	.0225	0%	.0206	0%
Au	ADL	35-1	940	.0140	0%	.0145	0%	.014	0%
Ag	ADL	37	762	.0111	0%	.0144	20%	.0147	40%
SiO/Ag	ADL	43	75/745	.0141	0%	.0199	20%	.0175	20%
Cu	ADL	59	675	.0121	0%	.0437	0%	.0713	0%
SiO/Cu	ADL	53	75/761	.0174	0%	.0212	10%	.0254	10%
Al	NRC	321	435	.0225	0%	.0229	0%	.243	0%
Au	Hastings	304B	825	.021	0%	.023	2%	.0225	30%
Au	Nat. Met.	322	212	.0211	0%	.027	0%	.0271	0%

TABLE III-14

SUMMARY OF COATING CONDITIONING TESTS

TEST SERIES C

CO_2 ATMOSPHERE AND TEMPERATURE OF 95°F

Film	Source	Sample No.	Th'k °A	ε Start	Tape Test	ε 50 hr.	Tape Test	ε 100 hr	Tape Test
Al	ADL	50	862	.0203	0%	.0192	0%	.0184	0%
Au	ADL	34-1	1020	.0152	0%	.0148	0%	.0187	0%
SiC/Ag	ADL	44	75/745	.0150	0%	.0142	0%	.0207	0%
SiO/Cu	ADL	54	75/761	.0170	0%	.018	0%	.0166	0%
Au	Hastings	333	953	.0259	0%	.0273	0%	.0299	0%
Au	Hastings	330A	1840	.0146	0%	.0146	0%	.0153	0%

TABLE III-15

SUMMARY OF COATING CONDITIONING TESTS

TEST SERIES S

SALT ATMOSPHERE AND TEMPERATURE OF 95°F

Film	Source	Sample No.	Th'k °A	ε Start	Tape Test	ε 50 Hr.	Tape Test	ε 100 Hr.	Tape Test
Al	ADL	51	862	.0191	0%	.0187	0%	.0200	0%
Au	ADL	33-2	455	.0154	0%	.0153	0%	.0152	0%
SiO/Ag	ADL	45	75/745	.0198	0%	.0179	50%	.0165	100%
SiO/Cu	ADL	55	75/761	.0228	0%	.0248	0%	.0255	0%
Au	Hastings	336	1050	.0228	0%	.0225	0%	.0202	40%
Au	Hastings	330B	2072	.0127	0%	.0160	0%	.0144	0%

TABLE II-16

COMMERCIAL METALLIZED FILM SUPPLIERS

USED IN PROGRAM

National Research Corporation
70 Memorial Drive
Cambridge, Mass. 02142

Supplier of Aluminum Metallized Films

Hy-Sil Manufacturing Company
28 Spring Street
Revere, Mass.

Supplier of Aluminum Metallized Films

Hastings & Company, Inc.
2314 Market Street
Philadelphia 1, Pennsylvania

Suppliers of Gold Metallized Films

Gomar Manufacturing Company
1501 W. Blancke Street
Linden, New Jersey

Suppliers of Silver Metallized Films

G. T. Schjeldahl Company
Box 170
Northfield, Minnesota 55057

Suppliers of Silver Metallized Films

National Metallizing Division
Standard Packaging Corp.
825 New York Avenue
Trenton 8, New Jersey

Suppliers of Gold Metallized Films

TABLE III-17

ARTHUR D. LITTLE, INC.
20 Acorn Park
Cambridge, Massachusetts 02140

13 September 1965
C-67180-02
Specification

Vacuum Metalized

Silver Coated Polyester Film

General

This specification establishes the requirements for polyester film consisting of a vacuum meatlized coating of silver and a protective coating of silicon monoxide on each side. The objective of the specification is the procurement of a well-bonded, highly reflecting (to infrared radiation) and protected silver coating which is to be used in an investigation of the performance of multi-layer insulations in the NASA space program being conducted by Arthur D. Little, Inc., under Contract NAS3-6283.

Substrate Material

The substrate material shall be DuPond Type S polyester film 1/4 mil in thickness. Film from an original mill wound roll is to be used for the coating.

Metal Coating

Both sides of the Polyester film are to be vacuum metalized with fine silver of 99.9 per cent minimum purity to a nominal thickness of 1000 Angstroms (.16 ohms per square). The thickness shall have a tolerance of -250 Angstroms and +500 Angstroms. These values represent a maximum film resistance of .22 ohms per square and a minimum film resistance of .11 ohms per square respectively.

The coated film is to be produced in a single continuous length. The vacuum metalized coating on each side of the film shall be produced in a single pass at a minimum deposition rate of 100 Angstroms per second. Higher rates up to 500 Angstroms per second are preferred. The metal vaporizing boats shall be shielded, in the film rolling direction, to limit the incident angle of metal vapor at the film to ± 20 degrees from the film normal. The vacuum in the region where metalizing is taking place shall be below 10^{-5} mm Hg.

TABLE III-17
(Cont'd)

ARTHUR D. LITTLE, INC.
20 Acorn Park
Cambridge, Massachusetts 02140

13 September 1965
C-67180-02
Specification

The vacuum metalized coatings are to be uniform over each surface within the limits specified above. The metal coatings are to have a bright lustre and be free from streaks, windows and pinholes except for pinholes present in the film. It is recommended that all film wind-rewind operations be done under vacuum conditions. The coating shall adhere to the polyester film to the degree that when scotch tape is rubbed onto any portion of the metal coating, the adhesive retains none of the metal when the tape is removed.

Silicon Monoxide Coating

The vacuum metalized silver is to be protected with a coating of silicon monoxide having a nominal thickness of 75 Angstroms. This thickness shall have a tolerance of -25 Angstroms and +75 Angstroms.

As in the case of the silver coating, the silicon monoxide coating is to be produced in a single pass. The coating shall be deposited at a rate not less than 15 Angstroms per second in a chamber vacuum less than 10^{-5} mm Hg.

The silicon monoxide coatings are to be uniform over each surface within the limits specified above. Further, the coating is to be free from streaks and windows. The coating's adherence shall be tested by means of the scotch tape test mentioned above for the silver coating.

Thickness Measurement of the Coatings

The primary determination of the thickness of the silver coatings shall be established from the resistivity of the metal in the wrought condition and the measured resistance of the coating in ohms per square. The thickness shall be computed from the relation,

$$t = \frac{\rho}{R} K$$

TABLE III-17

(Cont'd)

ARTHUR D. LITTLE, INC.
20 Acorn Park
Cambridge, Massachusetts 02140

13 September 1965
C-67180-02
Specification

where t = the coating thickness in Angstroms

ρ = the resistivity in the wrought condition of silver, 1.60×10^{-6} ohm-cm at 74°F

R = measured resistance of the coating in ohm per square

K = units conversion factor from cm to Angstroms; 10^8 Å per cm

The manufacturer's bid is to contain a detailed description of the measuring head and readout equipment used in the resistance measurement of the coating and a description of the technique used in making the measurement.

Samples are to be removed across the full width from either end of the processed film. A portion of the sample is to be used for measurements made by the manufacturer at the edges and at each six inches of width across the films on each side. These are to be certified and preserved. The remaining portion of each end sample (approximately 3 feet long by 2 feet wide), is to be delivered to Arthur D. Little, Inc. prior to shipment of the order along with manufacturer's measurements.

Spot measurements of the silver coating shall be made across the width of the film near the edges and at the quarter points at 200 foot intervals along the film length to establish the deposition rate and coating thickness. These measurements are to be obtained with a vibrating quartz crystal-type, thin film monitor or comparable thickness and rate measuring devices and are to be certified.

The thickness of the silicon monoxide and its rate of deposition are to be determined with a vibrating quartz crystal-type, thin film monitor, or comparable thickness and rate measuring device, during production of the coating. Measurements are to be made across the sheet near each edge and at the quarter points at 200 foot intervals along the film length. All measurements are to be certified.

TABLE III-17

(Cont'd)

ARTHUR D. LITTLE, INC.
20 Acorn Park
Cambridge, Massachusetts 02140

13 September 1965
C-67180-02
Specification

All certified data relating to the thickness of the silver and silicon monoxide films at the locations specified are to be supplied prior to or with the completed order at the time of delivery.

Handling and Shipment

Each of the two rolls of processed film are to be mounted on 3-inch diameter cores and suspended within their respective shipping containers. Packages are to be handled so the processed film is not damaged or wrinkled during shipment.

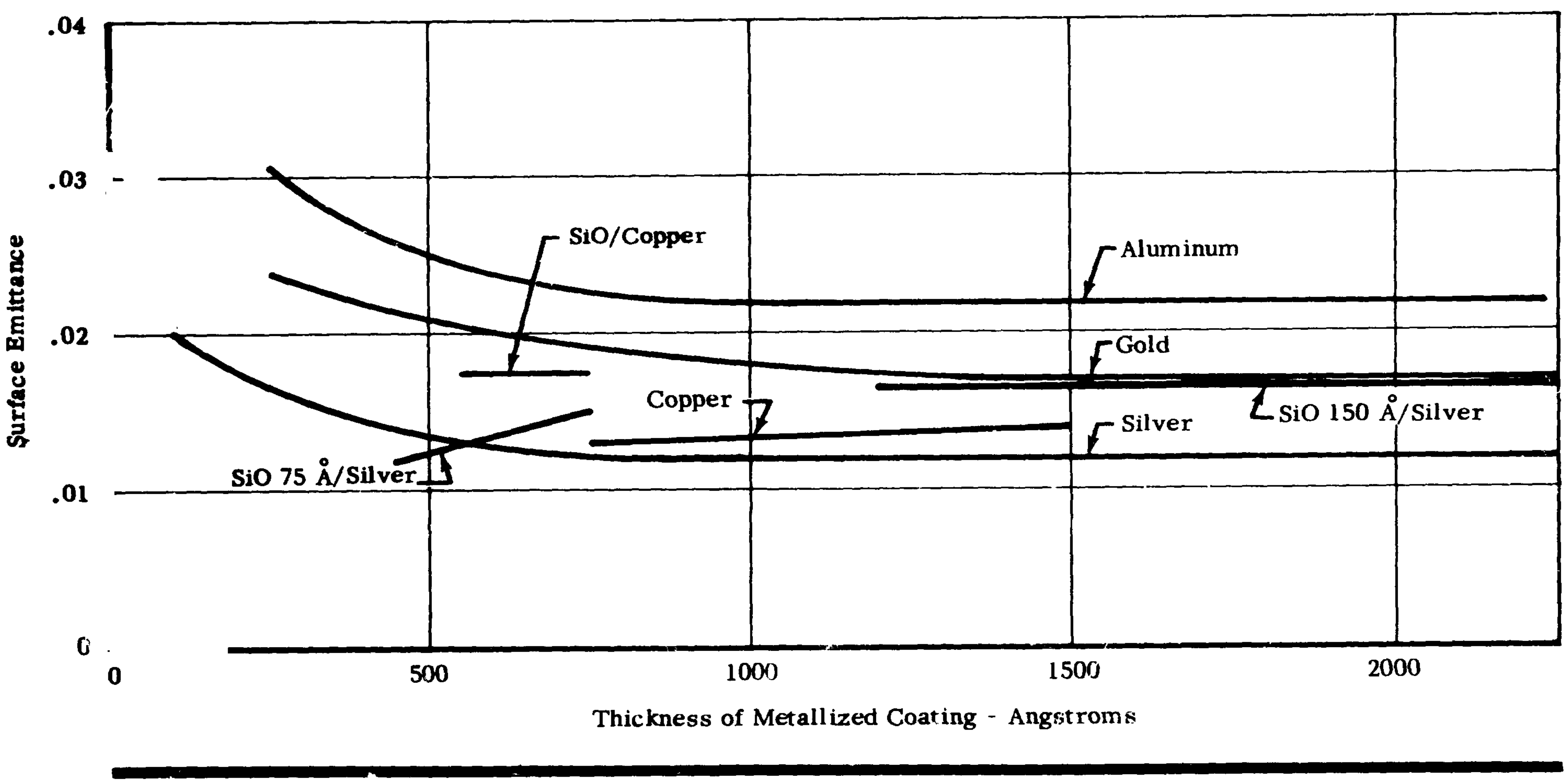

FIGURE III EMITTANCE OF VACUUM METALLIZED POLYESTER FILM AT 553°R FOR VARIOUS COATING MATERIALS AND THICKNESSES

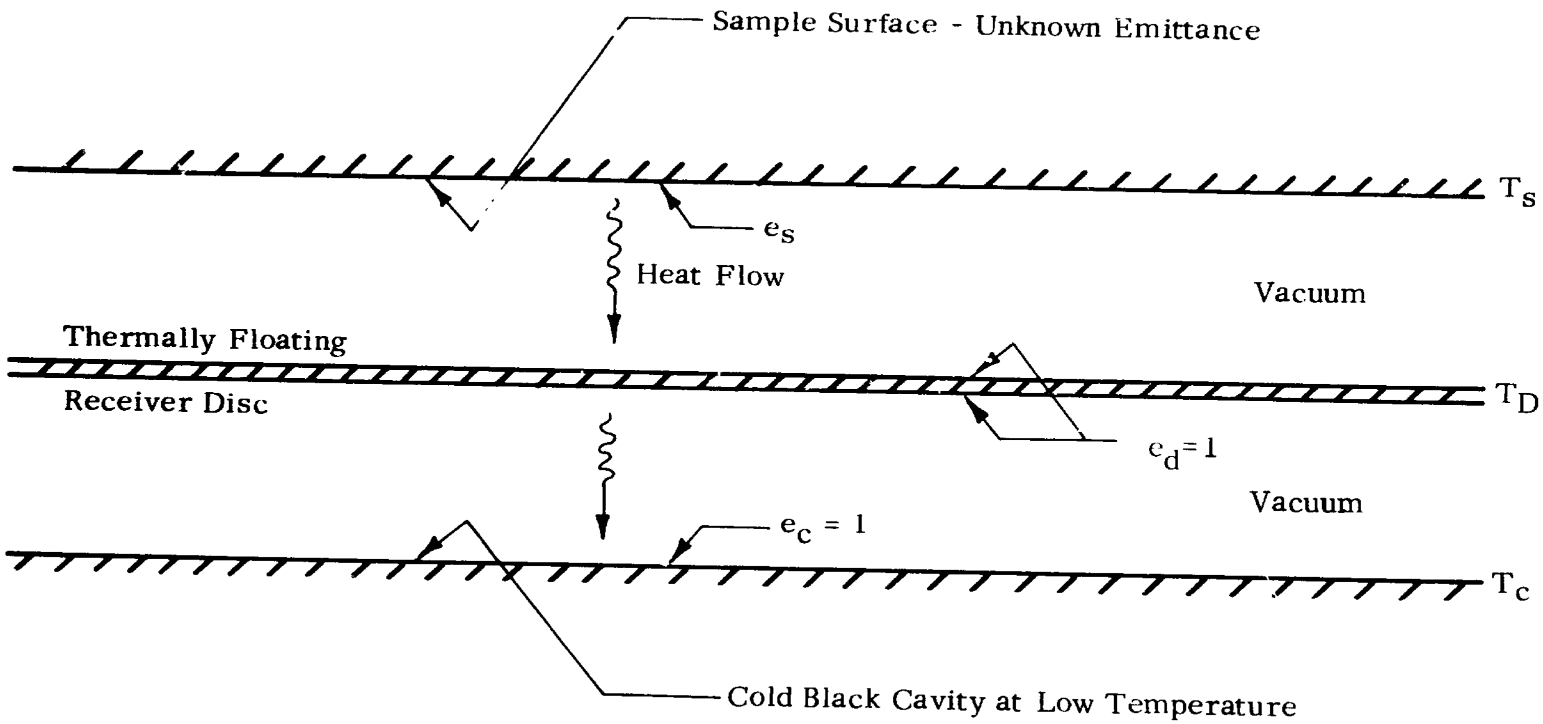

FIGURE III-2 IDEALIZED REPRESENTATION OF HEAT TRANSFER CONDITIONS IN EMISSOMETER

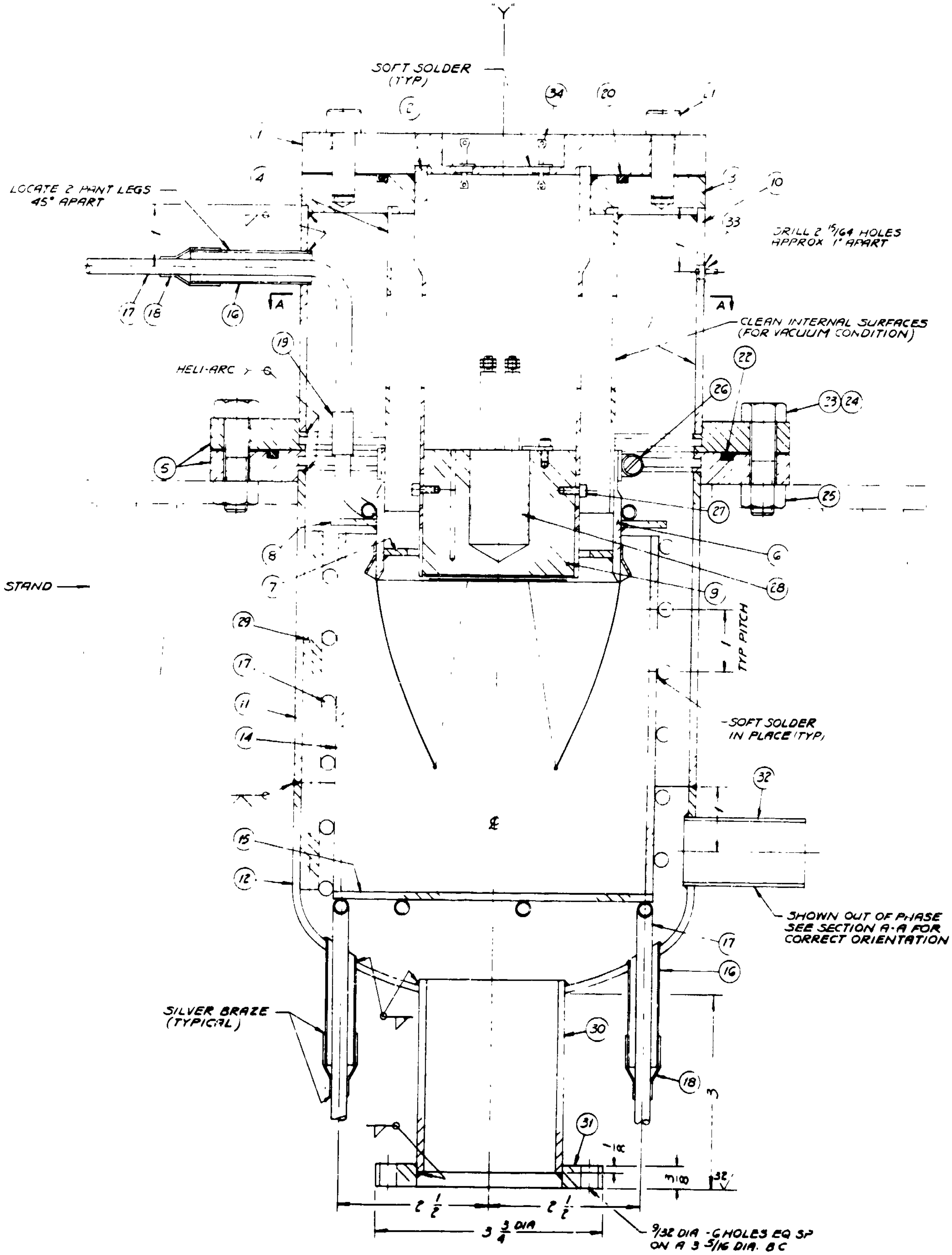

FIGURE III-3 MISSOMETER ASSEMBLY

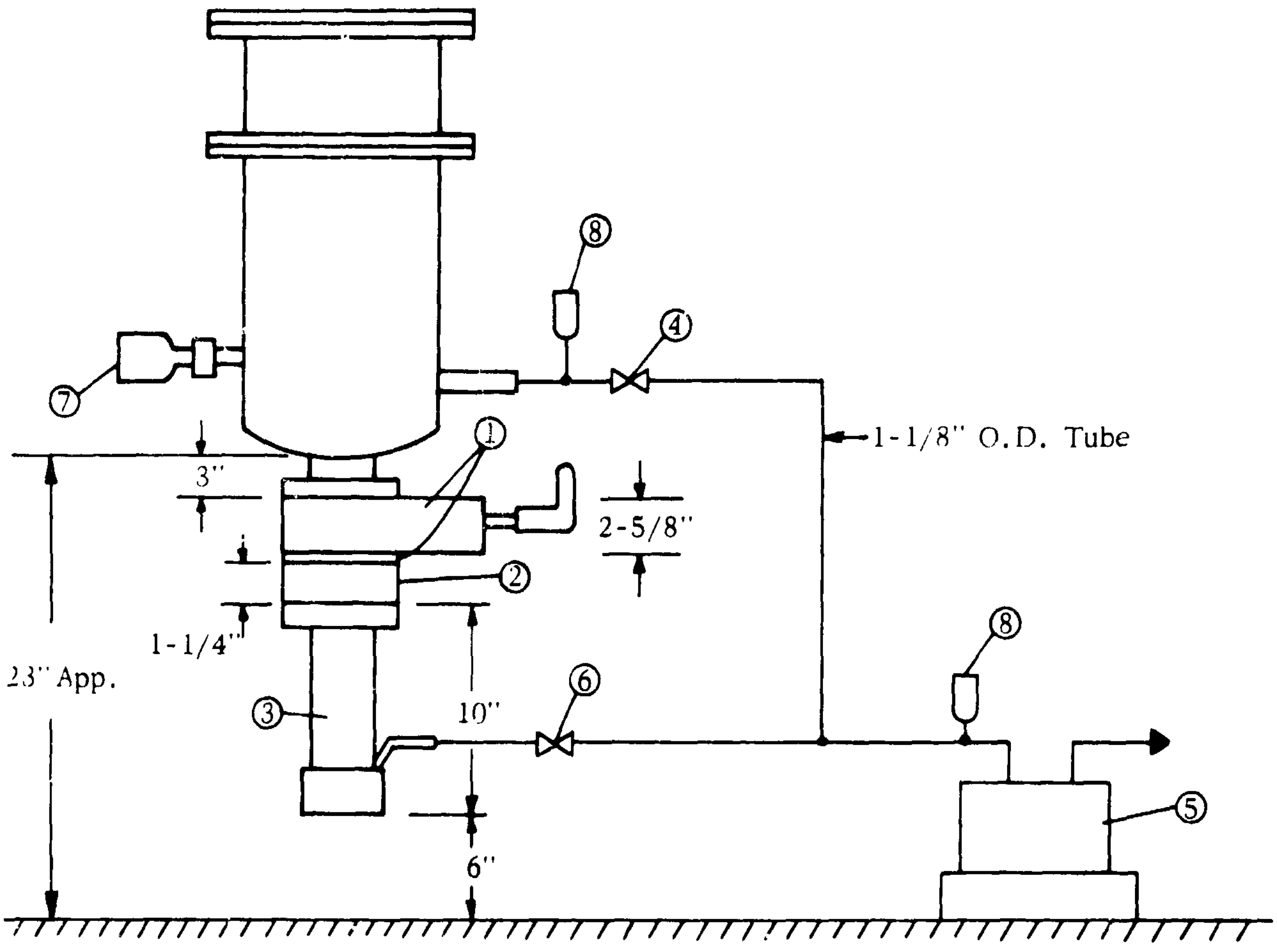

1 High Vacuum Gate Valve

2 Chevron Baffle

3 2" Diffusion Pump

4 Roughing Valve - Veeco Bellows Angle Type

5 5 CFM Roughing and Fore Pump

6 Foreline Valve

7 Ion Pressure Gage

8 Thermocouple Pressure Gage

FIGURE III-4 SCHEMATIC DIAGRAM OF EMISSOMETER VACUUM SYSTEM

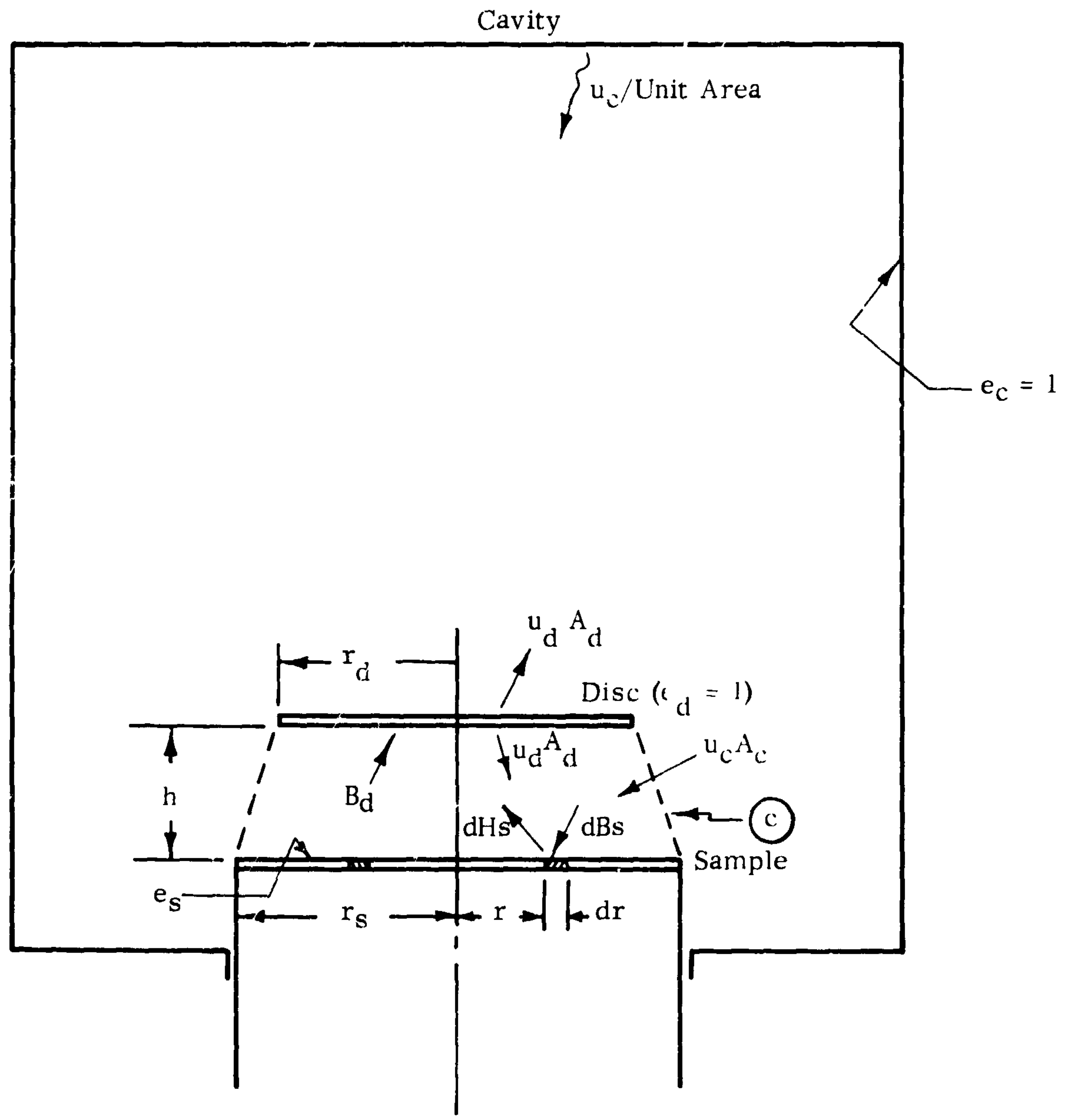

r_s = 1.250 ins.
r_d = 1.125 ins.
h = 0.040 ins.

FIGURE III-5 CONDITIONS FOR CALCULATION OF GEOMETRY ERROR

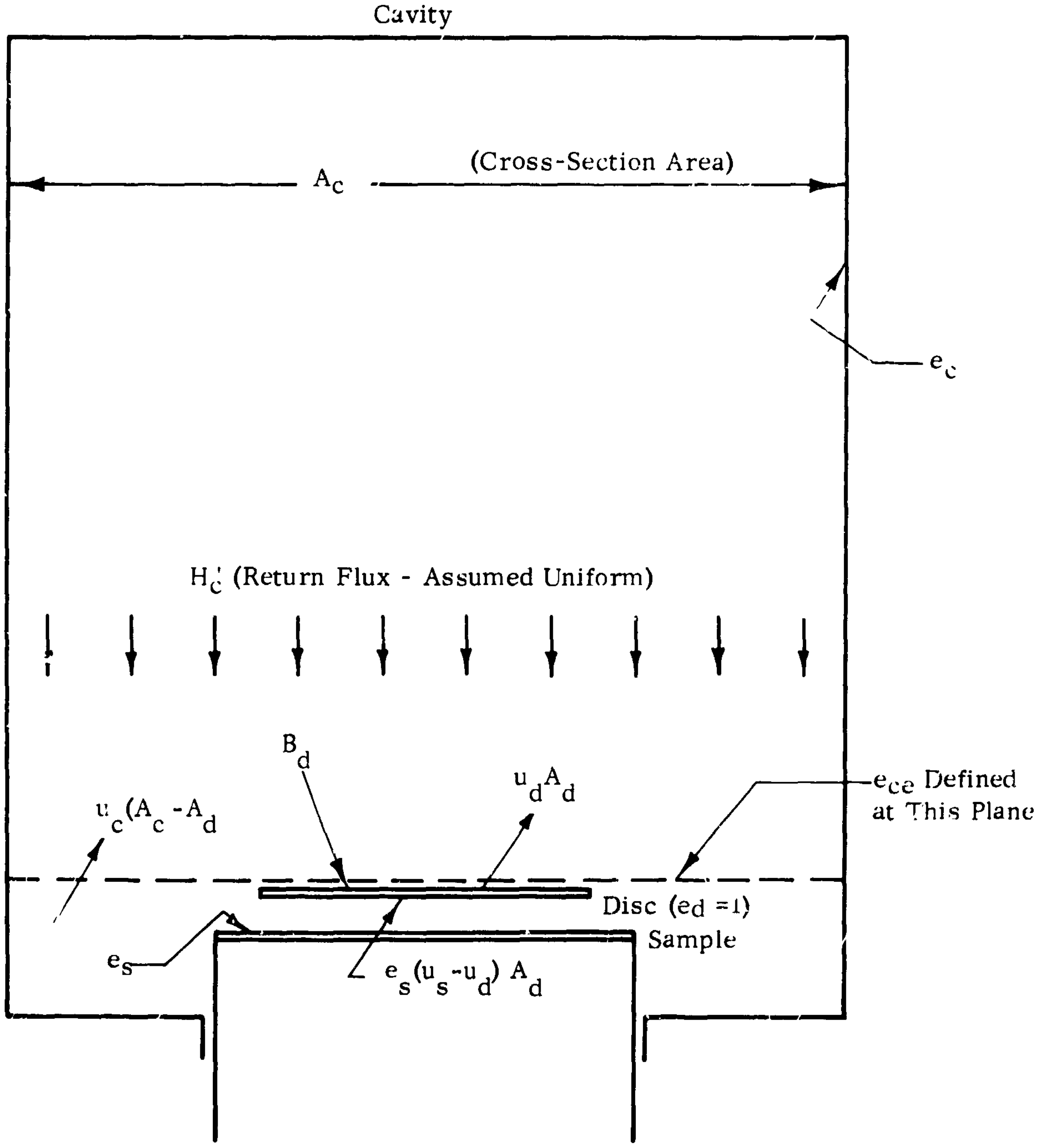

FIGURE III-6 CONDITIONS FOR CALCULATION OF CAVITY EMITTANCE ERROR

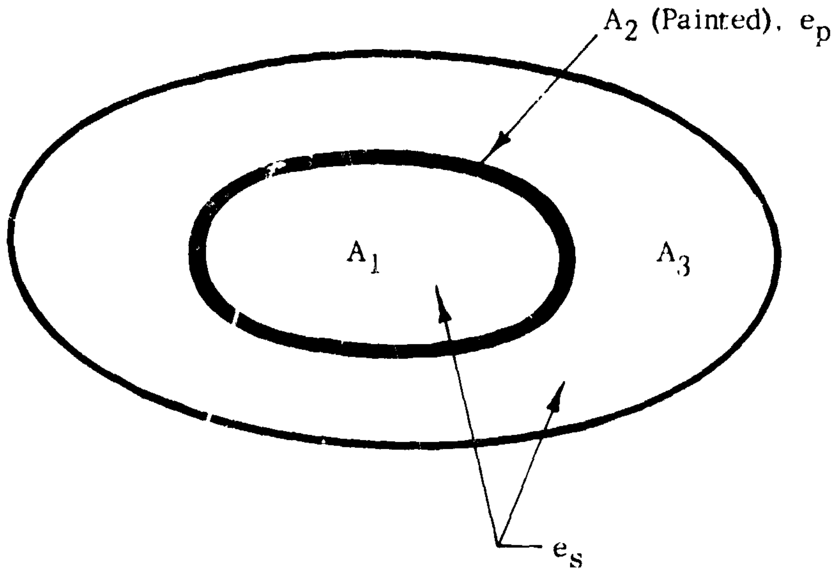

FIGURE III-7 CONFIGURATION FOR PAINTED SAMPLE ANALYSIS

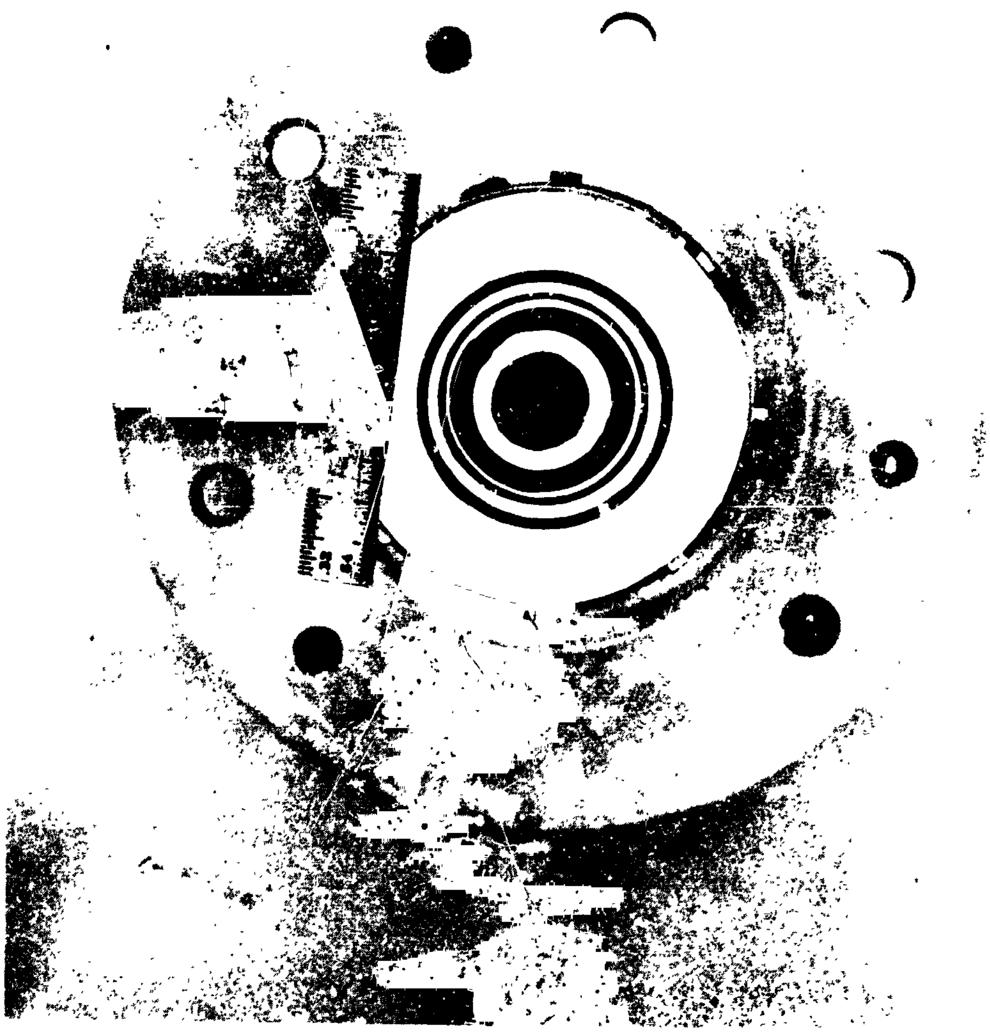

FIGURE III-8 ALUMINUM EMITTANCE SAMPLE WITH PAINTED CALIBRATION RINGS

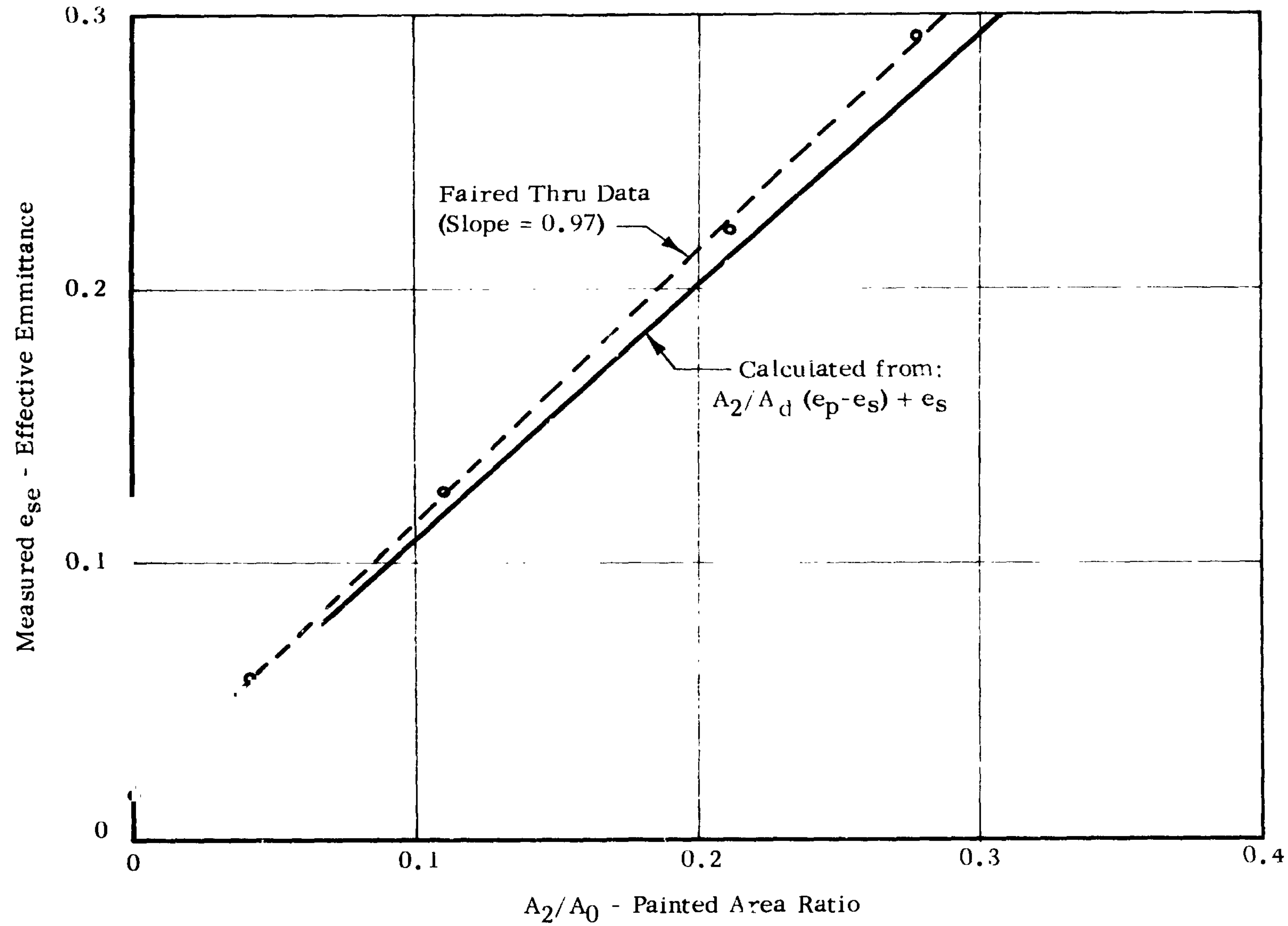

FIGURE III-9 MEASURED AND CALCULATED EFFECTIVE EMITTANCES

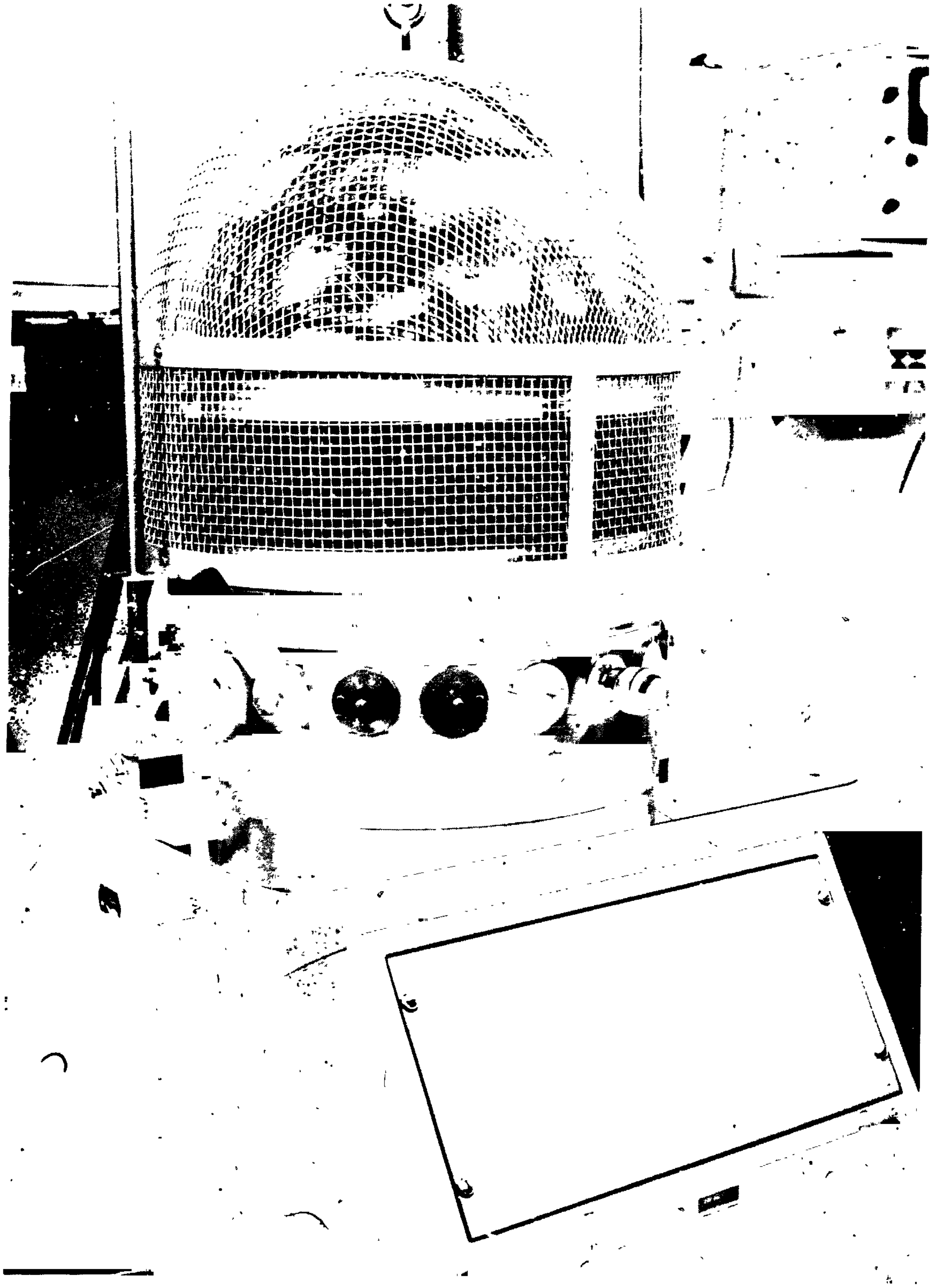

FIGURE III-10 EIGHTEEN-INCH BELL JAR

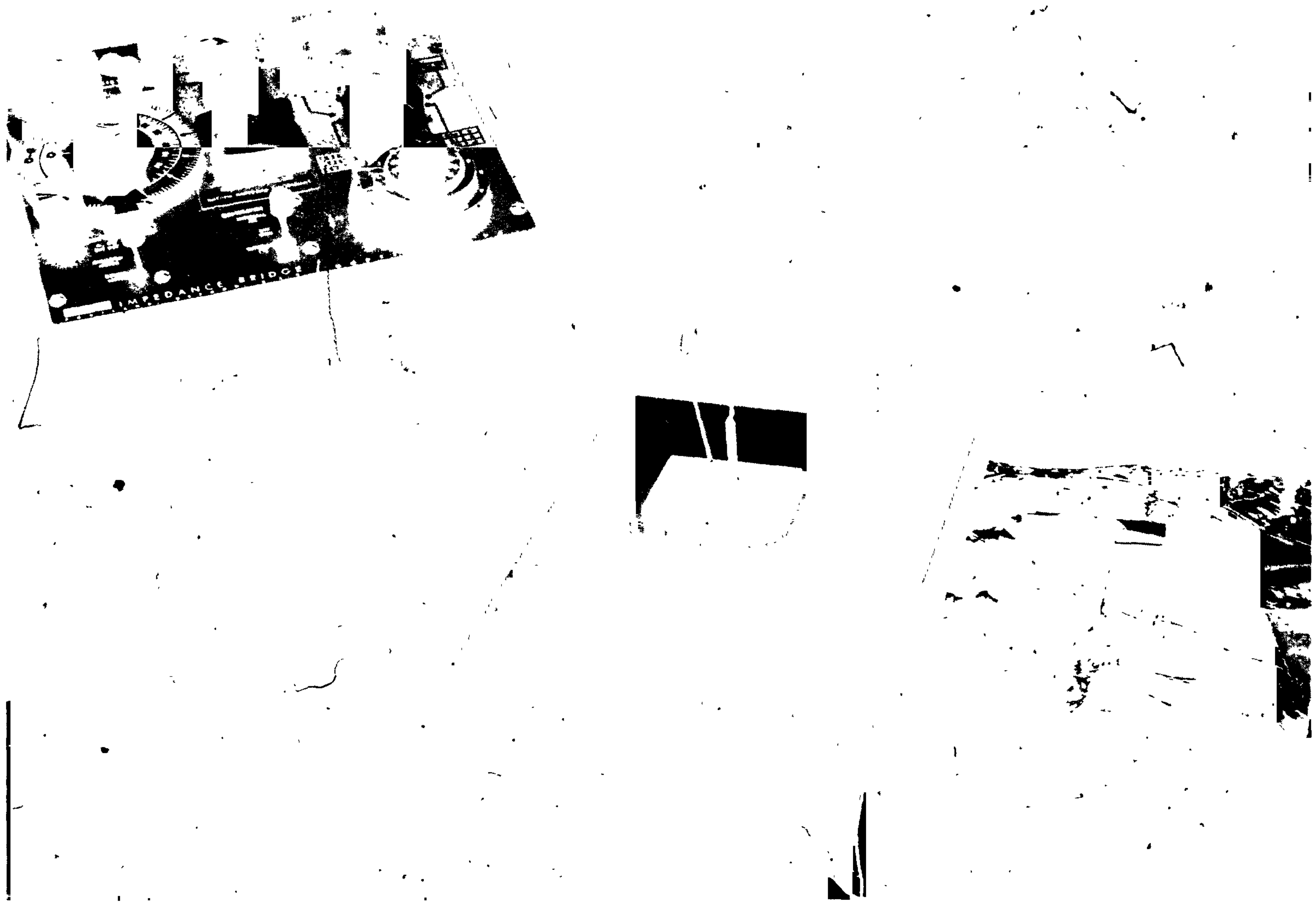

FIGURE III- 11   RESISTANCE MEASURING HEAD--PARALLEL KNIFE EDGE TYPE

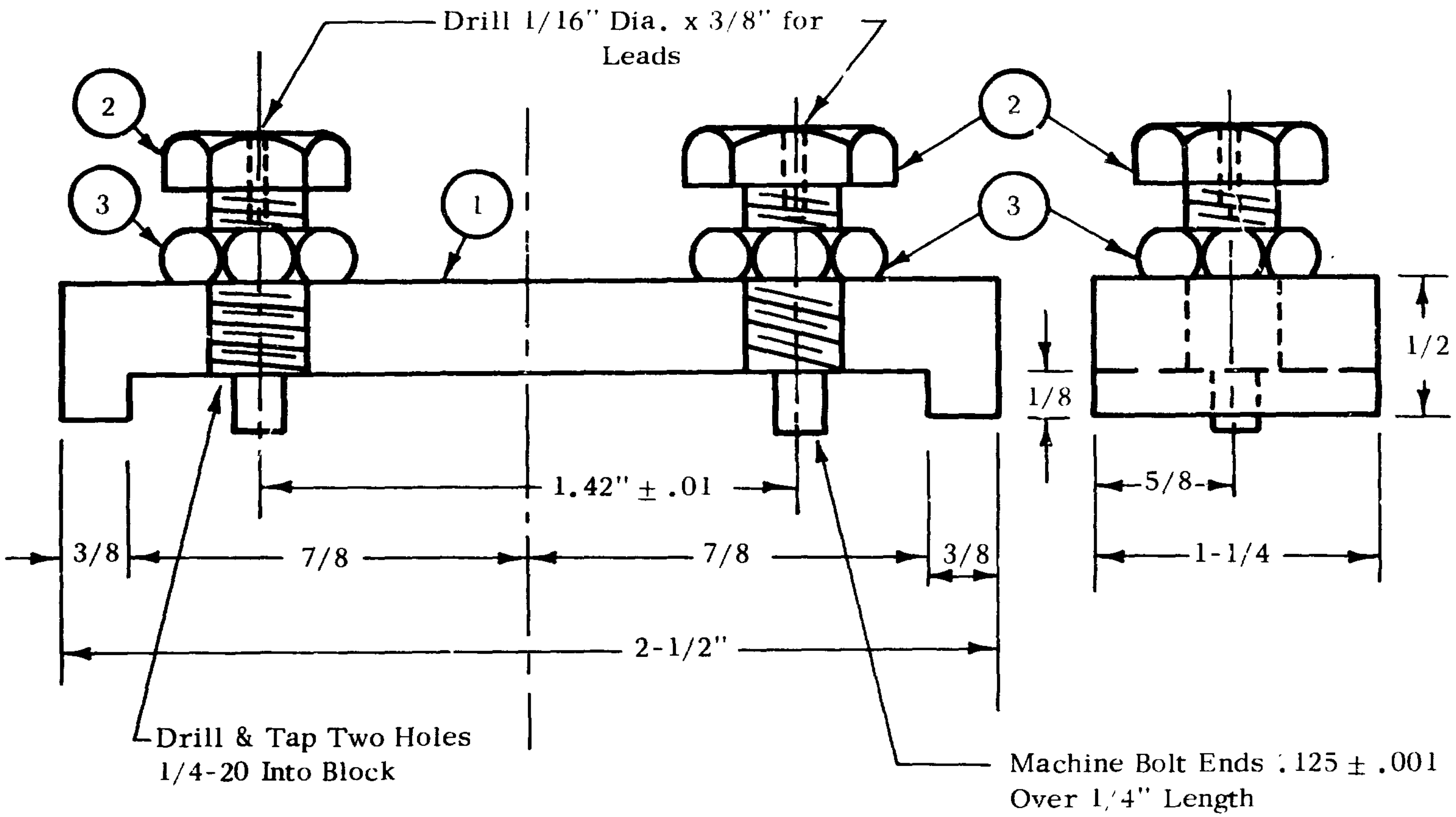

	Description	Size	No. Required
1.	Micarta Block	1/2 x 1-1/4 x 2-1/2	1
2.	Hex Head Aluminum Bolts	1/4 - 20 x 1-1/4	2
3.	Hex Head Aluminum Nuts	1/4 - 20	2

FIGURE III-12 RESISTANCE MEASURING HEAD--TWO-POINT TYPE

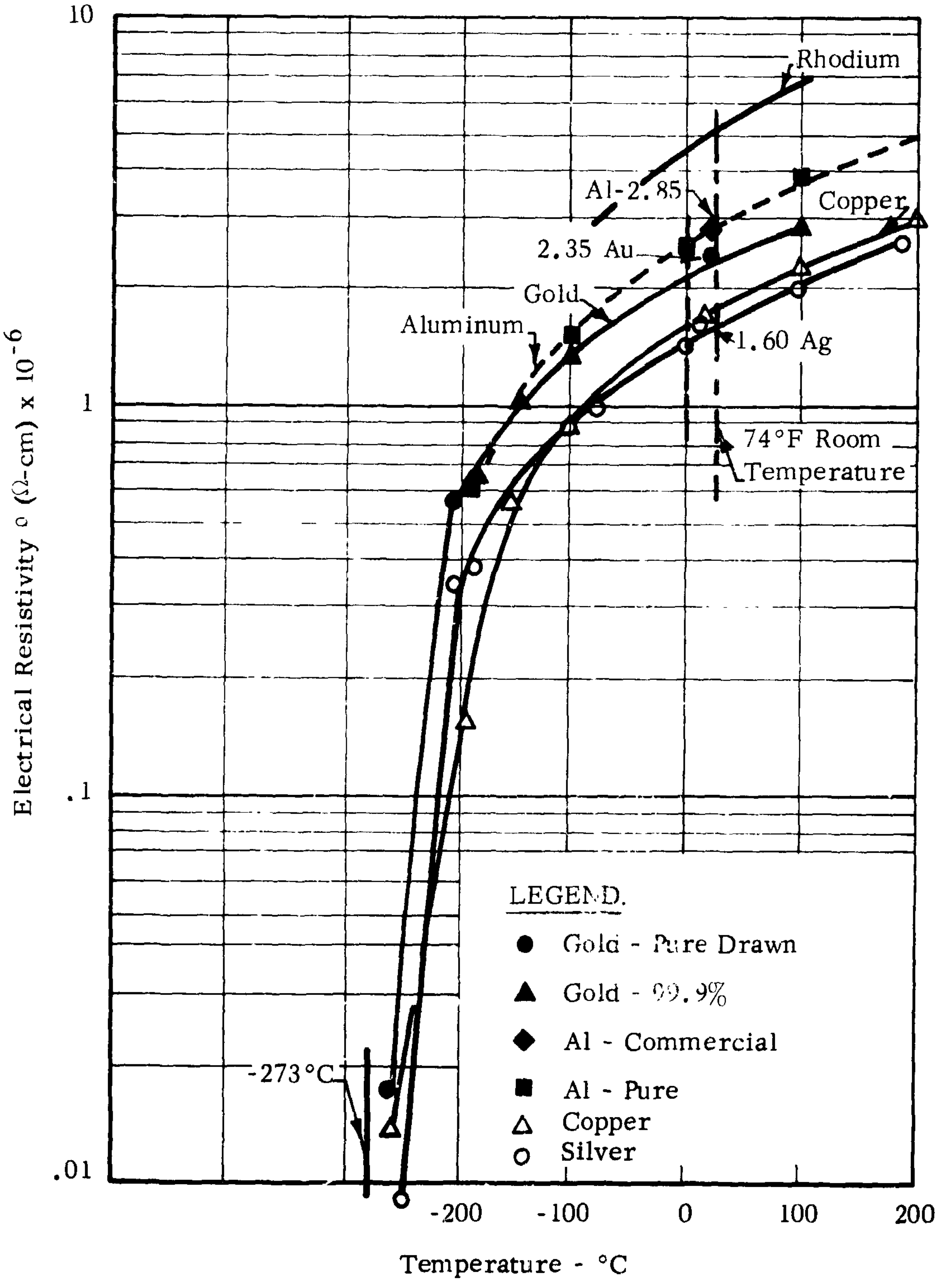

Source: Chemical & Physics Handbook

FIGURE III-13 RESISTIVITY OF WROUGHT COATING METALS

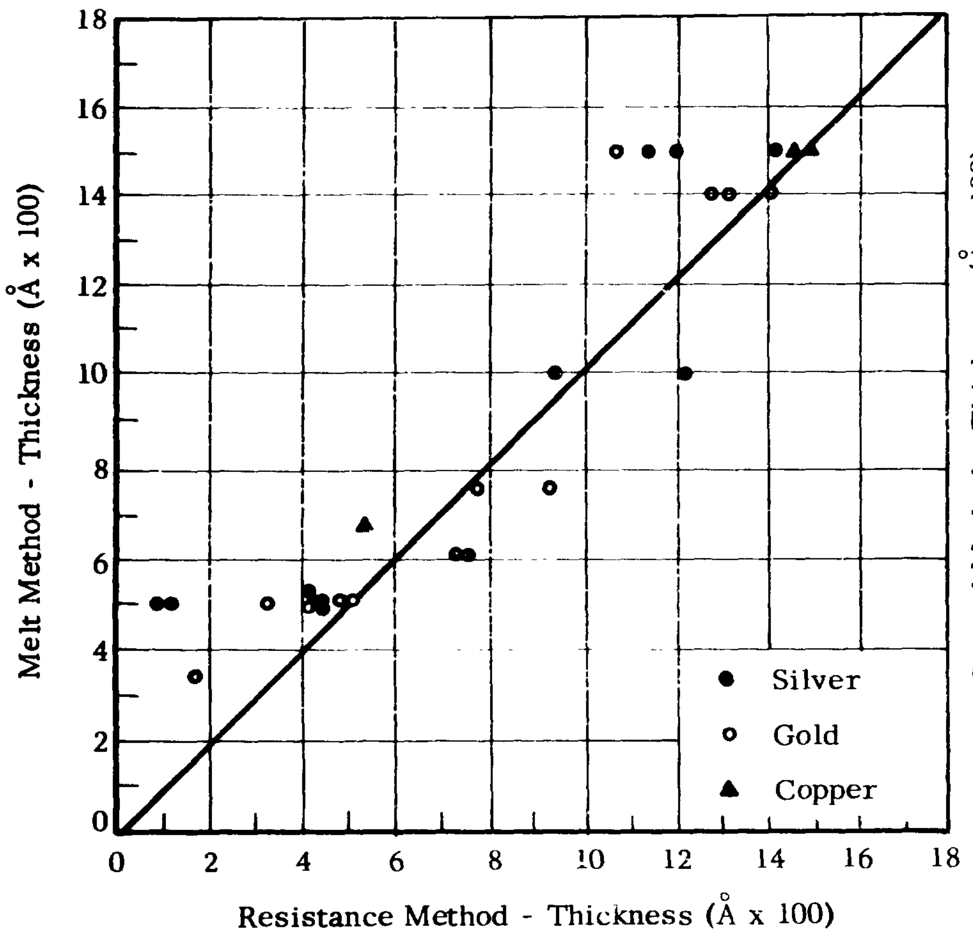

FIGURE III-14a COMPARISON OF RESISTANCE AND MELT THICKNESS MEASUREMENTS

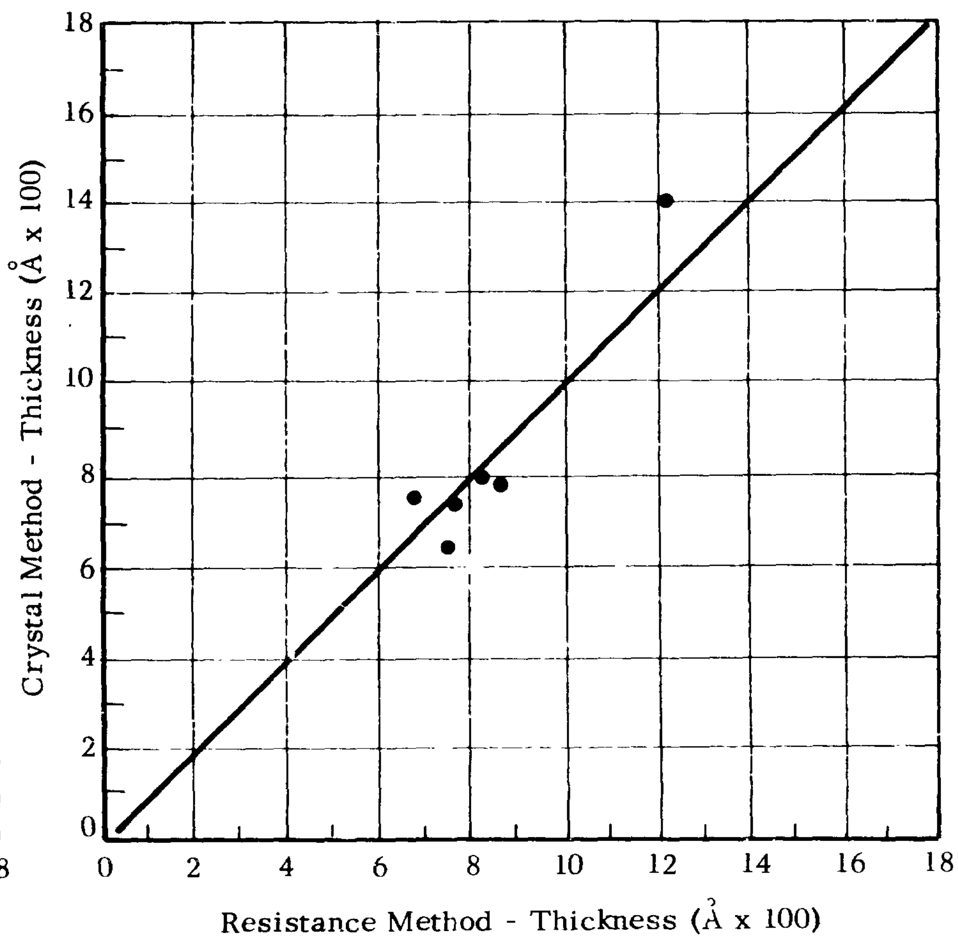

FIGURE III-14b COMPARISON OF RESISTANCE AND CRYSTAL THICKNESS MEASUREMENTS

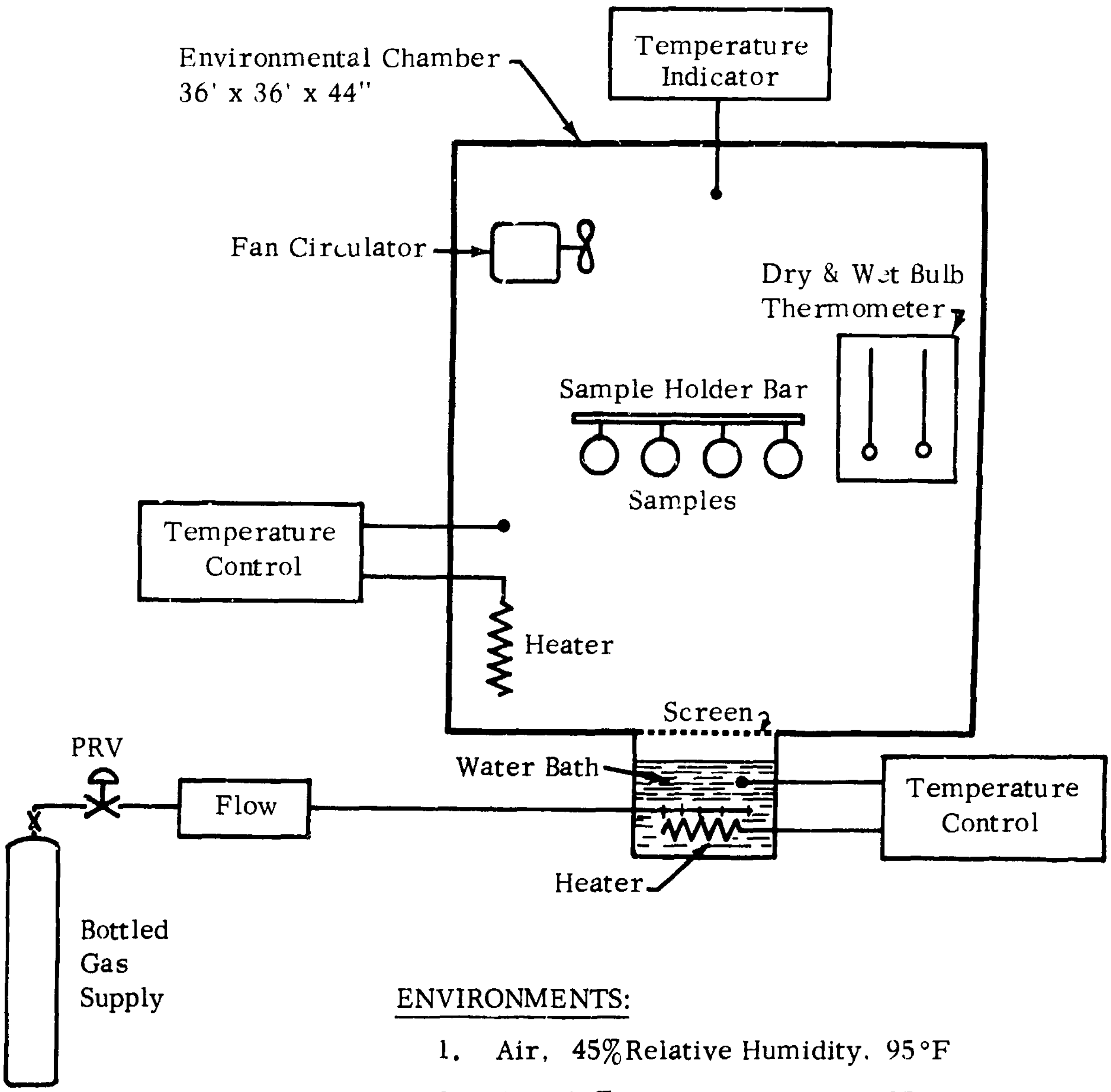

ENVIRONMENTS:

1. Air, 45% Relative Humidity, 95°F
2. Air, 95% Relative Humidity, 95°F
3. Salt Air, Saturated Water Vapor, 95°F
4. Carbon Dioxide, 95°F

FIGURE III-15 ENVIRONMENTAL CHAMBER

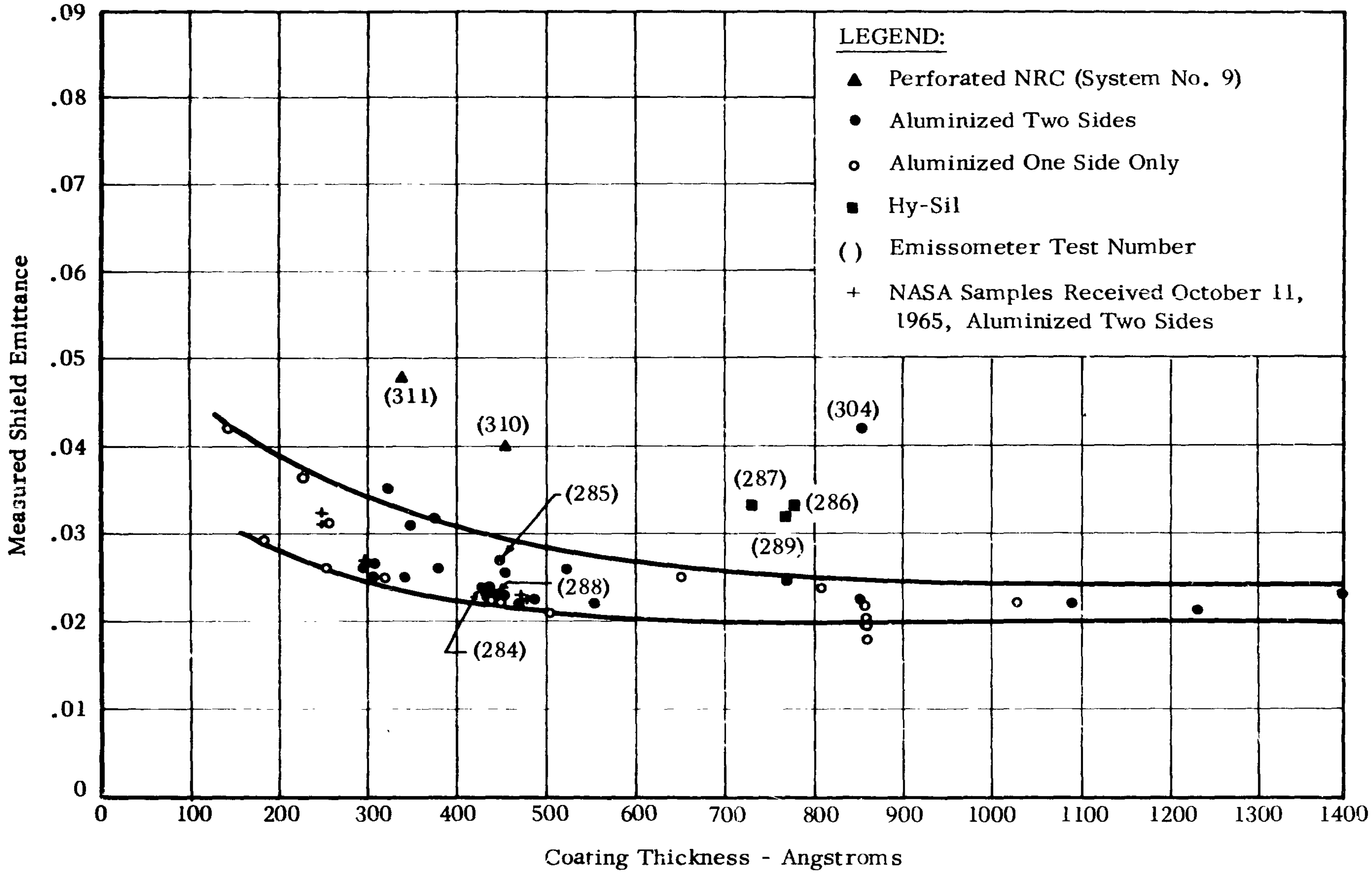

FIGURE III-16 ALUMINIZED MYLAR SURFACE EMITTANCE VS COATING THICKNESS

( ) Indicates Sample No.

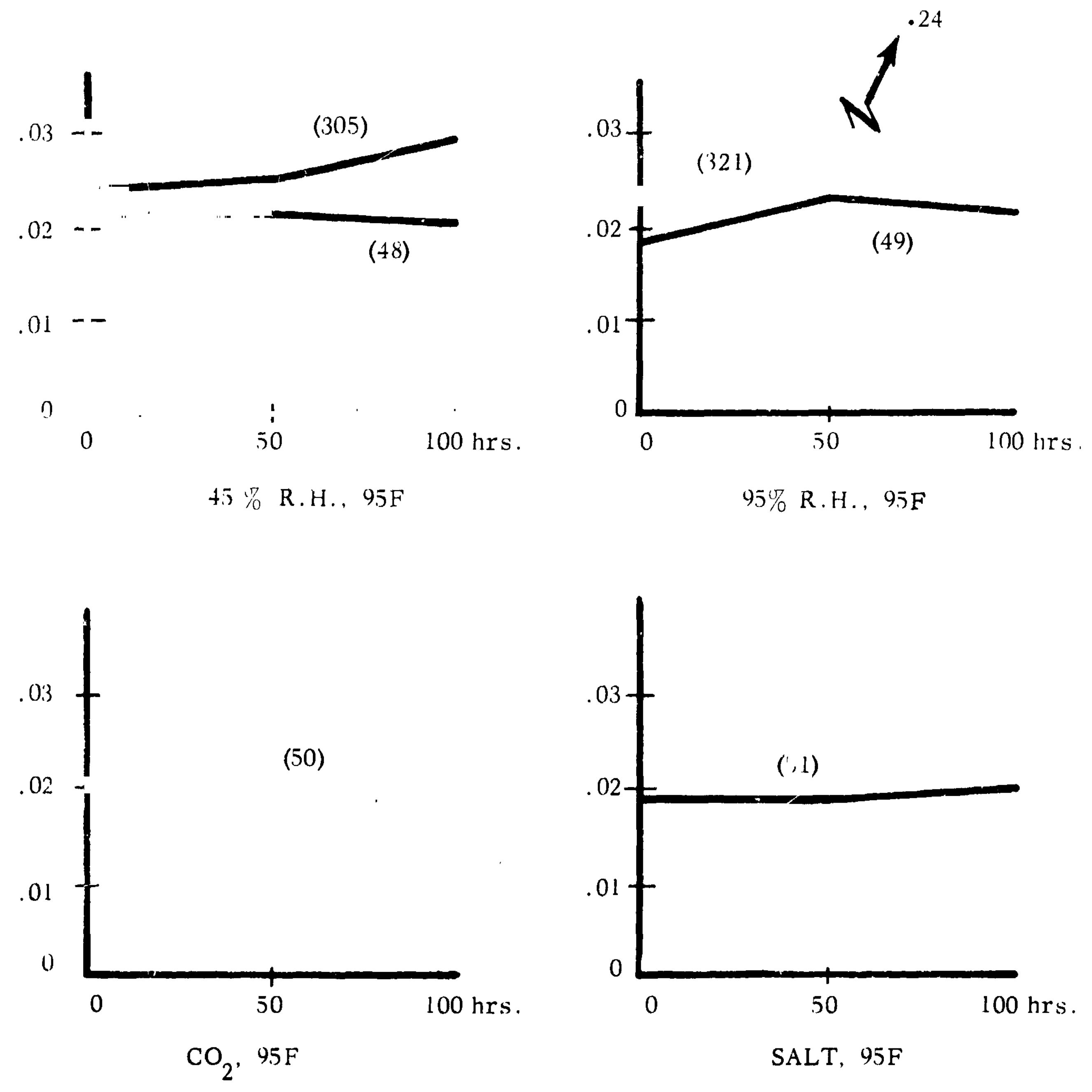

FIGURE III-17 EMITTANCE OF ALUMINUM EXPOSED TO VARIOUS ENVIRONMENTS FOR 50 AND 100 HOURS

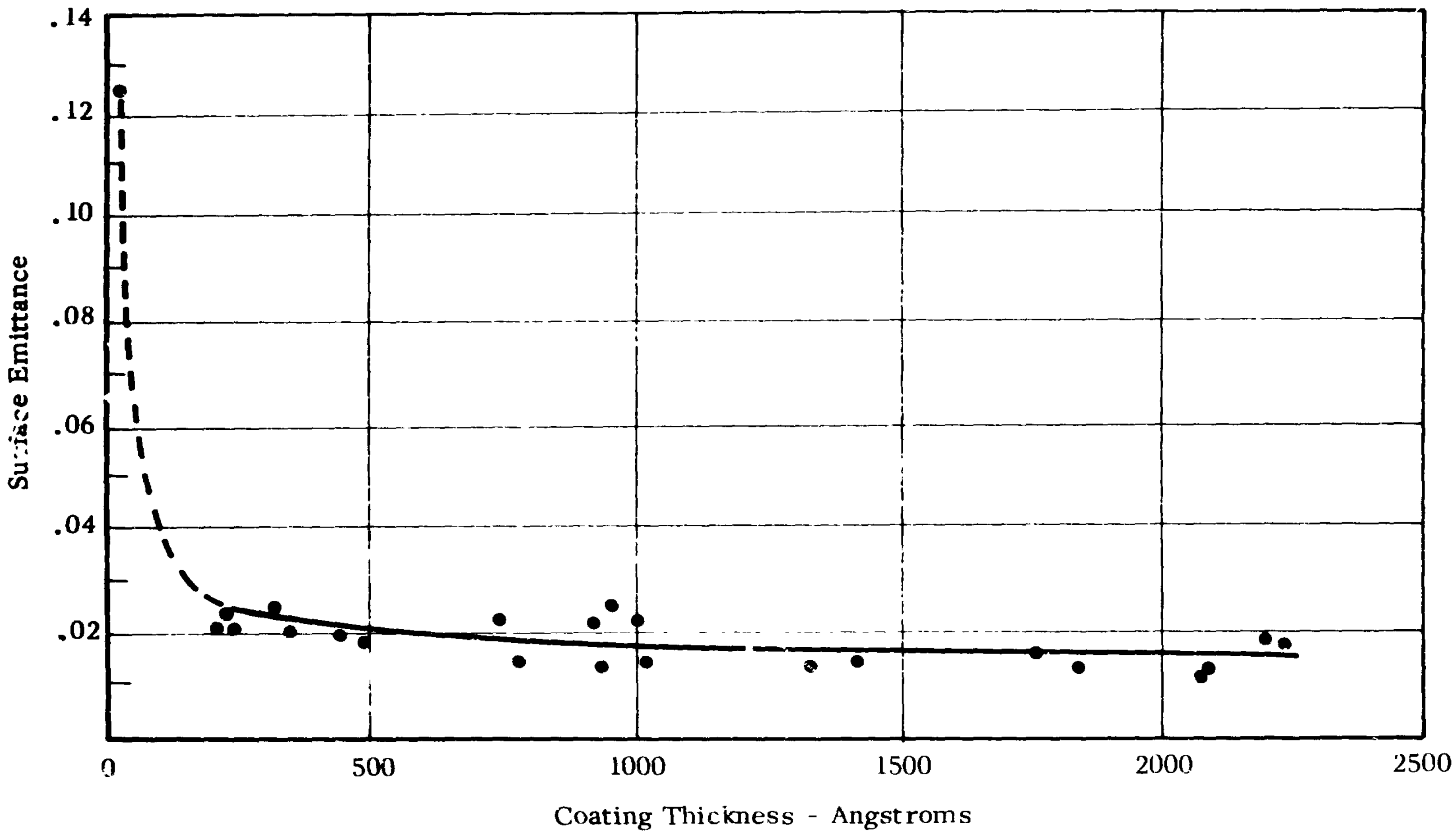

FIGURE III-18 GOLD METALLIZED POLYESTER FILM - EMITTANCE AND COATING THICKNESS

( ) Sample No.
▲ Coating Lift-Off During Scotch Tape Test

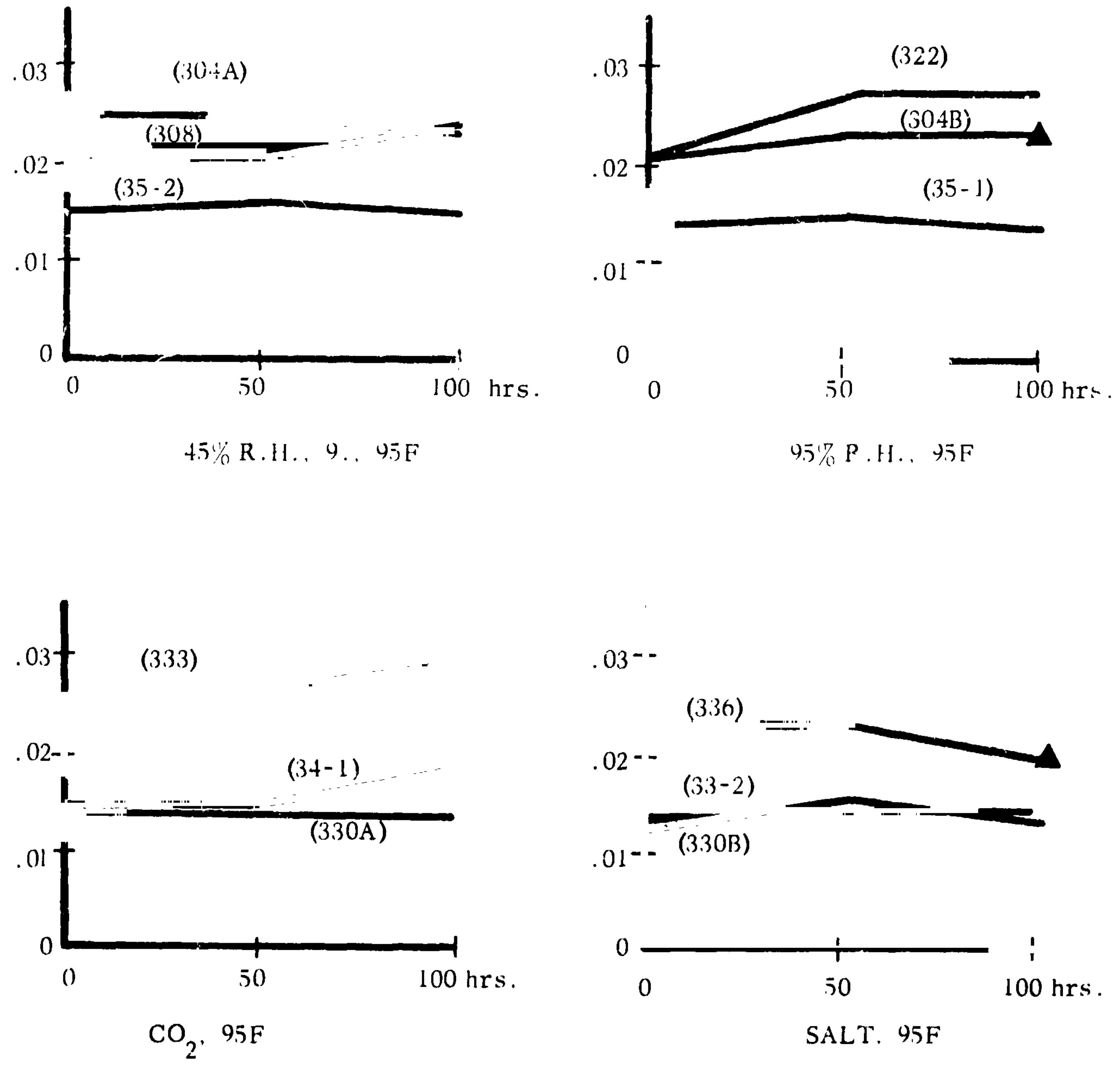

FIGURE III-19 EMITTANCE OF GOLD EXPOSED TO VARIOUS ENVIRONMENTS FOR 50 AND 100 HOURS

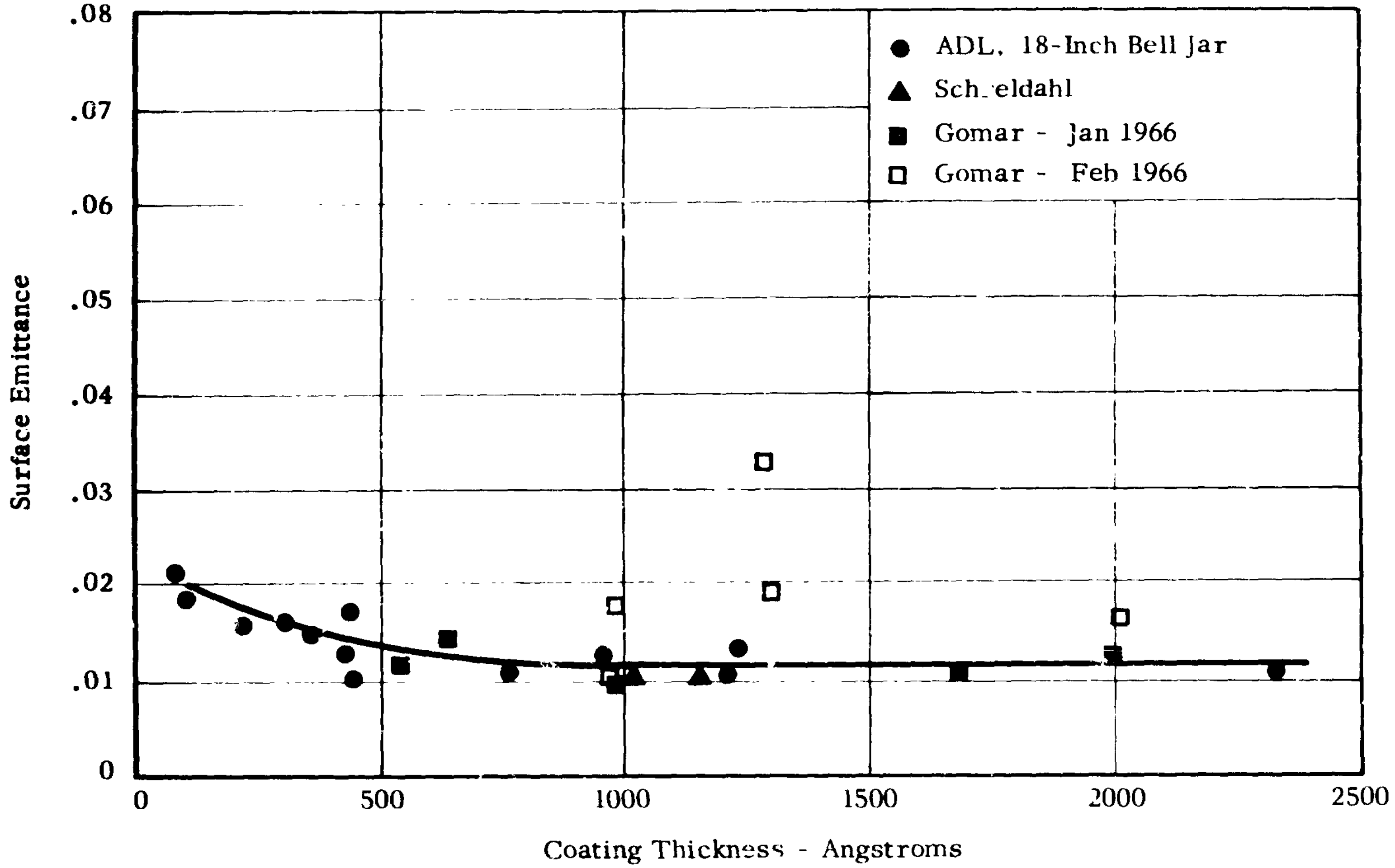

FIGURE III-20 SILVER METALLIZED POLYESTER FILM, EMITTANCE AND COATING THICKNESS

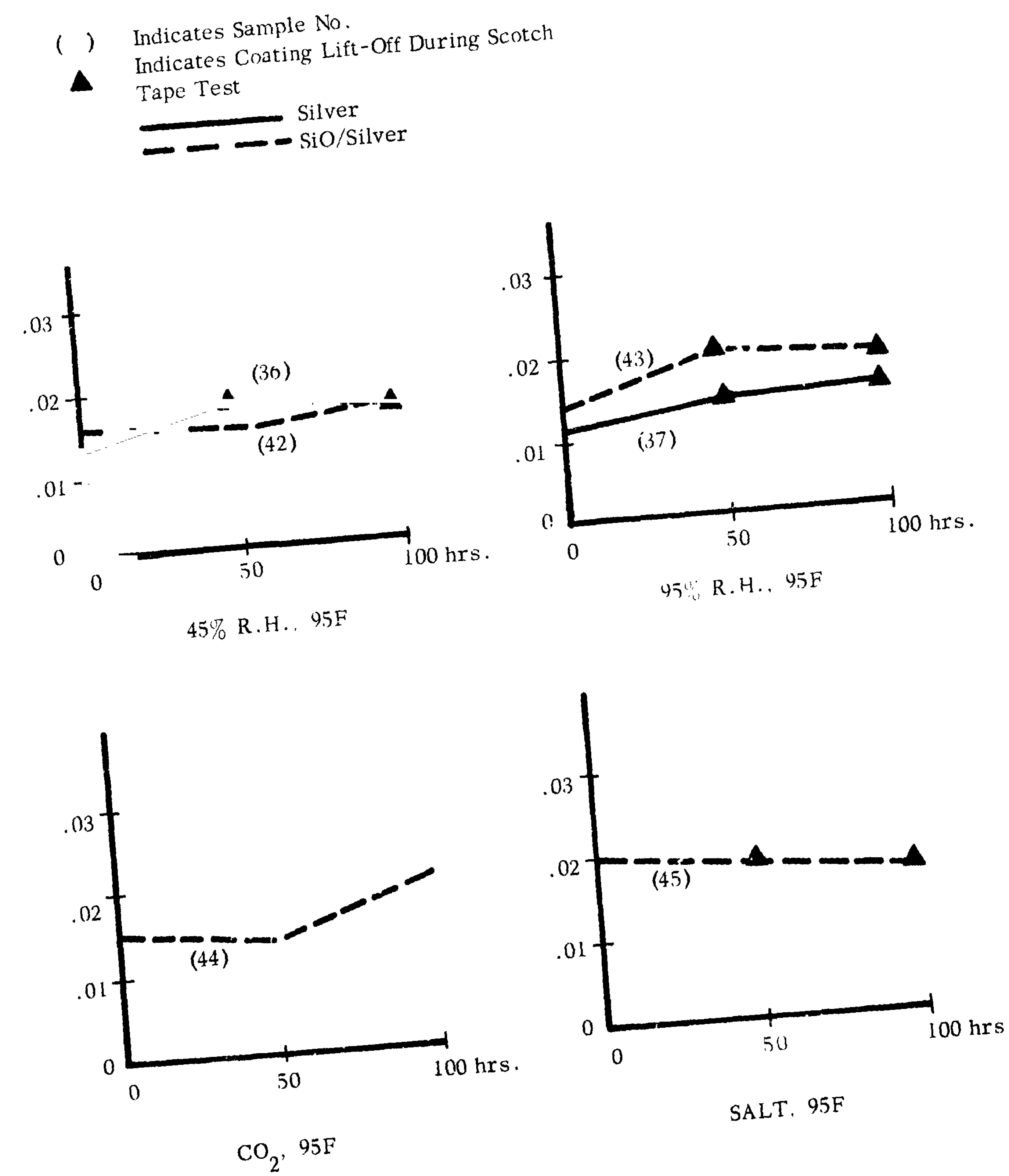

FIGURE III-21 EMITTANCE OF SILVER AND SiO/SILVER EXPOSED TO VARIOUS ENVIRONMENTS FOR 50 AND 100 HOURS

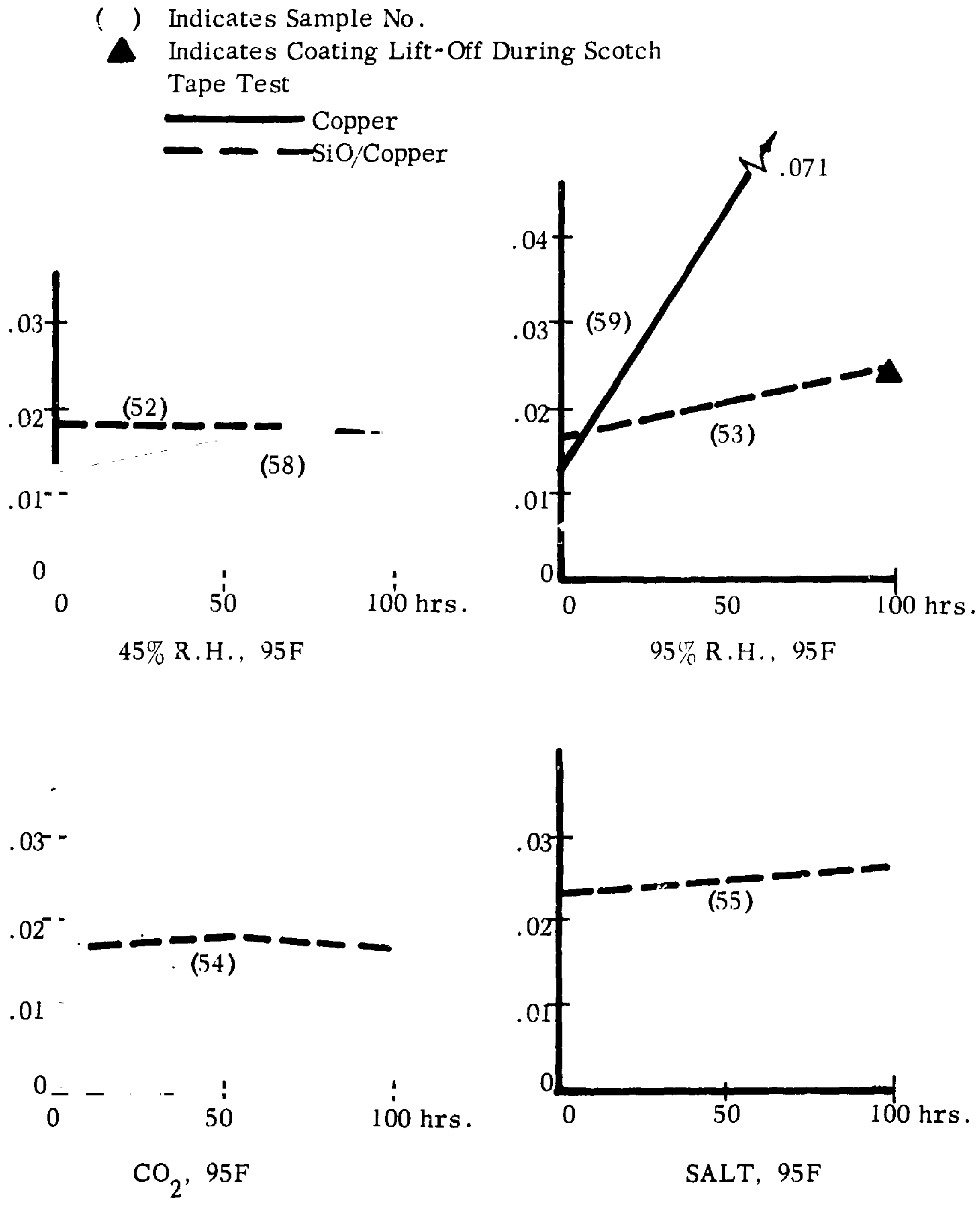

FIGURE III-22 EMITTANCE OF COPPER AND SiO COPPER EXPOSED TO VARIOUS ENVIRONMENTS FOR 50 AND 100 HOURS

REFERENCES

III

1. Holland. L., Vacuum Deposition of Thin Films, John Wiley & Sons, Inc., New York, 1958

2. Kline. S. J. and F. A. McClintock, "Describing Uncertainties in Single-Sample Experiments," Mechanical Engineering, January 1953.

3. Jenkins, R. J., C. P. Butler and W. J. Parker, "Total Hemispherical Emittance Measurements over the Temperature Range 77°K to 300°K," August 1963, U. S. Naval Radiological Defense Laboratory Technical Report 663, SSD-TDR-62-189.

4. Sparrow, L. U. Albers and E. R. G. Eckert, "Thermal Radiation Characteristics of Cylindrical Enclosures," Journal of Heat Transfer, February 1962, p. 73.

5. Knudsen, M., Kinetic Theory of Gases, John Wiley & Sons, Inc., New York, 1934.

PART IV

TASK II, INSULATED TANK CALORIMETER

TABLE OF CONTENTS

IV

LIST OF TABLES

IV

LIST OF TABLES (CONTINUED)

IV

LIST OF FIGURES

IV

LIST OF FIGURES (CONTINUED)

IV

LIST OF FIGURES (CONTINUED)

IV

IV. TASK II, INSULATED TANK CALORIMETER

A. Summary

This report summarizes the work carried out by Arthur D. Little, Inc. under Contract NAS3-6283 to develop and measure the thermal performance of multi-layer insulation systems. This is a continuation of the Insulated Tank Program effort initiated in February 1963 under Contract NASw-615 and carried on under Contract NAS3-4181.

1. Purpose

The purpose of this study was: (1) to select insulation materials which were expected to yield improved performances of multi-layer insulation systems; (2) to design and fabricate multi-layer insulation systems, apply them to calorimeter tanks, and measure and evaluate their thermal performance in a simulated space environment using liquid nitrogen as the heat sink; and (3) to develop practical methods of applying insulation to vehicle-type tanks and achieve the optimum thermal performance for the least weight of insulation.

2. Scope

We have designed, fabricated, and tested a total of seven multi-layer insulation systems. Four of these systems consisted of a foam substrate in addition to the multi-layers. One system contained a 6 inch diameter by 17 inch long penetration. Each system tested is described in Table IV-2. The thermal performance of each insulation system was measured in a test chamber which simulated the vacuum and a portion of the radiation spectrum found in the space environment. A group of seven experimental test series was conducted using the two test calorimeters and test chamber facilities fabricated under the previous contracts.

The heat flux and $\kappa\rho$ performance for each insulation system tested under space environment conditions are presented in Table IV-2 (Insulation Systems 8 thru 14). In addition the results obtained with systems in the two previous contracts are presented for comparison.

3. Conclusions

a. Commercial sources of good quality, low emittance shields have been identified (see Table III-16). These consist of polyester film, vacuum metallized on both sides with aluminum, silver, and gold. The best emittance values obtained with these coatings have been .025, .011 (the silver was unprotected and new; emittance degrades with time) and .017 respectively. One set of shields was obtained containing 1.9 per cent perforations for use in systems with expected gas leaks.

b. Commercial sources of lightweight spacer materials have been identified. These consist of glass fabric, silk nettings, and combinations of silk and foams. Single layers of these materials have unit weights of .0042, .0012 and .0037 pounds per square foot respectively as compared to .0018 pounds per square foot representative of the unit weight of 1/4 mil Mylar. Spacers consisting of multiple layers of glass fabric and multiple layers of silk netting have good low load thermal performance. Each of the spacers could be easily fabricated into multi-layer insulation systems.

c. In the current program, the measured heat fluxes for the five shield systems tested ranged from .31 to 1.06 Btu/hr ft^2. System No. 14 consisting of gold coated shields and silk netting spacers, produced a $\kappa\rho$ product of .000273 Btu-in-lb/hr ft^5°F, which is the lowest value obtained with any system in the entire tank program. The heat flux associated with this system was .33 Btu/hr ft^2 and is surpassed only by System 12 which produced a heat flux of .31 Btu/hr with a $\kappa\rho$ value of 0.0003 Btu-in-lb/hr ft^5°F. Further improvement in the $\kappa\rho$ product of the systems tested can be expected if the insulations are not required to sustain external pressure loadings.

d. The agreement in the insulation heat fluxes measured with tank calorimeter apparatus and with a flat plate thermal conductivity apparatus have been generally good. Also the predicted fluxes based on emittance measurements made on the shield surfaces with the emissometer instrument have been in good agreement with the measured system values. Thus, a great deal of confidence can be placed in the heat flux results obtained in the program.

e. Engineering relations have been developed to predict the effect of static gas pressure and gas flow in the insulation after certain empirical constants are evaluated. From tests conducted with helium gas in a five shield multi-layer insulation, a value for the gas accommodation coefficient of .65 was established for inner and outer boundary temperatures of -320 and 80°F.

Penetration heat flow and temperature gradients were successfully measured in eight tests for a variety of conditions. The experimental techniques used in this investigation were demonstrated to be valid for isolating the penetration heat flows for a wide variety of boundary conditions. The measured heat flow and temperature gradients for one set of conditions are predicted by the analytical model with good accuracy. Generally, however, the conditions selected for the experimental model were not covered by the analysis performed in a previous contract. The analytical model gives good promise of predicting the heat transfer phenomena occurring within the penetration.

The technique of using angles of aluminum foil to seal the joints formed by the shields of the tank and penetration insulation against radiation leaks appears to be both effective and practical. While the data can only be used to demonstrate this factor indirectly, there are no significant heat flows that could be identified with this part of the insulation system.

4. Recommendations

a. In the current program high thermal efficiencies were obtained with five shield multi-layer systems. However, the thermal protection provided by these systems is not sufficient for many contemplated space missions where fifty or more shields per system may be required. Thus the insulation systems developed under this contract should be investigated further with greater numbers of shields.

b. The current program has not included any studies in consideration of the permanent effects that vibration, acceleration and accoustic environments have on the thermal performance of multi-layer insulations. There is, undoubtedly, considerable work in progress in these areas. A portion of this effort should be directed towards further evaluation of the insulation systems developed in the current program which have been demonstrated to have excellent thermal-weight performance properties.

c. It is recommended that the experimental and analytical studies on pipe penetrations conducted in the current program be continued. Other penetration conditions should be explored both to confirm the analytical model selected and to obtain engineering information for optimizing penetration designs. The work completed in this program indicates that the techniques and equipment developed to date can be used successfully to obtain the required information.

It is recommended, therefore, that additional tests with the experimental model be performed. These tests should explore the combined effects of wall conduction, internal radiation and radial heat flow from the outside. Alternate insulating methods used at the outside of the penetration should be investigated also. Walls of the penetration cavity having a low emittance should be investigated to determine the effect on the heat flow.

d. Because of their wide variety, structural supports for space vehicle propellant tanks should be considered separately from propellant tank piping. While the scope of work of the present contract permitted no studies in this area, we believe that it deserves priority in any future investigations. It is recommended, therefore, that the necessary funding in this area for studies be provided.

B. Introduction

Cryogenic propellants, such as liquid hydrogen and liquid oxygen will be used in space vehicles for long duration missions provided they can be efficiently conserved. Normally the environment is at a higher temperature level than the propellants. This promotes a heat flow into the propellants and causes them to vaporize. The generated gases are subsequently lost from the system because they must be vented to space to prevent the rupture of the propellant tanks. This loss can be considerably reduced by thermal isolation of the propellants achieved through the use of efficient low-weight insulation of the multi-layer type.

Multi-layer insulations consist of a number of parallel and alternate layers of shields and spacers which form an envelope around the propellant tank. The shield surfaces have low emittances so as to restrict the transfer of heat by radiation. The spacers maintain the appropriate separation between shields and are constructed of low thermal conductivity materials to restrict the transfer of heat through the system by solid conduction. Under ideal conditions, the vacuum of outer space reduces the amount of interstitial gas present in the multi-layer system to a value where the heat transfer through the system by gas conduction is negligible. However, a realistic appraisal of the situation reveals that there is a small, but finite, probability that some slight leakage of cryogenic fluid will occur through cracks and other imperfections in the tank walls and joints. The flow of these gases through the insulation, and the subsequent increase in the pressure of the gas within the multi-layer will result in a heat flow by gas conduction.

The current investigation was conducted to develop combinations of shields and spacers that produce the lowest heat flow for the lowest system weight as well as to develop the techniques of applying the system to tanks. In addition an attempt was made in the study to evaluate the various modes of heat transfer in multi-layer insulations. In the current program seven insulation systems were applied to the four foot diameter calorimeter tanks. This brings to fourteen the total number of insulation systems tested in the three-year program. The shield materials have consisted of aluminum foil and polyester films vacuum metallized with aluminum, silver and gold. The spacers investigated included vinyl coated Fiberglas screen, silk and nylon nettings, glass fabric and a silk-foam composite.

One system tested in the current program contained a simulated pipe penetration of 6 inch diameter and 17 inches length. This study was undertaken with the purpose of establishing some experience with a physical system and achieving a correlation between the analytical and experimental data.

The heat flow through the insulation and in penetrations was measured with liquid nitrogen in the calorimeter tank. The test specimens were tested in a vacuum chamber which contained temperature controlled wall baffles. All systems were tested at high vacuum conditions.

In addition a number of tests were performed with a calibrated helium gas leak at the cold wall of the insulation to simulate propellant tank leaks in space.

C. Experimental Equipment and Procedures

1. Tank Calorimeter

The calorimeter is a vertical cylindrical vessel, 48 inches in diameter and 26 inches deep, having torispherical heads. The head was fabricated from 1/4 inch thick, oxygen-free, annealed copper because its high thermal conductivity promotes isothermal-temperature conditions in the cold boundary over wide ranges of liquid bath level and insulation heat flux levels. The vessel had a maximum internal working pressure 30 psi above the external pressure and a maximum external working pressure 15 psi above the internal pressure. The tank is supported from a support flange by a 5 inch, schedule 5, Type 304 stainless steel pipe that also acts as the tank vent. The 24 inch diameter support flange is mounted into the top of the vacuum chamber with bolts and O-ring seal. Additional details can be found in our final report on Contract NASw-615.

2. Cambridge Test Facilities

The Arthur D. Little, Inc., facilities located at Cambridge, Massachusetts, were used to conduct our test program. These facilities were limited to the use of liquid nitrogen test fluid. They consist of a 5 foot diameter vacuum chamber, 500 gallon liquid nitrogen supply tank, vacuum pumping system, cold guard and baffle supply systems, and the calorimeter vent gas measuring system.

During the space simulation tests, the calorimeter and its insulation system were installed in the 5 foot vacuum chamber in the position shown in Figure IV-1. The chamber contains two interior baffles; one located in the upper half and the other in the lower half of the chamber. Each can be independently maintained at liquid nitrogen or water temperature through the use of an external supply system.

The chamber and its associated systems are shown in Figure IV-2. The calorimeter is filled from a 500 gallon liquid nitrogen supply tank. This supply tank also provides the feed for the cold guard and chamber baffles when they are operated at liquid nitrogen temperatures. This is accomplished through use of a gravity tank which is elevated above the chamber. The tank support is a 4 inch column which also serves as feed line for the baffles and cold guard. The baffles vent to the gravity tank ullage space while the cold guard vents to atmosphere through a heat exchanger. The baffles can also be connected to the local water system when they are to be maintained at near room temperature.

The chamber is evacuated through use of a 10 inch oil diffusion pump and a mechanical fore pump. This system can achieve 10^{-5} mm Hg pressure with a clean and out-gassed system in less than one day. A longer period of up to several days has been required to achieve this same vacuum with new insulation systems. The insulation systems were generally tested with chamber operating vacuums in the range of 10^{-5} to 10^{-6} mm Hg Occasionally on long-run tests, vacuums below 10^{-6} mm Hg were achieved.

The boil-off gases vented from the calorimeter were brought to room temperature in an air-warmed heat exchanger. The gases were measured volumetrically in dry type, positive displacement meters and vented subsequently to the atmosphere.

3. Instrumentation

The primary measurements made periodically during each test consisted of the following:

a. Calorimeter vent gas flow, temperature and pressure
b. Vacuum chamber pressure
c. Local barometer
d. Liquid level capacitance gauge
e. Temperatures in the insulation system, on the chamber baffles, at the calorimeter cold guard, of the local environment, and others as required.

At the Arthur D. Little, Inc. facility, all temperatures and the barometer data were recorded on strip charts. In addition, these and all the other data were manually recorded.

4. Measured Heat Flux

We measured the shield temperature in each insulation system at select locations. Generally, the thermocouple sensors were located at the top, side and bottom or areas of the tank which are identified as the A, B and C locations respectively. These locations are shown in Figure IV-3. The thermocouple is identified by shield number and area location, i.e., sensor 5B is located on shield number five on the cylindrical section of the tank. Thermocouples are sometimes placed at other locations as in Insulation System No. 10. These locations are also identified by shield number and area, i.e., couple 5AB is located on shield number five in the region between the A and B positions. Exact locations are given in additional figures presented in subsequent sections.

The thermal performance of the insulation system has been measured over intervals of approximately 24 to 100 hours. Occasionally, it was necessary to accept intervals of shorter duration because of difficulties encountered with the facility subsystems after system temperature equilibrium had been achieved. During the measurement interval, the ullage pressure of the calorimeter varied directly as the barometric pressure, i.e., the calorimeter vented to the atmosphere through a low pressure drop system and no attempt was made to control the ullage pressure.

The heat passing through the insulation is reflected as stored energy in the calorimeter system and as vaporized liquid vented from the calorimeter. When no changes in the barometric pressure occur in the measuring interval, the energy transmitted through the insulation is evidenced primarily as vaporized liquid. An almost negligible amount of energy is stored in the calorimeter ullage.

When barometric pressure changes occur during the interval, the system temperature increases or decreases directly with this pressure. An increase in system temperature results in heat storage in the calorimeter tank metal, and the liquid and gas masses. A decrease in temperature results in a heat release. Barometric changes which do work on the thermodynamic system which comprises the calorimeter and its contents are also reflected as system energies.

A thermodynamic analysis[4] of the calorimeter system indicates that for the conditions under which our measurements were made, only two effects need be considered when evaluating the insulation heat flow. The first and most significant factor is the vented gas mass and the second factor is the liquid mass heat storage effect.

The total heat rate is computed from the total vaporized liquid mass vented in the data interval and the latent heat of vaporization of cryogen. The gas mass is computed from the integrated volume measurement of the calorimeter vent gas stream and its temperature and pressure at the metering point.

This measured heat flow is corrected for heat storage or heat release in the calorimeter liquid as follows: the average mass of the liquid in the tank during the data interval is established from the liquid-level measurement, tank-volume calibration, and liquid density. The increase or decrease in the saturation temperature of the bulk liquid at the end of the data interval is compared to that at the beginning and is determined from the change in the calorimeter ullage pressure. This is a function both of the local barometric pressure and the pressure loss in the vent system. From the change in the bulk temperature and the liquid specific heat at saturation, the total heat energy stored or released during the data interval was computed and converted into an hourly rate. Any heat stored during the data interval was added to the heat flow determined from the calorimeter boil-off; a release of heat during the data interval was subtracted.

5. Test Program

We fabricated seven insulation systems and conducted a series of tests with each system. A total of forty-five tests were performed in one or more of the following environments to measure the system heat flow:

a. Space vacuum and 300°K source radiation

b. Space vacuum and 77°K source radiation

c. Transient vacuum and 300°K source radiation

d. Helium gas flow in insulation system

e. Static pressure of helium gas in insulation system

f. Liquid nitrogen test fluid in calorimeter

The principal variables investigated with each system are summarized in Table IV-1. In Table IV-2 the description, conditions, and results obtained with each system are summarized except for System 10 which contains the 6 inch diameter penetration.

D. Experimental Systems and Results

1. Insulation Systems No. 8 and 9

a. Summary

This task is one of the several tasks undertaken in the insulated tank program. It was a combined experimental and analytical effort conducted to evaluate the thermal performance of multi-layer insulations with helium gas flowing outward through the system.

Two multi-layer insulation systems, each consisting of five shields, were placed onto the tank calorimeters. The shields of one system (No. 9) were perforated in order to permit the gas introduced at the underside of the insulation to vent readily. The two insulation systems were identical in all other respects. Thirty heat flow tests were performed with the two systems using liquid nitrogen in the tank and with various levels of gas flow and chamber back pressure. An engineering model was formulated and analyses were prepared for predicting the heat flows in each system at the various test conditions. A good check was obtained between the predicted and experimental values.

b. Introduction

Under ideal conditions, the vacuum of outer space reduces the amount of interstitial gas present in a multi-layer insulation to a value where the heat transfer through the system by gas conduction is negligible. A realistic appraisal of the situation, however, reveals that there is a small, but finite, probability that some slight leakage of cryogenic fluid will occur through cracks and other imperfections in the tank walls and joints. The flow of these gases through the insulation and the subs quent increase in the pressure of the gas within the multi-layer will result in a heat flow by gas conduction.

When a leak is present, the pressure of interstitial gas depends upon the size of the leak, the pressure of the gas prevailing outside of the system and the restriction presented to the gas flow by the shields and spacers. Normally, the spacers are formed by a fibrous material; therefore, being porous they offer little restriction to gas flow. The shields, however, are usually formed of continuous films and offer considerable restriction to gas flow.

For a given system and gas leak condition, it is possible to reduce the interstitial gas pressure by perforating the shields. These perforations allow the gas to vent more freely through the system. These same perforations allow heat energy in the form of radiation to also pass more freely through the system. Thus, while perforations decrease the gas conduction heat flow rate, they simultaneously increase the radiation heat flow rate. From previous[1] analytical studies of this situation, is has been determined that for a given system and gas leak rate, there is an optimum perforation fraction which produces the minimum net rate of heat flow in the system.

c. Multi-Layer Heat Transfer Relations

The general problems of low-pressure gas conduction between two parallel surface, j and j+1, have been treated by Kennard[2] and may be expressed as:

$$(Q/A)_{j,\ j+1} = f\ (\alpha)\ F_{j,\ j+1}\ (C_v + k/2)\ (T_{j+1} - T_j) \qquad (1)$$

The accommodation coefficient function f (α) is usually assumed constant with temperature, though this conclusion may not be valid. Further, if there is a constant leak rate ν_o , molecules/area-time, from the inner tank to the outside through shield slits, perforations, or other openings, a material balance over shield j yields,

$$\nu_o = \tau\ (F_{j,\ j-1} - F_{j,\ j+1}) \qquad (2)$$

F is the molecular flux and τ the perforated area fraction. The subscript numbering is such that the inner cold surface is designated as o and the shields numbered in increasing order 1, 2, ...n where n is the last shield or outer vessel wall. To combine Eqs. (1) and (2), it is readily seen that (Q/A) due to gas conduction varies in different layers (though as pointed out below, the sum of the gas conduction, radiation and solid conduction components must be the same between layers). For example, gas conduction between the inner tank and shield 1,

$$(Q/A)_{o,\ 1} = f\ (\alpha)\ F_{o,\ 1}\ (C_v + k/2)\ (T_1 - T_o) \tag{3}$$

However, from Eq. (2),

$$F_{o,\ 1} = \frac{\nu_o}{\tau} + F_{1,\ 2} = \frac{\nu_o}{\tau} + \frac{\nu_o}{\tau} + F_{2,\ 3} = \ldots$$

$$= \frac{n\nu_o}{\tau} + F_{n,\ n+1} \tag{4}$$

where $F_{n,\ n+1}$ represents the average molecular flux outside the insulation; in an absolute vacuum, $F_{n,\ n+1} = 0$. As $F_{n,\ n+1}$ is usually known Eq. (4) relates the unknown $F_{o,\ 1}$ to known parameters. Eq. (4) is substituted into Eq. (3) and similar operations carried out for $(Q/A)_{1,\ 2}, \ldots (Q/A)_{n-1,\ n}$. For the gas conduction between shields j and j+1, assuming C_v to be independent of temperature,

$$(Q/A)_{j,\ j+1} = f(\alpha)\ (C_v + k/2)\ (T_{j+1} - T_j)$$
$$[(n-j)\ \frac{\nu_o}{\tau} + F_{n,\ n+1}] \tag{5}$$

Considering next the radiation component between layers with an open area τ, it has been shown (2) that.

$$(Q/A)_{j,\ j+1}(\text{radiation}) = R\ \sigma\ (T_{j+1}^{\ 4} - T_j^{\ 4}) \tag{6}$$

Finally the solid component between layers may be expressed as:

$$(Q/A)_{j,\ j+1} = k_{sc}\ (T_{j+1} - T_j)/\delta \tag{7}$$

Neither k_{sc} nor δ can be well defined in a multi-layer insulation; however, the group (k_{sc}/δ) may be considered a valid proportional constant which does not vary between layers. The solid conduction component between inner and outer shields may then be expressed as:

$$(Q/A)_{o,\,n} = (k_{sc}/\delta)\,(T_n - T_o)/n \qquad (8)$$

The net heat flow between any two shields is given by the sum of Eqs. (5), (6), and (7) as $(Q/A)_{net}$. Also this heat flux is a constant so that

$$\sum_{j=o}^{n} \left[(Q/A)_{gas\ conduction} + (Q/A)_{radiation} + (Q/A)_{solid\ conduction}\right]_{j,\,j-1}$$

$$= n\,(Q/A)_{net} \qquad (9)$$

Substituting in the sum and simplifying,

$$(Q/A)_{net} = f(\alpha)\,(C_v + k/2)\left\{\frac{\nu_o}{\tau}\left[\sum_{j=1}^{n}\frac{T_j}{n} - T_o\right] + \left(\frac{T_n - T_o}{n}\right)F_{n,\,n+1}\right\}$$

$$+ \frac{R}{n}\,\sigma\,(T_n^4 - T_o^4) + (k_{sc}/\delta)\,(T_n - T_o)/n \qquad (10)$$

The temperatures in the (n-1) shields between the inner and outer shields must be known in order to solve Eq. (10). These could, in principle, be obtained from the use of the (n-1) simultaneous equations resulting from the sum of Eqs. (5), (6) and (7) applied to the (n-1) layers. Such a solution would almost certainly require machine computation due to the non-linear character of the equations. However, using experimental data, it will be shown later that Eq. (10) describes the various heat flow components.

d. Description of Insulation System

The experimental investigation was carried out with two companion insulation systems designated as Systems No. 8 and 9. Each consists of five shields mounted onto the Arthur D. Little, Inc. tank calorimeters. The systems are identical in all respects except that the shields of the second system contain perforations which give it a superior gas venting ability compared to the first system. The insulation system information presented in the subsequent discussion is also summarized in Table IV-3.

(1) Shields

The shields of both insulation systems were made up of 1/4 mil polyester film vacuum metallized with aluminum on each side. The coatings had a nominal thickness of 400 Angstroms and were produced by the National Research Corporation. The total hemispherical emittance of the unperforated coatings was .025 as measured with the Arthur D. Little, Inc. emissometer. After metallizing, one-half of the shield material was perforated by the Perforated Specialities Company, Inc. of New York City. The perforations consisted of nominal .047 inch diameter holes stamped 0.308 inches apart in one direction and 0.316 inches apart in the perpendicular direction.

In the first attempt to produce the shield material for the insulation systems, the perforating operation preceded the metallizing operation. These attempts were unsuccessful because: a) the perforations had weakened the film and it could not be easily handled in the metallizing equipment, and b) the wrinkling introduced in the film by the perforating equipment created windows in the coatings. Further, the handling of the film prior to the coating operation had resulted in the surface becoming contaminated with dust and oil marks which introduced imperfections in the coatings.

Since the coating imperfections increase the emittance of the coating surfaces, it was necessary to perform the metallizing operation before any other operations and handling. This required that the metallizing fabricator use a mill wound roll. The roll was unwound only in the metallizing chamber under vacuum until the required coatings were placed on the film. The metal coatings were not degraded when the films were perforated in subsequent operations.

(2) Spacer

Under Contract NAS3-4181, we demonstrated that netting spacers fabricated from nylon increased the insulation heat flux by inducing a pressure between the layers of the insulation. This pressure resulted from the high thermal contraction occurring in the spacers, particularly in the layers at the tank side when their temperature was lowered significantly below room temperature.

To eliminate the contraction-induced-effects, we investigated the use of glass fabrics which have a lower temperature coefficient of expansion than nylon and lower also than aluminum and stainless metals which are normally used for the construction of propellant tanks. The lightest fabric available is Style 104 glass fabric and is produced commercially in a plain weave for use primarily in the electrical industry. This material has a thickness of 2-1/2 mils and a weight per unit area about twice (.0042 lbs ft^3) that of 1/4 mil Mylar. All organic contaminants were removed from the fabric by a batch oven cleaning.

Glass fabrics had been tested previously with the K-apparatus and found to give good thermal performance at no-load conditions, but the performance was severly degraded when the insulation was loaded. Tests 2027 and 2029 conducted under Contract NAS3-4181, indicate the effect that loading has on heat flux of a MLI with glass fabric spacers (three layers of the type of fabric used by L'air Liquide per spacer). A 15 psi load produced almost a thousand fold increase in the heat flux over the no-load conditions (test results for 2029i and 2029e yielded heat flux values .28 and .246 Btu/hr ft^2 respectively for ten-shield systems).

Not withstanding its poor thermal performance under load, we used Style 104 fabric in the spacers for Insulation Systems 8 and 9 because of its low unit weight, low thermal contraction, availability, and the negligible effect that air contaminants and humidity have on glass materials.

Removal of sizing materials from the fabric during the oven cleaning process made the material difficult to handle especially when cut. Handling was considerably improved when all the cut edges of the material were bound with the use of 1/4 mil polyester film strips which were heat pressed to the fabric edges. The polyester strips were used also for binding two or more layers of fabric together and for producing hems in the material, i.e., for purse string binding on the spacers' side sheets.

(3) Insulation Application Method

Insulation Systems No. 8 and 9 were fabricated onto Calorimeter Tanks No. 2 and 1 respectively over 1/8 by 1/8 inch vinyl-coated Fiberglas net and 1/8 inch tubing which form the gas distributor for the helium leak system (see Appendix IV-E-1). The shields, as previously described, were made from 1/4 mil, Type S, DuPont Mylar that was vacuum metallized on both sides with aluminum. Each spacer was fabricated from two layers of Style 104, tafetta, oven-cleaned glass fabric. The fabricated systems each consisted of five shields and six spacers.

Each layer of insulation was applied in three segments, consisting of a top, bottom and side element. The side element was twenty-two inches wide and about thirteen feet long. Each side segment consisted of two layers of glass fabric and a layer of aluminized polyester film. The two glass fabric layers were bonded together at the edges through the use of 1/4 mil by 1 inch wide polyester stripping. The shield was then hand stitched to the glass fabric. A hem was placed into the fabric on each of the two long sides so that it could be fastened over the tank through the use of a draw string as shown in Figures IV-4 and IV-5. The shield was loosely stitched to the outside of the spacer. The portions of the shield that extend over the knuckle radii of the tank at top and bottom were slit every four inches; the glass fabric was not cut.

Each of the circular segments for the top and bottom of the tank was formed from two layers of glass fabric which were bonded together along the edge with Mylar. These were tucked under the drawn edge of the side segment and were held in place by the draw string on the side segment. The shields at the top and bottom were next placed over the glass spacers. However, instead of tucking them under the draw string, they were placed so as to overlap and directly contact with the side shield segment. These shield segments were held in place with scotch tape (See Figure IV- 6) until the next layer of spacers which provided permanent support for these shields have been attached to the tank.

As in all the tank insulation systems fabricated in the previous programs, three thermocouples were attached to each shield at the top, side and bottom sectors (see Figure IV-3).

e. System Test Conditions

Three types of tests were performed with the system. In each type a particular space or launch condition was partly simulated. These consist of the following:

1. space condition (standard test environment)
2. space condition with helium flow in the insulation
3. final phase of the launch conditions

(1) Space Condition

The standard space environment used in this program consists of chamber vacuums less than 10^{-5} mm Hg. The chamber baffles were operated at a nominal temperature of 80°F. Liquid nitrogen was used in the calorimeter tank and in the cold guard at the calorimeter neck. Vent gas flow measurements were taken after the calorimeter insulation achieved temperature equilibrium. These conditions prevailed in the tests noted below for each system.

Tests

System No. 8	System No. 9
III-1A1	III-2A1
III-1A2	III-2A2
III-1G	III-2A3
III-1N	III-2G
	III-2P

(2) Space Condition with Helium Flow in the Insulation

These tests were performed with all systems operating as in the conditions described above. In addition helium at a controlled flow rate up to 300 micron liters per second* was distributed to the

*Multiply micron-liters per second by 5.38 x 10^{-8} to obtain g-moles per second. Divide by the insulation area to obtain mass flow rate per unit area.

underside of the insulation system. The helium flow was pumped from the chamber with the ten-inch oil diffusion pump and mechanical fore pump system (see Figure IV-2). Because the vacuum pump capacity was limiting at the higher helium flow rates, higher chamber pressures prevailed during these tests than were permitted in the standard condition tests.

These conditions prevailed in the tests noted below for each system.

Tests

System No. 8	System No. 9
III-1B	III-2B
III-1C	III-2C
III-1D	III-2D
III-1E	III-2E
III-1F	III-2F
III-1H	III-2J
III-1J	III-2K
III-1K	III-2L
III-1L	III-2M
III-1M	III-2N

(3) Final Phase of the Launch Conditions

At the high helium leak rates, a gas pressure of approximately ten microns prevailed in the chamber space. By stopping the gas leak, with the vacuum and other systems continuing to operate as before, a partial simulation of the vehicle launch could be obtained producing a transient in the chamber pressure, calorimeter vent gas flow, and shield temperatures. These variants were monitored so that the insulation performance could be determined as a function of time. These conditions prevailed in Test III-1P with System No. 8 and in Test III-2Q with System No. 9.

f. Experimental Results and Discussion

The experimental results and significant conditions prevailing in the tests performed with Systems 8 and 9 are presented in Tables IV-4 and IV-5 respectively. The duration of the test shown in column five represents the period in which the insulation test specimen and system were at temperature equilibrium.

In column six the value of the average prevailing vacuum in the space simulation chamber is presented. During some tests the chamber pressure fluctuated as little as 20 per cent; in other tests it fluctuated as much as 100 per cent.

The value of the guard temperature is presented in column seven. The temperature was established with a thermocouple attached to the guard. This temperature is a measure of the heat flow from the guard to the calorimeter which is at a temperature of -320°F. The 8°F differential temperature produces a maximum heat flow to the calorimeter of 0.5 Btu/hr. This value is reduced somewhat because the cold gas venting from the calorimeter tends to carry away a portion of this heat flow.

In the next column the value of the helium leak rate is presented. This represents the total mass passing through the insulation system. As described in Appendix IV-E-1, the gas was evenly distributed at the underside of the insulation. In the perforated system the flow rate per unit area is obtained from the measured gas flow and the insulation area as established from the tank surface. A comparable value can be established for the non-perforated system recognizing, however, that the flow through the insulation takes place at the location of slits and joints in the shield.

The column labeled "total heat flow" shows the experimental value of the heat passing through the insulation. This value is obtained after all corrections have been applied to the volume flow rate of the boil-off and corrections have been made for the effect of changing barometric pressure on the heat storage in the liquid mass contained in the calorimeter.

The last column is the value of the measured flux adjusted to standard boundary conditions. Since the temperature of the chamber baffle varied from one test to another, the comparison of different insulations or of different tests performed with the same insulation cannot be properly made. A temperature of 80°F has been chosen as the standard value of the chamber baffle. Since radiation is the dominant mode of heat transfer (to be shown later), the measured heat flux was adjusted by a factor (T_s^4/T_m^4) where the subscripts on the outer boundary temperatures are the standard and measured temperatures respectively. This adjustment to standard conditions is made only for insulation systems evaluated under the standard space conditions and which do not contain penetrations.

Portions of the foregoing discussion apply also to the presentation of the experimental conditions and data in tabulations for the other insulation systems in subsequent sections of this report of the tank program.

(1) Standard Conditions, System No. 8

An average heat flux of 0.511 Btu/hr ft^2 (adjusted value) was obtained in 130 hours of test (III-1A, 1G and 1N) with the insulation at the standard conditions. This value compares with the value of 0.36 Btu/hr ft^2 computed for the radiation flux alone using a shield emittance value of 0.025 as obtained with the Arthur D. Little, Inc. emissometer instrument. The difference in the two values is 0.15 Btu/hr ft^2 and represents the heat flux due to solid conduction within the multi-layer. As will be demonstrated in a subsequent section, the chamber pressure was sufficiently low so that heat transfer within the multi-layer resulting from gas conduction may be considered negligible.

In the table below the values obtained with the 39.5 square feet of insulation mounted on the calorimeter tank are compared with the results obtained with the same insulation placed in the flat plate thermal conductivity apparatus (K-apparatus). These are, in turn, compared to the values computed from the shield surface emittance.

Test Equipment	Test No.	Measured Flux Btu/hr ft^2	Adjusted Flux Btu/hr ft^2	$\frac{(Q/A)_{adjusted}}{(Q/A)_{theoretical}}$	Remarks
Calorimeter Tank	III-1A1	.522	.518	1.44	-
Calorimeter Tank	III-1A2	.519	.512	1.42	-
Calorimeter Tank	III-1G	.490	.490	1.36	-
Calorimeter Tank	III-1N	.520	.505	1.40	-
K-Apparatus	3047a	.216	.466	1.30	at zero load prior to 15 psi load
K-Apparatus	3047j	.344	.740	2.05	at zero load after 15 psi load
Emissometer	284, 285, 288	-	.36	1.00	based on .025 emittance

The results obtained with the K-apparatus were for a ten-shield system and 70°F warm boundary. In accordance with our customary procedures, we have adjusted the experimental value to those that would be obtained in a five-shield system and 80°F warm boundary temperature. Also in accordance with these past procedures, we assume, when making these adjustments, that no conduction effects are present in the insulation system. On this basis the flux measured in the tank apparatus is in excellent agreement with that measured in the K-apparatus for Test 3047a. K-apparatus Test 3047j, performed after the insulation was unloaded from the 15 psi level shows a considerably higher flux.

Assuming that the computed value of .36 Btu/hr ft^2 is the actual radiation flux, then the average conduction flux for the tank system is about .15 Btu/hr ft^2 or 30 per cent of the total flux; the K-apparatus results indicate a 30 to 105 per cent increase in the total flux due to conduction for Tests 3047a and 3047j respectively. The $\kappa\rho$ product of the system based on the measured fluxes has a value of .00092 Btu-in-lb/hr-ft^5°R.

(2) Standard Conditions, System No. 9, Heat Flux Data

An average heat flux of 1.04 Btu/hr ft^2 (adjusted value) was obtained in 136 hours of test (III-2A, 2G and 2P) with the insulation at standard conditions. This compares with the value of 0.92 Btu/hr ft^2 computed for the radiation flux alone using a shield emittance value of .065. The difference in the two values is 0.12 Btu/hr ft^2 and represents the heat flux in the multi-layer due to solid conduction. The heat flux in the multi-layer due to gas conduction is negligible because of the low chamber pressure.

The heat fluxes measured both in the tank and K-apparatus systems are compared in the tabulation below. The tank fluxes are about 35 per cent lower compared to K-apparatus Test 3049a and about 55 per cent lower compared to K-apparatus Test 3049h.

Test Equipment	Test No.	Measured Flux $\frac{Btu}{hr\ ft^2}$	Adjusted Flux $\frac{Btu}{hr\ ft^2}$	$\frac{(Q/A)_{adjusted}}{(Q/A)_{theoretical}}$	Remarks
Calorimeter Tank	III-2A1	1.04	1.02	1.11	-
Calorimeter Tank	III-2A2	1.09	1.07	1.16	-
Calorimeter Tank	III-2A3	1.07	1.06	1.15	-
Calorimeter Tank	III-2G	1.02	1.04	1.13	-
Calorimeter Tank	III-2P	1.03	1.01	1.10	-
K-Apparatus	3049a	.658	1.41	1.53	at zero load prior to 15 psi load
K-Apparatus	3049h	.742	1.60	1.74	at zero load after 15 psi load
Computed	-	-	0.92	1.00	based on .063 effective shield emittance

The heat flux of a multi-layer insulation is increased when perforations are added. The openings in the shield transmit radiation which otherwise would be blocked. The degree to which the flux is increased is given by the following relation for small closely spaced holes, low emittances, and small perforated area fractions:

$$(Q/A)_{\tau} = (Q/A)_{o}\left(1 + \frac{2\tau}{\varepsilon}\right) \qquad \text{(Reference 1, p. II-121)}$$

where $(Q/A)_o$ = radiation flux without perforations, Btu/hr ft^2

τ = perforated area, fractional per cent

ε = shield emissivity (unperforated value)

In the process of building up Insulation System No. 9, emittance measurements were made on samples of the perforated shields. It is important, however, to point out that the values obtained could not be used directly in computing the insulation performance because the effective emittance of the material as measured in the emissometer is different from the effective emittance of a floating shield in a multi-layer insulation system. The basis of this difference is that the perforated areas are sealed by the tape that is used to attach the sample onto the sample holder of the emissometer. As the tape has an emittance approaching 1.0, the perforations are replaced with high emittance surfaces. The effective emittance for this situation is given approximately by the relation,

$$\varepsilon_1' = \varepsilon_o\left(1 + \frac{\tau}{\varepsilon_o}\right)$$

Thus, for an aluminized surface emittance, ε_o = .025, the computed effective emittance of shields with τ =.0188 perforation is .044 which compares with the measured values of .048 and .040 obtained with the emissometer in Tests 310 and 311 respectively. (See Part III)

However, the effective emittance, ε', of perforated shields in an actual calorimeter system is given by the relation:

$$\varepsilon'_2 = \varepsilon_o \left(1 + \frac{2\tau}{\varepsilon_o}\right) \qquad \text{(Reference 2, p. IV-8)}$$

The effective emittance of the shields computed from this relation is 0.063. From this value the radiation flux of 0.92 Btu/hr ft^2 is obtained for System No. 9.

(3) Space Conditions With Helium Flow, Systems No. 8 and 9, Heat Flux Data

The heat fluxes measured in Systems No. 8 and 9, while helium was passing through multi-layers, consists of four components. Two of these components, the radiation and solid conduction fluxes, were established in the preceeding discussions. The two remaining components are associated with the interstitial helium gas; the first is the result of base gas pressure existing inside of the system as a result of the static pressure outside of the system and the second is the result of gas pressure within the insulation that results from the directional flow of gas through the system. The relations for establishing the magnitude of these components were presented previously in Equation (10).

To illustrate the fact that Equation (10) describes these various heat flux components, it is applied to experimental results obtained in Test Series III-1 and III-2 with the calorimeter tank wherein all the parameters were measured experimentally or determined indirectly. The technique of obtaining all the parameters is outlined in Table IV- 6.

Considering first System No. 9 the radiation and solid conduction contributions were very nearly constant and equal to 0.92 and 0.12 Btu/hr ft^2 respectively. The total heat flux varied from 1.02 to about 1.415 Btu/hr ft^2 as ν_o and/or $P_{external}$ increased. To illustrate the final form of Eq. (10) for these tests,

$$(Q/A)_{net} = f(\alpha)\ (\theta_1 + \theta_2) + 1.04 \qquad (11)$$

where $\theta_1 = 2.26 \times 10^{-6}\ \nu_o \left(\sum_{j=1}^{6} \frac{T_j}{6} - 150 \right)$

$$\theta_2 = 3.16 \times 10^{-3}\ P$$

and ν_o is expressed in g moles/cm^2-sec, P in mm Hg, and T in °R; T_j values were determined experimentally as ν_o and P were varied. A plot of measured $(Q/A)_{net}$ against the sum of θ_1 and θ_2 should give a straight line with a slope $f(\alpha)$. Such a plot is shown in Figure IV-7 and, although there is some experimental scatter, a linear relation is a good approximation. $f(\alpha)$ was found to be 0.5. From the method of defining $f(\alpha)$ in the nomenclature, if $\alpha_j = \alpha_{j+1}$, then the accommodation coefficient may be estimated since $f(\alpha) \rightarrow \alpha/(2-\alpha) = 0.5$, $\alpha = 0.67$. In Figure IV-7, the data points represent tests where ν_o varied from 0 4.14×10^{-10} g moles/cm^2-sec and P from 6.5×10^{-7} to 2.4×10^{-3} mm Hg. The computed and experimental heat flux values are compared in Table IV-7 and show an average deviation of 6.2 per cent.

Equation (10) was also applied to the data obtained with System No. 8. As indicated previously, this system is similar in all respects to System No. 9 except that no perforations were used and all the gas venting had to occur from slits, joints and other openings in the insulation. The value of τ was not known, but it was expected to be small. From the identity of the two systems, the assumption was made that the functional value of the accommodation factor is the same for both systems, i.e., $f(\alpha) = 0.5$. Using Equation (10) a value of $\tau = 0.0014$ was obtained. This gave a good check between the calculated and experimental heat fluxes. A plot of the experimental (Q/A) as a function of $\theta_1 + \theta_2$ using the indicated $f(\alpha)$ and τ, is shown in Figure IV-8. The pertinent variables computed, fluxes and experimental fluxes are presented in Table IV-8. The average values of the radiation and solid conduction fluxes are 0.36 and 0.15 Btu/hr ft^2 respectively as previously established in the standard conditions tests.

The comparisons presented in the table between the computed and experimental fluxes are in excellent agreement considering the wide variations in helium flow and chamber pressure. The average deviation computed for this test series is 4.4 per cent. The chamber pressure was varied over the range from 6.5×10^{-7} to 2.4×10^{-3} mm Hg. The helium flow was varied in the range from 0 to 300 micron-liters per second.*

The data in Tables IV-7 and IV-8 for no helium flow in the systems show the small value computed for the gas conduction flux, $(Q/A)_{gc}$, compared to the radiation and solid conduction fluxes. For example in Test III-2A2 the gas conduction flux represents about 8 per cent of total flux at a chamber pressure of 5×10^{-5} mm Hg. In Test III-2G the value of this flux is reduced to less than 1 per cent at a chamber pressure of 5.8×10^{-6} mm Hg. In Tests III-2P, III-1A, 1G and 1N this flux is an even smaller percentage of the total because of the low chamber pressure levels that prevailed in the tests.

(4) Temperature Gradients in Multi-Layer Insulation Systems No. 8 and 9

The temperatures of the shields in each multi-layer attain new values for every helium gas load. Also, there is a definite pattern to the successive temperature distribution that occurs as the gas load varies. This can be seen in Figure IV-9 from the temperature plots for each of Tests III-1A through III-1G. Only the temperatures on the side sheet, location B, are shown.

The temperature distribution for zero gas load, Test III-1A, approximates the theoretical temperature distribution for a true floating shield system. Increasing the gas load to 4.5 micron-liters per second has little effect on the temperature distribution and results in only a 10 per cent increase in the measured heat flux. A further increase to 30.5 micron-liters per second reduces the temperature of No. 1 shield to very near the value it achieves ultimately at a gas load of 168 micron-liters per second. This would indicate that, in spaces close to the tank, gas conduction quickly becomes the predominant heat transfer mode. On the other hand, the temperature of shield No. 4 assumes its ultimate value only gradually with increasing gas load. This would indicate that the helium gas pressure in the space on both sides of shield No. 4 is increasing at a more moderate rate.

*Multiply micron-liters per second by 5.38×10^{-8} to obtain g-moles per second. Divide by the insulation area to obtain mass flow rate per unit area.

The shield temperature gradients measured for Systems No. 8 and 9 appear significantly different from one another. For example the temperatures of shield No. 1, as shown in Figure IV-9, are reduced significantly as the gas load is increased from 4.5 to 63 micron-liters per second. On the other hand, in System No. 9 the No. 1 shield temperatures shown in Figure IV-10 decline more gradually with increasing gas load. Also, the temperature gradient curve for System No. 9 appears to become displaced parallel to itself, while in System No. 8 the shape of the gradient, particularly at the inner shield changes drastically.

The foregoing temperature data apply to the first tests performed with each system in which the chamber pressures were higher than in the latter tests in each series. However, the effect of helium flow in the latter system produces similar effects on the temperature gradients. Again in System No. 8 there is a drastic downward shift in those temperatures of shields closest to the tank wall.

This is exhibited in Figure IV-11 where the experimental shield temperatures are shown versus the helium leak flow rate as obtained in various Tests III-1H through III-1N. The effect of the gas in the multi-layer is to place a low heat flow resistance in parallel with the high radiation heat flow resistance, and, thereby, reduce the effectiveness of the shields in the radiation mode. Stated in another way, the gas in the multi-layer has the effect of removing shields from the cold side as the gas leak flow is increased.

The distribution of temperature in the multi-layer is shown as a function of helium gas load in Figure IV-12 for System No. 9. It is to be noted that for this perforated system as before, the shield temperatures are not effected as drastically as those of System 8.

The heat fluxes from the two systems are very nearly equal at a helium gas load of 120 micron-liters per second. The corresponding tests are III-1J and III-2M. The shield temperature distribution that prevails in these tests is compared in Figure IV-13.

The shield distribution obtained in Test III-1J is illustrative of an insulation where the heat flow is conduction dominated; Test III-2M is illustrative of an insulation where the heat flow is radiation dominated.

(5) Transient Condition, Systems No. 8 and 9

The helium gas load to Insulation System No. 8 was reduced to zero in test III-1P after being maintained at a load of 168 micron-liters per second for several hours. The boil-off from the calorimeter and chamber pressure were monitored until steady-state values were achieved. From the boil-off rate, the instantaneous calorimeter heat flow and heat flux were computed. The latter is presented as a function of time along with chamber pressure in Figure IV-14. Although the chamber achieves equilibrium pressure at 10^{-6} mm Hg in about 75 minutes, the initial transient is very rapid and pressures below 10^{-5} are achieved in the first few minutes. The heat flux on the other hand, starts out at a value 7.2 Btu/hr ft^2 and achieves 97 per cent of its approach to equilibrium in about three hours. The average heat flux rate in this interval is 2.6 Btu/hr ft^2 and indicates a gradual decline in the value of the flux.

The temperature gradients in the multi-layer are shown in Figure IV-15 at the beginning and later times during the transient. The gradient at three hours and fifteen minutes after the start of the transient has almost the same values as the theoretical gradient. The gradient at fifteen minutes is almost identical to the steady-state gradient presented in Figure IV-9 for Test III-1C. A similar comparison can be drawn between the gradient at one hour and fifteen minutes and the steady-state gradient of Test III-1B. The gradient at the start of the transient is linear within the multi-layer. This was obtained at a helium leak rate of 168 micron-liters per second, the same rate used in Test III-1F. However, this through-put was at the maximum capacity of the pumping system and on one occasion (Test III-1F), the chamber pressure was held to 6 x 10^{-4} mm Hg. Variations in performance of the pump caused the chamber pressure to rise to 15 microns. This high pressure produced a correspondingly higher heat flux, i.e., 7.2 Btu/hr ft^2 and a more linear temperature gradient than obtained in Test III-1F. (In actual time Test III-1P was performed immediately following Test III-1F.)

While the temperature gradients for the transient test at fifteen minutes and at 75 minutes correspond very closely to the steady-state gradients for Tests III-1C and III-1B respectively, heat fluxes do not correspond because of the apparent lag existing in the response of the calorimeter tank and liquid to rapid changes in the heat input.

A test, III-2Q, was performed to monitor the decay in the insulation heat flux taking place in Insulation System No. 9 when the helium gas leak is discontinued. The test conditions were similar to those prevailing in Test III-1P. Prior to start of the test, the helium leak rate was increased to 280 micron-liters per second. The chamber pressure and flux were stabilized over a period of three hours. Prior to start of the transient, the chamber pressure was constant to a value of 5 microns and the heat flux was constant at a value of 7.85 Btu/hr ft^2. At the start of the test, the helium flow was terminated and the calorimeter boil-off and shield temperatures were monitored. In Figure IV-16 are presented the transient values of the chamber pressure and insulation heat flux. The shape and duration of these transients are very nearly the same as those obtained with Insulation System No. 8.

The temperature gradients in the multi-layer are presented in Figure IV-17 for various times during the transient. These gradients are similar in form to the gradients obtained at steady-state conditions for the various helium leak rates (See Figure IV-10). The rise in the cold boundary temperature indicated in Figure IV-17 is due to the 1/2 inch of foam insulation present on Calorimeter No. 1. At the high heat flux rates a noticeable temperature differential is produced across this insulation resulting in a rise in the temperature of the foam-multi-layer interface.

The temperature gradients in System 9 appear to achieve their equilibrium value in about one hour compared to approximately two hours for System 8. The more rapid response of Insulation System 9 is not confirmed by the return of the heat flux to equilibrium values. Both Systems 8 and 9 require about four hours to reach heat flux equilibrium. This latter result may be, therefore, indicative of the response time of the calorimeter tank and liquid and vent system rather than of the insulation systems. This view is supported by the fact that the starting heat flux values for both Tests III-1P and III-2Q were comparable (7.2 and 7.85 respectively) and shapes of the heat flux curves are very nearly the same.

g. Conclusions

(1) An engineering model was formulated and analyses were prepared for predicting the gas conduction heat flows in a perforated and unperforated multi-layer. A good check was obtained between the predicted and the experimental values for the systems studied. The analysis is expected to be applicable to other similarily conducted insulation systems provided the gas rates, fractional openings and gas accommodation coefficients can be estimated accurately.

(2) Heat flux values of 0.15 and 0.12 Btu/hr ft^2 were estimated for the solid conduction heat flux in the unperforated and perforated systems respectively. These values represent a significant fraction of the total measured fluxes amounting to about 30 per cent in System 8 and about 12 per cent in System 9. The agreement between the two measured values reflects the similarity of the two systems.

(3) Good agreement was obtained between the heat fluxes with the measured values of the tank calorimeter and the K-apparatus.

(4) The accommodation coefficient of helium gas in the two systems studied was estimated to have an average value of 0.65.

(5) The fraction of open area in the shields of Insulation System No. 8, represented by the slits and joints, is estimated to be .0014.

(6) The two systems showed comparable heat flux values (1.10 Btu/hr ft^2) at a helium leak rate of 120 micron-liters per second of helium flow introduced at the underside of the insulation systems. Below this helium leak rate the unperforated system

(System No. 8) produced lower heat fluxes; at greater helium leak rates the perforated system (System No. 9) produced lower heat fluxes. The heat flux with no helium flow was approximately .51 and 1.04 Btu/hr ft for Systems No. 8 and 9 respectively.

(7) The temperature distribution in the shields of System 8 differs significantly from that of System 9 when there is a helium gas flow in the multi-layer.

2. Insulation System No. 10

a. Introduction

As a result of the Arthur D. Little, Inc. tank program conducted under the current and previous contracts with NASA Lewis Research Laboratory, eleven multilayer insulation systems have been tested in simulated space environments and, in some cases, in ground environments. From these studies, an understanding of the insulation application techniques and performance has been developed. While the work in this area continued, it was also recognized that considerable emphasis should be placed on the problems associated with passing stuuctural supports, instrument wiring and piping through the multilayer insulations with minimum weight and heat leak penalties. The fabrication of a pipe penetration in a multilayer was undertaken with the purpose of establishing some experience with physical systems and of achieving a correlation among the theoretical and experimental data.

A number of theoretical concepts valuable for this study were developed in previous NASA contracts and summarized in a final report(3) prepared during the previous Contract NAS3-4181. In an early period of the same contract, an experimental system was fabricated which consisted of a three-inch copper penetration (simplified strong-short physical model) placed through a five-shield multilayer insulation system. The measured heat flow for this penetration obtained in a single series of tests,did not correlate with those predicted from our earlier theory.(3) Subsequently, the insulation system was accidentally destroyed when the test facility became flooded. Thus, no further corroborating tests could be performed which would have produced insight into the different results obtained with the experimental and analytical models.

The situation in which a propellant line on a spacecraft passes through the multilayer insulation on a cryogenic propellant tank has been treated analytically. The results of this work have been published in the aforementioned contract and are presented in Reference 3 and summarized in the following disucssion.

Heat passes through a penetration from the outside to the tank by several paths. These paths are illustrated in Figure IV-18. There is a heat flow by direct radiation from one end of the penetration to the other. For penetrations with large length-to-diameter (L/D) ratios, the value of this flow can be quite small because of the small view factors invovled. A second radiation path involves the interaction of the walls and ends of the tube. The heat flow by this path is dependent only on the emittance of the tube ends and the (L/D) ratio when the walls are nonconducting. For conducting and zero emittance tube walls, the heat flows are independent and, therefore, can be separately determined and summed. For a conducting and nonzero emittance tube, however, the heat flows by the two paths are dependent and cannot be summed because of the nonlinearity of heat flow phenomena.

The radial heat flow into the penetration is moderated by an external multilayer or other insulation. This heat flow will vary along the length of the penetration because: a) the penetration wall temperature increases with distance away from the propellant tank and b) this same gradient will be present in the insulation in certain configurations and will produce conduction in the insulation parallel to the penetration axis. The radial heat can interact with the other heat flow mechanisms unless it is made negligibly small in comparison to them.

The experimental program initiated during the current contract has been designed to explore and confirm the predicted effects indicated above. A six inch diameter by seventeen inch long penetration was fabricated and installed onto the forty-eight inch diameter Arthur D. Little, Inc. tank calorimeter. Provisions were made to alter: a) the temperature of the warm end of the penetration, b) the emittance of the penetration tube and ends, and c) the magnitude and gradient of the radial heat flux. Details of physical model are presented in the following section.

b. Description of Six Inch Pipe Penetration

The penetration simulation was a stainless steel pipe with a .032 inch wall, six inches in diameter and seventeen inches long. This produced a length-to-diameter ratio of 2.84 which is very close to the ratio used for the analysis presented in Reference 3. The pipe was connected into the bottom of Calorimeter No. 2 which contains Insulation System No. 8. At the tank end, the pipe was thermally shorted to the calorimeter tank. A cap (which contained an electrical heater) was attached to the pipe at the free end and was thermally insulated. Dimensions and other details of the pipe penetration are presented in Figure IV-19.

The pipe exterior was insulated with fifty shields of aluminized polyester film and one hundred spacers of Style 104 glass fabric. This system was made up of five insulation blankets each containing ten shields. At the corner where the tank and penetration insulation meet each blanket of ten shields was interleafed with one tank shield using an aluminum two mil foil angle formed into a circle. The angles seal the juncture of the shields of the two systems and thus eliminate direct radiation paths to the tank from the outside. The details of this joint are shown in Figure IV-20.

The large number of shields on the penetration were calculated to achieve a close approach to an adiabatic wall. The surface area of the tube is approximately 2.3 sq. ft. A fifty shield system with inner and outer boundaries at 140 and 540°R respectively would result in a heat flux of about .05 Btu/hr-ft^2. For these boundary conditions, therefore, the total radial heat flow to the penetration wall would be about 0.12 Btu/hour. Generally, however, the inner boundary temperatures (penetration wall) increase with distance away from the tank. For a linear wall gradient of 140 to 540°R the heat flow is about 75 per cent, or the value .09 Btu/hr., for a constant wall temperature of 140°R. Thus the radial heat leak to the penetration for the conditions chosen is about 1 per cent of the penetration heat leak due to wall conduction for the 140 to 540°R wall gradient.

Because of the usually small temperature difference between the warm end of the penetration and the environment (chamber baffles) and the small area of the end (.2 sq. ft.), fewer shields are required at this location. Thus, even for a differential temperature 400°R (140°R inner and 540°R outer) the maximum expected radiation heatflow is of the order of 0.1 Btu/hr.

The warm end of the penetration was sealed at first using aluminum foil. Details of this system are shown in Figure IV-21a. However, as the early tests were run, it became evident that a significant heat flow was passing through the insulation at the cap. This was traced specifically to the micarta ring shown in the figure. Thus, prior to test III-3A7, the cap insulation was altered to conform to the details shown in Figure IV-21b. The main difference between the two methods is that in the former, the insulation at the cap butts to the side insulation. In the latter configuration, the cap insulation overlapped the side insulation.

In a well-designed insulation penetration, the heat leak will be less than a few Btu/hr. It is difficult to measure this level of heat flow in an experimental system such as the tank calorimeter in which the heat flow is of the order of 20 Btu/hr ft^2. To obtain meaningful heat leak data for the penetrations, it is necessary to increase the penetration heat flow and, in some cases, reduce the tank surface heat flow while still maintaining the necessary relation between the experimental and analytical models. The penetration heat flow was increased by providing a heat source at the free end of the penetration so that the temperature at this location could be controlled independently of the chamber baffles and at a high level (up to 850°R). The heat leak to the surface of the calorimeter tank is reduced by operating the chamber baffles with liquid nitrogen. In combination these techniques were able to produce penetration heat leaks that were comparable to tank surface heat leak, and, in some cases, significantly greater than the tank surface heat leak.

c. Test Conditions

The principal test conditions are summarized in Table IV-9. Additional information is provided in the following discussion.

(1) Test III-3A1

This test was performed with warm baffles (nominal 80°F) and zero electric power to the heater at the end cap. Because the entire penetration was insulated, the calorimeter heat flow should have been very nearly the same as that obtained in Test 1A1 before the penetration was introduced into the system. Instead, the end cap stabilized at a value of -158°F indicating a heat flow in the penetration.

(2) Tests III-3A2 and 3A3

In these tests the temperature of the chamber baffles was held at the same level as that used in Test 3A1. All three tests differ in the magnitude of the electrical heating introduced at the penetration end cap. The electrical heat input was increased to 9.05 Btu/hr in Test 3A2 and to 20.2 Btu/hr in Test 3A3. There was an increase in the end cap temperatures to 14°F and 143°F in these tests respectively.

(3) Tests III-3A4 and 3A5

Test 3A4 was performed with the same electrical heat input to penetration as in Test 3A3. In Test 3A4, however, the chamber baffles were cooled to liquid nitrogen temperatures. In Test 3A4, the end cap temperature decreased 23°F compared to Test 3A3 for the same end cap power input. In Test 3A5, the baffles were maintained at liquid nitrogen temperatures and the electrical heat input to the end cap was increased to 51.2 Btu/hour. The end cap reached a new temperature of 285°F.

(4) Test III-3A6

This test was performed with all chamber baffles at liquid nitrogen temperatures and zero electric power to the end cap heater in order to determine the heat flow to the calorimeter tank through its support and other components. Because of the low boil-off rate from the calorimeter and the increasing barometric pressure during the test, the calorimeter vent had to be shut to prevent back flow in the vent lines. The heat leak to the calorimeter was then determined from the rise in the absolute ullage pressure over a period of time. This procedure could be used because the copper wall of the calorimeter acts as an equilibrator to reduce the temperature stratification in the liquid which would otherwise take place.

(5) Tests III-3A7 and III-3A8

Tests 3A7 and 3A8 were performed after the insulation surrounding the warm end of the penetration was modified. The heat flow and temperatures in the penetration measured in previous tests had given us indications that the insulation at the cap was of poor design and permitted a large heat flow to pass through the penetration under certain conditions.

The two insulation methods used with the "A" penetration end cap are shown in Figure IV-21. The original insulation system consisted of five shields of aluminum foil and spacers of 0.1 inch Scott foam. A micarta ring separated the penetration end cap insulations and served to position the insulation. The newer technique utilized aluminized Mylar shields which overlapped the penetration insulation. Spacers formed from Scott foam were used to separate the shields at the flat section of the cap. Style 104 glass fabric was used as a spacer on the cylindrical section of the penetration.

Test III-3A7 is comparable to Test III-3A1 and was performed with warm baffles and zero electrical power to the heater end cap. At thermal equilibrium the end cap achieved a temperature of 220°R.

Test III-3A8 was performed with warm chamber baffles and an electrical heat input to the penetration end cap. The heat input was adjusted during the experiment to a value that produced a cap temperature of 91°F which is very close to the temperature of the chamber baffles (80°F). This test is also comparable to Test III-3A3 which has a slightly higher cap temperature.

d. Experimental Results and Discussion

The heat flows measured in the penetration with the tank calorimeter are presented in column 10 of Table IV-9. These data are also presented in Figure IV-22 as a function of the penetration warm end temperature. The corresponding temperature gradients in the wall of the penetration are shown in Figure IV-23.

In tests 3A1, 2 and 3, the penetration heat flow was determined from the difference between that obtained with and without the penetrations; Test IV-1A2 produced a heat flow of 20.5 Btu/hr and was used as the representative value of the system heat flow without a penetration. In Test 3A4, 5 and 6 the heat flow through the tank insulation was negligible because of the small temperature difference between the tank wall and chamber baffles. Thus, except for a negative correction of 0.5 Btu/hr (tank support heat leak), the penetration heat flow corresponded to the actual measured heat flow. The penetration heat flow for Test 3A7 was calculated from the penetration wall temperature gradient. The power required at the end cap to maintain it at $551^{o}R$ was used as the penetration heat flow for Test 3A8.

Analytical predictions of the penetration heat flow were attempted based on the generalized results presented in Reference 3. However, for all conditions tested except those of Test 3A5, the μ factors (ratio of wall conduction heat flow to the emitted radiation from the warm end) were outside the range of values considered in the analysis[(3)]. In Test 3A5 the experimental value is larger than, the predicted value by 10 per cent.

An expedient approach was taken to determine the relation of the data to maximum-minimum boundary limits. One of the lower limits was represented by the wall conduction in the absence of internal radiation effects. The second lower limit was established for the radiation heat transfer assuming no wall conduction, i.e., analytical condition for $\mu = 0$. Note: This is evaluated from analysis, Reference 3, and is less than total emitted energy. These values are shown in Figure IV-22. It is to be noted that conduction predominates below 550°R and above this value radiation predominates. An upper limit was also established which was taken as the sum of conducted heat flow and the total energy emitted from the warm end which has a surface emittance of 0.9. This is shown on Figure IV-22 as a third curve. All three curves have an asymptote at about 150°R.

As can be seen from Figure IV-22, the majority of the data lie within maximum-minimum limits. The data of Test 3A1 are the most notable exception in that the experimental value is larger than the maximum limits by approximately 50 per cent. A curve (shown dotted) can be passed through the data representing penetration heat flows above 10 Btu/hr. This same curve can be obtained coincidentally by summing the radiation component obtained from the analysis and conduction only heat flows at each temperature level. An alternate to the calorimeter method was used to evaluate the penetration heat flow. Since the temperature gradient in the penetration at the tank end was known from the experimental data the wall conduction flow could be computed. These computed values correlate well with the calorimeter determined heat flows as shown in Figure IV-24. It should be noted that wall conduction should be always smaller than the total because of radiation effects.

It was noted from the data that on occasion there was a greater than 10°F difference between the temperature measured at the end of the penetration (1/4 inch copper plate) and the calorimeter tank. This was probably due to poor thermal contact existing in the area where the two contact each other. The temperature difference appears to be proportional to the heat flow which tends to provide some support for the hypothesis. This correlation is shown in Figure IV-25 where, except for two points, the trend is confirmed.

A further check of the analytical model was obtained from a comparison of the temperature distribution in the penetration wall. The computed temperature distribution for a penetration with L/D of 3.0, wall and end emittance of 1.0 and μ factor of .081 is presented in Figure 6 of Reference 3. These conditions, including the warm end temperature are closely approximated by Test 3A4. The comparison between the two is shown in Figure IV-23. The curves correspond very well except at the cold end of the penetration where the predicted and experimental temperatures are different. Further, the warm end gradients for Tests 3A3 and 3A8 also correspond well with the predicted gradient though the μ factor for these tests is larger by a factor of about 2.5. This would indicate that for values above 0.1, the μ factor has a relatively small influence on the temperature distribution and also on the heat flow in the penetration.

Some additional comments are necessary with regards to the data obtained in Tests 3A7 and 3A8. It is recalled that both of these tests were performed after the insulation at the warm end of the penetration had been modified. In each test, if the predicted penetration and tank insulation heat flows are summed and subtracted from the measured values, a substantial residual remains. In the case of Test 3A7, this residual is 7.3 Btu/hr; for Test 3A8, it is 8.7 Btu/hr. The source of this residual was investigated subsequent to Test 3A8.

After the system was removed from the chamber, it was observed that the penetration insulation had changed its position. This shifting of the insulation may have two principal effects. First, it is possible for the penetration insulation to introduce a compressive load into the tank insulation because its weight, approximately 1.8 lbs, became suspended from the tank insulation. Second, the shifting of the insulation may have caused the special corner joint to become disassembled resulting in the opening of gap (radiation holes) and/or shorting of shields at different levels of the insulation.

The penetration insulation was subsequently given a careful inspection. It was determined that the insulation had moved away from the tank and along the axis of the penetration a distance of from 7/8 to 1 inch. While under test, this insulation was thus suspended from 1/8 x 1/8 inch mesh vinyl coated Fiberglas net. This support system consisted of a side sheet and bottom circle; the top gores of the side sheet were held in place by a drawstring.

The insulation from the six inch penetration was carefully removed and each of the five blankets, each consisting of ten shields and glass fabric spacers, were inspected particularly where they joined the tank multilayer. Blanket No. 5 had slipped from behind the aluminum foil corner joint all along its circumference. Blankets No. 2 and 1 had also slipped away from their aluminum corner joints along distances of two and one half and five inches respectively. In all other cases, the joint of the multilayers were found to be very much like they had been installed. The description of the joint in the instances cited could not be used to account for approximately 8.2 Btu/hr noted above.

Our next approach was to estimate the compressive loads in the tank multilayer that may have been induced by the weight of suspended penetration insulation. Our analysis indicates that the upper and lower knuckle radii of the tank were principal areas where the insulation loading was introduced. The area affected was approximately 10.5 sq. ft. and the estimated loading pressure was .002 psi.

The heat flux under load for the insulation in question was measured in the K-apparatus in Test 3041. The data indicate a flux of .7 Btu/hr ft^2 at a .002 psi loading for a ten shield system. We expect the heat flux to double to a value of 1.4 Btu/hr ft^2 for a five shield system at the same loading pressure. In Test III-1A1 (System 8) we measured an average heat flux of .52 Btu/hr ft^2 for the same insulation system before the penetration was added (making it System No. 10). If this value is subtracted from the adjusted K-apparatus flux, we obtain a value of .9 Btu/hr ft^2 as the possible increase in the insulation flux for the loaded insulation area.

The above results obtained for an area of 10.5 sq ft loaded to approximately .002 psi, producing an added heat flux of .9 Btu/hr ft^2 result in an estimated heat rate of about 9.45 Btu/hr. This value compares with values of 7.3 and 8.7 estimated from the data of Tests III-3A7 and 3A8 respectively. The temperature conditions at the penetration for these latter two tests were radically different. Thus, the heat flows in question are not likely to be as close as they are unless they are the result of occurrences on the tank insulation, away from the penetration, where the conditions for the two tests remain constant. Thus, from the foregoing it is concluded that the unexpected results obtained in these tests is due to the loading of the tank insulation by the weight of the hanging penetration insulation.

e. Conclusions

(1) The experimental techniques used in this investigation were demonstrated to be valid for isolating the penetration heat flows for a wide variety of boundary conditions.

(2) Penetration heat flow and temperature gradients were successfully established in the eight tests performed. The measured heat flow and temperature gradients for one set of conditions are predicted by the analytical model with good accuracy. Generally, however, the conditions selected for the experimental model were not covered by the analysis. The analytical model gives good promise of predicting the heat transfer phenomena occurring within the penetration and should, therefore, be enlarged to cover a larger variety of experimental and practical conditions.

(3) The technique of using angles of aluminum foil to seal the joints formed by the shields of the tank and penetration insulation against radiation leaks appears to be both effective and practical. While the data can only be used to demonstrate this factor indirectly, there are no significant heat flows that could be identified with this part of the insulation system.

f. Recommendations

(1) It is recommended that the experimental and analytical studies on pipe penetrations conducted in the current program be continued. Other penetration conditions must be explored both to confirm the model selected and to obtain engineering information for optimizing penetration designs. The work just completed indicates that the techniques and equipment developed to date can be used successfully to obtain the required information.

(2) It is recommended that a minimum of two additional test series be performed. Each should explore the combined effects of wall conduction, internal radiation, and radial heat flow from the outside. A different insulating method should be used at the outside of the penetration for each case. The walls of the penetration cavity would be lined with aluminum foil to produce a low wall emittance compared to the completed tests.

(3) It is recommended that additional analytical work be performed to provide close support to the experimental program.

3. Insulation System No. 11

a. Introduction

Insulation System No. 11, like previous systems, contains five shields. It was fabricated and tested because of the emphasis placed on the program for the continued development of lightweight-low heat flux systems. A silk netting was used for the spacer in this system which is of considerably lower weight than the glass fabric spacers used in Systems No. 8 and 9 or other previously tested systems. Since the shields for this system and System No. 8 are identical, the test results provide a basis for comparing the thermal performance of the spacer materials.

System No. 11 is also to serve in the transition from aluminized shields used in former systems to the higher performance shields having silver and gold coatings to be used in subsequent systems. Silk and combinations of silk and foam were used in the remaining systems developed in the program. This approach is in accord with that taken throughout the program of introducing one major variable change per insulation system.

b. System Description

(1) Shields

The five shields of this system are 1/4 mil polyester film metallized on both sides with aluminum. This material was produced by the National Research Corporation and is from the same rolls from which Systems 8 and 9 were produced. Some typical coating thickness and emittance measurements taken on samples of the material gave the results tabulated below.

The following data give an average emittance value of .025 at an average thickness of 396 Angstroms. Further, the adherence of the aluminum coatings to the polyester film was excellent. All tests made on the material in the as received condition showed no coating lift-off when the scotch tape test was made at various locations adjacent to material use for the shields.

Emittance Test No.	Coating Thickness (°A)	Emittance
284	430	.0236
285	450	.0273
288	445	.0227
300	346	.0251
301	455	.0226
307	380	.0266
312	310	.0250
314	350	.0311
320	430	.0240
322	307	.0264
323	455	.0255
391	376	.0316
414	376	.0250
452	435	.0229

(2) Spacers

Each spacer consisted of two layers of silk netting. At a weight of .0012 lbs/ft per layer, it is the lightest fabric identified in the study. This weight is also two-thirds the value of 1/4 mil polyester film and, therefore, has the potential of producing one of the lightest multi-layer insulations possible.

The expansion coefficient of silk is not accurately known. Attempts to measure the coefficient early in the current program with an inexpensive extensometer were not successful. The experience with System No. 6 (during the preceeding program) in which nylon net was used as a spacer, indicated that allowance should be made to avoid insulation loading induced by the thermal contraction of the netting. Thus two layers of silk netting were used in the system so that expansion slits could be placed in the spacer side sheets. The slits are placed two feet apart in each layer at alternate locations to prevent shield shorting.

A second purpose for the two layers of silk per spacer results from data obtained with the flat plate thermal conductivity apparatus which indicates that, for a given spacer, increasing the number of layers decreases the heat flux under load.

(3) Application

The shields and spacers of System No. 11 were applied in the same manner as those of Systems 8 and 9. The top and bottom sections were made up of circles of shields and spacers. The spacer side sheet was not slit or gored but was instead provided with a hem at top and bottom through which a purse string was provided. The purse string held both the side sheet and ends in place. This construction is shown in Figures IV-26 and IV-27.

At the calorimeter tank vent support, the insulation was extended under the cold guard shield to within 3/4 inches of the vent line. This approach was used because the application and centering of the top sections of the insulation was accomplished more easily. The space between the end of the shield and the vent was buffered with 1/16 inch thickness of Scott foam. The opening between the neck shield and top of tank was approximately 1/2 inch. The details of this construction are shown in Figure IV-28.

Additional detail information concerning the insulation system is presented in Table IV-11.

c. Test Conditions

A total of three tests were performed with the system all of which were at the standard test conditions. Tests III-4a and 4c were identical. Test III-4b differed from the others in that no liquid nitrogen flow was provided in the cold guard contrary to the usual procedures. The altered procedure was used to establish the magnitude calorimeter neck heat flow in the absence of any refrigeration.

d. Experimental Results and Discussion

In Tests III-4a and 4c encompassing 96 hours a heat flux of 0.48 Btu/hour was obtained. Based upon a shield emittance of 0.025 the system radiation flux has a calculated value of 0.36 at the stated boundary conditions. The conduction flux, representing the difference between the measured and radiation values, is estimated at 0.12 Btu/hr ft^2. Negligible gas conduction heat flux is expected because of the low chamber pressures (below 10^{-6}mm Hg). The system $k\rho$ product has a value of .00331 as established from the measured flux and unit weight of the insulation.

The configuration of the insulation at the calorimeter support may have increased the calorimeter heat flow as compared to the condition where the edge of the insulation is guarded by the cold guard shield. If the buffer zone effect of the foam at the shield edges is neglected, the flow of heat from the edges to the tank is estimated to be less than 10 per cent of the total calorimeter heat flow. Thus, a lower conduction flux would be predicted for the system than previously indicated. Based on the heat transfer results obtained in Tests III-4a and 4c, the performance of System No. 11 is negligibly better than that of System 8 (Tests III-1A, 1G and 1N). However, as its unit weight is less than half that of System 8 (.023 compared to .059 lbs/ft^2) the $k\rho$ performance is improved by a factor of almost 2.8. On this basis System 11 is superior to System 8 and all previous systems tested in the tank program.

The temperature distribution in the multi-layer is conventional and corresponds fairly well with the theoretical values. However, there is a noticeable temperature gradient in the shields; the temperatures in the shields at the top of the tank are lower than those at the side and bottom of the tank. This gradient is believed to be produced by the discontinuity in the insulation at the vent. This effect has been observed in other systems tested on the calorimeter, but is not considered a serious effect.

In Test III-4b the total heat flow to the calorimeter was 45.3 Btu/hr. Thus the non-refrigerated neck was adding 26 Btu/hr to the calorimeter in comparison to the 19.3 Btu/hr passing through the insulation. The approximately 135 per cent increase in the insulation heat flow represents maximum error that can be associated with measured heat flux established in Tests III-4a and 4c.

4. Insulation System No. 12

a. Introduction

Insulation System No. 12 is identical to System No. 11 in all respects except that the aluminum coated shields have been replaced with silver coated ones. The new shields have the lowest surface emittance of any tested previously in the tank program. It is the objective of this test series, therefore, to compare the system performance of the improved shields with those using aluminum surfaces.

b. System Description

Insulation System No. 12 consists of five shields and six spacers. The shields are 1/2 mil polyester film metallized on both sides with silver. The spacers are made up of two layers of silk netting.

(1) Shields

The material for the shields was purchased from Gomar Manufacturing Company. The coating thickness and emittance measurements taken on samples of similarily coated materials produced the following results:

Coating Source	Sample No.	Coating Material	Coating Thk °A	Emittance Test No.	Emittance
Gomar	337A	Silver	1680	467	.0109
Gomar	337B	Silver	1650	468	.0103
Schjeldahl	327A	Silver	1150	457	.0104
Schjeldahl	327B	Silver	1050	458	.0102
ADL	20-1	Silver	953	364	.012
ADL	20-2	Silver	1230	365	.013
ADL	25-1	Silver	1210	337	.011
ADL	27-1	Silver	2325	335	.011

The emittance values obtained with the Gomar material are comparable to those obtained with silver coatings produced at Arthur D. Little, Inc. and by the G. T. Schjeldahl Company.

Approximately twenty thickness measurements were made on each side of the material used for the shields. The coating on one side of the roll surface showed thicknesses that were generally in the range of 1000 to 1300 Angstroms; a low value of 595°A and a high value of 1600°A were also measured on the same side. The thickness of the outside roll surface was generally in the range of 1700 to 2200 Angstroms. A low reading of 1530°A and a high reading of 2520°A were also measured on the same side.

The adherence of the silver coating to the 1/2 mil polyester film was generally very poor. In the scotch tape test, approximately 80 to 100 per cent of the coating was lifted away from the film at all locations tested on the outside surface of the roll and half the inside surface. One half of the inside surface showed no coating lift-off when the scotch tape test was made at various locations.

Although the adhesion of the silver coating to the film was very poor and unsatisfactory for general use in MLI, the material was used in System 12 because the thermal performance of the shields could be demonstrated without their becoming mechanically degraded during the tests. The sample materials produced by Schjeldahl and Gomar, indicate that the required adhesion can be achieved in commercial practice though it was not achieved in the materials used in System No. 12.

As previously indicated, polyester film 1/2 mil in thickness was used as the carrier for the silver coatings. This was adopted as an expedient in terms of time and cost of producing the coatings. There is every indication that the same coatings can be produced on 1/4 mil film when it is required.

To limit the degradation of the emittance of the silver coatings, the shields were applied to the tank in the period of one week after receipt of the material. During this time the completed portion of the system on the calorimeter was purged with vaporized liquid nitrogen to further retard the tendency for the coatings to tarnish in the shop environment. After completion of the fabrication, the system was placed immediately into the space simulation chamber.

(2) Spacers

The silk netting spacers used in System No. 12 were those used previously in System No. 11. The shields and spacers were applied in a manner identical to those of System 11. For further information and details see Table IV-13. The completed system is shown in Figure IV-29.

c. Test Conditions

Test III-5A was performed with the insulation system under the standard conditions. The calorimeter utilized liquid nitrogen in the tank and cold guard. The chamber baffles were maintained at near 80°F by use of the temperature controlled water recirculation system. A vacuum of 2×10^{-6} mm Hg was achieved in the chamber.

Tests III-5b and 5C were performed with environmental pressures at 2.5×10^{-4} and 1×10^{-3} mm Hg respectively. This condition was established by bleeding helium gas at a constant rate through a capillary into the chamber. The increased gas load on the vacuum pumping system resulted in its operation at a higher inlet pressure. The helium was admitted directly into the chamber in Test III-5B and into the inlet of the pumping system in Test III-5C. In this manner there was no gas flow through the multi-layer insulation as had been the case in the III-1 and III-2 test series (performed with the unperforated and perforated insulation systems respectively).

d. Experimental Results and Discussion

A chamber pressure of 2×10^{-6} was achieved during the performance of Test III-5A. This pressure level is well below that at which heat transfer in the multi-layer by molecular conduction becomes significant. Then the remaining modes of heat transfer in the multi-layer are by radiation and solid conduction. The experimental flux as determined by Test III-5A is representative of the heat transfer in these two modes.

The experimental conditions and results are summarized in Table IV-14. The heat flow measured in ~3 hours of test was .306 Btu/hr ft^2. This resulted in a system $\kappa\rho$ product of .000300 x Btu-in-lb/hr ft^{5}°F. The flux compares with .48 Btu/hr ft^2

obtained with System No. 11 in 96 hours of test. The low emittance shields resulted in a .18 Btu/hr ft^2 improvement in the heat flux.

A further comparison can be made from the computed values of the radiation flux. The shields used in System No. 11 have been yielding emittance of about .025. As indicated previously, the measured emittance of the silver shields is about .011. The computed radiation flux for each system and the resulting solid conduction flux, which are obtained from the measured and computed radiation fluxes, is presented in the table below.

Insulation System	Average Shield Emittance	Measured Flux (Btu/hr ft^2)	Calculated Radiation Flux (Btu/hr ft^2)	Solid Conduction Flux (Btu/hr ft^2)
11	.025	.48	.36	.12
12	.011	.31	.16	.15

In System No. 11, the solid conduction is estimated to be .12 Btu/hr ft^2. This is comparable to the value (.15 Btu/hr ft^2) determined for System No. 12. The two conduction fluxes are expected to be very nearly the same because the systems were identical in all respects except for the shields.

The improved shields have reduced the radiation flux very nearly to the estimated value of the conduction flux. It appears, therefore, the thermal performance of the insulation can be improved further by reducing the solid conduction flux through the use of improved spacers.

The distribution of temperature in the multi-layer at the cylindrical section of the tank is shown in Figure IV-30. The theoretical distribution using the measured shield emittance is presented for comparison. There is good agreement between the two temperature distributions.

Tests III-5B and III-5C were performed to test the validity of the relations used to predict the performance of a multi-layer when an interstitial gas is present. The engineering relations were presented in Section D-1-c of Part IV of this report. The results of the computation are presented in Table IV-15. The principal element in the computation is the gas conduction heat flux which was established from the level of helium pressure obtained in the chamber during each test. Further the computation considers the effect of the accommodation coefficient for helium. The functional dependence of the heat flux on the accomodation coefficient was established from the data obtained in Systems No. 8 and 9.

Since the boundary temperatures in all three tests were very nearly the same, the radiation and solid conduction fluxes are assumed to remain unchanged in the three tests. The total computed flux is the sum of the radiation, solid conduction, and gas conduction fluxes. In Table IV-15 these are compared to the experimental fluxes. The results show a deviation of -6.7 and +7.8 per cent for tests III-5B and III-5C when the computed values are compared to the experimental values.

The distribution of the temperature in the multi-layer at the cylindrical section of the tank for each of the three tests are shown in Figure IV-30. The effect of increasing chamber pressure is readily apparent in the trend toward a linear distribution of temperatures. The theoretical distribution of temperatures based on the measured shield emittance and low gas pressure is also shown in the figure.

5. Insulation System No. 13

a. Introduction

During the course of this program a spacer was developed having low weight and excellent thermal properties. This spacer consists of strips of foam attached in a regular pattern to a single layer of silk netting. Based on studies reported in Part II, the insulation heat flux is only moderately affected by pressure loadings in the range of zero to 0.1 psi compared to most other insulations. Thus, the properties of this composite material are very attractive. The spacer was, therefore, fabricated into a tank system (System No. 13) for further study.

b. System Description

Insulation System No. 13 consists of five shields and six spacers. The shields are 1/2 mil polyester film metallized on both sides with silver. The spacers are a composite of a layer of silk netting and foam strips that are bonded to the silk. The system has a unit weight of .038 lbs/ft^2 and a theoretical thickness of 0.33 inches (sum of thickness of all materials).

(1) Shields

The material for the shields was purchased from Gomar Manufacturing Company and is from the same production roll from which the shields for System No. 12 were produced. Thus, the previous discussion pertaining to the shields of System No. 12 is also applicable.

Additional emittance measurements were made on the silver coated 1/2 mil polyester film. Samples were taken on the roll at center width both preceding and following the material used for the shields on System No. 13. These data are summarized below in Table IV-16 and include the data obtained on roll from System No. 12.

The material used in the shields of System No. 13 appear to have a higher average emittance than would be expected from previous information. This emittance degradation may be due to the aging of silver and/or from the wrinkling present in the inner portions of the roll induced quite probably during the rewind process in the coating operation. From previous data, we also recognize that aging does occur. No surface deterioration of the coating could be observed under visual magnification. Therefore, for the current work, it is assumed that the surfaces have an average emittance of .017.

(2) Spacers

The spacers for this system are a composite of silk netting and foam strips. In the unloaded condition the shields become spaced approximately 0.1 inches. This large thickness causes the low load performance of the MLI to be much improved over other systems.

The first component of the spacer system was made up of silk netting manufactured by Heathcoat Ltd. of England which is the same as that used on Systems No. 11 and 12. The material is identified as Jordan Marsh Company 5517 bridal veil. It has an average thickness of .0035 inches and a weight .0012 lbs/ft^2. A single layer is used as the carrier for the foam.

The second component of the spacer is a Scott flexible foam having an average 2 lb/ft^3 density and sixty pores per inch. The foam was cut into sheets 1/16 inch thick and then die cut to 1/4 x 2-1/4 inch strips. These strips were then attached to the silk netting in the pattern shown in full scale in Figure IV-31 (1/4 mil polyester film heated to the melting point was used for the attachment of the center of the foam strip to the silk). The foam covers 25 per cent of silk area and adds .0025 lbs/ft^2 to the weight of the silk making a total spacer weight .0037 lbs/ft^2.

The foam pattern was developed to provide a low insulation weight and a 5 to 10 per cent support area that is practically independent of the relative orientation among spacers. If all the foam strips in each spacer were perfectly aligned one over the other, the maximum support area would be 25 per cent. Or, if any two adjacent layers are completely aligned such that the foam stirps do not overlay one another, the minimum support area would be zero per cent. However, with the pattern selected the chances of complete alignment of the pattern is quite small. The reason for this is that very small rotations and translations of one spacer relative to another tends to produce general misalignment of the spacers which in turn produces support through the foam amounting to 5 to 10 per cent of the total netting area. Figure IV-32 shows five layers of foam in a random stacking.

(3) Application

Each shield layer was made of three segments consisting of two ends and a side sheet. The ends were circles approximately 42 inches in diameter. The side sheet was formed from 2 feet wide material wrapped around the cylindrical section of the tank. The upper and lower edges of the side sheet were slit every 3-1/2 inches for a distance of 7 inches from the edges. These slit segments were made to conform over the knuckle radii of the tank and were lapped under the end circles.

The spacer layers were also made up of three segments consisting of two ends and a side sheet. The ends were circles of material about thirty-eight inches in diameter. The side sheet was formed from from two foot wide material wrapped around the cylindrical section of the tank as shown in Figure IV-33. Three inch wide gores were cut into the edges of the side sheet for a distance of 6-1/2 inches. These were made to conform to the knuckle radii and were butted and sewn to the end circles. See Figure IV-35 for spacer application to tank.

Additional spacer, shield and system data and information are presented in Table IV-17.

(4) Neck Detail

The insulation configuration at the calorimeter support was different for each of the two tests performed with the system. The details are shown in Figure IV-34. Prior to Test III-6A, the insulation was fluffed out to a thickness of almost one inch. During the performance of Test III-6A, the insulation had settled about 1/2 inch and opened a circular gap about 1/2 inch wide between the neck shield and outer shield of the insulation. Calculations indicated that a significant amount of radiation energy could pass through this opening and that the neck insulation should be modified.

The modified neck configuration was made to correspond to that used with the earlier insulation systems. The insulation and spacers were cut away from the neck area on a 9-1/8 inch diameter circle. The neck shield was extended to within 1/8 inch of the tank surface so as to completely guard the edges of the insulation. A copper angle was bolted to the neck shield to block any 300°K radiation that might enter the insulation system through the space between the neck shield and edge of the tank insulation.

c. Test Conditions

Two tests were performed with this system. In each the test condition corresponded to those of the standard environment, i.e., liquid nitrogen in the tank, less than 10^{-5} mm Hg vacuum and 80°F chamber baffles. As noted above the neck detail used in both tests were different.

d. Results and Discussion

A chamber pressure less than 2×10^{-6} mm Hg was achieved during the performance of all tests. This pressure level is well below that at which heat transfer in the multi-layer by molecular conduction becomes significant. Thus, the remaining dominant modes of heat in the multi-layer are by radiation and solid conduction.

The experimental results and conditions for the III-6 test series are summarized in Table IV-18. As indicated the heat flux measured in eighty hours of test was .41 Btu/hr ft^2 for Test III-6A. System No. 12 gave a result of .31 Btu/hr ft^2 for the identical conditions and the identical system, except for the spacers. However, System No. 13 was expected to produce a comparable or lower heat flux than System No. 12. Since the neck shield was shortened by about 1/2 inch in System No. 13 compared to System No. 12, it was the most likely cause of the high flux. Thus, the neck configuration was modified as was discussed previously.

The neck modification resulted in a significant improvement of the heat flux. Values of 0.33 and 0.34 Btu/hr ft^2 were measured in Tests III-6B1 and 6B2 respectively. Based upon these values and a unit weight of .0377 lbs/ft^2 the $\kappa\rho$ product has a value of .000377 Btu-in-lb/hr-ft^5-°F.

The computed radiation flux of the system has a value of .248 Btu/hr ft^2 using 0.017 for shield emittance and temperature boundaries corresponding to the experimental conditions. The difference of this flux and the experimental flux corresponds to the solid conduction flux of the system which has a value of 0.08 Btu/hr ft^2.

It is interesting to compare Systems 12 and 13 which have the same shields but different spacers. First, the solid conduction flux of the former is almost twice that of the latter and the composite spacer has, therefore, produced a significant improvement. This is balanced by the effect of shield deterioration which occured in going from System 12 to System 13. The net result is that under the conditions tested and based on the $\kappa\rho$ product, System 12 is the superior of the two. Furtner, System 13 is more difficult to fabricate. However, if the shields of System 13 had an emittance of 0.011, as in System 12, then the $\kappa\rho$ performance of System 13 would have a value of about .000276 units Btu-in-lb/hr ft^5-°F making it the superior of the two systems. In addition, System 13 has a better load handling ability than System 12, which may be of considerable worth in some space systems.

Two samples of System 13 were tested in the K-apparatus. One system (Test 3075) had five shields and the other (Test 3076) had ten shields. The results obtained with these are 0.28 and 0.34 Btu/hr ft^2 respectively as adjusted to standard conditions. These compare quite well with the value of 0.33 Btu/hr ft^2 obtained with System 13 and the value of 0.25 Btu/hr ft^2 computed for the radiation flux alone. The system heat flux as a function of loading pressure is discussed in Part II of this report. See Table IV-19 for comparison.

The temperature distribution in the shields of the multi-layer are shown in Figure IV-36 for Tests III-6A and 6B. The shield temperatures measured during Test 6A at the "a" location are considerably depressed compared to the measurements made at the other locations and to the theoretical distribution. This is seen to be the result of neck configuration (see Figure IV-34a). Additional temperature measurements were made after the neck configuration was modified (see Figure 34b). During the change over a number of thermocouple leads were cut leaving only five intact. The temperatures at the "b" and "c" location appear not to have changed while the 5a location temperature was increased about 30°F. This increase is an indication that all other "a" temperatures also increased.

e. Conclusions

(1) Of the twelve systems evaluated in the tank program over a three-year period, System 13 is one of the four best systems for heat flux and $\kappa\rho$ product with even greater promise for a superior system had the silver coating not degraded.

(2) The emittance of the silver coated shields used in System 13 was significantly greater than the emittance of the same shields used in System 12 though considerable care was taken to keep the shields protected from noxious atmospheres.

(3) The silk-foam spacer used in System 13 is very effective in reducing the solid conduction component of heat flux in the zero load condition. The combination spacer also represents a feasible construction method.

6. Insulation System No. 14

a. Introduction

System No. 14 was the last system to be evaluated in the tank program. It consisted of gold coated polyester film and silk netting spacers. From studies conducted on both of these components, there were indications that a low $\kappa\rho$ product system could be fabricated. From the work accomplished under the Emissometer Program (Part III of this report), it was established that emittance values of about .017 could be obtained with gold coatings (greater than 1500 Angstrom thickness). This represented an improvement of 25 per cent compared to the emittance of aluminum coatings. Further, a source was found for the commercial production of these coatings in roll form which were of excellent quality.

The spacer component of the system had been evaluated both in the K-apparatus and in the tank program. In the former its heat flux-loading performance was evaluated in Tests 3042, 3071 and 3077 (see Part II) and found to be comparable to the test which included foam and silk-foam spacers. In the tank program the techniques of application developed in the fabrication of Systems 11, 12 and 13 indicated that thermal contraction effects of the spacer could be controlled and high heat leaks resulting from temperature induced loading pressures could be eliminated.

Thus, the fabrication of System 14 was the logical result of the prior development efforts conducted in the K-apparatus, Emissometer, and tank programs.

b. System Description

Insulation System No. 14 consists of five shields and six spacers. The shields are 1/4 mil polyester film metallized on both sides with gold. The spacers are made up of three layers of silk netting. The system has a unit weight of 0.028 lbs/ft^2 and a theoretical thickness of 0.057 inches (sum of the thicknesses of all materials). The system is shown in Figure IV-37.

(1) Shields

The shields were made up from materials obtained from the Hastings & Company, Inc. of Philadelphia in three different lots. Shields No. 1 and 2 were made up from 100 ft^2 of purchased sample material with approximately 2000 Angstroms gold coatings and an average emittance of .0160. Shields 3, 4 and part of shield 5 were made up from a second purchase of 180 ft^2 of production material having a coating thickness of 2000 to 3000 Angstroms and an average emittance of 0.0175. A small portion of shield 5 was made up from a 50 ft^2 sample coated with 23K gold instead of 24K gold used in the others. The 23K coatings had an inferior emittance but represented about 2 per cent of the total shield area. The average emittance for all shields was 0.0172. The shield emittance data is summarized in Table IV-20.

The gold coatings were of excellent quality. All samples showed no coating lift-off with the scotch tape test. The coatings also showed a high brilliance indicative of small grain structure. Tests of gold coatings in various environments (See Part III) indicated that they also have a stable emittance value.

(2) Spacer

For information concerning the silk netting spacers, refer to previous discussions and to System 14 Specification, Table IV-21.

(3) Application

The shields were made up and applied in the same manner as the shields of the other systems discussed previously.

The spacers were made up of the usual three segments. The ends were circles of material about 38 inches diameter; the side sheets were formed from 2 feet wide material. Three inch wide gores were cut into the edge of the side sheet for conforming the spacer over the knuckle radii. All joints were butted. Each layer of each spacer was applied spearately and the edges of the three segments were stitched together to hold the spacers and shields in place. All gores and slits in the side sheets of alternate layers were staggered to cover all openings.

c. Experimental Results and Discussion

One test of 96 hours duration was performed with the system at the standard environmental condition. The vacuum in the space simulation chamber averaged 2×10^{-6} mm Hg making any gas conduction heat transfer effect negligible in comparison to the radiation and solid conduction heat transfer.

The experimental results and conditions for Test III-7 are summarized in Table IV-22. The measured heat flux was 0.325 Btu/hr ft^2. Based upon the average shield emittance (.0172) of the system, a value of 0.25 Btu/hr ft^2 was computed for the radiation flux. Combining this with the measured value of the heat flux results in a solid conduction flux value of 0.075 Btu/hr ft^2. The $\kappa\rho$ product of the system is .000273 and represents the lowest value of any system evaluated in the tank program.

Systems 13 and 14 have the same thermal performance and also the same proportions of radiation and solid conduction heat fluxes. However, because of its smaller unit weight, the $\kappa\rho$ product of System 14 is almost 40 per cent less than that of System 13. Based upon the results obtained in the tank program, System 14 appears the superior of the two systems at the zero pressure load condition.

A heat flux of 0.315 Btu/hr ft^2 was measured on a sample of System 14 in the K-apparatus. The temperatures of the cold and warm boundaries were -320°F and 70°F respectively. The adjusted heat flux, therefore, has a value of 0.34 Btu/hr ft^2 which is within 3 per cent of tank measured value.

The temperature distribution in the shields of the multi-layer are shown in Figure IV-38. The side sheet temperatures coincide almost identically with the theoretical distribution. The temperatures in the bottom head were measured 8 inches off center and shield temperatures are distributed at higher levels than at the side of the tank. The opposite effect takes place for the top shields where the temperature is measured 12 inches off center. As indicated previously, this trend is characteristic of the temperatures measured on most of the other systems.

The significant differences between the upper and lower heads are: a) the calorimeter vent support passes through the top located insulation only and b) the side and bottom segments of the insulation are supported from the top layer which may result in an induced pressure in this upper segment. The difference in the distribution may be caused by one or both of the construction differences. As indicated in the discussions of System 8 and 9, conduction effects, whatever their nature (solid or gas conduction), tend to linearize the temperature distributions. Also, the top shield temperature may be lower because of the edge guarding accomplished by the neck shield. The combination of edge guard and pressure loading is seen to be the cause for the lower temperature in the top head.

d. Conclusions

(1) System No. 14 has the lowest $\kappa\rho$ product of any insulation testsd in the tank program. It is made up of shields consisting of gold coatings that have low stable emittances. The spacer is lightweight and would be capable of supporting the insulation in an acceleration environment. We consider System 14 to be superior to all other systems tested.

TABLE IV-1

INSULATION SYSTEMS AND VARIABLES INVESTIGATION

Insulation System No.	Principal Independent Variables Investigated
8	a) Glass fabric spacers
	b) Helium gas flow in multi-layer
9	a) Glass fabric spacers
	b) Perforated shields
	c) Helium gas flow in multi-layer
10	a) Penetration warm end temperature
	b) Penetration radiation environment
11	a) Silk netting spacer
	b) Aluminum coated polyester film
12	a) Silk netting spacer
	b) Silver coated polyester film
13	a) Combination silk-foam spacer
	b) Silver coated polyester film
14	a) Silk netting spacer
	b) Gold coated polyester film

TABLE IV-2

TANK PROGRAM - MULTI-LAYER INSULATION PERFORMANCE SUMMARY

Insulation System Description						Test Data						
System[1][2] No.	Shield Materials	Spacer Materials	Application Method	Other	System Weight[3] (lbs/ft^2)	Test No.	Ave. Vac. (mm Hg)	Measured Heat Flux ($Btu/hr\ ft^2$)	Ave. Baffle Temp. (°F)	Adjusted Heat Flux[5] ($Btu/hr\ ft^2$)	Kρ Product ($Btu\text{-}in\text{-}lb/hr\ ft^5\ °R$)[6]
1	Aluminum foil 2 mil	Screen, vinyl coated Fiberglas 1/8 x 1/8 in. mesh, 1 layer per spacer	Ends: pressure formed shields and formed spacers; Sides: gored shields and spacers	—	.236	I-3D2, 3[4] I-7	0.4×10^{-6} 1.0×10^{-6}	0.66 0.44	79 40	0.66 0.61	.00467 .00345
2	1/4 mil polyester film aluminized one side	Screen, vinyl coated Fiberglas 1/8 x 1/8 in. mesh, 1 layer per spacer	Ends: slitted shield circles formed spacer; Sides: gored shields and spacers	—	.104	I-4A, B, C, D	4.0×10^{-6}	0.80	48	1.02	.00266
4	Aluminum foil, 1/2 mil	Screen, vinyl coated Fiberglas, 1/8 x 1/8 in. mesh, 1 layer per spacer	Ends: pressure formed shields and formed spacers. Sides: gored shields and spacers	—	.131	II-1A	0.7×10^{-6}	0.37	48	0.47	.00158
5	1/4 mil polyester film aluminized two sides	Screen, vinyl coated Fiberglas, 1/8 x 1/8 in. mesh, 1 layer per spacer	Ends slit shield circles and formed spacers; Sides: gored shields and spacers	Urethane foam substrate, 1/2 in. thick, foamed in place, outer vapor barrier	.104	II-9A	1.3×10^{-6}	0.71	68	0.78	.00228
6	1/4 mil polyester film aluminized two sides	Nylon netting, 1 layer per spacer	Ends: slit shield and spacer circles; Sides gored shields and spacers	—	.025	II-7	1.2×10^{-6}	1.04	74	1.11	.00072
7	1/4 mil polyester film aluminized two sides	Nylon netting, 1 layer per spacer	Outer five layers formed into blanket; Ends, slit circles; Sides: gored	System made up of System No. 5 with 5 layer blanket type system added	.047	II-8	0.7×10^{-6}	0.78	73	0.83	.00110
8	1/4 mil polyester film aluminized two sides	Glass fabric, Style 104 2 layers per spacer	Ends, circles for both shields and spacers; Side, slit shields, purse string spacers	—	.059	III-1A	1.3×10^{-6}	0.52	81	0.53	.000920
9	1/4 mil polyester film aluminized two sides perforated 1.88%	Glass fabric, Style 104 2 layers per spacer	Ends, circles for both shields and spacers; Side: slit shields, purse string spacers	Urethane foam substrate Same as System No. 5	.059	III-2A	3.0×10^{-5}	1.06	83	1.04	.00186
11	1/4 mil polyester film aluminized two sides	Silk netting, 2 layers per spacer	Ends: circles used for both shields and spacers; Sides slit shields, purse string spacers	Urethane foam substrate Same as System No. 5	.023	III-4A, C	2.0×10^{-6}	0.48	80	0.48	.000331
12	1/2 mil polyester film silver coated two sides	Silk netting, 2 layers per spacer	Ends: circles used for both shields and spacers; Sides: slit shields, purse string spacers	Urethane foam substrate Same as System No. 5	.032	III-5A	2.0×10^{-6}	0.31	79	0.31	.000300
13	1/2 mil polyester film silver coated two sides	Silk netting, 1 layer combined with Scott foam strips except outer spacer 1 layer silk only	Ends: circles used for both shields and spacers; Sides: slit shields, gored spacers	Urethane foam substrate Same as System No. 5	.038	III-6B	2.0×10^{-6}	0.33	80	0.33	.000377
14	1/4 mil polyester film gold coated two sides	Silk netting, 3 layers per spacer except outer spacer is 1 layer	Ends: circles used for both shields and spacers; Sides: slit shields, gored spacers	—	.028	III-7	2.0×10^{-6}	0.33	80	0.33	.000273

Notes:
1. All systems contain 5 radiation shields except for System No. 7 which contain 10 shields.
2. Insulation surface area is approximately 40 square feet.
3. Insulation weight given is for multilayer only and does not include foam present on Systems 5, 9, 11, 12, and 13.
4. Test performed with liquid hydrogen in calorimeter, all others performed with liquid nitrogen.
5. Measured heat flux adjusted for warm boundary temperature of 80°F.
6. Kρ product is based on measured value of heat flux.

TABLE IV-3

INSULATION SYSTEMS NO. 8 & 9 - SPECIFICATION

Description:	The system consists of five shields of polyester film, aluminized on both sides, and six spacers, each consisting of two layers of glass fabric.	
Shield:		
Material:	DuPont, Type S, polyester film, coated on both sides with vapor deposited aluminum to a nominal thickness of 375 Angstroms.	
Thickness:	.00025 inches	
Weight:	.0018 lbs/ft^2	
Emissivity:	.025	
Side Geometry:	Ungored; purse string top and bottom	
Head Geometry:	Slit circles	
Joint Design:	All seams overlapped	
Perforations:		
System No. 8:	None	
System No. 9:	1.88 per cent of shield surface	
Spacer:		
Material	Two layers of taffeta glass fabric, Style 104, heat cleaned	
Thickness:	.0050 inches (measured value)	
Weight:	.008 lbs/ft^2	
Density:	16.0 lbs/ft^3	
Filament Diameter:	.00021 inches (51 filaments in fill, 102 in warp)	
Open Area:	50 per cent (approximately)	
Side Geometry:	Ungored; two layers of glass fabric to be attached to each shield	
Head Geometry:	Circles; two layers of glass fabric, top circle slit along one radii.	
Joint Type:	Overlapped	
Boundary Emissivity:	System 8	System 9
Calorimeter Tank:	.86 at -320°F	Approx. .35 at -310°F
Chamber Baffles:	.93 at 80°F	.93 at 80°F
System Properties:		
Surface Area:	39.5 ft^2(System No. 8); 39.8 ft^2(System No. 9)	
Weight:	.059 lbs/ft^2	
Thickness:	.0313 inches	
Weight Density:	22 lbs/ft^3	
Shield Density:	190 shields per inch (unity stacking factor)	
Figure of Merit: (wt. basis)	2.7	

TABLE IV--4

TANK INSULATION PROGRAM

Insulation System No. 8, Test Series III-1 Data Summary, Calorimeter No. 2

Insulation System:	Five radiation shields of polyester film aluminized on both sides and six spacers each consisting of two layers of Style 104 glass fabric.
Test Facility:	ADL/Cambridge test facility
Penetrations or Gaps:	None
Boundary Conditions:	Warm boundary: nominal 80°F, .93 surface emittance. Cold Boundary: -320°F, .86 surface emittance
Tank Surface Area:	39.5 ft^2 based on outer surface of calorimeter tank.

Test No.	Tank Liquid	Data Period Date&Time	to Date&Time	Test Time (hrs)	Ave. Vac. (mm Hg)	Guard Liq/Temp (°F)	Helium(1) Leak Rate $\left(\frac{\mu\text{-}\ell}{sec.}\right)$	Total Heat Flow $\left(\frac{Btu}{hr}\right)$	Measured Heat Flux $\left(\frac{Btu}{hr\ ft^2}\right)$	Ave. Skin Temp (°F)	Adjusted Heat Flux $\left(\frac{Btu}{hr\ ft^2}\right)$
III-1A1	LN_2	7/23/0830	7/26/0830	72	1.2×10^{-6}	-312	0	20.6	.522	81	.518
III-1A2	LN_2	7/26/0830	7/27/0830	24	1.3×10^{-6}	-312	0	20.5	.519	82	.512
III-1B	LN_2	7/28/1200	7/29/0830	20.5	1.1×10^{-5}	-312	4.5	22.8	.577	82	-
III-1C	LN_2	7/29/1200	7/30/0830	20.5	3.0×10^{-5}	-312	31	29.0	.735	81	-
III-1D	LN_2	7/30/1230	7/31/0830	20.0	6.5×10^{-5}	-312	63	39.4	.995	82	-
III-1E	LN_2	7/31/2030	8/2/0830	36.0	1.5×10^{-4}	-312	116	47.4	1.20	82	-
III-1F	LN_2	8/4/2100	8/5/0830	11.5	6.0×10^{-4}	-312	168	78.[illegible]	1.98	80	-
III-1G	LN_2	8/5/1630	8/6/1030	18.0	4.0×10^{-6}	-312	0	19.4	.49	80	.49
III-1H	LN_2	9/30/0830	9/30/1130	3.0	4.0×10^{-5}	-312	66	33.0	.84	83	-
III-1J	LN_2	9/30/1630	10/1/1030	18.0	5.0×10^{-5}	-312	117	44.1	1.12	84	-
III-1K	LN_2	10/1/1330	10/1/1530	2.0	7.5×10^{-5}	-312	190	54.4	1.38	83	-
III-1L	LN_2	10/1/1730	10/1/2300	5.5	1.0×10^{-4}	-312	270	65.0	1.65	83	-
III-1M	LN_2	10/2/1000	10/2/1200	2.0	1.3×10^{-4}	-312	300	69.9	1.77	83	-
III-1N	LN_2	10/4/1630	10/5/0830	16.0	4.8×10^{-7}	-312	0	20.6	.520	84	.505
III-1P	LN_2			Transient helium flow test							

(1) micron liters per second at 80°F

TABLE IV- 5

TANK INSULATION PROGRAM

Insulation System No. 9, Test Series III-2, Data Summary, Calorimeter No. 1

Insulation System:	Composite insulation system consisting of a 1/2 inch thickness of foam substrate and five radiation shields of perforated polyester film aluminized on both sides. Shields are separated with (six spacers each consisting of) two layers of Style 104 glass fabric.
Test Facility:	ADL/Cambridge test facility
Penetrations or Gaps:	None
Boundary Conditions:	Warm boundary: nominal 80°F, .93 emittance; cold boundary: nominal -310°F .35 emittance
Tank Surface Area:	39.8 ft^2 based on outer surface of the 1/2 inch foam substrate

Test No.	Tank Liquid	Data Period Date&Time to	Date&Time	Test Time (hrs)	Ave. Vac. (mm Hg)	Guard Liq/Temp (°F)	Helium(1) Leak Rate ($\frac{\mu\text{-}\ell}{sec.}$)	Total Heat Flow ($\frac{Btu}{hr}$)	Measured Heat Flux ($\frac{Btu}{hr\ ft^2}$)	Ave. Baffle Temp (°F)	Adjusted Heat Flux $\frac{Btu}{hr\ ft^2}$
III-$2A_1$	LN_2	8/13/0830	8/20/1630	56	1×10^{-5}	-311	0	41.3	1.04	83	1.02
III-$2A_2$	LN_2	8/21/2100	8/23/0830	35.5	5 x 10-5	-312	0	43.5	1.09	83	1.07
III-$2A_3$	LN_2	8/25/1830	8/26/0830	14.0	4.5×10^{-6}	-312	0	42.5	1.07	81	1.06
III-2B	LN_2	8/27/2200	8/28/1330	15.5	1.4×10^{-4}	-312	8.5	51.2	1.29	81	-
III-2C	LN_2	8/29/1130	8/30/0830	21.0	1.1×10^{-4}	-311	30	48.[illegible]	1.22	80	-
III-2D	LN_2	8/30/1630	8/31/1230	20.0	2.6×10^{-4}	-311	66	55.4	1.39	79	-
III-2E	LN_2	8/31/1630	9/1/0830	16.0	4.3×10^{-4}	-311	121	66.7	1.68	79	-
III-2F	LN_2	9/1/1630	9/2/1105	18.6	2.4×10^{-3}	-310	168	166	4.15	78	-
III-2G	LN_2	9/2/2000	9/3/0930	13.5	5.8×10^{-6}	-311	0	40.2	1.02	78	1.04
III-2J	LN_2	9/22/1500	9/22/2100	6	1.7×10^{-4}	-312	293	55.6	1.4	84	-
III-2K	LN_2	9/22/2300	9/23/1300	14	1.1×10^{-4}	-312	241	48.2	1.21	83	-
III-2L	LN_2	9/23/1600	9/23/1900	3	8.3×10^{-5}	-312	190	50.6	1.27	83	-
III-2M	LN_2	9/23/2030	9/24/0830	12	5.5×10^{-5}	-312	120	44.5	1.12	83	-
III-2N	LN_2	9/24/1030	9/24/1430	4	$3.8 \times 10^{-[illegible]}$	-312	70	40.3	1.02	83	-
III-2P	LN_2	9/24/1630	9/25/0930	17	$6.5 \times 10^{-[illegible]}$	-312	0	40.8	1.03	83	1.01

(1) micron liters per second at 80°F

TABLE IV-6

EVALUATION OF EQUATION PARAMETERS

Term in Eq. (10)	Value or Method of Expression
$(Q/A)_{net}$	The heat flux was measured experimentally by boil-off of liquid nitrogen in the calorimeter.
$f(\alpha)$	unknown
ν_o	Helium gas was allowed to flow out evenly over the cold inner surface. Values ranged from 0 to 4.14×10^{10} g moles/cm^2-sec
τ, ε	The radiation shields were perforated aluminized Mylar with an open area fraction = 0.019. The measured emissivity of the shields without perforations was 0.025
T_η, T_j, T_o	The outer shield temperature, T_η, was held at 540°R; the inner, T_o, 150°R, and the temperature of the five shields between were measured.
$C_v + k/2$	For helium, $C_v = (3/2)k$, so this term is 2k or 2 cal/g mole - °K = 2 Btu/lb mole-°R
η	Five shields were used, with inner and outer walls (η, o). In the gas and solid conduction terms, $\eta = 6$ since there are 6 gas conduction spaces; in the radiation term, $\eta = 5$ since the inner and outer surfaces are essentially black.
$F_{\eta,\ \eta + 1}$	The molecular flux exterior to the insulation was determined from kinetic theory in terms of external temperature and pressure. The temperature was held constant at 540°R but the pressure varied in different tests. $F_{\eta,\ \eta + 1}$ is a linear function of the pressure.
R, σ	The radiation constant was calculated from $\epsilon' T$ as defined in the nomenclature, σ is 0.173×10^{-8} Btu/hr-ft^2-°R^4.
(k_{sc}/δ)	This constant is not known. It is found by applying Eq. (10) to experiments where ν_o was zero and $P_{(external)}$ measured.

TABLE IV-7

SYSTEM NO. 9

COMPARISON OF PREDICTED AND MEASURED HEAT FLUXES

PERFORATED SHIELDS WITH HELIUM GAS FLOW

Test No.	ν_o (μ-ℓ/sec)	Chamber Pressure (mm Hg)	$(\theta_1 + \theta_2)$	$(Q/A)_{gc}$ $f(\alpha)(\theta_1 + \theta_2)$	$(Q/A)_r$	$(Q/A)_{sc}$	$(Q/A)_{net\ theor}$	$(Q/A)_{exp}$	Per Cent Deviation
III-2A$_2$	0	5×10^{-5}	.158	.079	.92	.12	1.12	1.07	+4.7
III-2B	8.5	1.4×10^{-4}	.446	.223	.92	.12	1.26	1.29	-2.3
III-2C	30	1.1×10^{-4}	.373	.187	.92	.12	1.23	1.22	+0.8
III-2D	66	2.6×10^{-4}	.863	.434	.92	.12	1.47	1.39	+5.8
III-2E	121	4.3×10^{-4}	1.436	.768	.92	.12	1.81	1.68	+7.7
III-2F	168	2.4×10^{-3}	7.59	3.795	.92	.12	4.84	4.15	+16.6
III-2G	0	5.8×10^{-6}	.018	.009	.92	.12	1.05	1.02	+2.9
III-2J	293	1.7×10^{-4}	.739	.369	.92	.12	1.41	1.40	+0.7
III-2K	241	1.1×10^{-4}	.574	.257	.92	.12	1.30	1.21	+7.5
III-2L	190	8.3×10^{-5}	.394	.197	.92	.12	1.24	1.27	-2.4
III-2M	120	5.5×10^{-5}	.258	.129	.92	.12	1.17	1.12	+4.5
III-2N	70	3.8×10^{-5}	.170	.085	.92	.12	1.23	1.02	+19.5
III-2P	0	6.5×10^{-7}	.002	.001	.92	.12	1.04	1.03	+1.0
								average deviation	16.21

$$\theta_1 = 2.26 \times 10^{-6}\, \nu_o \left(\sum_{j=1}^{6} \frac{T_j}{n} - T_i \right)$$

$$\theta_2 = 3.16 \times 10^{3} P$$

Multiply micron-liters per second by 5.38×10^{-8} to obtain g-moles per second. Divide by the insulation area to obtain mass flow rate per unit area.

TABLE IV-8

INSULATION SYSTEM NO. 8
COMPARISON OF PREDICTED AND MEASURED HEAT FLUXES
NON-PERFORATED SHIELDS WITH HELIUM GAS FLOW

Test No.	ν_o $\frac{\mu \ell}{sec}$	Chamber Pressure (mm Hg)	$\theta_1+\theta_2$	(Q/A) $f(\alpha)[\theta_1+\theta_2]$ Btu/hr ft^2	$(Q/A)_r$ Btu/hr ft^2	$(Q/A)_{sc}$ Btu/hr ft^2	$(Q/A)_{net\ theor.}$ Btu/hr ft^2	$(Q/A)_{exp.}$ Btu/hr ft^2	Per Cent Deviation
III-1A	0	1.3×10^{-6}	.004	.002	.36	.15	.51	.516	-1.2
III-1B	4.5	1.1×10^{-5}	.076	.038	.36	.15	.55	.577	-4.7
III-1C	31	3.0×10^{-5}	.357	.179	.36	.15	.69	.735	-6.1
III-1D	63	6.5×10^{-5}	.705	.353	.36	.15	.86	.995	-13.5
III-1E	116	1.5×10^{-4}	1.360	.680	.36	.15	1.19	1.20	-0.1
III-1F	168	6.0×10^{-4}	3.150	1.575	.36	.15	2.09	1.98	+5.6
III-1G	0	4.0×10^{-6}	.012	.006	.36	.15	.52	.49	+6.1
III-1H	66	4.0×10^{-5}	.654	.327	.36	.15	.84	.84	0.0
III-1J	117	5.0×10^{-5}	1.052	.526	.36	.15	1.04	1.12	-7.1
III-1K	190	7.5×10^{-5}	1.597	.799	.36	.15	1.31	1.38	-5.1
III-1L	270	1.0×10^{-4}	2.186	1.093	.36	.15	1.60	1.65	-3.0
III-1M	300	1.3×10^{-4}	2.420	1.210	.36	.15	1.72	1.77	-2.8
III-1N	0	4.8×10^{-7}	.0015	.0007	.36	.15	.51	.52	-1.9
								average deviation	14.41

$$\theta_1 = 3.1 \times 10^{-5} \; \nu_o \left(\sum_{j=i}^{6} \frac{T_j}{n} - T_i \right)$$

$$\theta_2 = 3.16 \times 10^{3} P$$

Multiply micron-liters per second by 5.38×10^{-8} to obtain g-moles per second. Divide by the insulation area to obtain mass flow rate per unit area.

TABLE IV-9

TANK INSULATION PROGRAM

Insulation System No. 10, Test Series II-3 Data Summary, Calorimeter No. 2

Insulation System:	This is System No. 8 consisting of 5 radiation shields of polyester film aluminized on both sides and six spacers consisting of two layers of Style 104 glass fabric into which a 6 inch diameter by 17 inch long penetration has been placed.
Test Facility:	ADL/Cambridge test facility
Penetrations or Gaps:	6 inch diameter, 17 inches long insulated with 50 shields.
Boundary Conditions:	Boundary temperatures will vary as noted below.
Tank Surface Area:	39.5 ft^2 based on outer surface of calorimeter tank.

Test No.	Tank Liquid	Data Period Date&Time	to Date&Time	Test Duration (hrs)	Ave. Vac. (mm Hg)	Guard Liq/Temp (°F)	Total Heat Flow (Btu/hr)	Elect. Heat to End Cap (Btu/hr)	Estimated Penetration Heat Flow (Btu/hr)	Ave. Baffle Temp. (°F)	End Cap Temp (°R)
III-1A2 (1)	LN_2	7/23/0830	11/26/0830	24	1.3×10^{-6}	-312	20.5	NA	NA	82	NA
III-3A1	LN_2	11/18/0830	11/20/0830	48	8×10^{-7}	-312	28.2	none	7.7	83	302
III-3A2	LN_2	11/21/0830	11/22/1630	32	5×10^{-6}	-312	35.1	5.05	14.6	82	474
III-3A3	LN_2	11/23/1630	11/24/1130	19	5×10^{-6}	-311	43.6	20.2	23.1	83	584
III-3A4	LN_2	11/25/0830	11/26/1230	28	7×10^{-7}	-312	16.9	20.1	16.4	-301	561
III-3A5	LN_2	11/27/0830	11/28/0830	24	7×10^{-7}	-312	43.6	51.2	43.1	-303	745
III-3A6	LN_2	11/30/0830	12/3/0830	72	2×10^{-6}	-312	0.87	none	0.4	-303	220 to 145
III-3A7	LN_2	12/26/1100	12/27/0830	2[illegible].5	8×10^{-7}	-312	29.3	none	1.5	80	220
III-3A8	LN_2	12/28/0900	12/29/0900	24	7×10^{-7}	-312	44.5	15.3	15.3	80	550

Notes: (1) Test III-1A2 data is presented to show comparison between data obtained for the insulation system with and without penetration.

TABLE IV-10

ANALYTICAL AND EXPERIMENTAL HEAT FLOW SUMMARY

	Experimental				Calculated				
			Penetration						
Test No.	Measured Calorimeter Heat Flow (Btu/hr)	Exper. Penet. Heat Flow (Btu/hr)	Warm End Temp. (°R)	Cold End Temp. (°R)	Wall Conduct. Heat Flow (Btu/hr)	Total Warm End Emitted Heat Flow (Btu/hr)	μ Factor[1]	q Factor Figure I-5[1]	Predicted Penetration Heat Flow (Btu/hr)
III-3A1	28.2	7.7	302	144	3.0	2.8	1.1	N.E.[2]	N.E.(2)
III-3A2	35.1	14.6	474	151	6.5	17.0	0.38	N.E.	N.E.
III-3A3	43.6	23.1	584	150	8.7	39.0	0.22	N.E.	N.E.
III-3A4	16.9	16.4	561	161	8.0	33.3	0.24	N.E.	N.E.
III-3A5	43.6	43.1	745	190	11.1	104.0	0.1	.37	38.5
III-3A6	0.87	0.4	220 to 145	142	0.4	0.2	0	N.E.	N.E.
III-3A7	29.3	1.5	220	145	1.2	0.8	1.5	N.E.	N.E.
III-3A8	44.5	15.3	550	179	7.5	31.0	0.24	N.E.	N.E.

[1]See Reference 3

[2]Not evaluated; outside range or analysis

TABLE IV-11

INSULATION SYSTEM NO. 11, SPECIFICATION

Description:	The system consists of five shields of polyester film aluminized on both sides and six spacers each consisting of two layers of silk netting. System applied to Calorimeter No. 1 over 1/2 inch Urethane foam.
Shield:	
Material:	DuPont, Type S, polyester film, coated both sides with vapor deposited aluminum.
Thickness:	Film .00025 inches; coating 400 Angstroms
Weight:	.0018 lbs/ft^2
Emissivity:	.025 average
Side Geometry:	Straight gores 4 to 5 inches wide
Head Geometry:	Full circles
Joints:	All seams overlapped and contacting
Spacer:	
Material:	Two layers of silk netting Jordan Marsh No. 5517
Thickness:	.007 inches
Weight:	.0024 lbs/ft^2
Density:	4.1 lbs/ft^3
Filament Dia:	.0004 inches
Open Area:	84 per cent
Side Geometry:	Gored; purse string top and bottom, 10 inch slits spaced 2 feet apart at the center of each layer for the purpose of minimizing contraction effects. Slits in each layer are at alternate positions to prevent shorting of shields.
Head Geometry:	Full circles
Joints:	All joints are overlapped. Outer edges of head spacers are tucked under purse string used to attach side spacer.
Boundary Emissivity:	
Calorimeter Tank:	.35 at -320°F
Chamber Baffles:	.93 at 80°F
System Properties:	
Surface Area:	39.8 ft^2
Weight:	.0234 lbs/ft^2
Thickness:	.040 inches
Weight Density:	6.3 lbs/ft^3
Shield Density:	138 shield per inch (unity stacking factor)
Figure of Merit: (wt. basis)	1.2

TABLE IV-12

TANK INSULATION PROGRAM

INSULATION SYSTEM NO. 11, TEST SERIES III-4 DATA SUMMARY, CALORIMETER NO. 1

Insulation System:	Five radiation shields of polyester film aluminized on both sides and six spacers consisting of two layers of silk netting
Test Facility:	ADL/Cambridge Test Facility
Penetrations or Gaps:	None
Boundary Conditions:	Warm Boundary: 80°F, .93 emittance Cold Boundary: -320°F, .35 emittance
Tank Surface Area:	39.8 ft^2 based on outer surface of the 1/2 inch foam substrate

Test No.	Tank Liquid	Data Period Date&Time	to Date&Time	Test Duration (hrs)	Ave. Vac. (mm Hg)	Guard Liq/Temp (°F)	Total Heat Flow (Btu/hr)	Measured Heat Flux (Btu/hr ft^2)	Ave. Baffle Temp. (°F)	Adjusted Heat Flux Btu/hr ft^2
III-4A	LN_2	12/13/0830	12/16/0830	72	1×10^{-6}	-312	19.24	.484	80	.484
III-4B(1)	LN_2	12/17/0830	12/18/0830	24	5×10^{-6}	+ 2	45.3	NA	80	NA
III-4C	LN_2	12/19/1630	12/20/1630	24	6×10^{-7}	-312	19.39	.487	80	.487

Notes: (1) Test was performed with no cold guard liquid nitrogen refrigeration flow.

TABLE IV-13

INSULATION SYSTEM NO. 12, SPECIFICATION

Description:	The system consists of five shields of polyester film silverized on both sides and six spacers each consisting of two layers of silk netting. System applied to Calorimeter No. 2.
Shield:	
Material:	DuPont, Type S, polyester film, coated both sides with vapor deposited silver.
Thickness:	Film .00050 inches; coating, Side A, 1100 Angstroms, Side B, 2000 Angstroms
Weight:	.0036 lbs/ft^2
Coating Emittance:	.011 average
Side Geometry:	Straight gores 4 to 5 inches wide
Head Geometry:	Full circles
Joints:	All seams overlapped and contacting
Spacer:	
Material:	Two layers of silk netting, Jordan Marsh No. 5517
Thickness:	.007 inches
Weight:	.0024 lbs/ft^2
Density:	4.1 lbs/ft^3
Filament Dia:	.0004 inches
Open Area:	84 per cent
Side Geometry:	gored; purse string top and bottom, 10 inch slits spaced 2 feet apart at the center of each layer for the purpose of minimizing contraction effects. Slits in each layer are at alternate positions to prevent shorting of shields.
Head Geometry:	Full circles
Joints:	All joints are overlapped. Outer edges of head spacers are tucked under purse string used to attach side spacer.
Boundary Emittances:	
Calorimeter Tank:	.35 at -320°F
Chamber Baffles	.93 at 80°F
System Properties:	
Surface Area:	39.5 ft^2
Weight:	.0324 lbs/ft^2
Thickness:	.045 inches
Weight Density:	8.7 lbs/ft^3
Shield Density:	133 shields per inch (unity stacking factor)
Figure of Merit: (wt. basis)	1.7

TABLE IV-14

TANK INSULATION PROGRAM

Insulation System No. 12, Test Series III-5 Data Summary, Calorimeter No. 2

Insulation System:	Five radiation shields of polyester film metallized on both sides with silver and six spacers consisting of two layers of silk netting.
Test Facility:	ADL/Cambridge Test Facility
Penetrations or Gaps:	None
Boundary Conditions:	Warm boundary: 80°F; .93 emittance Cold boundary: -320°F; .35 emittance
Tank Surface Area:	39.8 ft^2 based on outer surface of the 1/2 inch foam substrate

Test No.	Tank Liquid	Date&Time	to Date&Time	Test Duration (hrs)	Ave. Vac. (mm Hg)	Guard Liq/Temp (°F)	Total Heat Flow (Btu/hr)	Measured Heat Flux (Btu/hrft^2)	Ave. Baffle Temp. (°F)	Adjusted Heat Flux (Btu/hr ft^2)
III-5A	LN_2	1/20/0830	1/24/0030	88	2×10^{-6}	-315	12.21	.306	79	.308
III-5B	LN_2	2/1/0930	2/2/0830	23.5	2.5×10^{-4}	-312	39.80	.750	80	.750
III-5C	LN_2	2/2/1040	2/3/0840	22	1×10^{-3}	-312	69.44	1.75	30	1.75

TABLE IV-15

INSULATION SYSTEM NO. 12

COMPARISON OF PREDICTED AND MEASURED HEAT FLUXES
NON-PERFORATED SHIELDS STATIC HELIUM GAS PRESSURE

Test No.	ν_o $\frac{\mu-\ell}{sec}$	Chamber Pressure (mm Hg)	θ_2	$(Q/A)_{gc}$ $f(\alpha)\ \theta_2$	$(Q/A)_R$ Btu/hr ft^2	$(Q/A)_{sc}$ Btu/hr ft^2	$(Q/A)_{theor}$ Btu/hr ft^2	$(Q/A)_{exp}$ Btu/hr ft^2	Per Cent Difference
III-5A	0	2×10^{-6}	0	0.003	.16	.15	.31	.31	-
III-5B	0	2.5×10^{-4}	.798	.394	.16	.15	.70	.75	-6.7
III-5C	0	1×10^{-3}	3.160	1.580	.16	.15	1.89	1.75	+7.8

$\theta_2 = 3.16 \times 10^3 P$

$f(\alpha) = 0.5$ See Part IV, D-1f of report

TABLE IV-16

SILVER COATED 1/2 MIL POLYESTER FILM (1)

SHIELD - EMITTANCE DATA SUMMARY

INSULATION SYSTEM NO. 13

Sample (2) From System/Shield	Sample No.	Coating Material	Coating Thk(°A)	Emittance Test No.	Emittance
12/1	337A	Silver	1680	467	.0109
12/1	337B	Silver	1650	468	.0103
12/5	338A	Silver	1400	484	.0218
12/5	338B	Silver	2000	480	.0116
13/1	340	Silver	985	510	.0175
13/1	340	Silver	985	511	.0179
13/1	341	Silver	1000	513	.0101
13/3	342	Silver	1000	514	.0103
13/5	345	Silver	1000	531	.0187
13/5	346A	Silver	1290	529	.0342
13/5	346B	Silver	2210	530	.0158

(1) Material purchased from Gomar Manufacturing Company.

(2) Emittance measurements on System No. 13 were made about one month after those made on System No. 12.

TABLE IV-17

INSULATION SYSTEM NO. 13, SPECIFICATION

Description:	Five radiation shields of polyester film metallized on both sides with silver and five inner spacers each consisting of a layer of silk netting combined with foam strips covering 25 per cent of the spacer area. A sixth silk netting spacer, without foam strips, was applied over the fifth shield. The multi-layer was applied on Calorimeter No. 1 over a 1/2 inch foam substrate and vapor barrier.
Shield:	
Material:	DuPont, Type S, polyester film
Thickness:	Film .0005 inches; Silver coating, Side A, 1100 Angstroms, Side B, 2000 Angstroms
Coating Emittance:	.017
Side Geometry:	Straight gores 4 to 5 inches wide
Head Geometry:	Full Circles
Joints:	All seams overlapped and contacting
Spacer:	
Material:	One layer of silk netting Jordan Marsh No. 5517 and Scott foam, sixty pores per inch Strips 1/4"x2 1/4"x1/16"
Thickness:	.065 inches
Weight:	.0037 lbs/ft^2
Density:	.67 lbs/ft^3
Open Area:	
Netting:	84 per cent
Spacer:	75 per cent
Side Geometry:	Gored edges of side sheet
Head Geometry:	Full circles
Joints:	All joints butted
Boundary Emittances:	
Calorimeter Tank:	.35 @ -320°F
Chamber Baffles:	93 @ 80°F
System Properties:	
Surface Area:	39.8 ft^2
Weight:	.0377 lbs/ft^2
Thickness:	.334 inches
Weight Density:	1.36 lbs/ft^3
Shield Density:	Fifteen shields per inch (theoretical)
Figure of Merit: (wt. basis)	2.03

TABLE IV-18

TANK INSULATION PROGRAM

INSULATION SYSTEM NO. 13, TEST SERIES III-6 DATA SUMMARY, CALORIMETER NO. 1

Insulation System:	Five radiation shields of polyester film metallized on both sides with silver and six spacers each consisting of a layer of silk netting combined with foam strips covering 25 per cent of the spacer area. Insulation placed over 1/2 inch foam substrate and vapor barrier.
Test Facility:	ADL/Cambridge Test Facility
Penetrations or Caps:	None
Boundary Conditions:	Warm Boundary: 80°F, .93 Emittance; Cold Boundary: -320°F, 0.35 Emittance
Tank Surface Area:	39.8 ft^2 based on outer surface of the 1/2 inch foam substrate

Test No.	Tank Liquid	Data Period Date&Time	to Date&Time	Test Duration (hrs)	Ave. Vac. (mm Hg)	Guard Liq/Temp (°F)	Total Heat Flow (Btu/hr)	Measured Heat Flux (Btu/hr ft^2)	Ave. Skin Temp. (°F)	Adjusted Heat Flux (Btu/hr ft^2)
III-6A	LN_2	2/18/0830	2/21/1630	80	$.9 \times 10^{-6}$	-312	16.3	.41	80	.41
III-6B1	LN_2	3/3/0830	3/4/0630	24	2×10^{-6}	-312	13.0	.33	80	.33
III-6B2	LN_2	3/4/1630	3/6/1330	45	1×10^{-6}	-315	13.5	.34	80	.34

TABLE IV-19

INSULATION SYSTEM NO. 13

COMPARISON OF CALORIMETER TANK AND K-APPARATUS

HEAT FLUX RESULTS

Test Apparatus	Test No.	Insulation Description: Shields	Insulation Description: Spacers	Zero Load Data: Insulation Thickness (in)	Zero Load Data: Measured Flux(1) Btu/hr ft^2	Zero Load Data: Adjusted Flux(2) Btu/hr ft^2
Tank	III-6B	(5) Silver on 1/2 mil Mylar	(6) Silk and flex foam	N.A.	0.33	0.33
Flat Plate	3075	(5) Silver on 1/2 mil Mylar	(6) Silk and flex foam	.808	.258	0.28
Flat Plate	3076	(10) Silver on 1/2 mil Mylar	(11) Silk and flex foam	1.365	.156	0.34

Notes: (1) Flat plate tests were performed at -320°F cold plate and 70°F warm plate

(2) Measured heat fluxes adjusted to 80°F warm boundary and five shield system

TABLE IV-20

INSULATION SYSTEM NO. 14

SHIELD EMITTANCE DATA SUMMARY

GOLD COATED 1/4 MIL POLYESTER FILM

Sample From System/Shield	Sample No.	Roll No.	Coating Thickness (Angstroms)	Emittance Test No.	Emittance
14/1	351B	122265	2440	542	.0201
14/1	351A	122265	2080	545	.0145
14/1	330B	122265	2072	465	.0127
14/1	330A	122265	1840	463	.0146
14/2	352A	122265	2680	550	.0176
14/2	352B	122265	3340	551	.0166
14/2	353B	21166	3360	549	.0173
14/3	353A	21166	2200	546	.0195
14/3	343B	21166	3100	527	.0176
14/3	343A	21166	2220	526	.0190
14/4	354B	21166	2140	548	.0146
14/4	354A	21166	1740	547	.0166
14/5(circle)	333	101565	953	486	.0259
14/5(circle)	336	101565	1050	503	.0228

Note:

1. Average emittance shields 1 and 2 0.0160
2. Average emittance shields 3, 4, 75% of 5 0.0175
3. Average emittance shield 5(25%) 0.0243
4. Computed average emittance - all shields 0.0172

TABLE IV-21

INSULATION SYSTEM NO. 14, SPECIFICATION

Description:	Five radiation shields of polyester film metallized on both sides with gold and five inner spacers each consisting of three layers of silk netting. The sixth and outer spacer consisted of one layer of silk netting; the multi-layer was applied over Calorimeter No. 2.
Shield:	
Material:	DuPont, Type S, polyester film
Thickness:	Film .00025 inches; Gold coatings, 1000 to 3000 Angstroms
Emittance	.0172 average for all shields
Geometry:	Sides, straight gores 4 to 5 inches wide Head, full circles
Joints:	All seams overlapped and contacting
Spacer:	
Material:	Three layers of silk netting, Jordan Marsh No. 5517
Thickness:	.0105 inches
Weight:	.0036 lbs/ft^2
Density:	4.1 lbs/ft^3
Open Area:	84 per cent
Geometry:	Side, gored edges of side sheet; Head, full circles
Joints:	All joints butted
Boundary Emittances:	
Calorimeter Tank:	.86 at -320°F
Chamber Baffles:	.93 at 80°F
System Properties:	
Surface Area:	39.5 ft^2
Weight:	.0282 lbs/ft^2
Thickness:	.0573 inches
Weight Density:	5.9 lbs/ft^3
Shield Density:	100 shields per inch (theoretical)
Figure of Merit: (wt. basic)	1.50

TABLE IV-22

TANK INSULATION PROGRAM

INSULATION SYSTEM NO. 14, TEST SERIES III-7, DATA SUMMARY, CALORIMETER NO. 2

Insulation System:	Five radiation shields of polyester film metallized on both sides with gold and six spacers each consisting of three layers of silk netting.
Test Facility:	ADL/Cambridge test facility
Penetrations or Gaps:	None
Boundary Conditions:	Warm Boundary: 80°F, 0.93 emittance; Cold Boundary: -320°F, 0.86 Emittance
Tank Surface Area:	39.5 ft^2 based on calorimeter tank surface area

Test No.	Tank Liquid	Data Period Date&Time	to Date&Time	Test Duration (hrs)	Ave. Vac. (mm Hg)	Guard Liq/Temp (°F)	Total Heat Flow (Btu/hr)	Measured Heat Flux (Btu/hr ft^2)	Ave. Skin Temp (°F)	Adjusted Heat Flux (Btu/hr ft^2)
III-7	LN_2	3/17/0830	3/21/0830	96	2×10^{-6}	-311	12.8	.325	80	.325

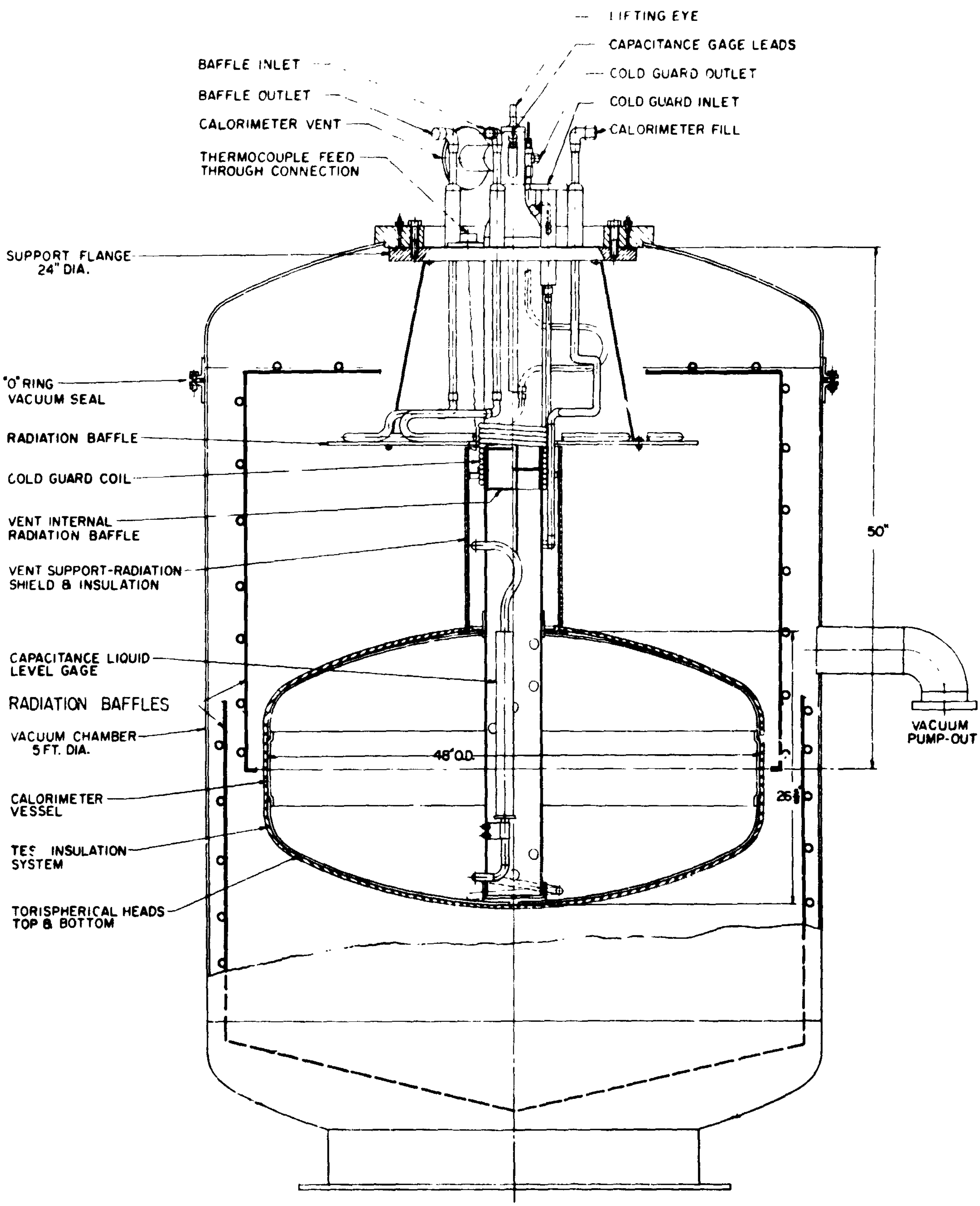

FIGURE IV-1. CHAMBER AND CALORIMETER ASSEMBLY

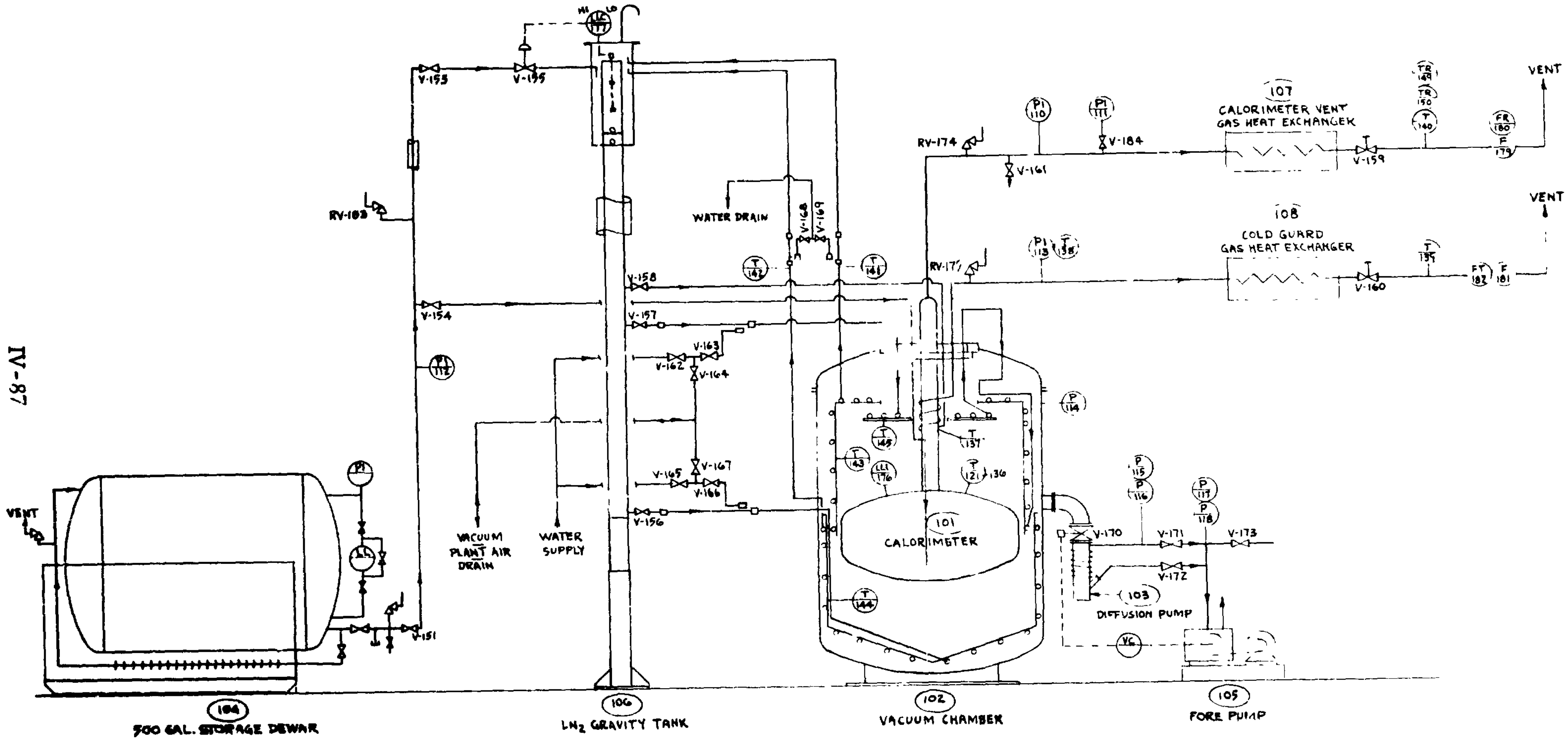

FIGURE IV-2 FLOW SCHEMATIC, TANK INSULATION TEST FACILITY

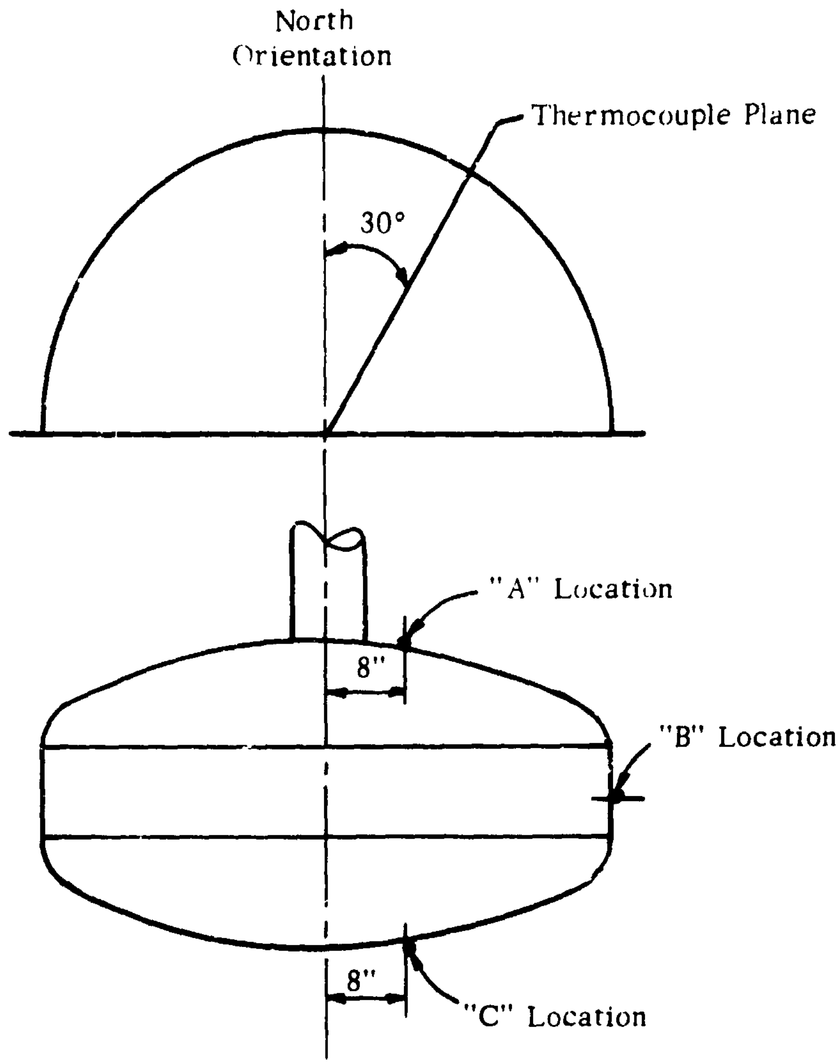

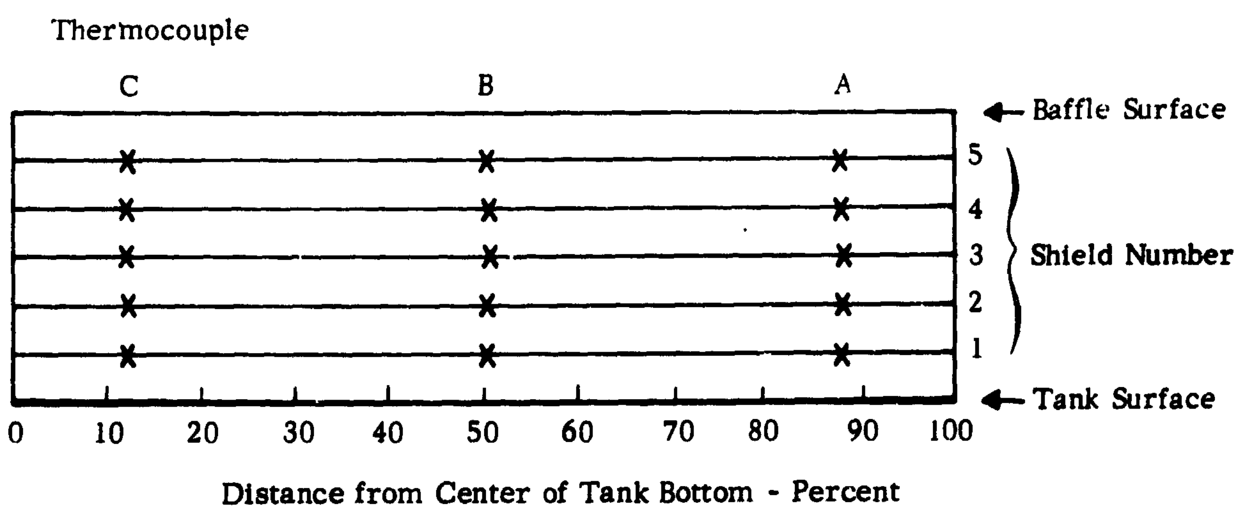

FIGURE IV-3 INSULATION SYSTEM, THERMOCOUPLE LOCATIONS

FIGURE IV-4 INSULATION SYSTEM NO. 8

FIGURE IV-5 INSULATION SYSTEM NO. 8, BOTTOM

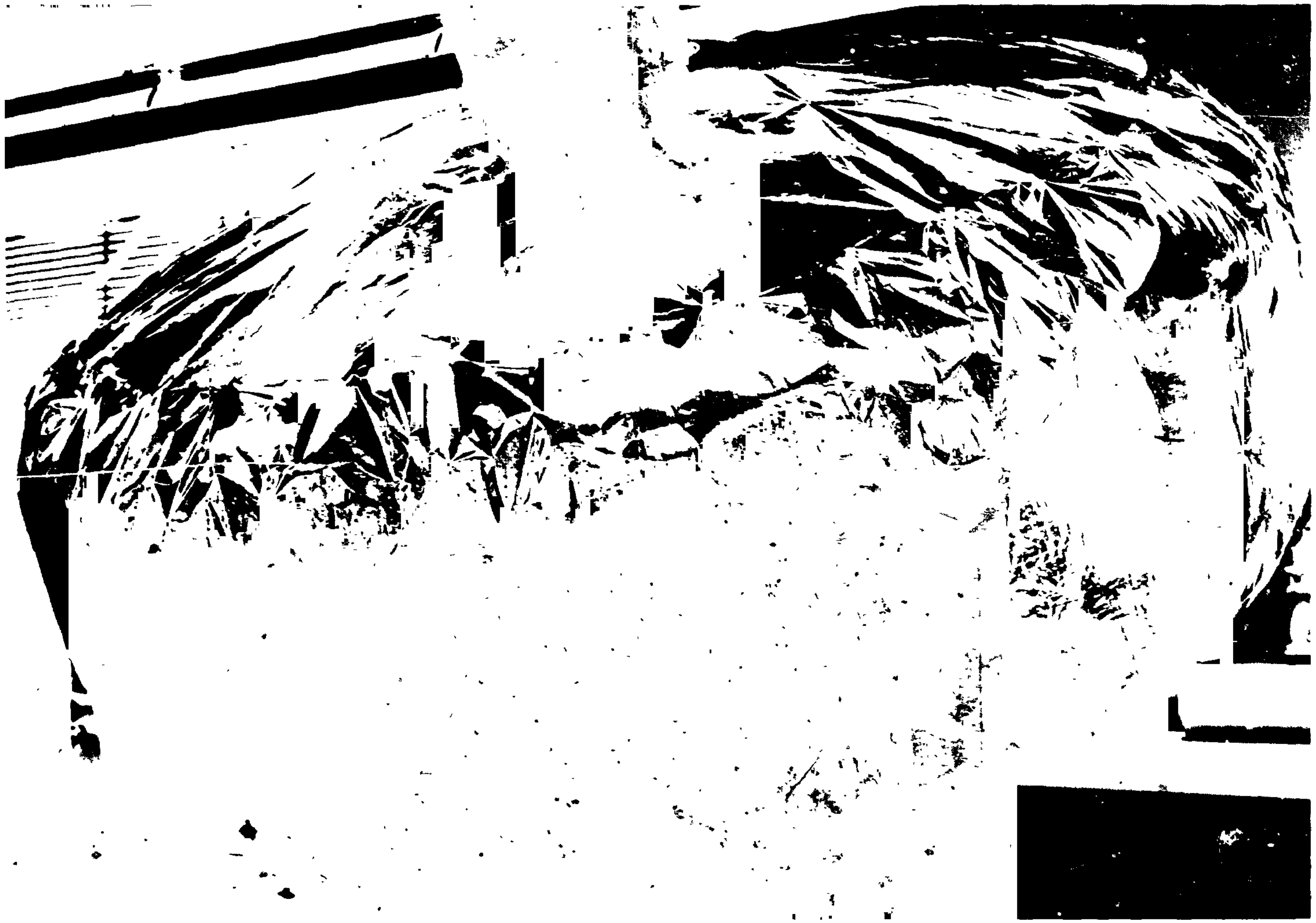

FIGURE IV-6 INSULATION SYSTEM NO. 9, FIRST PERFORATED SHIELD

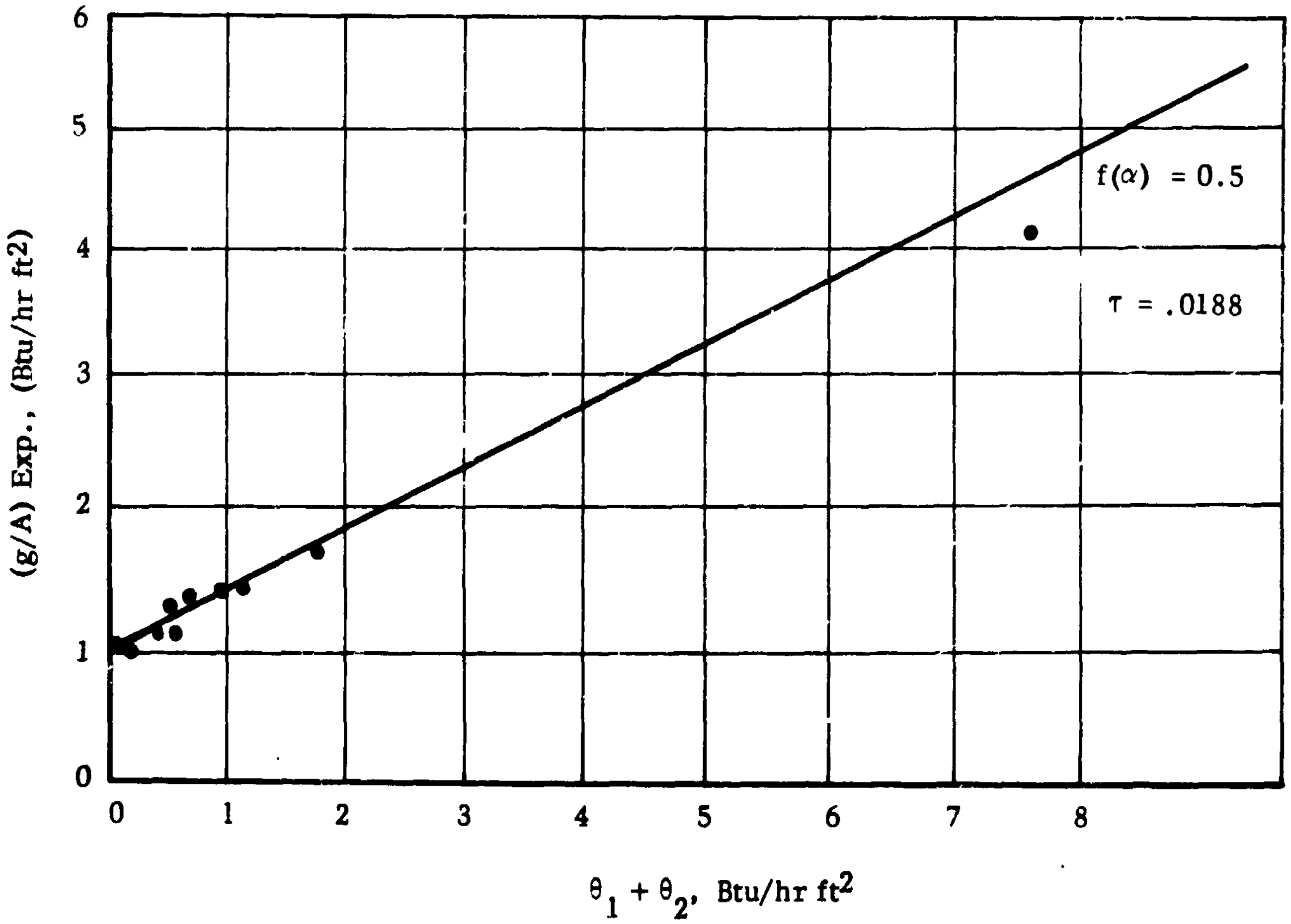

FIGURE 7 INSULATION SYSTEM NO. 9, COMPUTED GAS CONDUCTION HEAT FLUX FACTOR VERSUS MEASURED HEAT FLUX

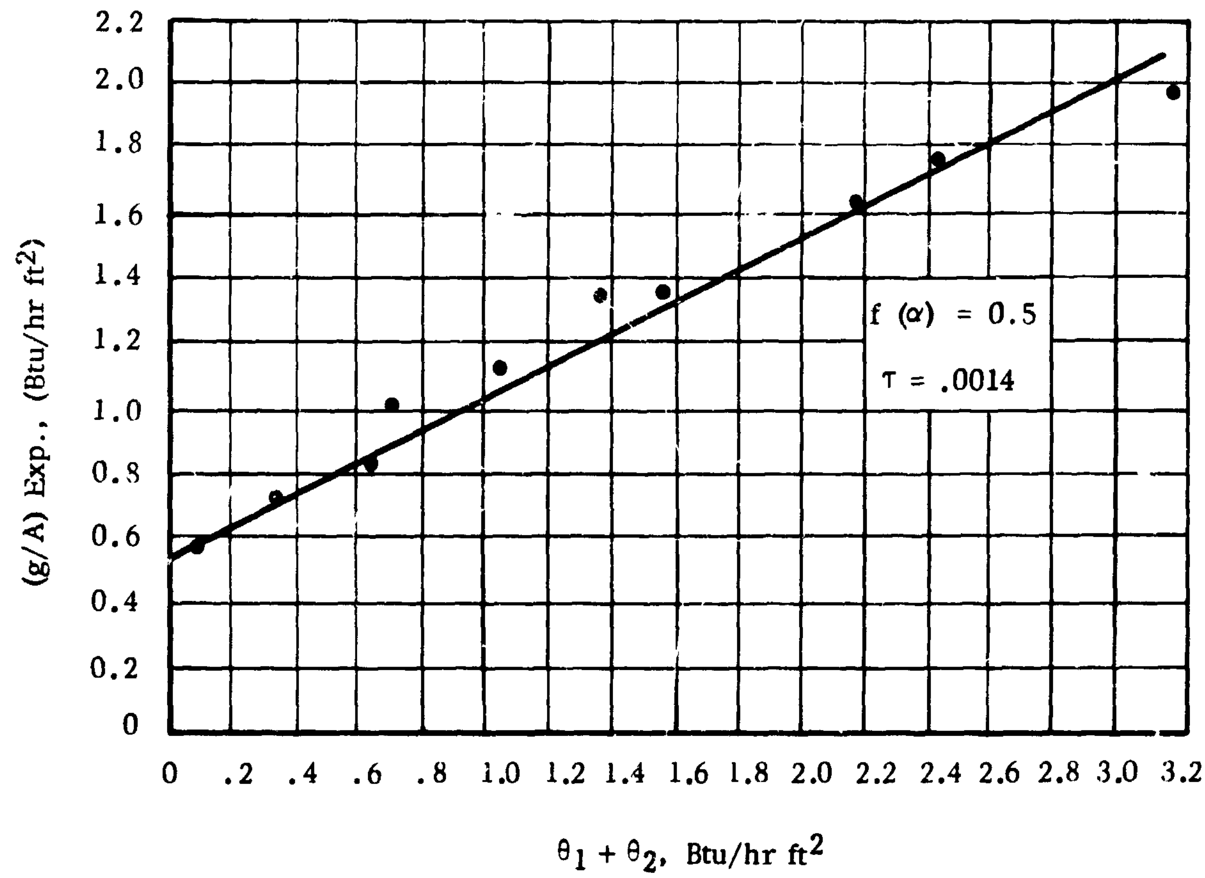

FIGURE 8 INSULATION SYSTEM NO. 8, COMPUTED GAS CONDUCTION HEAT FLUX FACTORS VERSUS MEASURED HEAT FLUX

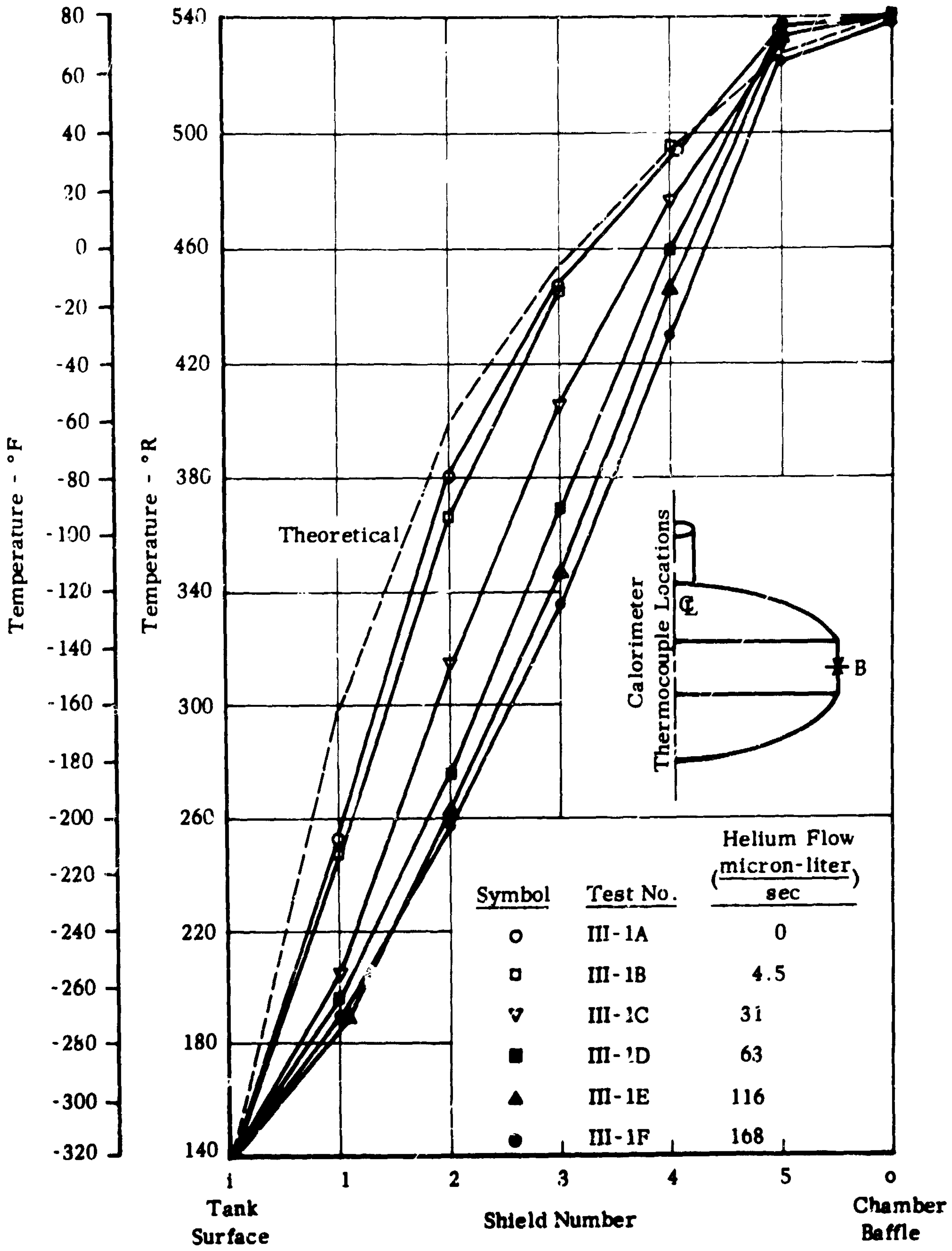

FIGURE IV - 9 INSULATION SYSTEM NO. 8--SHIELD TEMPERATURE GRADIENTS FOR VARIOUS HELIUM LEAK RATES

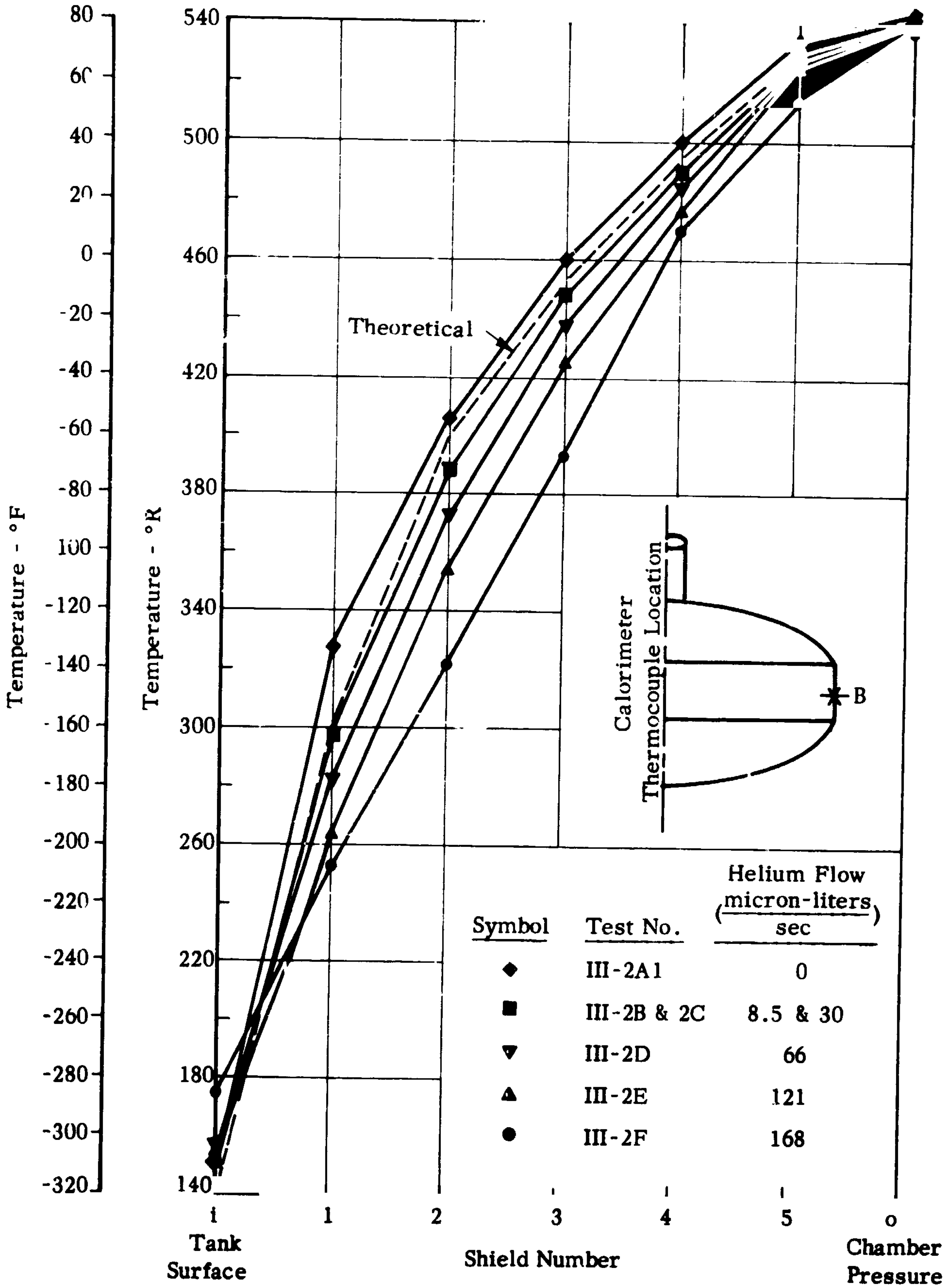

FIGURE IV-10 INSULATION SYSTEM NO. 9 · SHIELD TEMPERATURE GRADIENTS FOR VARIOUS HELIUM LEAK RATES

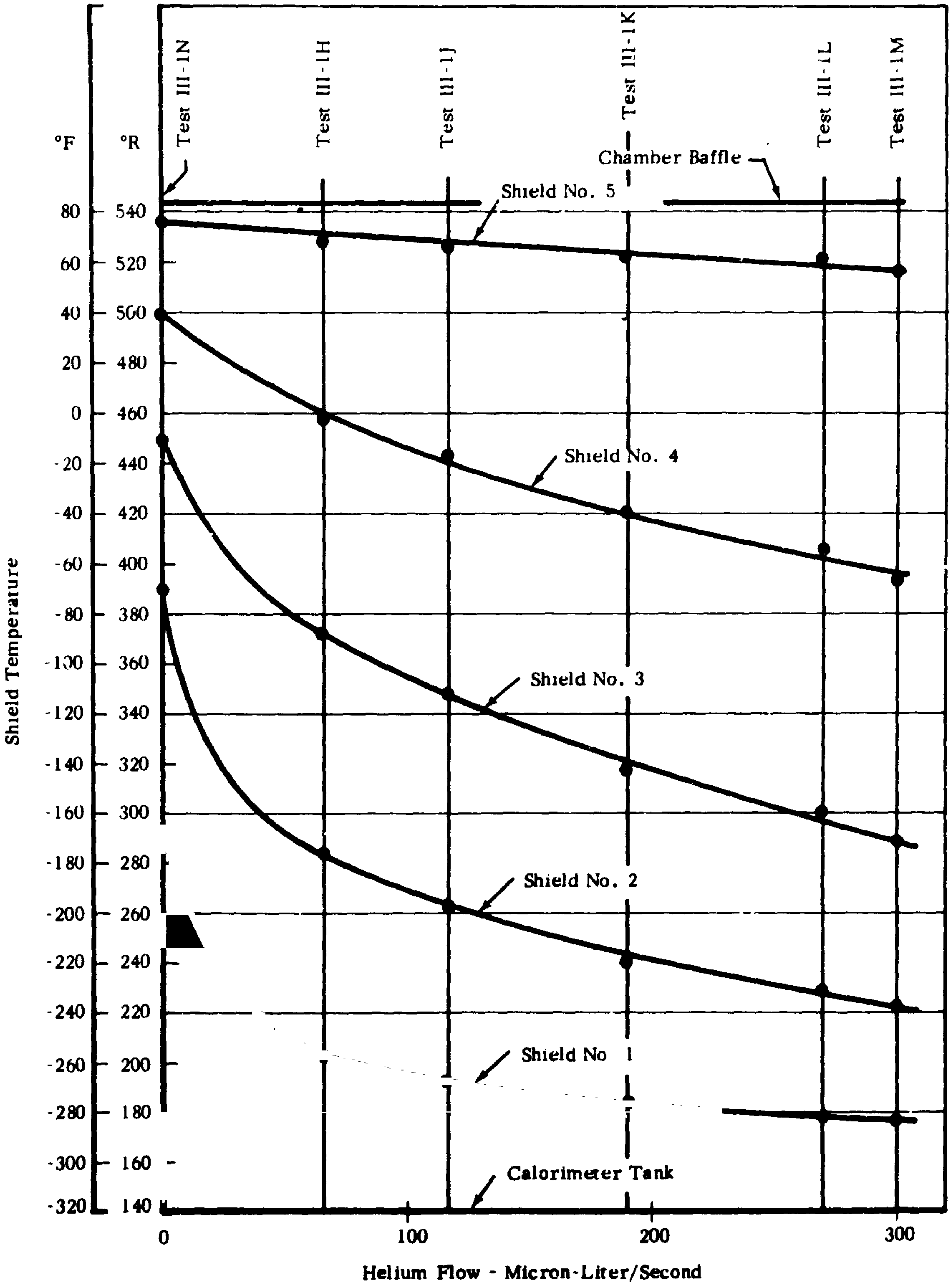

FIGURE IV-11 INSULATION SYSTEM NO. 8, SHIELD TEMPERATURE VERSUS HELIUM GAS LOAD

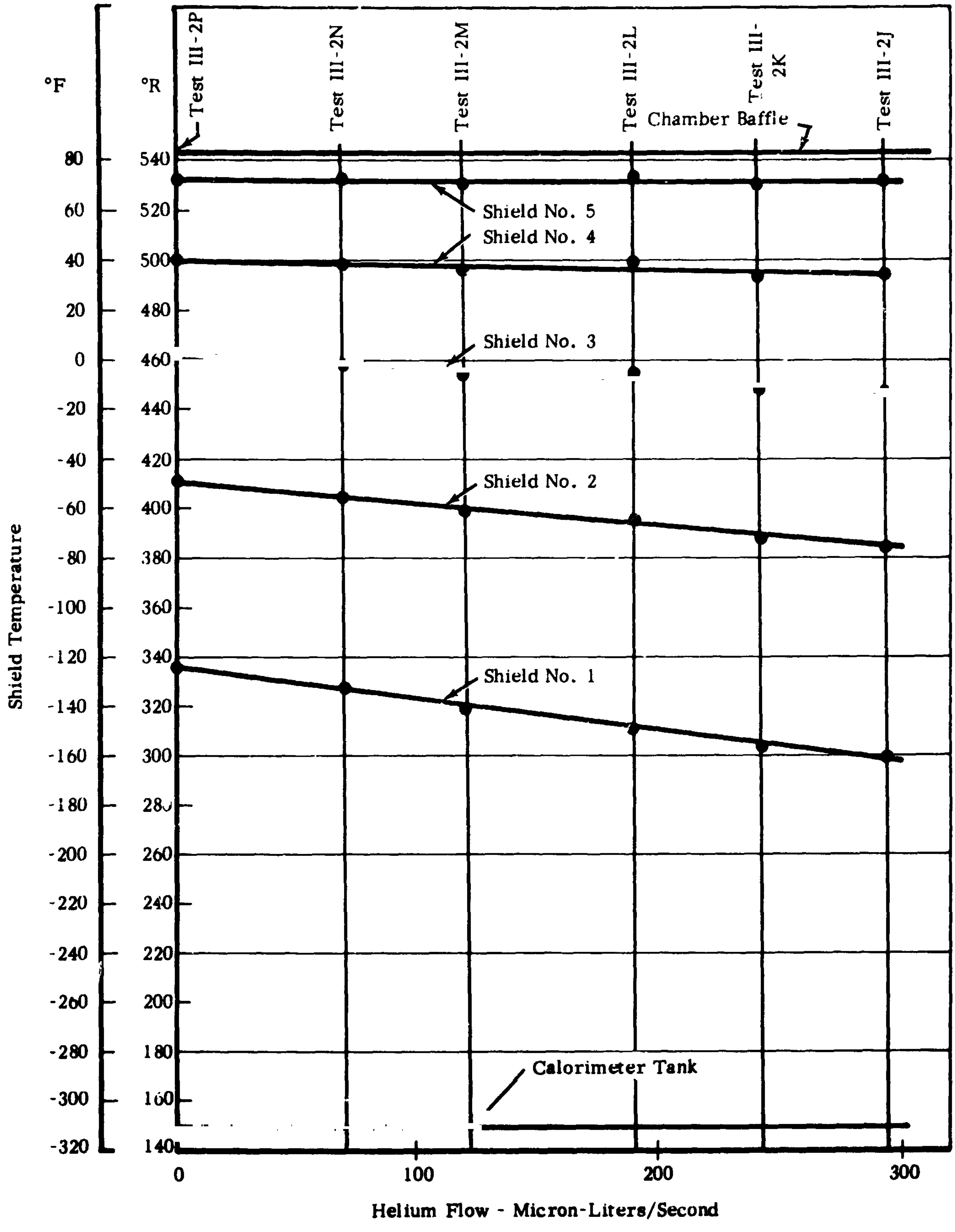

FIGURE IV-12 INSULATION SYSTEM NO. 9, SHIELD TEMPERATURE VERSUS HELIUM GAS LOAD

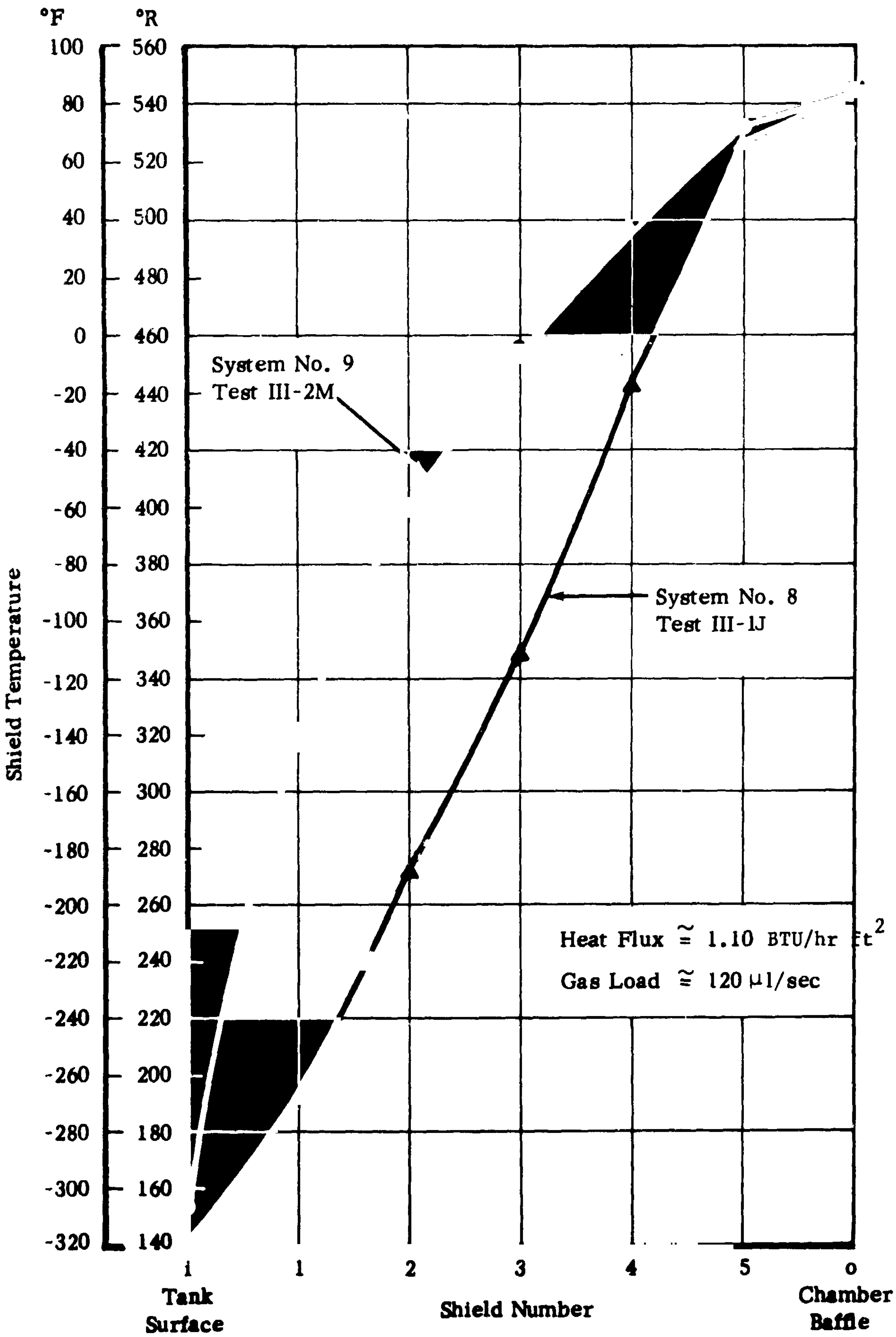

FIGURE IV-13 INSULATION SYSTEMS 8 AND 9--COMPARISON OF SHIELD TEMPERATURES FOR EQUAL HEAT FLUXES AND HELIUM GAS LOAD

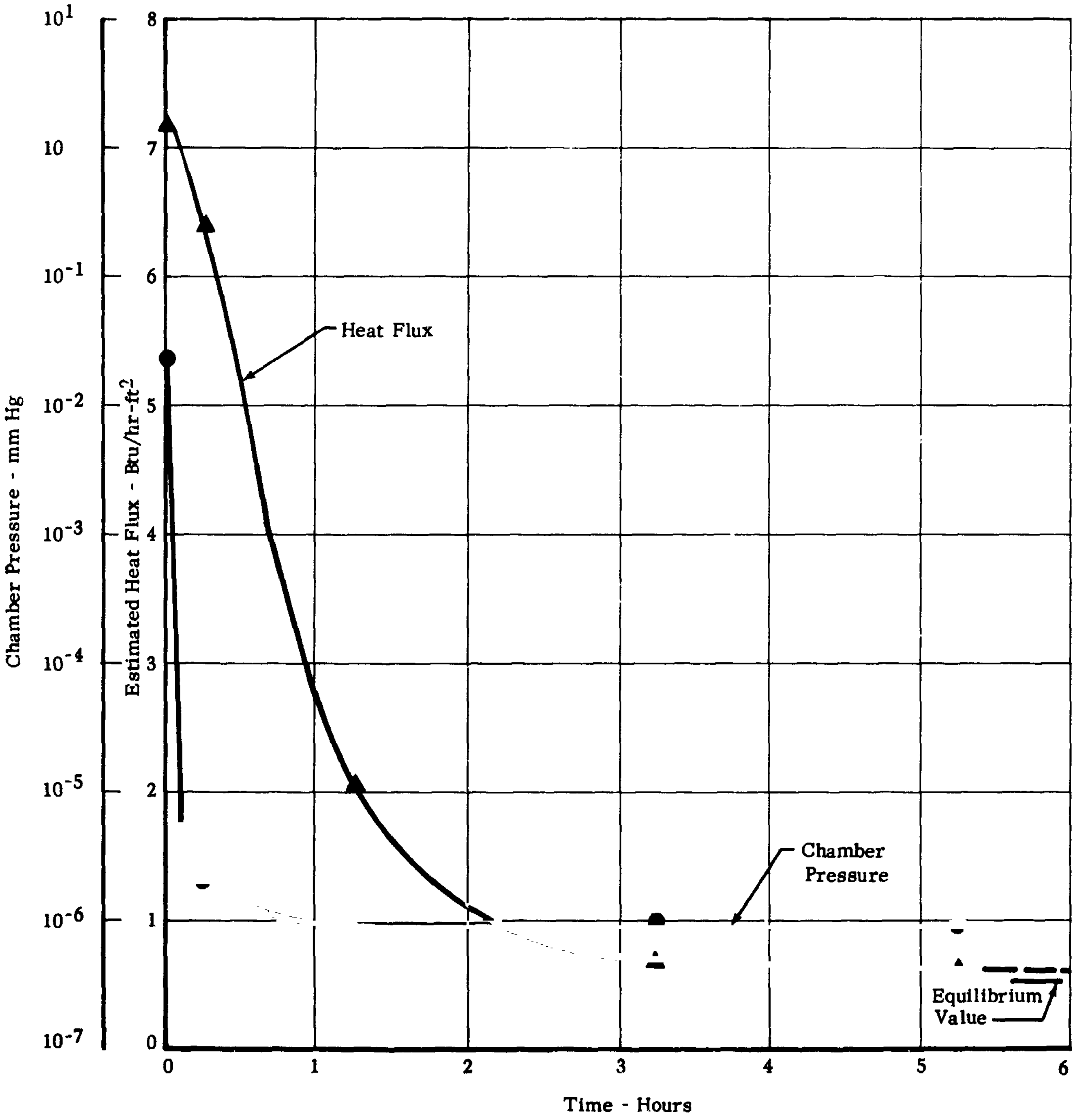

FIGURE IV-14 INSULATION SYSTEM NO. 8, TEST III-1P, HEAT FLUX TRANSIENT

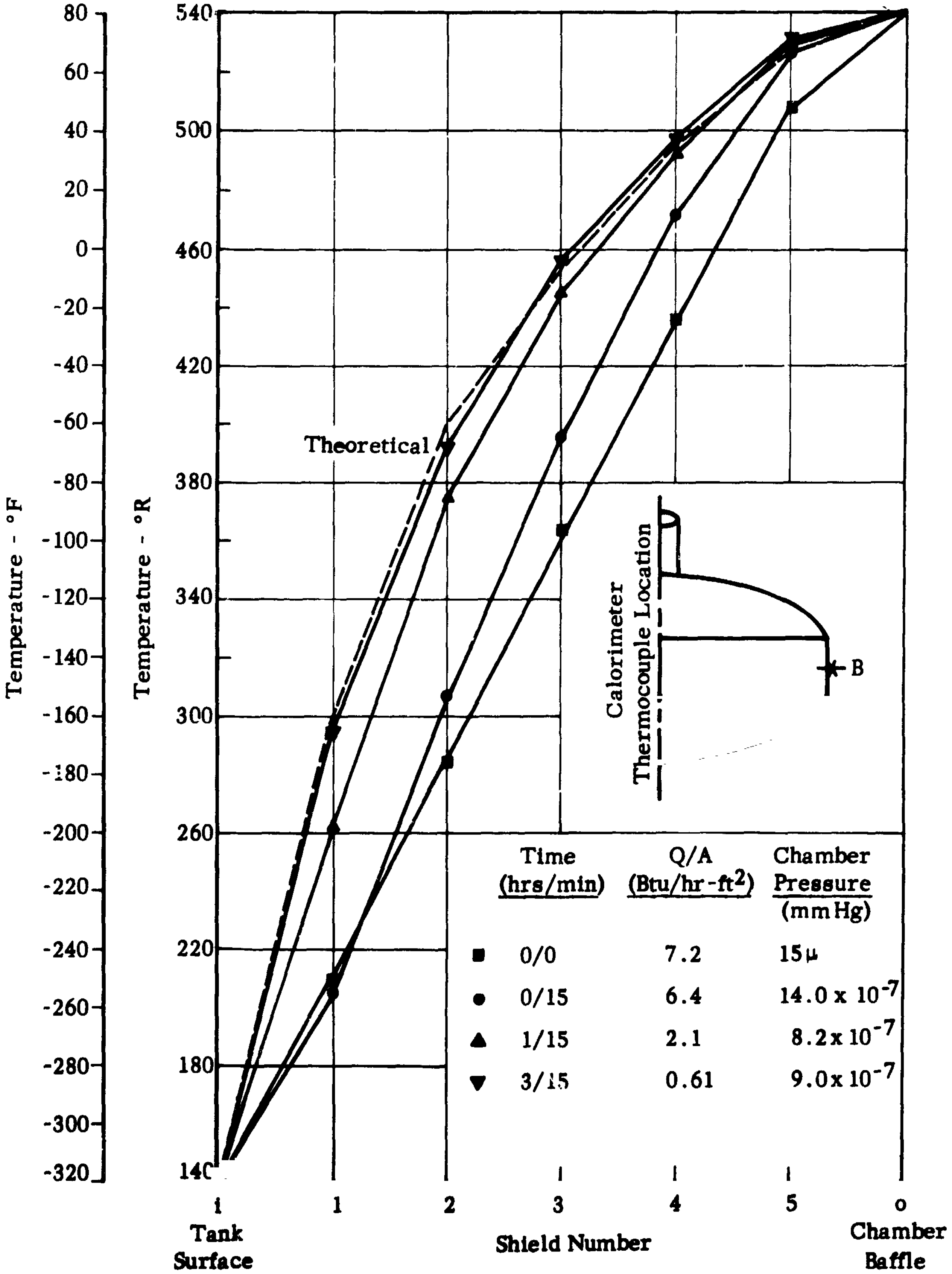

FIGURE IV-15 INSULATION SYSTEM NO. 8, TEST III-1P, SHIELD TEMPERATURE GRADIENTS AT VARIOUS TIMES DURING TRANSIENT

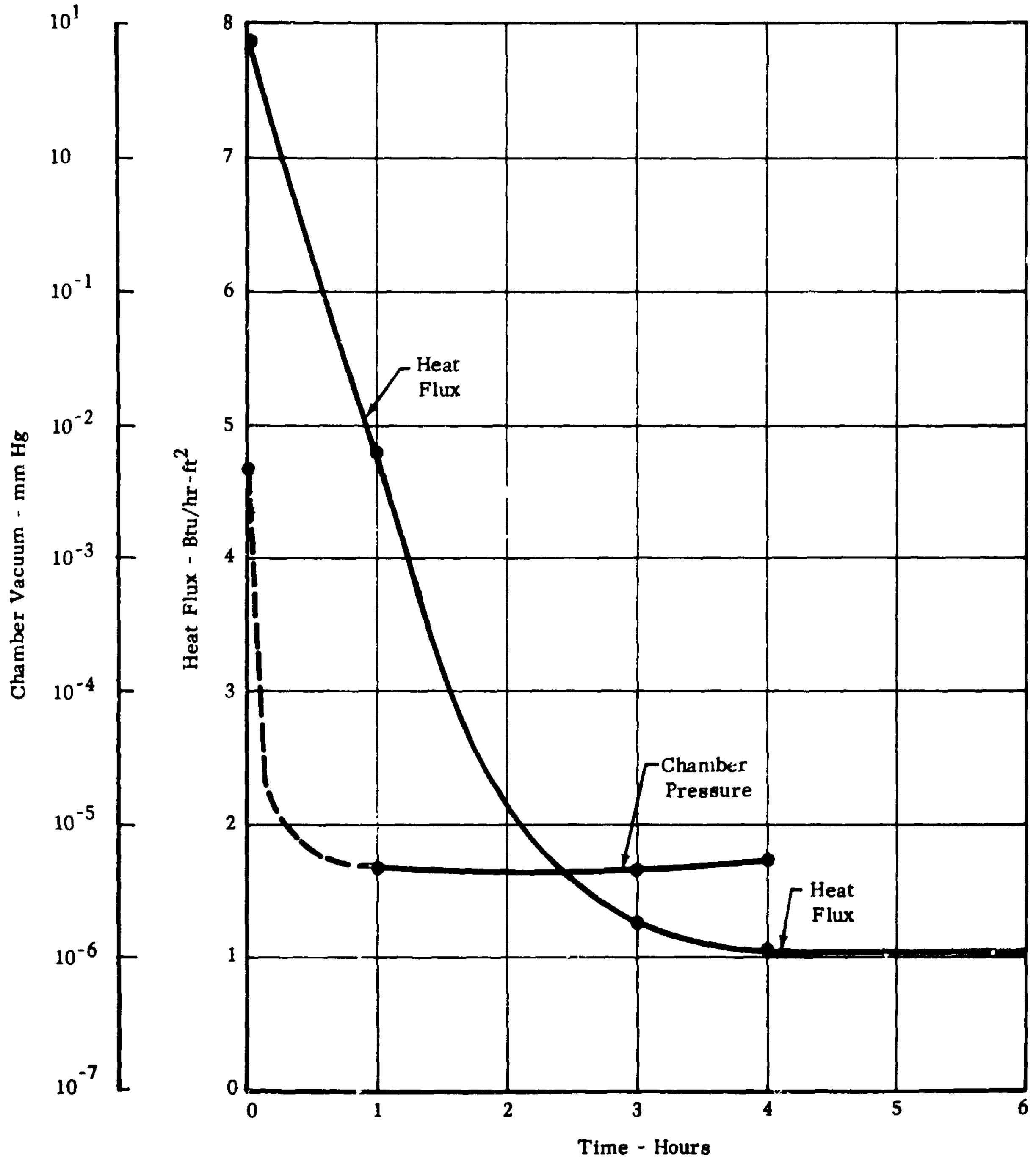

FIGURE IV- 16 INSULATION SYSTEM NO. 9--TEST III-2Q--HEAT FLUX TRANSIENT

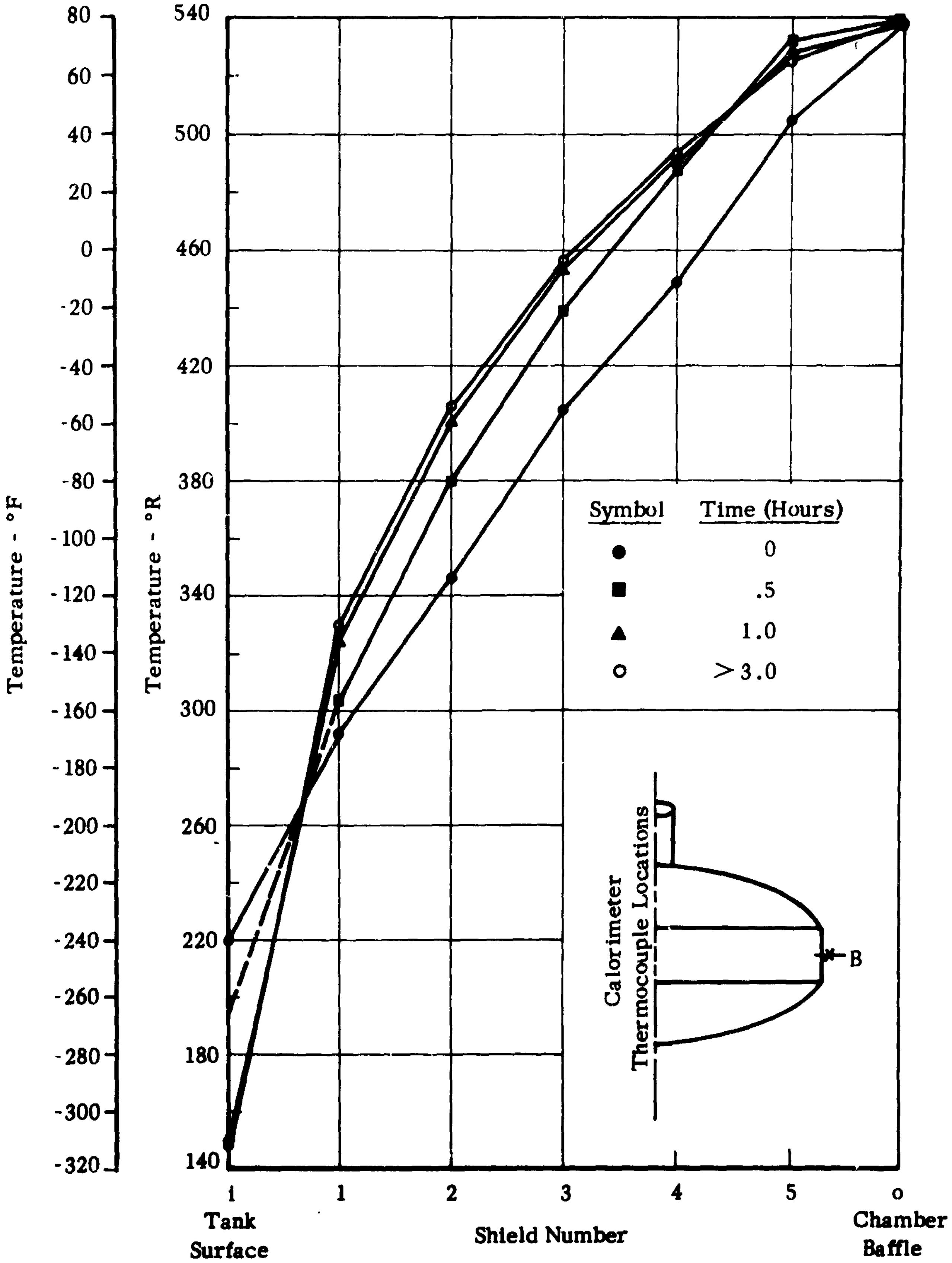

FIGURE IV- 17 INSULATION SYSTEM NO. 9--TEST III--2Q -TEMPERATURE GRADIENTS AT VARIOUS TIMES DURING TRANSIENT

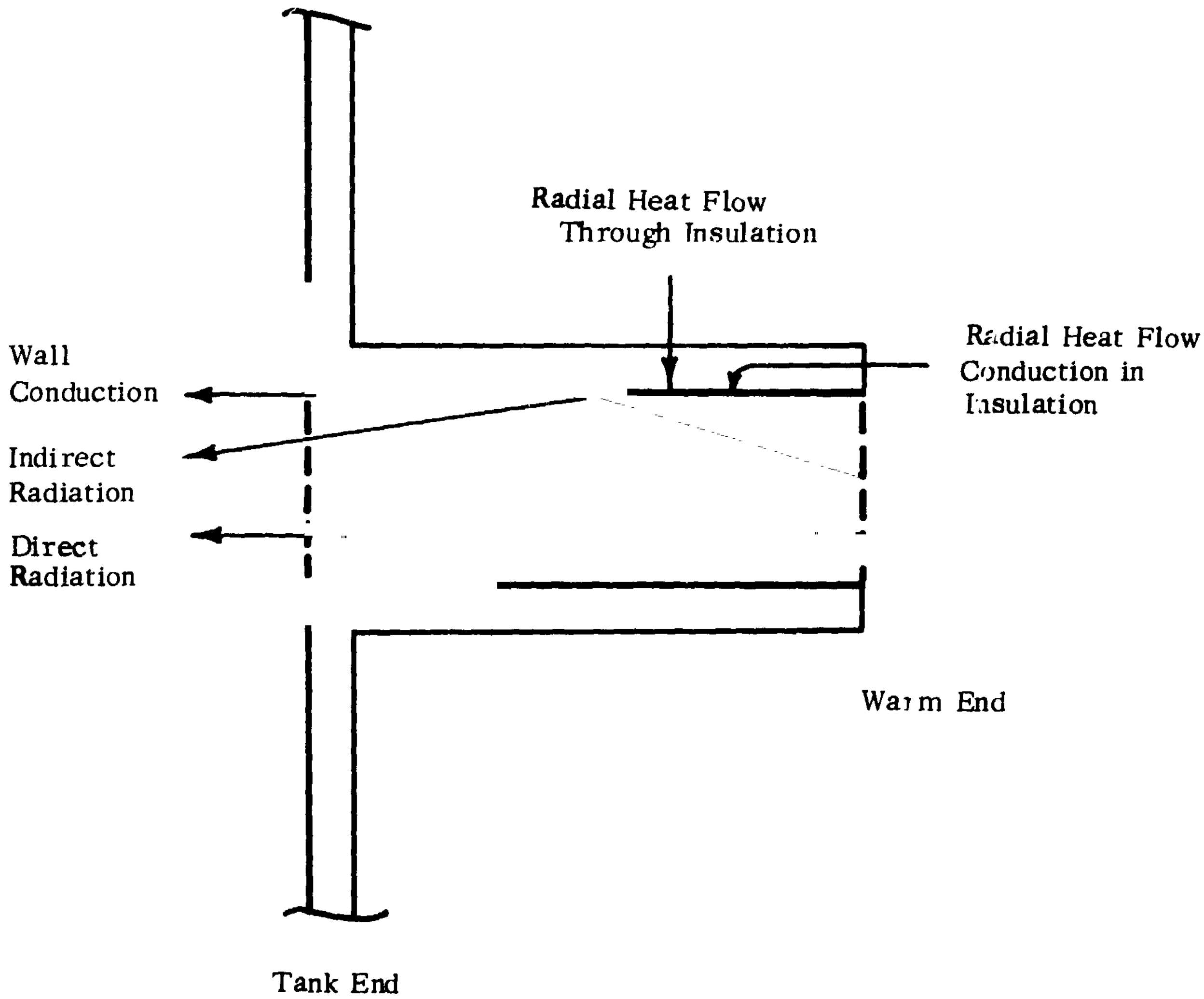

FIGURE IV-18 PENETRATION HEAT FLOW PATHS

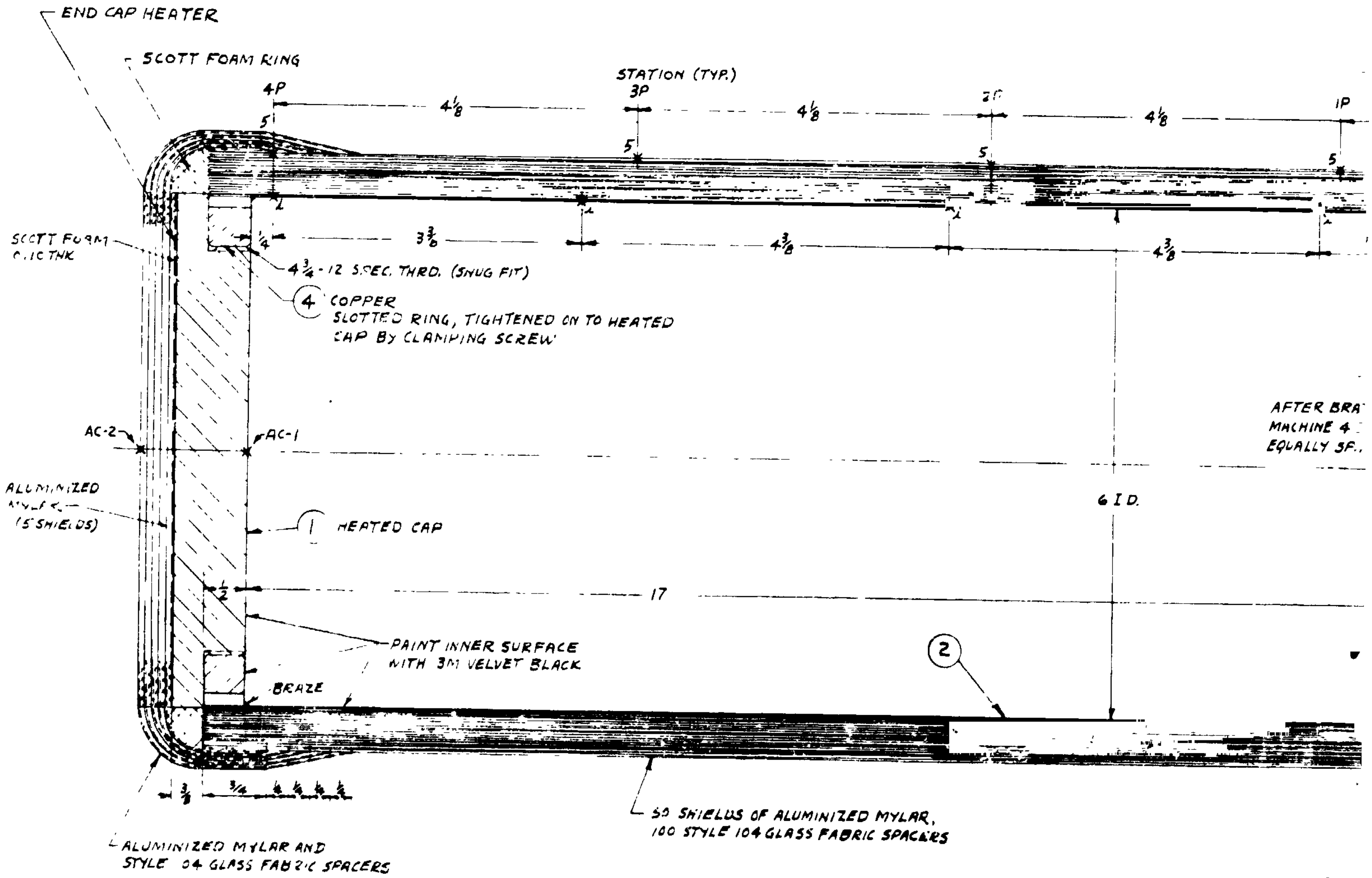

LEGEND

THERMOCOUPLE	DESCRIPTION
0P-1 THRU 4P-1	WALL PENETRATION
0P-2 AND 2P-2	NO. 2 SHIELD
0P-5 THRU 4P-5	NO. 5 SHIELD
AC-1	CAP
AC-2	OUTSIDE INSULATION - CAP
5C-1 THRU 5C-6	NO. 5 SHIELD - TANK BOTTOM
S-1	STUD THERMOCOUPLE

FIGURE IV-19 INSULATIC
PENETRA

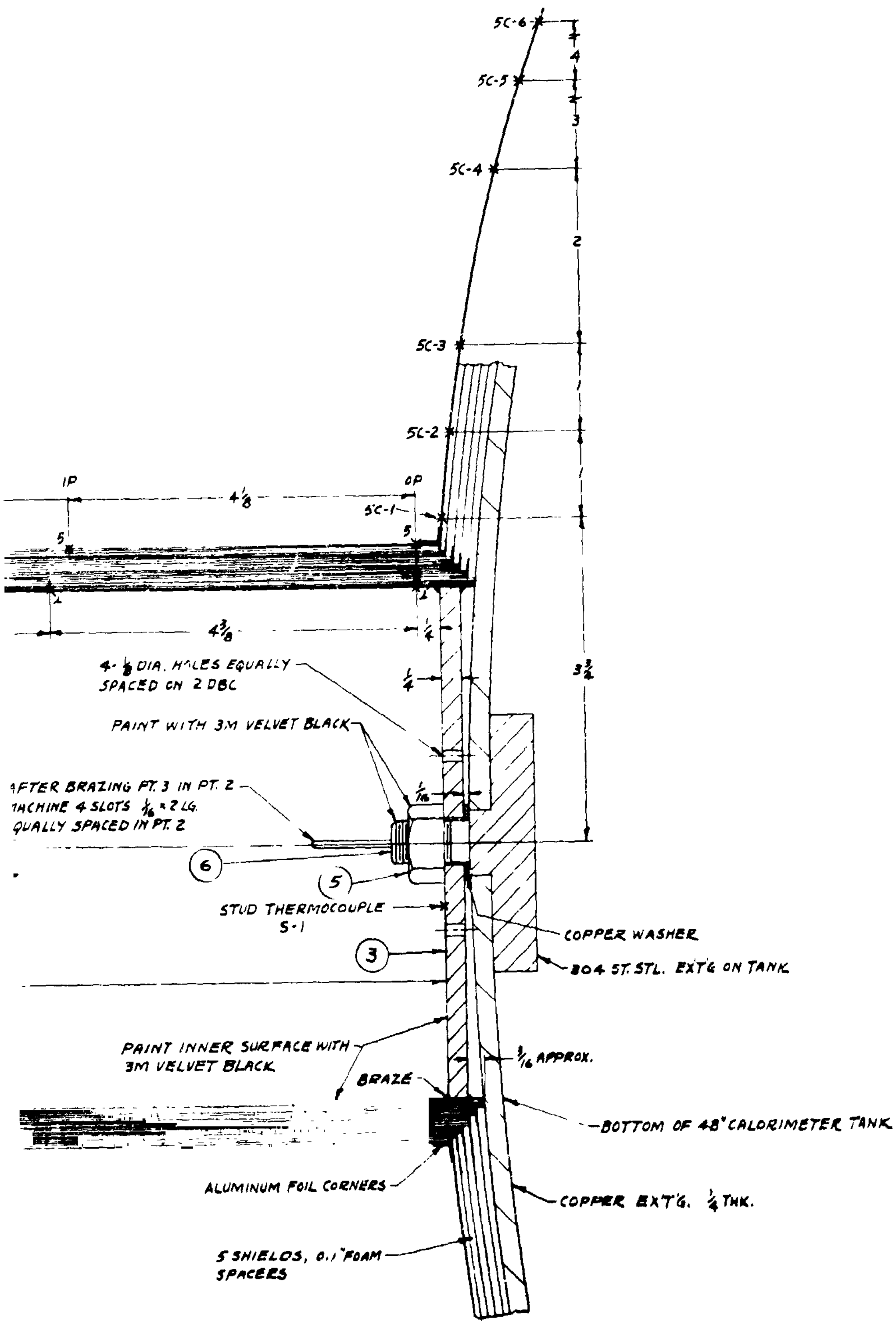

ITEM NO	QTY REQ	PART OR IDENTIFYING NO.	NOMENCLATURE OR DESCRIPTION	MATERIAL
6	1		STUD (WELD TO TANK)	304 ST. STL. 1/2-13UNC × 1 1/2 LONG
5	1		HEX. NUT	ST. STL. 1/2-13UNC
4	1	B3522-028	BASE RING	COPPER
3	1	B3522-027	CLAMPING PLATE	COPPER
2	1	B3522-026	PIPE SIMULATION ELEMENT	304 ST. STL.
1	1	B3522-024P2	HEATED CAP	ALUMINUM

LIST OF PARTS

.ATION SYSTEM NO. 10, TEST PIPE
TRATION DETAIL

IV-104-2

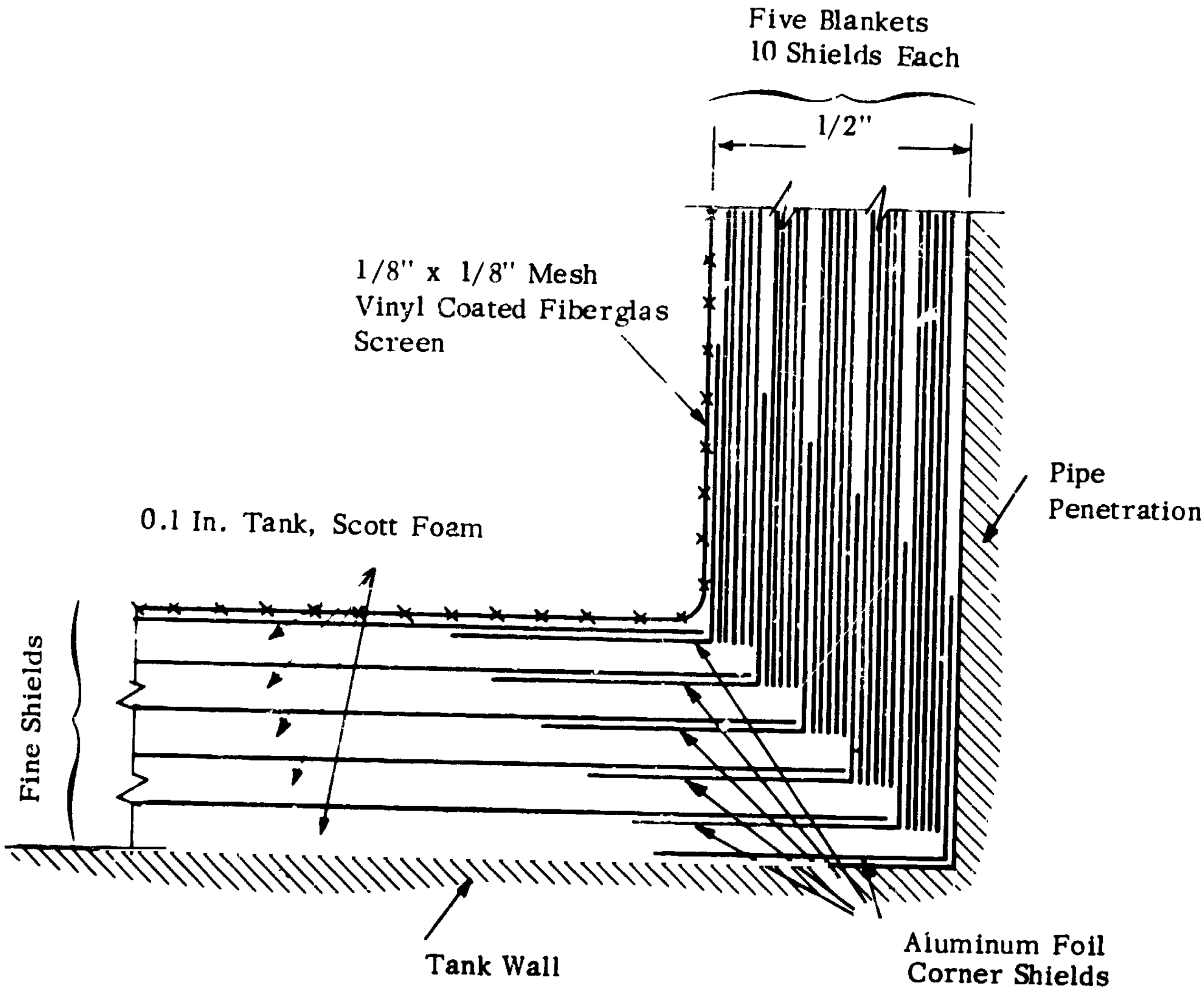

FIGURE IV-20 INSULATION SYSTEM NO. 10, PIPE PENETRATION CORNER DETAIL

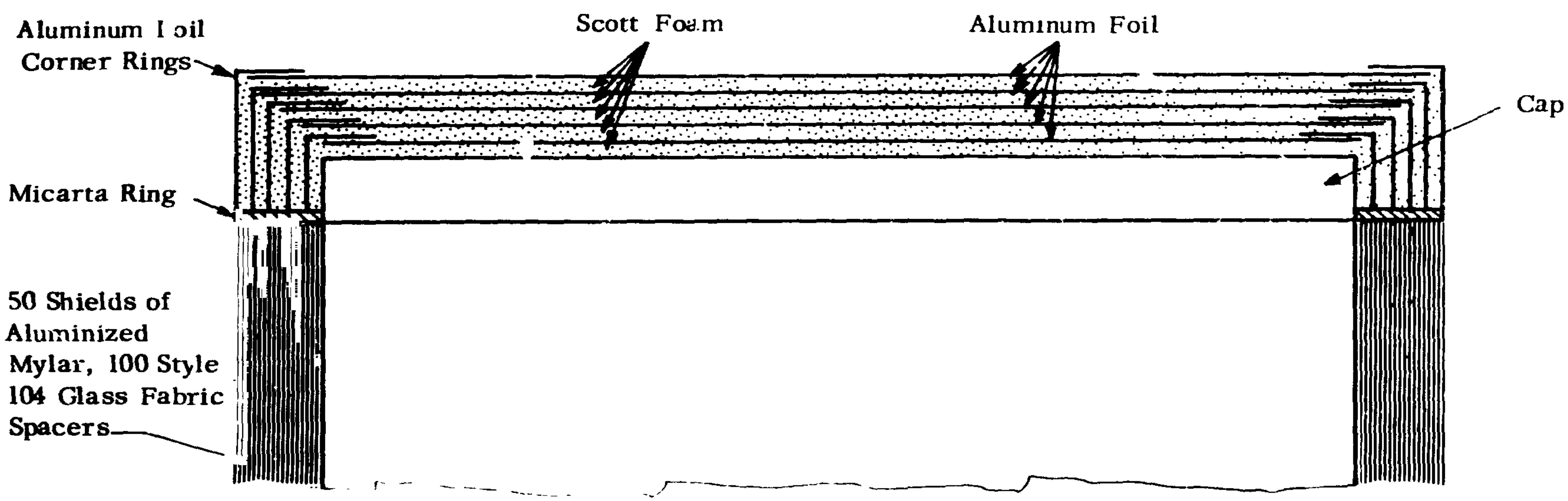

(a) "A1" Cap With Aluminum Foil Insulation - Tests 3A1 through 3A6

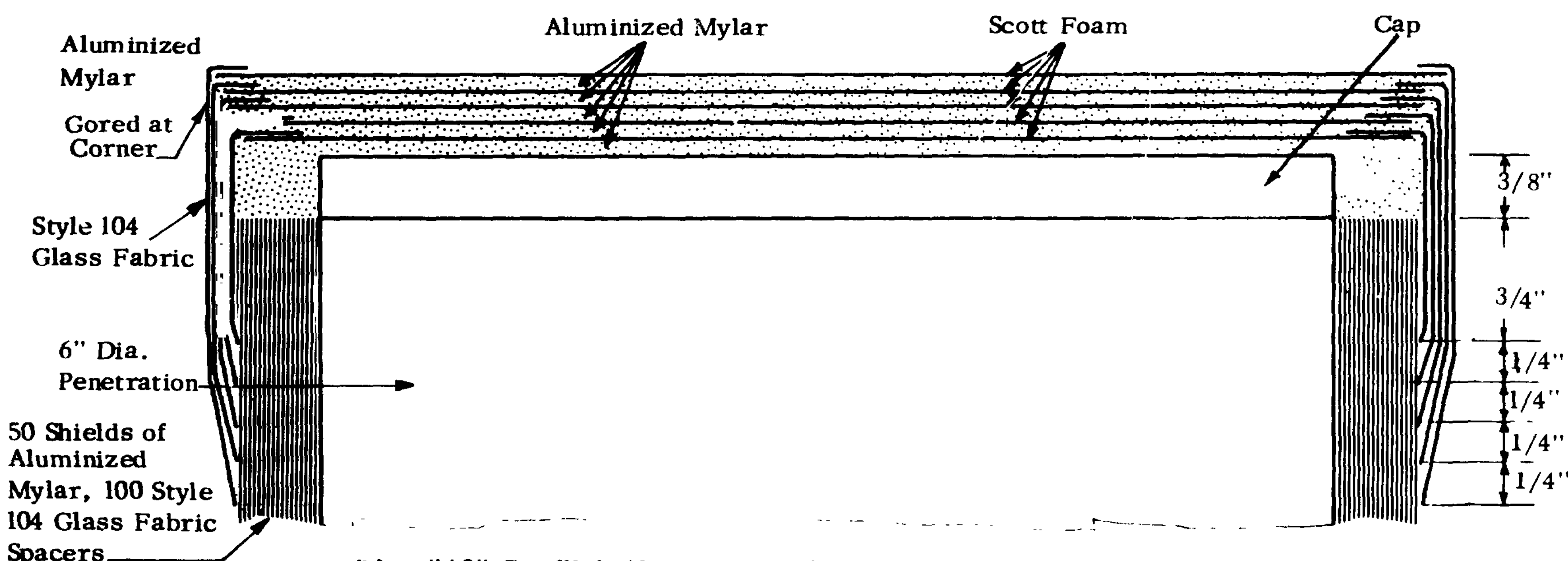

(b) "A2" Cap With Aluminized Mylar Insulation Tests 3A7 through 3A8

FIGURE IV-21 INSULATION SYSTEM NO. 10, END CAP INSULATION DETAIL

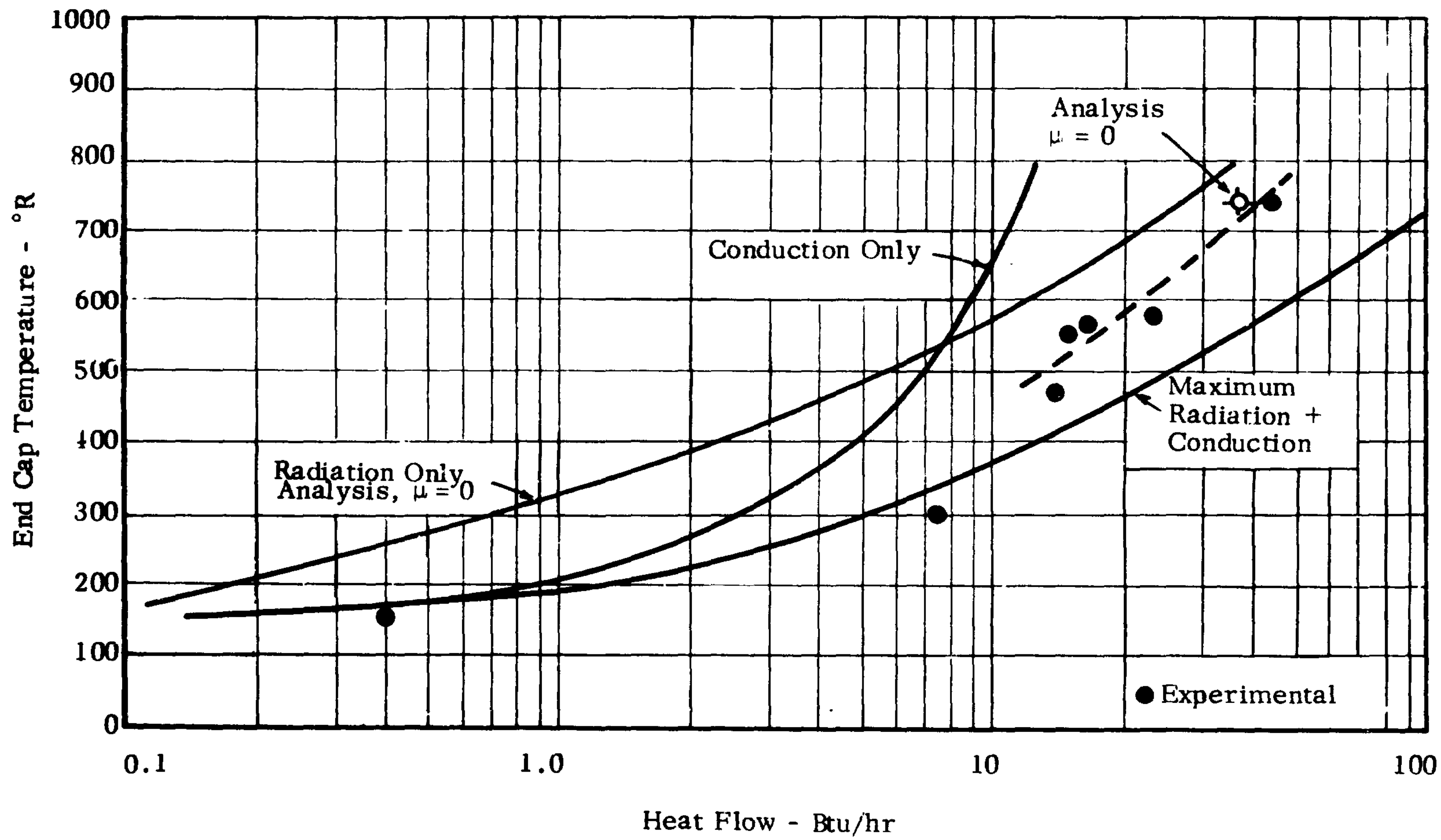

FIGURE IV-22 PENETRATION HEAT FLOW COMPARISON OF ANALYTICAL LIMITS AND EXPERIMENTAL AS A FUNCTION OF END CAP TEMPERATURE

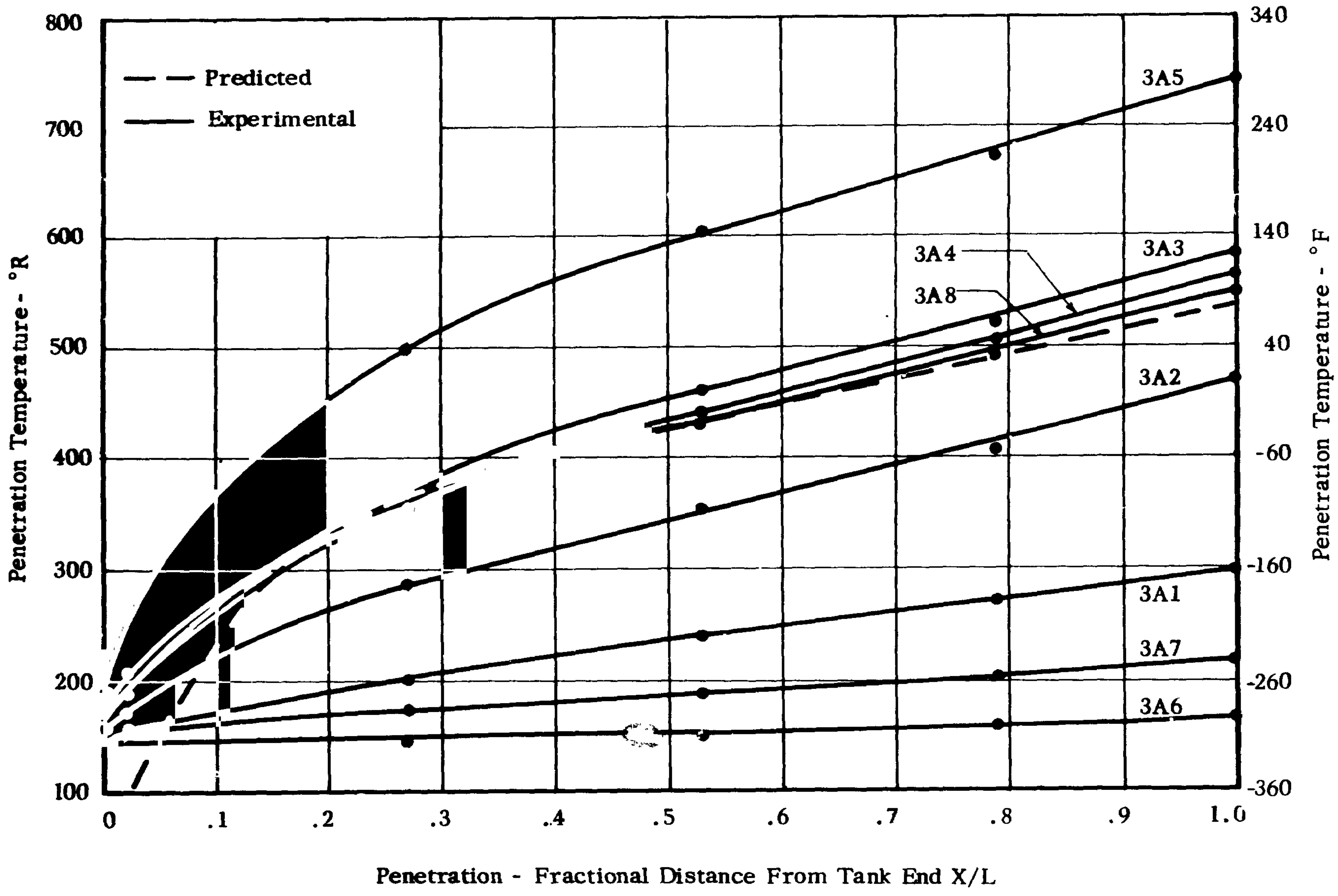

FIGURE IV-23 INSULATION SYSTEM NO. 10, TEMPERATURE DISTRIBUTION IN 6" x 17" PENETRATION TESTS III-3A1 THRU III-3A8

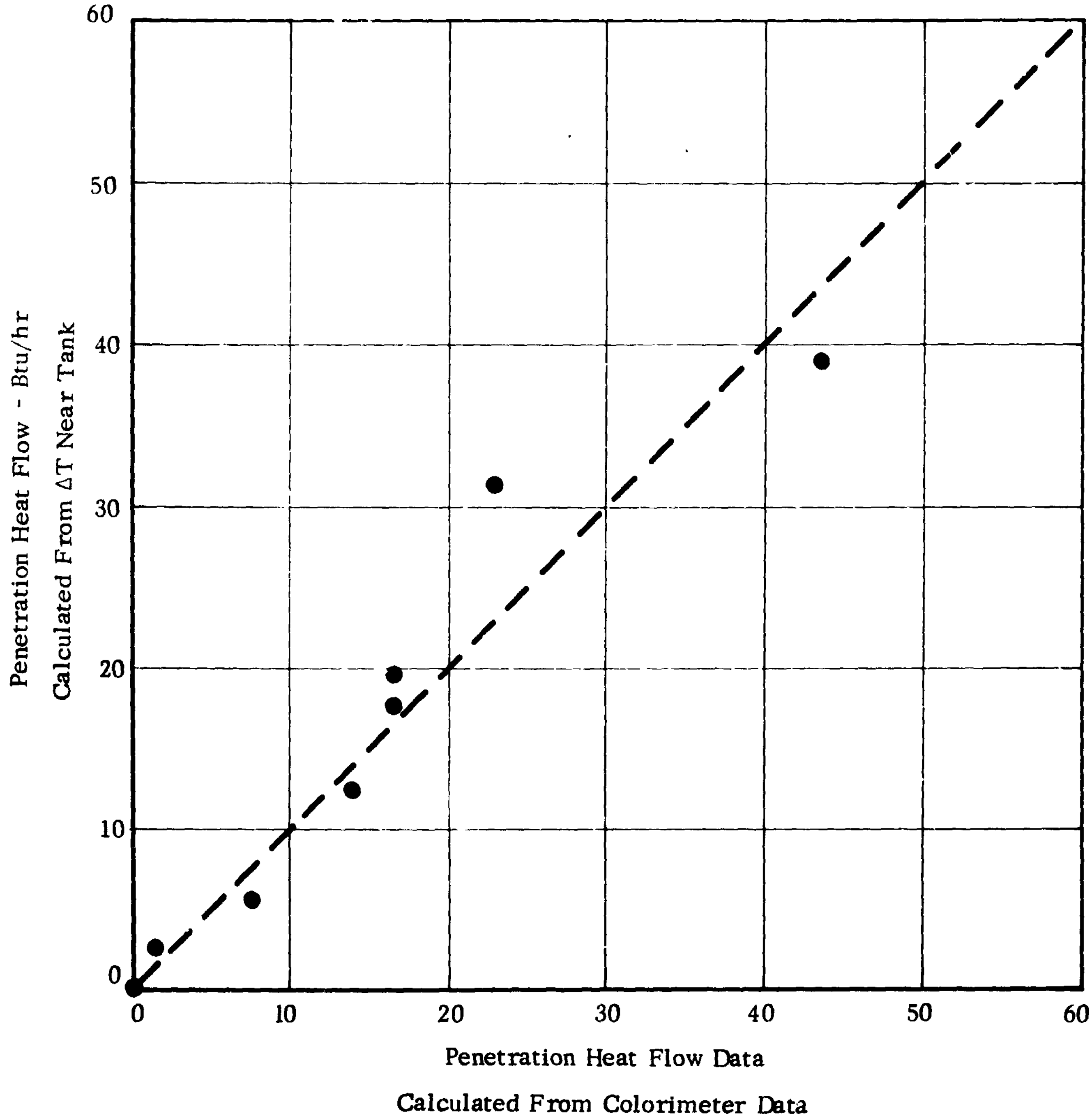

FIGURE IV-24 INSULATION SYSTEM NO. 10, PENETRATION HEAT FLOW COMPARISON OF EXPERIMENTAL RESULTS

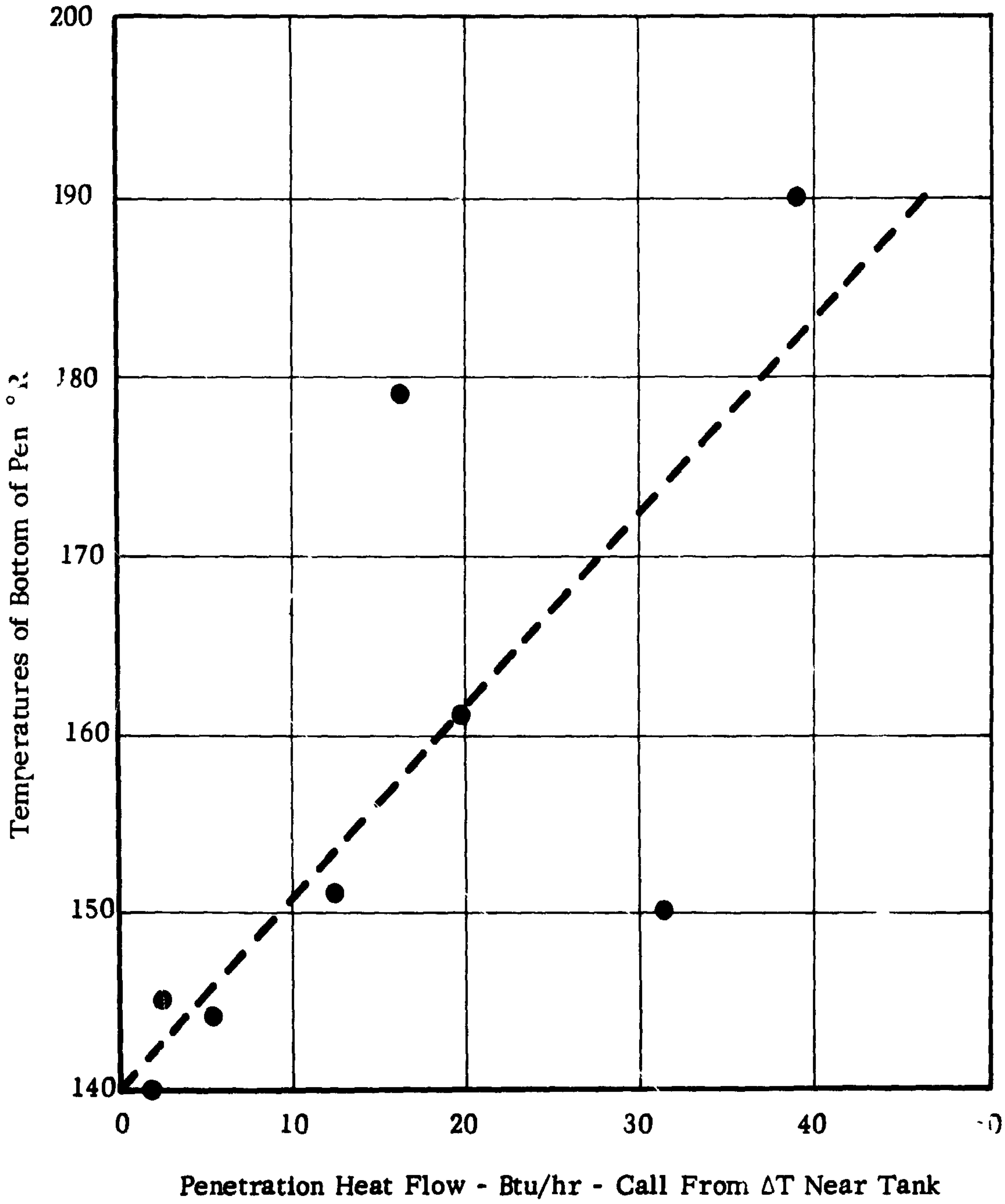

FIGURE IV-25 INSULATION SYSTEM NO. 10, TEMPERATURE OF PENETRATION COLD END AS A FUNCTION OF PENETRATION HEAT FLOW

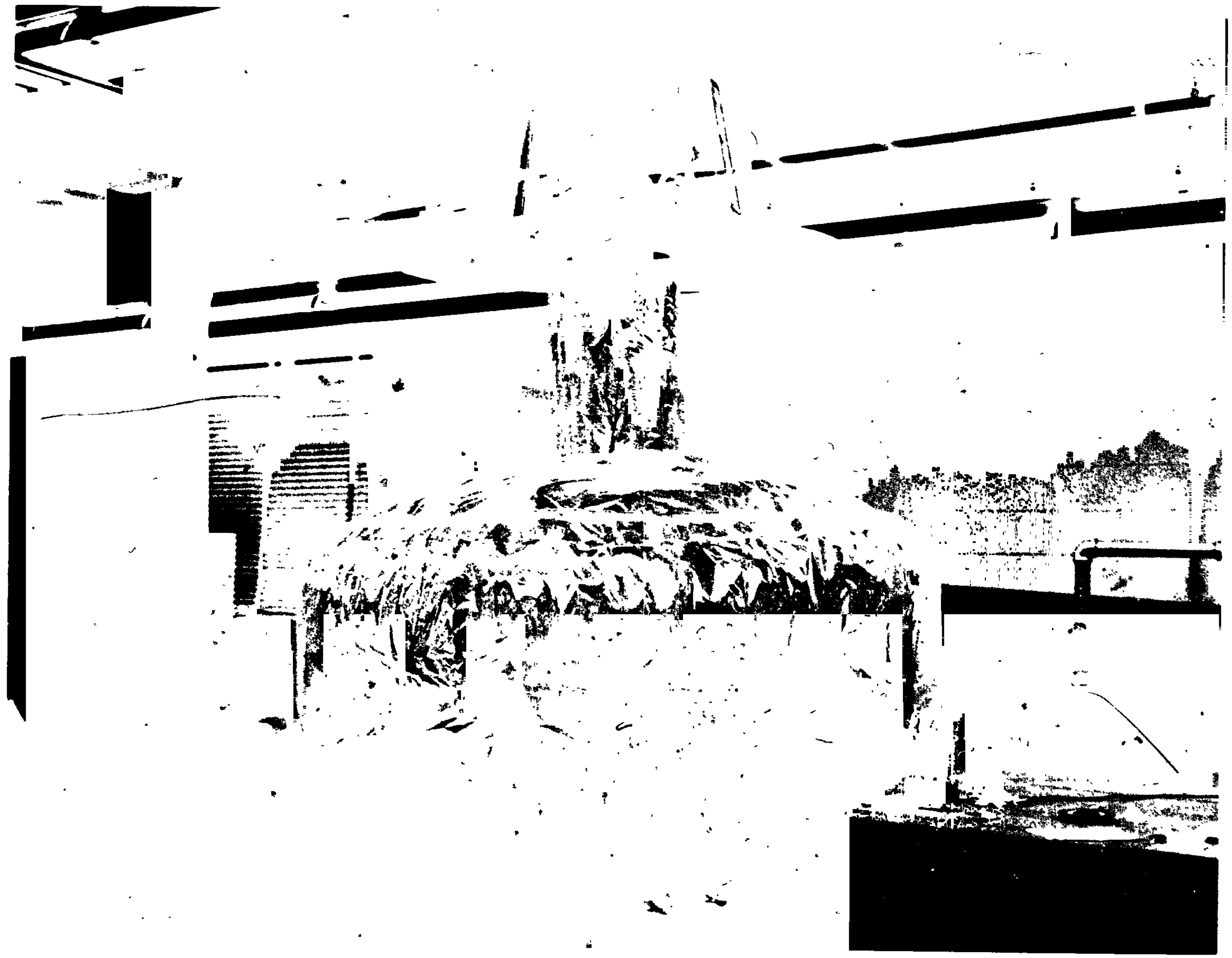

FIGURE IV-26 INSULATION SYSTEM NO. 11

FIGURE IV-27 INSULATION SYSTEM NO. 11, BOTTOM VIEW

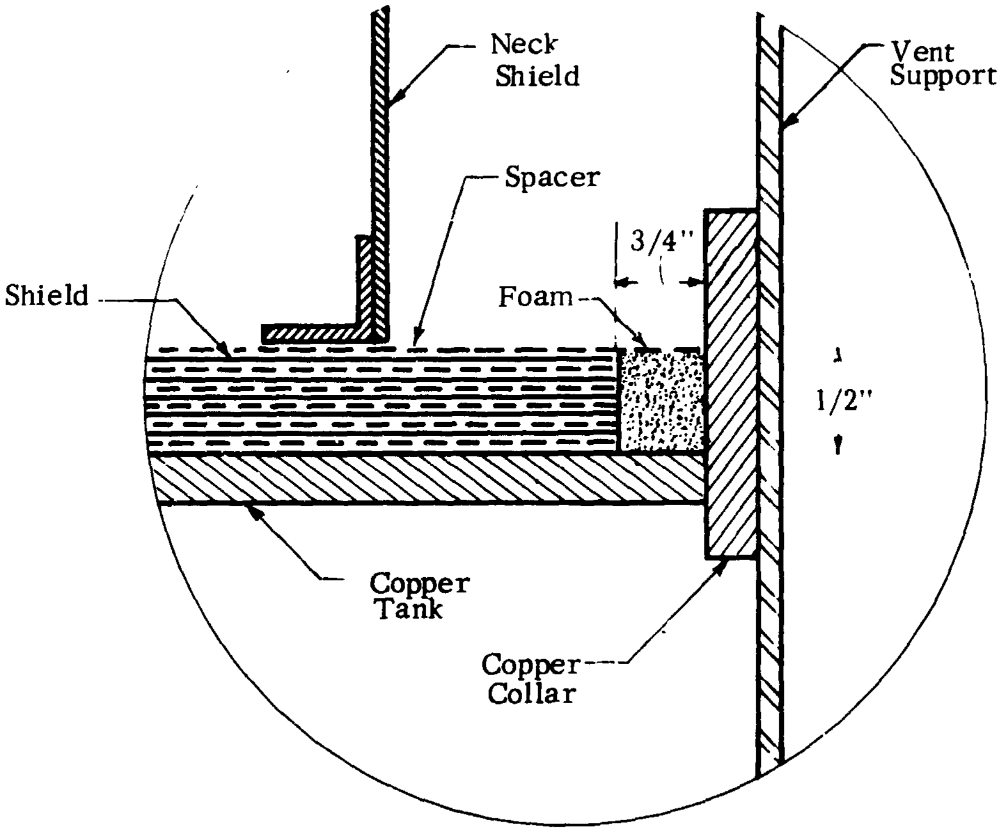

FIGURE IV-28 INSULATION SYSTEM NO. 11, NECK DETAIL

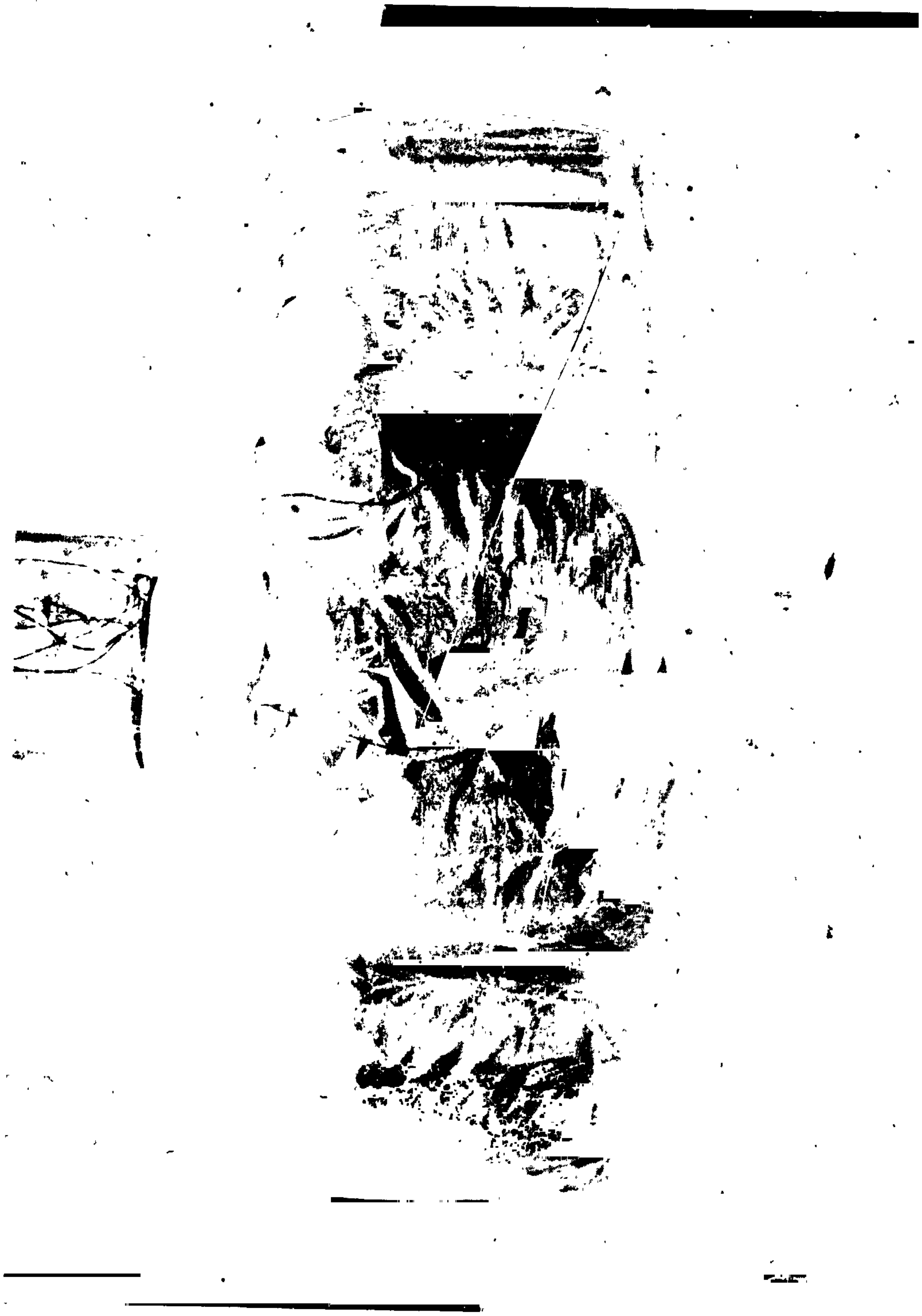

FIGURE IV-29 INSULATION SYSTEM NO. 12

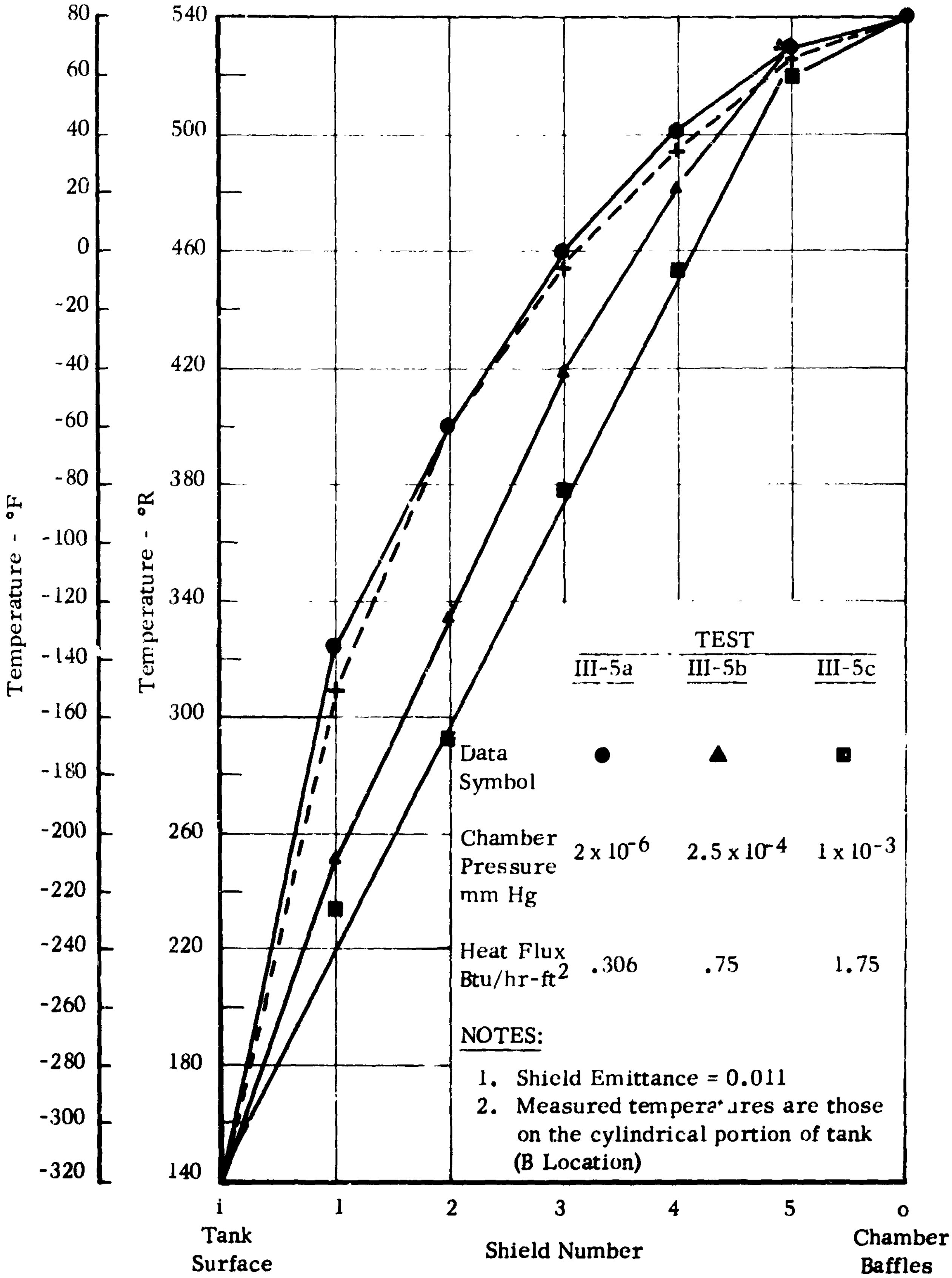

FIGURE IV-30 INSULATION SYSTEM NO. 11, SHIELD TEMPERATURE DISTRIBUTION

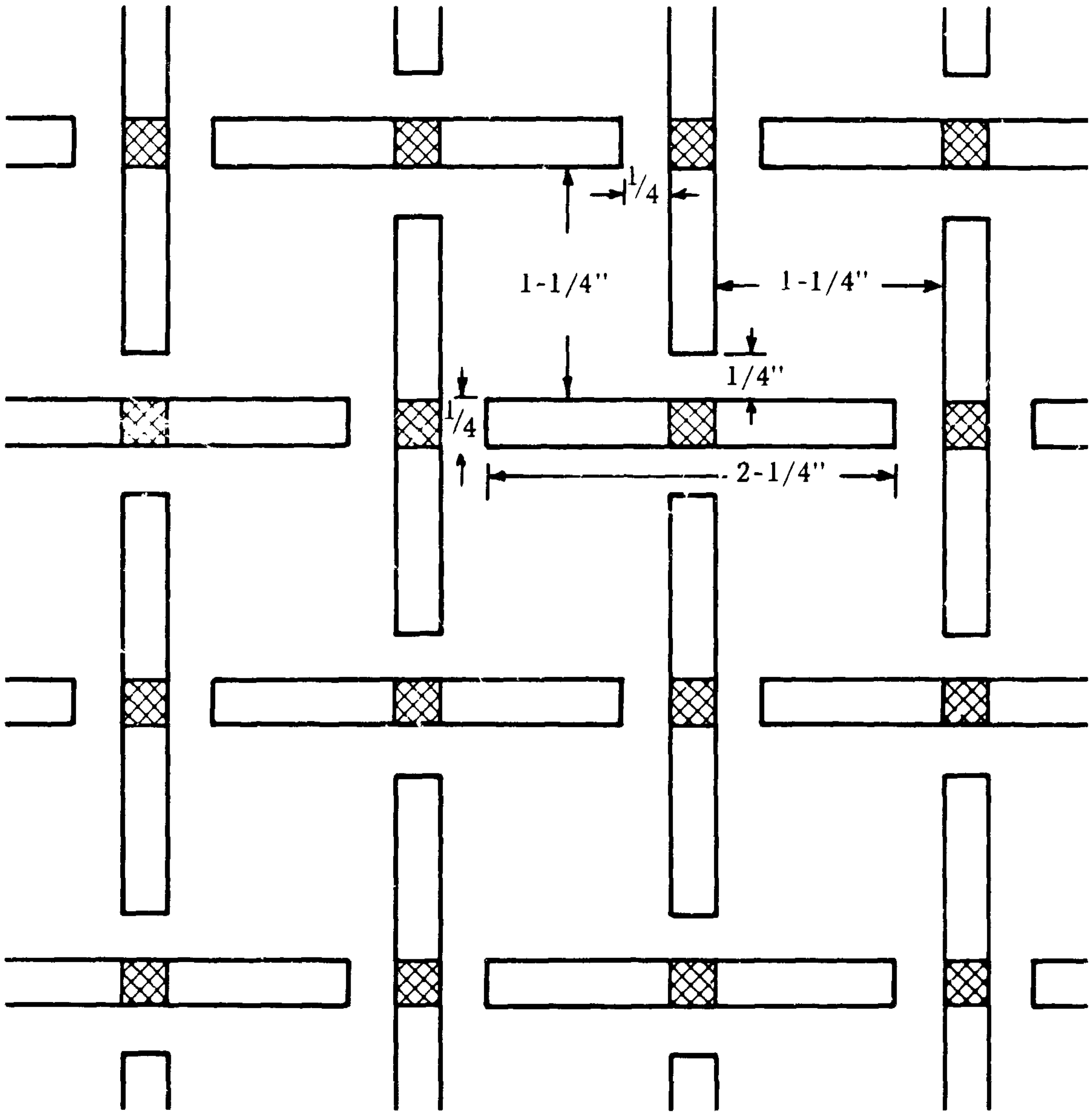

FIGURE IV-31 INSULATION SYSTEM NO. 13, SILK FOAM SPACER, FULL SCALE PATTERN

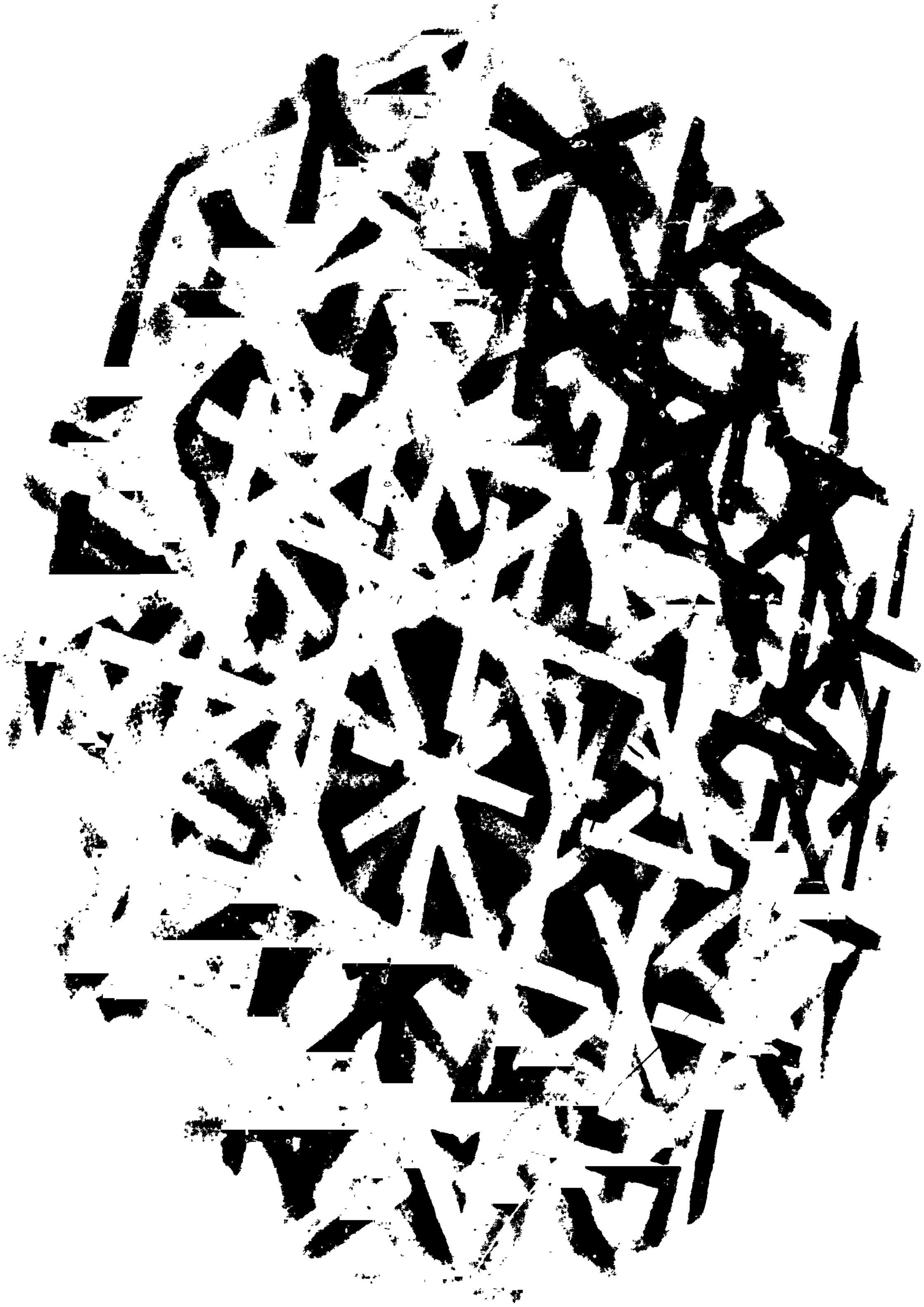

FIGURE IV-32 INSULATION SYSTEM NO. 13, SILK-FOAM SPACER PILE

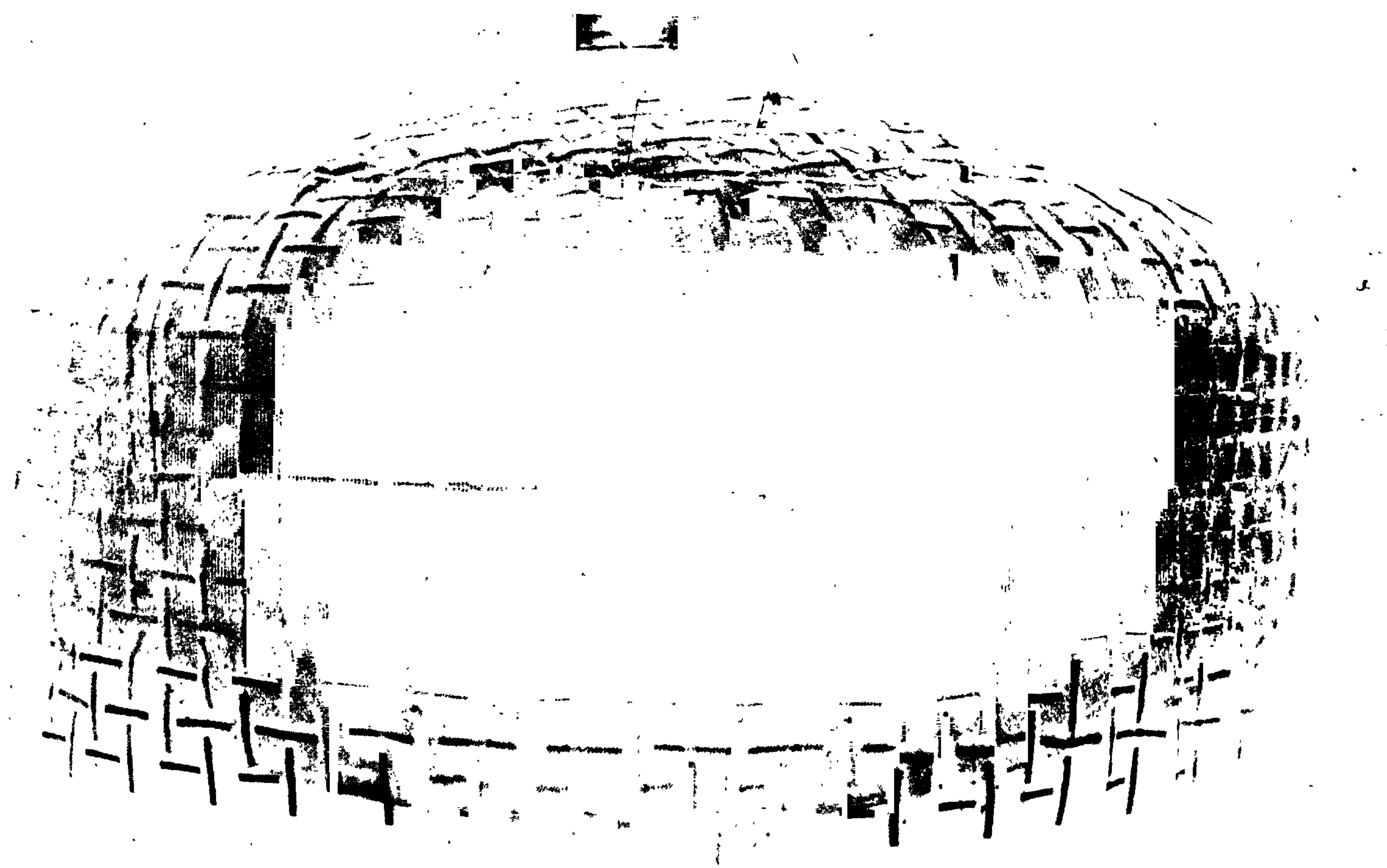

FIGURE IV-33 INSULATION SYSTEM NO. 13, SILK-FOAM SPACER, PARTLY APPLIED TO TANK

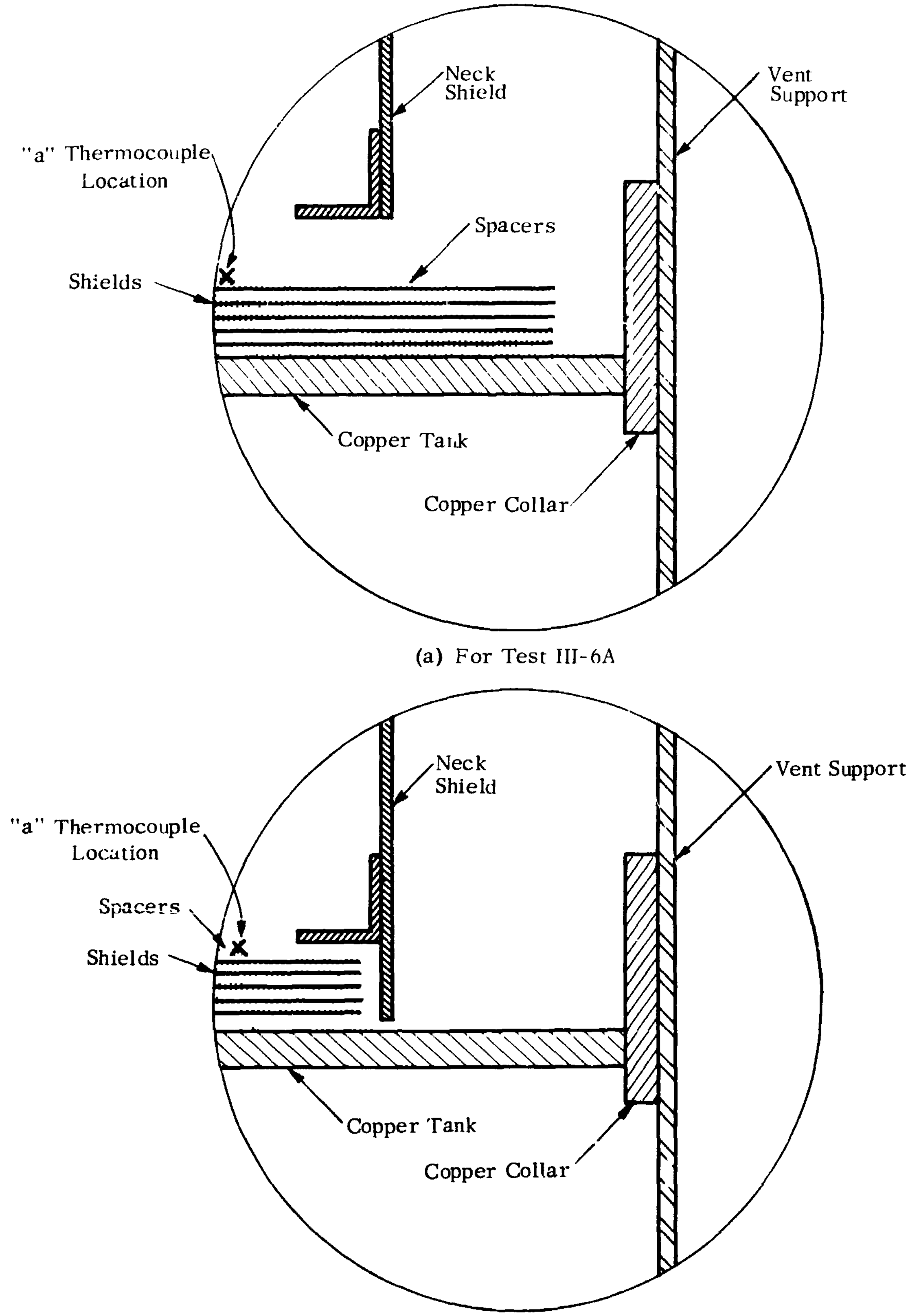

(a) For Test III-6A

(b) For Test III-6B

FIGURE IV-34 INSULATION SYSTEM NO. 13, NECK DETAIL

FIGURE IV-35 INSULATION SYSTEM NO. 13

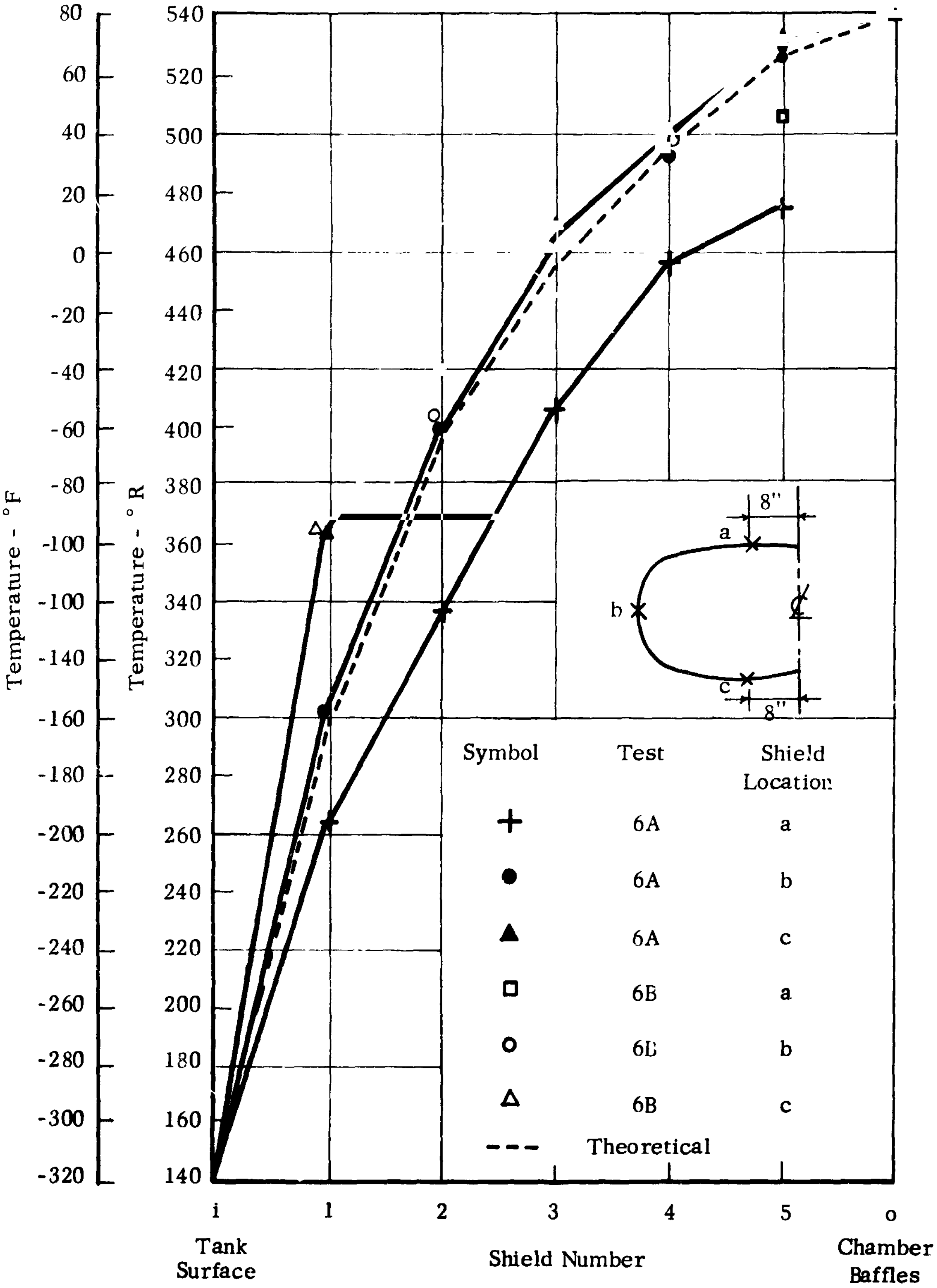

FIGURE IV-36 INSULATION SYSTEM NO. 13, SHIELD TEMPERATURE DISTRIBUTION

FIGURE IV-37 INSULATION SYSTEM NO. 14

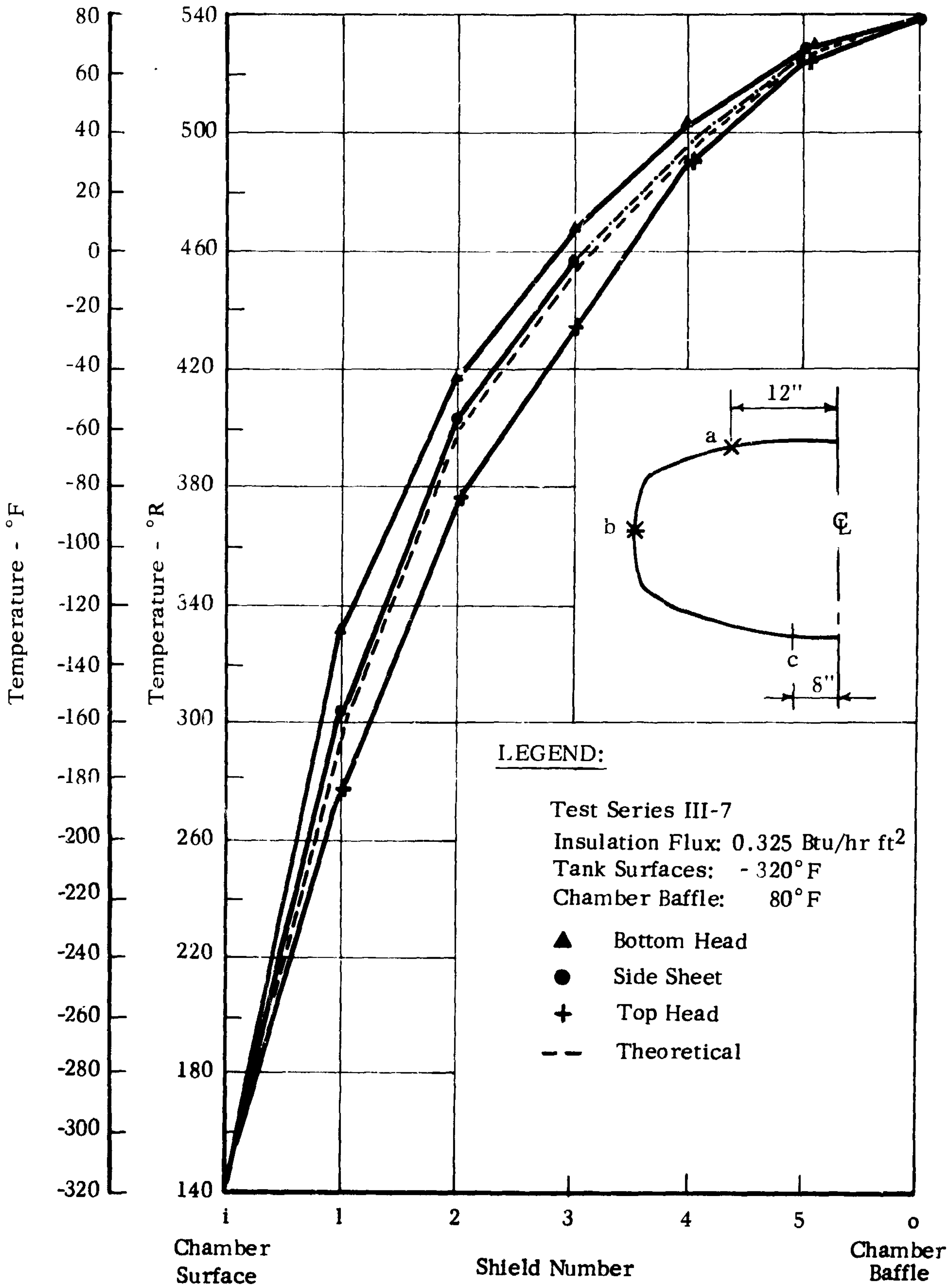

FIGURE IV-38 INSULATION SYSTEM NO. 14, SHIELD TEMPERATURE DISTRIBUTION

NOMENCLATURE

A	area, usually ft^2
c	average molecular velocity
C_v	heat capacity, Btu/lb mole °R, at constant volume
C_p	heat capacity, Btu/lb °R, saturated at constant pressure
$f(\alpha)$	Kennard's[2] function for the accommodation coeffiicent; between surfaces j and j+1, $f(\alpha) = (\alpha_j \alpha_{j+1}/\alpha_j - \alpha_{j+1} - \alpha_j \alpha_{j+1})$
F	average molecular flux = $Nc/4$
k_{sc}	thermal conductivity of the spacer-shield sandwich
N	molecular (or mole) density
Q	heat flow, usually Btu/hr
R	function of emissivity and open area = $[\frac{\varepsilon+(2-\varepsilon)\tau}{(2-\varepsilon)(1-\tau)}]$
T	temperature, absolute °R
λ	latent heat of vaporization, Btu/lb
m	mass, liquid or gas, lbs; m^v, gas mass; m^ℓ, liquid mass

GREEK

α	accommodation coefficient
δ	shield spacing
ε	emissivity
σ	Stefan-Boltzmann constant
ν_o	gas leak rate, mass (or moles)/area-time
τ	open area fraction in the multi-layer insulation

REFERENCES

1. "Liquid Propellant Losses During Space Flight," Report No. 65008-00-04, Contract NASw-615, p. II-36-47 (October 1963) Arthur D. Little, Inc., Cambridge, Massachusetts.

2. Kennard, Earle, H., Kinetic Theory of Gases, McGraw-Hill Book Company, New York, (1938), p. 315-318.

3. Bonneville, J. M., "Design and Optimization of Space Thermal Protection for Cryogens - Analytical Techniques and Results," Report No. 65958-02-01, Contract NAS3-4181, Appendix B, (December 18, 1964), Arthur D. Littie, Inc., Cambridge, Massachusetts. NASA CR54190.

4. "Basic Investigation of Multi-layer Insulation Systems," Report No. 54958-00-04, Contract NAS3-4181 (October 30, 1964), Arthur D. Little, In Inc., Cambridge, Massachusetts. NASA CR54191.

APPENDIX IV- A

CALIBRATED HELIUM LEAK SYSTEM

1. Introduction

The helium leak system provides a known gas flow at the underside of the multi-layer insulation. The maximum design rate is 340 micron-liters per second.* Based on theoretical considerations, this will produce a doubling of the heat flux in Insulation System No. 9 which is perforated in the amount of 2 per cent. As the leak system was to be used also with Insulation System No. 8 (openings occur at the gore and joint sections where the actual area is unknown but believed to be small), we selected a minimum leak rate one hundred times smaller than the maximum rate.

2. Helium Leak System

The required leak rates were achieved by fixing the flow, from a pressurized cylinder containing helium, through use of a capillary tube. The desired flow rate is established by the appropriate setting of the pressure level of the helium in the cylinder. The actual flow rate during the experiment is calculated for a given time interval from the change in the gas pressure within the cylinder and the change in temperature of cylinder occurring from beginning to end of the interval.

The principal components of the helium leak system are shown schematically in Figure IV-39. The capillary (HFC-8) is placed in series between the helium cylinder (CY-10) and the helium distributor located on the calorimeter tank which is in turn placed in the evacuated environmental chamber. The pressure upstream of the capillary is measured with a high accuracy pressure gauge (P-7) and the temperature of the helium cylinder is measured with a thermocouple attached to the cylinder wall. To increase the pressure level or replenish the helium in the cylinder, a valved connection is provided to the helium supply (CY-11).

*The leak rate is presented as micron-liters per second throughout this report. Multiply these values by 5.38×10^{-8} to obtain g-moles per second. Divide by tank area to obtain mass flow per unit area.

3. Capillary

The range of upstream capillary pressures selected to produce the required range of flows was 10 to 100 psia. Under these conditions of pressure, the gas is in viscous flow and can be predicted from the compressible form of Poiseuille's equation[1] with the downstream pressure assumed negligible:

$$Q_{\mu \ell} = \frac{5.236 \times 10^{-4}}{\eta} \frac{a^4}{L} \frac{P^2}{2} \qquad (1)$$

Through use of the above equation, it was determined that the required flow of 350 micron-liters per second would be obtained with a .005 inch I.D. tube 60 inches long at an upstream pressure of 100 psi.

The capillary device was fabricated by winding the length of stainless steel capillary tube onto a 1 inch diameter threaded core. The core was then inserted into a copper sleeve and soldered and sealed to the sleeve. An end cap was soldered to the sleeve at each end of the capillary to permit fit up into the system with 1/4 inch tubing sizes. Figure IV-40 shows the pertinent details of the capillary.

4. Leak Distribution

A gas leak distributor was installed on both calorimeter tanks to assure a uniform pressure of helium over the entire inner surface of the insulation systems. The distributor was made from 1/8 inch tubing providing six outlets at the tank surface as shown in Figure IV-41. Four outlets are located on the cylindrical sections of the calorimeters at equal circumferential spacings. A fifth opening is located at the bottom center of the calorimeter and the sixth in the top head sector.

The tubing on the tank is copper while the tubing passing through the support flange, down the vent support to the tank is stainless steel. This stainless steel tubing is also given two wraps around the cold guard and soldered to it for good thermal contact in order to bring the temperature of the leak gas to within 8°F of the temperature of the calorimeter tank. Thus, the heat carried by the helium into the insulation is reduced to a negligible quantity.

Two layers of 1/8 x 1/8 inch polyvinyl coated Fiberglas net are placed over the tank surface to provide additional space between tank surface and insulation system. The purpose of this space is to assure a uniform distribution of pressure in the helium gas at the tank surface.

5. Capillary Calibration

Calibration of the capillary flow restrictor was accomplished simultaneous with its use in the helium leak tests in the following manner: the number of moles of gas in the helium cylinder at any time is given by the equation of state for an ideal gas by the relation:

$$N_m = \frac{PV}{R_o T} \tag{2}$$

As the helium cylinder volume is fixed, Equation 2 can be differentiated with respect to N_m, P and T to give the difference equation (Equation 3) for the mole flow rate.

$$\frac{\Delta N_m}{\Delta\theta} = \frac{V}{R_o T \Delta\theta} \left(\Delta P - P \frac{\Delta T}{T} \right) \tag{3}$$

By rearrangement of Equation 3 and use of appropriate units, the flow of any gas in micron-liters per second is given by,

$$Q_{\mu\ell} = \frac{V}{\Delta\theta} \left(\Delta P - P \frac{\Delta T}{\bar{T}} \right) \tag{4}$$

where all quantities and increments on the right hand side are obtained from measurements taken at the beginning and end of the experiment.

The calibration data for the helium leak system were obtained during the performance of Test Series III-1 and III-2. The results are tabulated in Table IV-23 and compared to the predicted values in Figure IV-42. At the higher cylinder pressures, the predicted and measured values are in excellent agreement. At the 15 psia level, the variation between the values is attributed to limitations in accurately measuring the small pressure decrement during the approximately 20 hour test interval.

TABLE IV-23

HELIUM CAPILLARY CALIBRATION DATA

Test No.	Helium Cylinder Pressure (psia)	Helium Flow Rate micron-liters / sec.
III-1B	14.80	4.45
III-1C	29.43	30.5
III-1D	43.77	66
III-1E	56.75	116
III-1F	70.74	168
III-2B	15.34	8.5
III-2C	27.59	29.7
III-2D	43.68	66
III-2E	58.27	121
III-2F	70.97	168

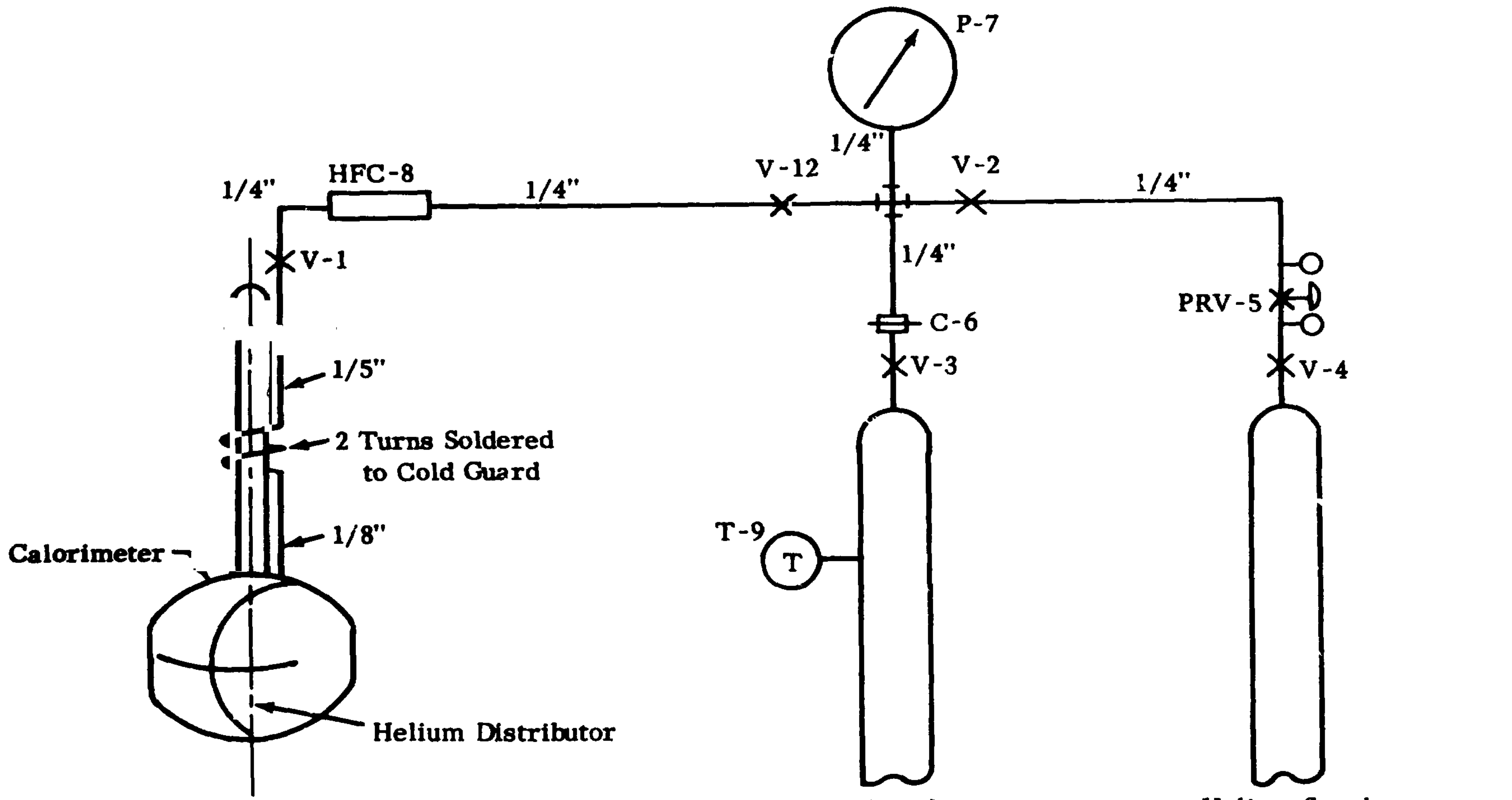

LEGEND:

V-1	Hoke Val Valve	P-7	Wallace & Tiernan Pressure Gage, 0-100 psi
V-2	Hoke Val Valve	HFC-8	Helium Flow Capillary
V-3	Cylinder Valve	T-9	Thermocouple
V-4	Cylinder Valve	Cy-10	Helium Cylinder
PRV-5	Pressure Regulator, 0-3000 Inlet, 0-200 Outlet	Cy-11	Helium Charging Cylinder
C-6	CGA 350 Helium Cylinder Connector	V-12	Hoke Vacuum Shut-Off Valve

FIGURE IV-39 HELIUM LEAK SYSTEM--FLOW SCHEMATIC

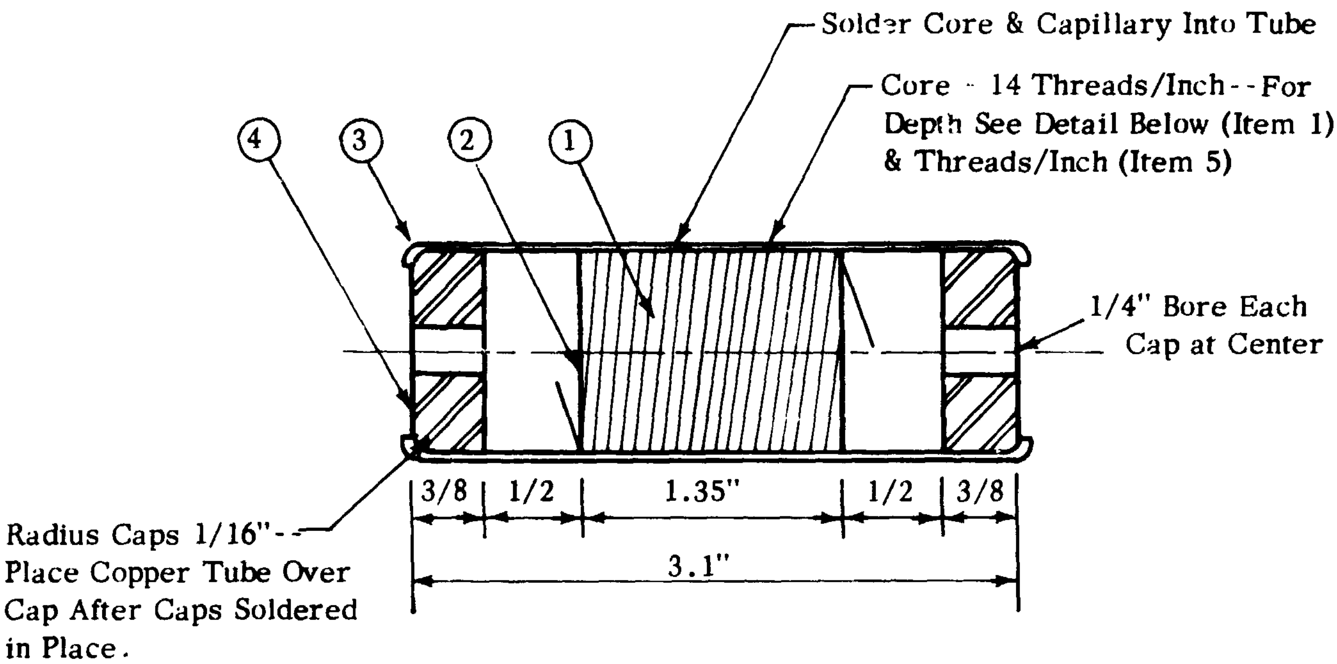

Item No.	Qty. Req.	Identifying Ratio	Description	Material
1	1	Capillary	.010 OD x .005 ID x 60 In.	Stainless
2	1	Core	~1" OD x 1.35"	Brass
3	2	Tube	1-1/8" OD x .065 Wall x 3-1/4	Copper
4	4	Cap	~1" OD x 3/8"	Brass

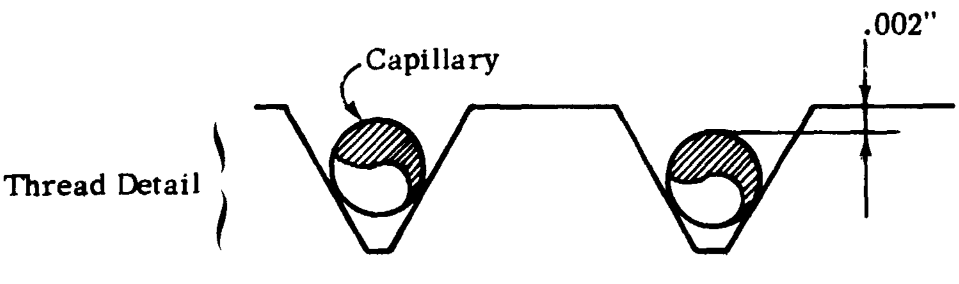

FIGURE IV-40 HELIUM FLOW CAPILLARY

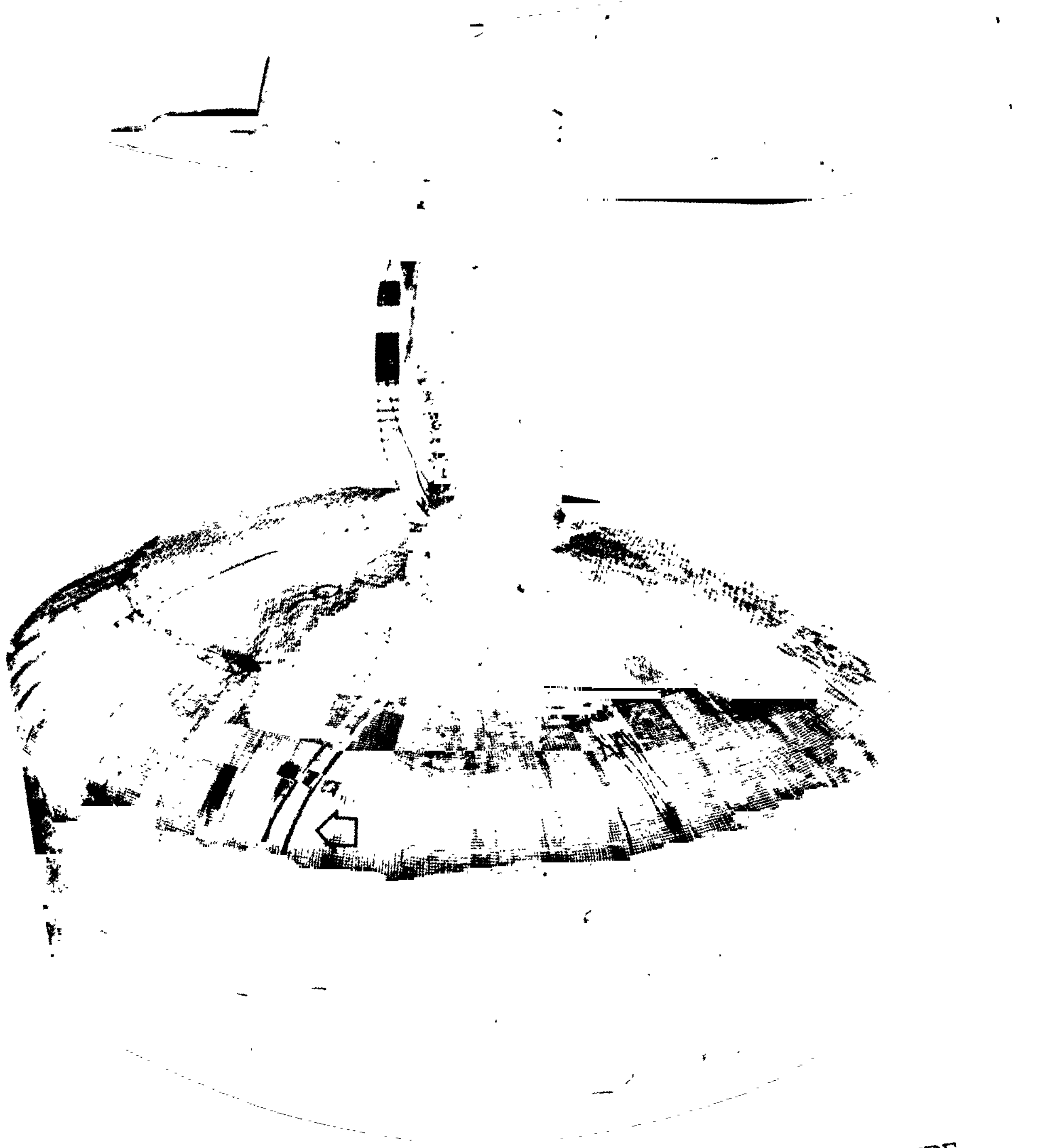

FIGURE IV-41 DISTRIBUTOR FOR HELIUM LEAK AT UNDERSIDE OF MULTI-LAYER INSULATION

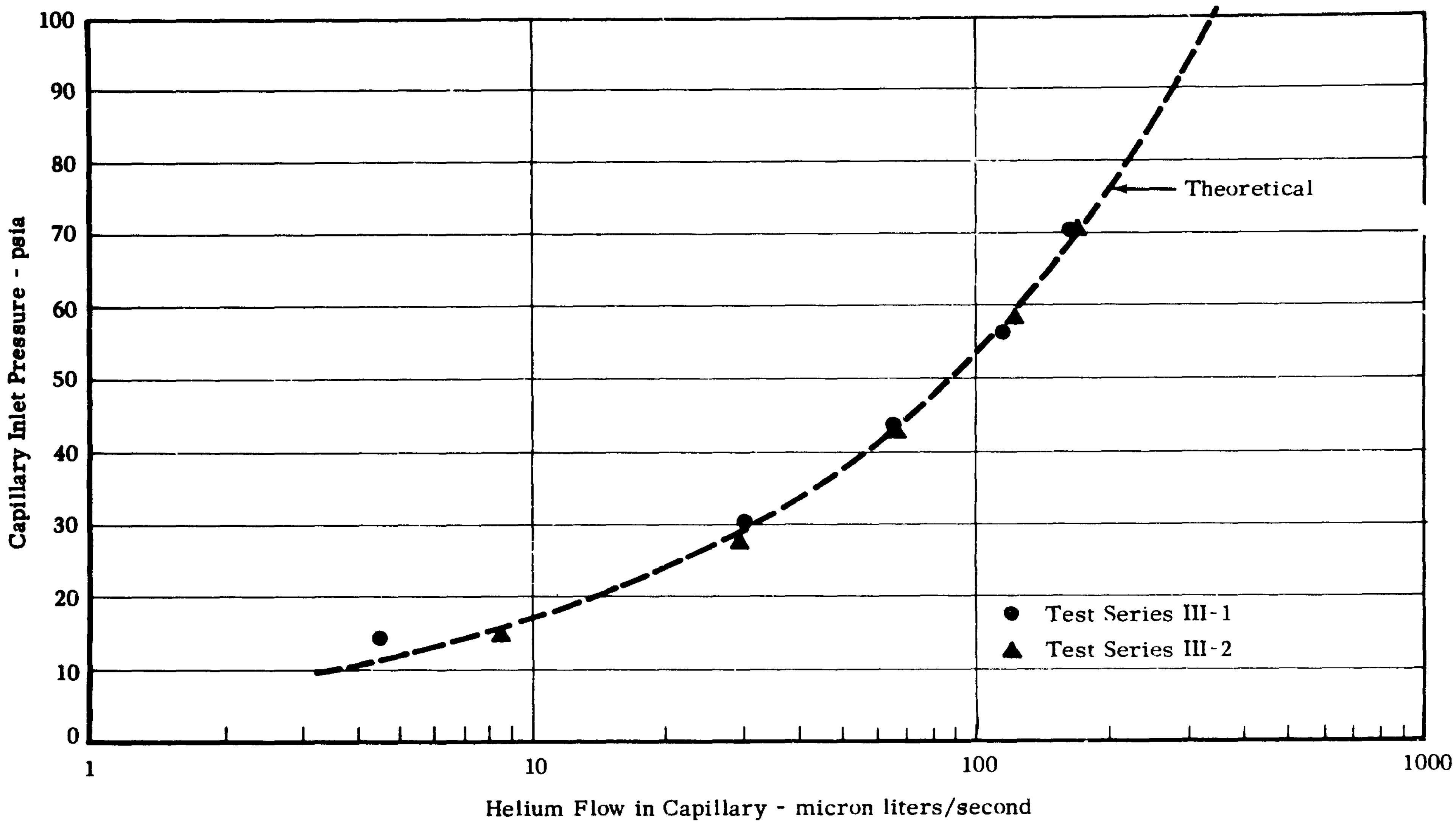

FIGURE IV-42 60-INCH CAPILLARY--PRESSURE VS FLOW CALIBRATION, HELIUM GAS

NOTATION

a	Inside radii of capillary; (cm)
L	Length of capillary; (cm)
N_m	Moles of gas
P	Pressure in the helium cylinder upstream of capillary
$Q_{\mu\ell}$	Flow rate of gas; (micron)(liters)/(sec) multiply micron-liters per second by 5.38×10^{-8} to obtain g-moles per second. Divide by the insulation area to obtain mass flow rate per unit area
R_o	Universal gas constant; (mm) (liters)/(gram-mole)(°K)
T	Temperature of gas in the capillary; temperature of gas in the cylinder; $\bar{T}$, average cylinder temperature in a time increment; (°K)
V	Cylinder volume; (liters)

Greek

η	Viscosity coefficient (grams)/(cm)(sec)
θ	Time; (sec)

REFERENCES

APPENDIX IV-A

1. Dushman, S. Scientific Foundations of Vacuum Techniques, John Wiley, New York (1949).